TE WHARE WĀNANGA O TE ŪPOKO O TE IKA A MĀUI

VICTORIA
UNIVERSITY OF WELLINGTON

Oligocene to early Miocene glacimarine sedimentation of the central Ross Sea, and implications for the evolution of the West Antarctic Ice Sheet

by

Christoph Kraus

A thesis submitted to
Victoria University of Wellington
in partial fulfilment of the requirements for the degree of
Master of Science
in Geology

Antarctic Research Centre
Victoria University of Wellington
2016

"Because now we've come to understand that what happens here [Antarctica] and in the north [Arctic] affects every one of us, no matter where we live on this planet"

Sir David Attenborough

ABSTRACT

Today the West Antarctic Ice Sheet (WAIS) is grounded mostly below sea level on a landward-sloping continental shelf, making it sensitive to oceanic temperature and circulation changes. However, recent reconstructions of the Cenozoic bedrock topographic evolution of West Antarctica have suggested that the WAIS may have first formed as a terrestrial ice sheet at the Eocene-Oligocene boundary (34 Ma), when there was up to 20% more land area in West Antarctica. At some point during the Oligocene to mid-Miocene (34-14.5 Ma) vast areas of West Antarctica became an over-deepened marine continental shelf, as is observed today. Atmospheric CO_2 also fluctuated between 600 and 200 parts per million (ppm) during this time period. Constraining the development of a marine-based WAIS during these climates with significant CO_2 fluctuations is critical in the context of understanding the sensitivity of ice sheet systems to environmental change.

In order to better constrain the development of the WAIS this study re-examined the Oligocene to early Miocene aged sediment cores recovered from the central Ross Sea, a principal drainage area of the WAIS, at Deep Sea Drilling Project Site 270 (77° 26.48' S, 178° 30.19' W). Using high-resolution visual core descriptions, as well as grainsize analysis to identify changes in ice-rafted debris and characterise the background sedimentation, six lithofacies were recognised. By incorporating new geochemical and magnetic susceptibility data, as well as existing information of the palynology and foraminifera, with the facies, six lithostratigraphic units were recognised. Together with the existing Ross Sea seismic framework the lithostratigraphic units were used to reconstruct the glacial history of the central Ross Sea during the Oligocene to early Miocene.

The late Oligocene was examined in detail, because the decreasing or invariant atmospheric CO_2 values appear to contradict the contemporaneous $\delta^{18}O$ records which imply a climatic warming and/or ice volume loss. This study shows that marine terminating ice masses of substantial size were present in West Antarctica for much of the late Oligocene, and displayed at least one significant advance. These ice masses were likely centred on the Central High and Marie Byrd Land based on the seismic stratigraphy and ice-rafted debris provenance. Only during the latest Oligocene (~23.4 Ma) do the sediments at DSDP 270 indicate a (local) reduction in ice volume in the central, and possibly eastern, Ross Sea. Plausible causal factors of this retreat include tectonic subsidence, and/or the culmination of a climatic warming. Either way, this deglaciation may have contributed to the decrease $\delta^{18}O$ shift during the latest Oligocene recorded in many far-field sites.

Furthermore, the Mi-1 glaciation has previously been suggested to represent the first significant marine-based advance of the WAIS, and has been linked to ocean and climate cooling. At DSDP 270, the Mi-1 appears to have terminated the aforementioned period of a (local) glacial minimum. However, the lack of ice overriding evidence in the core and the seismic data suggests that the WAIS did not extend as far north as DSDP Site 270. This indicates that the WAIS did not advance to the continental shelf edge during Mi-1.

Finally, spectral analyses of the late Oligocene aged sediments at DSDP 270 revealed the presence of all three orbital cycles, and a switch from eccentricity to obliquity dominated cyclicity. This is congruent with coeval near and far-field records, and represents the first evidence of an orbital forcing of West Antarctic ice volumes during the Oligocene.

Acknowledgements

Thank you to my family for teaching me to always be curious, and always believing in me. Without your continued support of everything I do, none of this would have been possible.

An meine Familie: danke das ihr immer an mich geglaubt, und das ihr mich gelehrt habt immer Interesse an neuen Dingen zu zeigen. Ohne eure Unterstützung in allem was Ich tue wäre diese These nie machbar gewesen.

Most of all, thank you Jasmine for your continued love and support (including proof-reading), even when I spent hours at university. You are amazing.
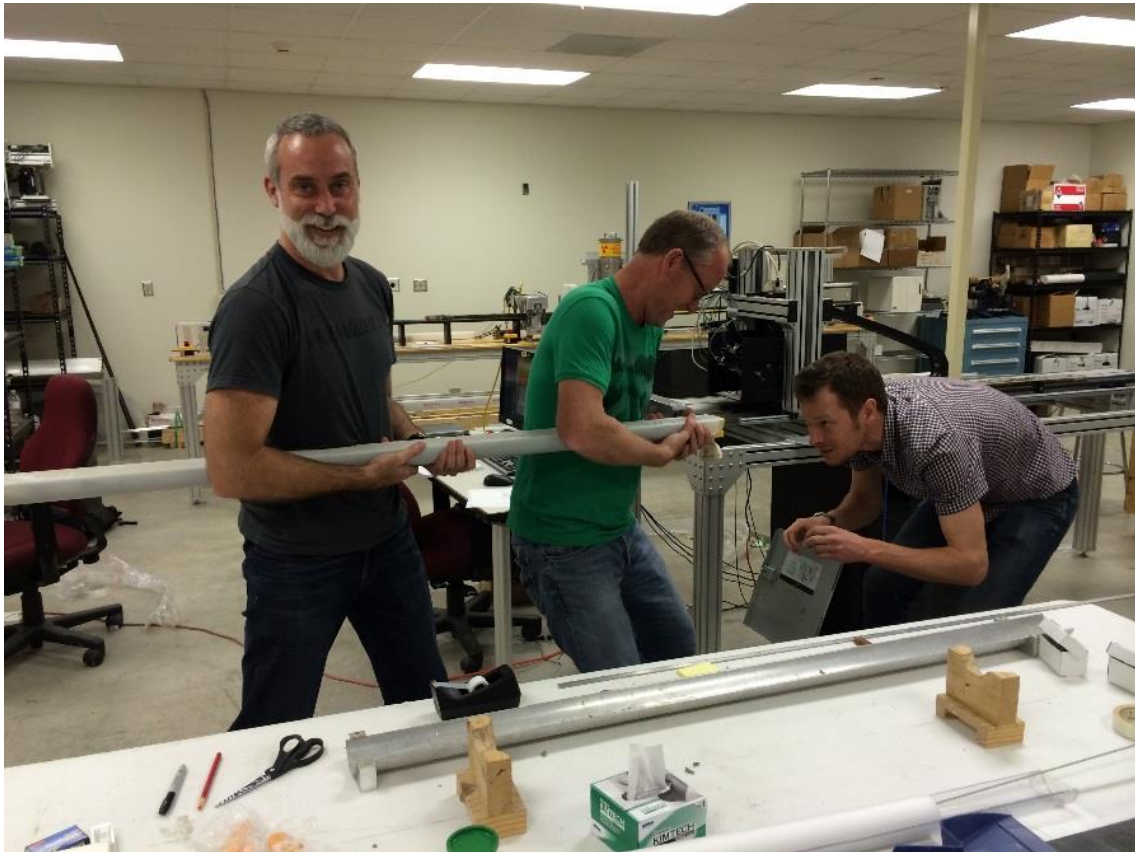
The core retrieval process …

TABLE OF CONTENTS

LIST OF FIGURES, TABLES, AND EQUATIONS

Figures

Tables

Equations

ABBREVIATION INDEX

µA	microamp
µm	micrometre
AABW	Antarctic Bottom Water
ASM	average spectral misfit
CIA	chemical index of alteration
CIROS	Cenozoic Investigation in the Western Ross Sea (drilling project)
cm	centimetre
CO_2	carbon dioxide
CRP	Cape Roberts Project
DSDP	Deep Sea Drilling Project
EAIS	East Antarctic Ice Sheet
EECO	Early Eocene Climatic Optimum
EHA	evolutive harmonic analysis
EOT	Eocene-Oligocene transition
GRAPE	gamma ray attenuation porosity evaluator
H_2O_2	hydrogen peroxide
HCl	hydrochloric acid
ICP-MS	inductively coupled plasma mass spectrometry
IODP	Integrated Ocean Drilling Program (now International Ocean Discovery Program)
IRD	ice-rafted debris
JAMSTEC	Japan Agency for Marine-Earth Science and Technology
ka/kyr	thousand years before present / thousand years (duration)
kV	kilovolt
m	metre
Ma/Myr	million years before present / million years (duration)

MAT	mean annual temperature
mbar	millibar
mbsf	metres below sea floor
mm	millimetre
MMCO	middle Miocene Climatic Optimum
MMCT	middle Miocene climate transition
MSSTS	McMurdo Sound Sediment and Tectonic Studies Project
MTM	multitaper method
ODP	Ocean Drilling Project
PCA	principle component analysis
PSICAT	Paleontological Stratigraphic Interval Construction and Analysis Tool
rpm	revolutions per minute
RSS	Ross Sea seismic sequence
RSU	Ross Sea unconformity
SHALDRILL	Shallow Drilling on the Antarctic Continental Margin (drilling project)
TAM	Transantarctic Mountains
WAIS	West Antarctic Ice Sheet
WARS	West Antarctic rift system
XRF	X-ray fluorescence

Chapter One

INTRODUCTION

1.1 Context and motivation

The West Antarctic Ice Sheet (WAIS) is largely grounded on a landward-sloping continental shelf several kilometres below sea level (Bindschadler, 2006), a bathymetric configuration that is hypothesized to lead to marine ice sheet instability (Schoof, 2007). If all of this potentially unstable marine-based ice in WAIS were to melt, it would raise global sea levels by ~3.3 m (Bamber et al., 2009). Consequently, the WAIS has been the focus of many studies assessing its vulnerability in response to warming oceans both in the geological past, and the present. Moreover, atmospheric carbon dioxide (CO_2), a principle agent in regulating the temperature of Earth (Lacis et al., 2010), has been steadily increasing from preindustrial levels of ~280 ppm and recently surpassed 400 parts per million (ppm) for the first time in ~3 million years (Myr) (IPCC, 2013). Ice sheet models and geological records from Antarctica suggest that when CO_2 last exceeded 400 ppm, the marine-based parts of the WAIS melted (Naish et al., 2009; Pollard and DeConto, 2009). However, far-field sequence stratigraphic records and isotope-based reconstructions suggest sea levels rose by as much as 22 ± 10 m (Miller et al., 2012), which implies a loss of parts of the marine-based sectors of East Antarctica (Cook et al., 2013; DeConto and Pollard, 2016; Golledge et al., 2015). Consequently, 400 ppm is suggested as the threshold beyond which all marine based ice (23 m sea level equivalent; 39% of all Antarctic ice) disappears (Foster and Rohling, 2013; Fretwell et al., 2013; IPCC, 2013). This includes ice from the subglacial basins of East Antarctica, which account for as much as 18 m of potential sea-level rise (e.g. Cook et al. (2013); Patterson et al. (2014)). At present several studies are already observing rapid thinning of Antarctic glaciers (e.g. Pritchard et al. (2009)), as well as substantial thinning of the West Antarctic ice shelves which buttress the WAIS and prevent accelerated flow of grounded ice (Paolo et al., 2015; Pritchard et al., 2012; Rignot et al., 2013). Furthermore, models coupled to observational data suggest that a marine ice sheet collapse of the Thwaites Glacier Basin in West Antarctica may already be underway (Joughin et al., 2014).

In order to place the modern changes into context, many researchers have attempted to constrain the past history of WAIS variability in warmer-than-present climates, to identify thresholds for marine-based ice sheet collapse (McKay et al., 2009; Naish et al., 2009; Pollard and DeConto, 2009; Scherer et al., 1998). However, accurate reconstructions of past sea level contributions resulting from WAIS retreat events rely on constraining the correct boundary conditions, such as the evolution of topography beneath the ice sheet. Reconstructions accounting for tectonic rifting and glacial erosion of West Antarctica suggest that there was up to 20% more land area in West Antarctica at the Eocene-Oligocene boundary ~34 million years ago (Ma), with the margin characterised by a shallow seaward dipping continental shelf (Fig. 1.1; Wilson et al., 2013). This has two consequences: (1) terrestrial ice sheets do not displace sea water, so the same volume of ice would have greater sea level contribution than a marine-based ice sheet that displaces sea water; and (2) as terrestrial ice sheets nucleate at high elevations, they can form in a warmer climate than marine ice sheets which require significant cooling at sea level. Subsequent overdeepening of the continental shelves may have resulted in a smaller ice sheet with less frequent ice sheet advances even as the background climate state may have gradually cooled through the late Cenozoic. It is now thought that the WAIS may have formed as a

terrestrial ice sheet at the same time as the terrestrial ice sheet first developed in East Antarctica, ~34 Ma (Wilson and Luyendyk, 2009; Wilson et al., 2012). Since 34 Ma, vast areas of West Antarctica have subsided to several kilometres below sea level but the evolution of the WAIS from the early terrestrial ice sheet to the marine-based ice sheet that characterised the Plio-Pleistocene glacial cycles is largely unconstrained. Atmospheric CO_2 has varied between 600 and 200 ppm over the past 34 Ma (Beerling and Royer, 2011; Zhang et al., 2013), and thus determining the threshold for the development of a marine-based WAIS is important in identifying the response of ice sheet systems to changes in environmental forcings. Furthermore, in light of the new topographic reconstructions it is appropriate to review the potential contribution of an early WAIS to two prominent climatic events of the time; the late Oligocene warming (~27-23.5 Ma) and the transient Mi-1 glaciation (23 Ma) (Zachos et al., 2001a).
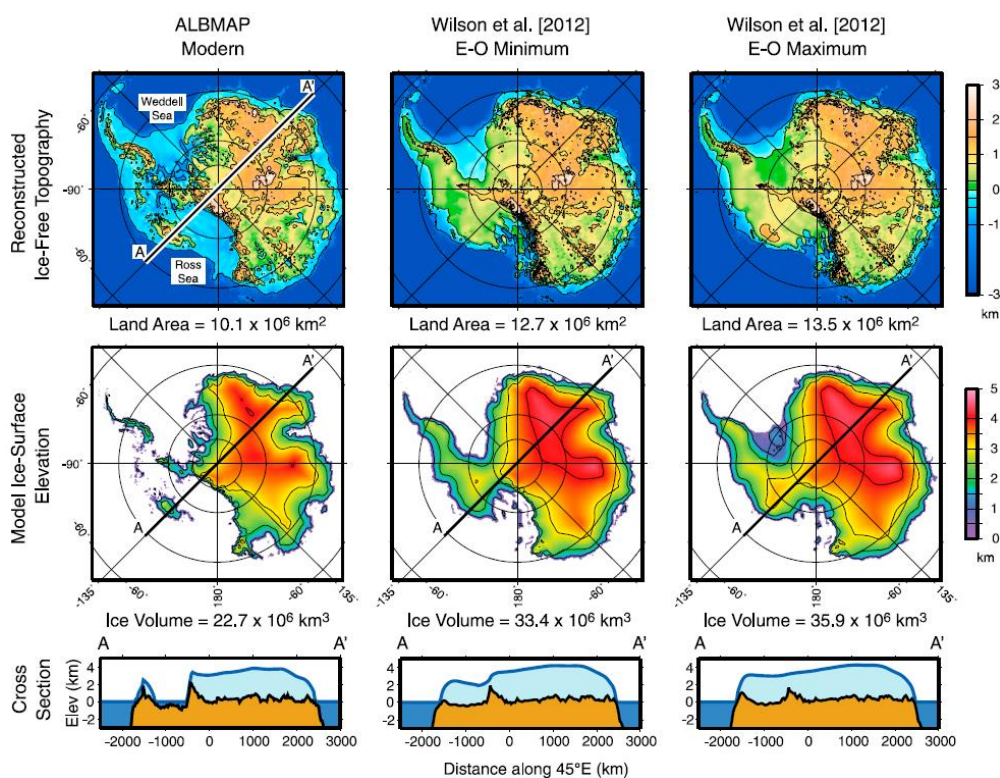
Fig. 1.1: Reconstruction of maximum and minimum bedrock topography at the Eocene-Oligocene transition, compared to the modern topography. Shown at the bottom are modelled ice volumes which could be accommodated by the topography (Wilson et al., 2013).

The up to 1 ‰ long-term decrease in $\delta^{18}O$ beginning possibly as early as ~27 Ma, and leading into the Mi-1 glaciation at ~23 Ma (Fig. 1.2), is commonly interpreted as a significant warming event, characterised by a deep sea warming of Antarctic bottom waters and deglaciation of large parts of the Antarctic ice sheets (De Man and Van Simaeys, 2004; Zachos et al., 2001a). However, atmospheric CO_2 concentrations, though poorly resolved over this time period, appear to decrease, or remain invariant (Beerling and Royer, 2011; IPCC, 2013; Zhang et al., 2013). It has been hypothesized that this conundrum may be resolved if the drop in $\delta^{18}O$ values reflects either a major change in Antarctic Bottom Water Formation (Pekar et al., 2006), or, alternatively, an ice sheet volume response to a crustal subsidence of West Antarctica (Fig. 1.3; Levy et al. (2014, unpub.); McKay et al. (2016)).

The latter scenario assumes that the WAIS initially grew as a terrestrial ice sheet (e.g. Wilson et al. (2013)) but as subsidence caused the West Antarctic bedrock to dip below sea level at a time (Oligocene), and atmospheric CO_2 levels and ocean temperatures remained too high to support a marine-based ice sheet (Foster and Rohling, 2013), significant volumes of ice may have been lost.

Following the marine transgression of the West Antarctic continental margin, ice sheets would not be able to advance across the continental shelf until CO_2 values fell below the threshold for marine-based ice sheets (which is modelled at ~400 ppm) and ocean temperature cooled sufficiently. Atmospheric values of CO_2 are first thought to have dropped below 400 ppm prior to the Oligocene-Miocene boundary (Beerling and Royer, 2011; IPCC, 2013; Zhang et al., 2013), making this time period a candidate for initiation of a marine-based ice sheet advance in West Antarctica. This time is marked by a brief (~200 ka), yet abrupt, ~1 ‰ positive $\delta^{18}O$ excursion (Fig. 1.2), and has been termed the Mi-1 event (Miller et al., 1991; Zachos et al., 2001b). The Mi-1 event is argued to represent an expansion of ice volume in Antarctica to ~125% of the present day East Antarctic Ice Sheet volume (Pekar and DeConto, 2006), a volume similar to that modelled for the Last Glacial Maximum in Antarctica (Golledge et al., 2013). Expansions of Antarctic ice volumes of this magnitude likely required an advance of the WAIS to the continental shelf edge assuming modern day bathymetry (DeConto et al., 2008; Pollard and DeConto, 2007). The Mi-1 glaciation is believed to have been triggered by a decrease in atmospheric CO_2 (and by inference temperatures) to below 400 ppm (Beerling and Royer, 2011; IPCC, 2013; Zhang et al., 2013), coupled with a low seasonality orbital configuration (cold summers) resulting from nodes (low variance) in obliquity and minima in eccentricity cycles (Liebrand et al., 2011; Pälike et al., 2006b; Zachos et al., 2001b).
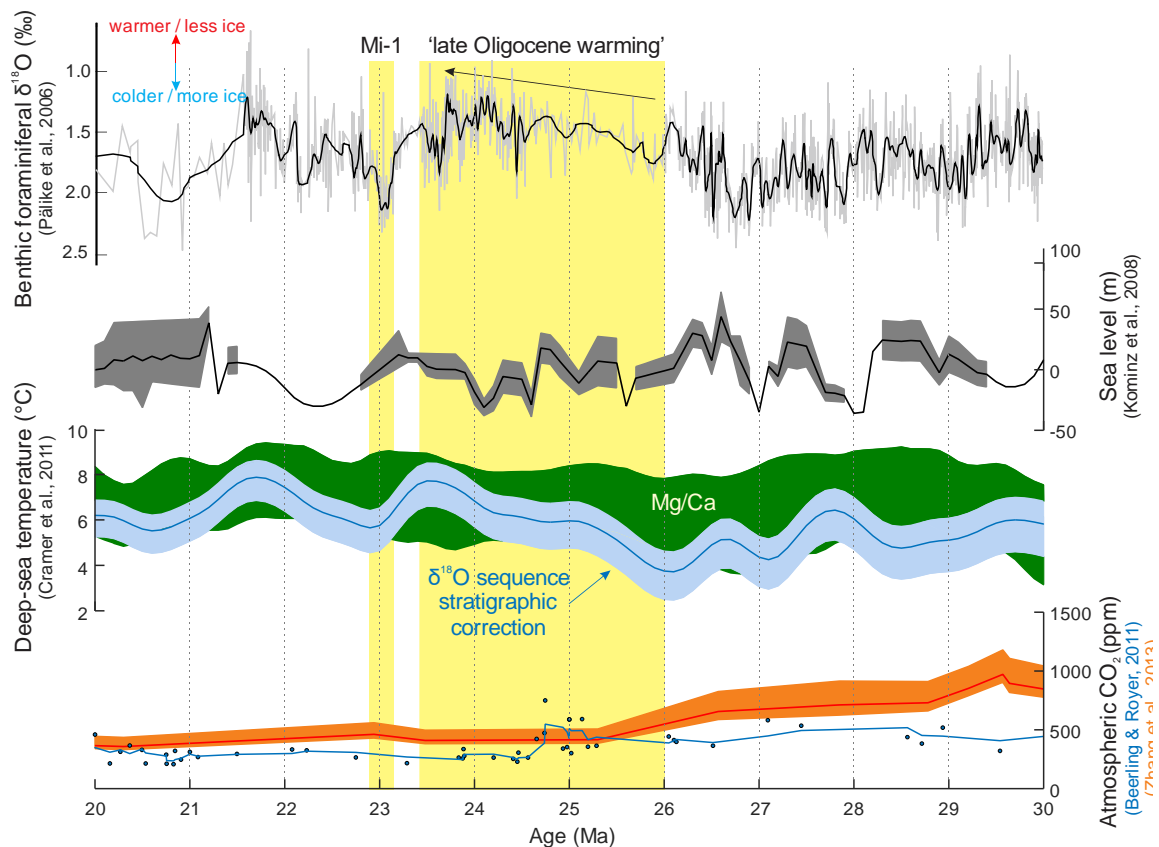
Fig. 1.2 (overleaf): Indicators of environmental change between 30 and 20 Ma: benthic foraminiferal $\delta^{18}O$ proxy of ice volume and temperature (black line is a 20-point robust loess smoothing; Pälike et al., 2006b); far-field passive margin sea level estimates, where the black line indicates the best fit with estimated sea-level lowstands bounded by maximum and minimum estimates in grey (Kominz et al., 2008); deep ocean temperatures derived from removing the ice volume component from benthic $\delta^{18}O$ records using passive margin backstripped sea level records (blue), and low resolution Mg/Ca records (green) (Cramer et al., 2011); atmospheric CO_2, compiled from several sites using various proxies (blue dots, with a 3-point moving average) (Beerling and Royer (2011), and references therein), as well as from a single site using alkenone-based reconstructions (ODP 925; orange) (Zhang et al., 2013).

Fig. 1.3: Potential change of West Antarctica and the WAIS during the Oligocene (Wilson et al., 2013), related to benthic $\delta^{18}O$ data (Zachos et al., 2008) and agents of climate forcing (O – obliquity (Laskar et al., 2004); T – possible tectonic forcing; G- greenhouse gases). Please note that this is only a conceptual illustration of possible changes (modified from Levy et al. (2014, unpub.)).

1.2 Study location

This study investigates Oligocene to early Miocene aged glacimarine sediment cores recovered from Deep Sea Drilling Project (DSDP) Site 270 (77° 26.48' S, 178° 30.19' W; Fig. 1.4) on the flank of a bathymetric high ('Central High') in the central Ross Sea by the *Glomar Challenger* on DSDP Leg 28 (Hayes and Frakes, 1975). The central Ross Sea is a key location from which the evolution of the WAIS can be studied because: (1) it is a principle drainage area of the WAIS (De Santis et al., 1999; Fahnestock et al., 2000; Golledge et al., 2013); (2) the morphology and sedimentation it was shaped under are the direct influence of the waxing and waning of the WAIS (De Santis et al., 1999); and (3) computer models have shown it to be sensitive to oceanic, atmospheric and tectonic influences (DeConto et al., 2007; Golledge et al., 2012; Pollard and DeConto, 2009; Wilson et al., 2013). Moreover, ice-rafted pebbles in the sediments at DSDP 270 are thought to be sourced from Marie Byrd Land (Barrett, 1975a), giving further evidence for a West Antarctic glacial influence on sedimentation at this site.

In addition to potentially covering the time interval which contains the late Oligocene warming and the Mi-1 glaciation (between Ross Sea unconformities 6 and 5; Fig. 1.4B), DSDP Site 270 records a terrestrial to marine transgression. As such, this core is an ideal candidate to test the aims and hypotheses outlined below.

Fig. 1.4 (overleaf): (A) Map showing the location of DSDP 270 (dot with cross) in the Ross Sea, and greater Antarctica (inset map). The solid line across DSDP 270 shows the approximate location of seismic line BGR80-07 which is depicted in (B). Arrows indicate modern ice flow lines (Barrett, 1999; Fahnestock, 2000; Rignot et al., 2011), dash-dot lines indicate ice flow divides (Rignot et al., 2008), and the heavy dashed line denotes the modern divide between the WAIS and East Antarctic Ice Sheet (EAIS). White (grey) lines represent bathymetric (topographic) contours, mapped in metres relative to mean sea level. (B) Southeast to northwest running seismic image (line BGR 80-07) showing core location DSDP 270, 271, and 272, with respect to the regional Cenozoic seismic stratigraphy, and the six prominent Ross Sea unconformities (RSU; coloured) defined by De Santis et al. (1995). Figure modified from one provided by collaborator L. De Santis.

(A)
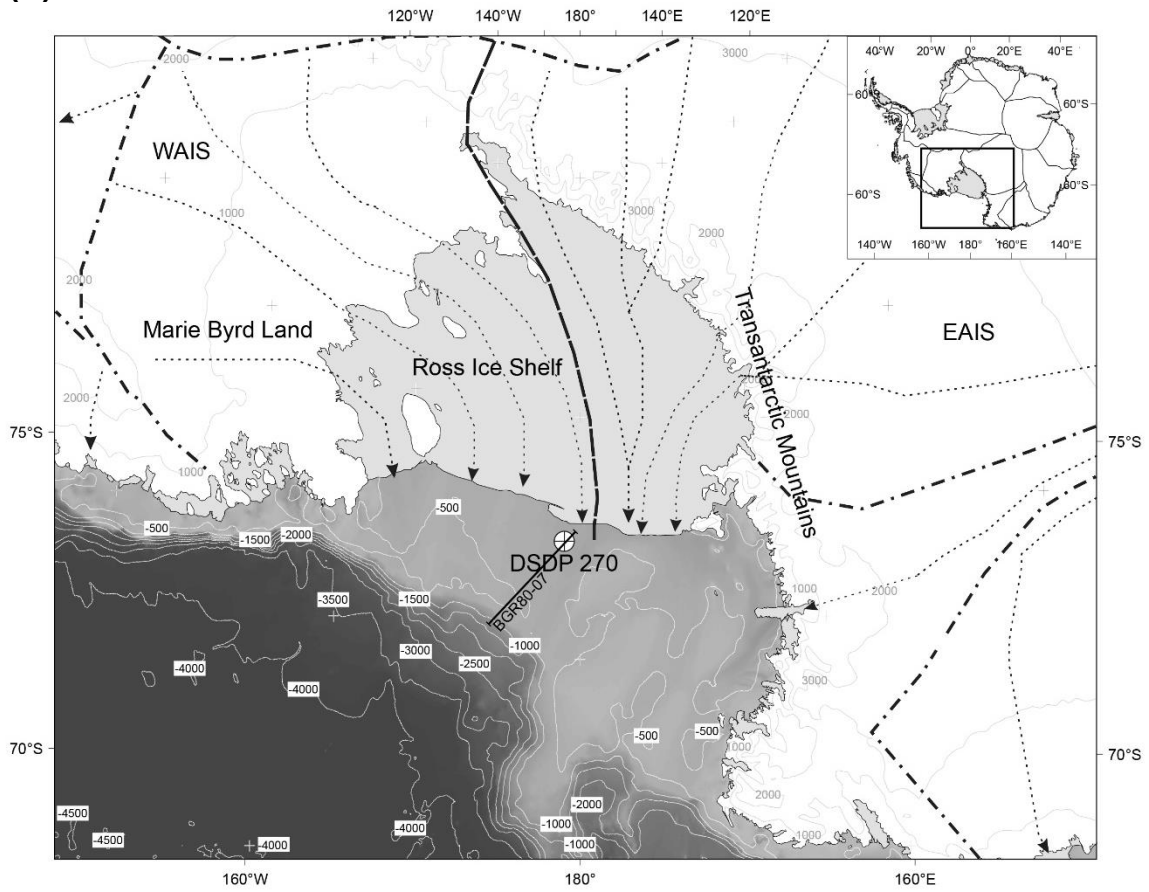
(B)
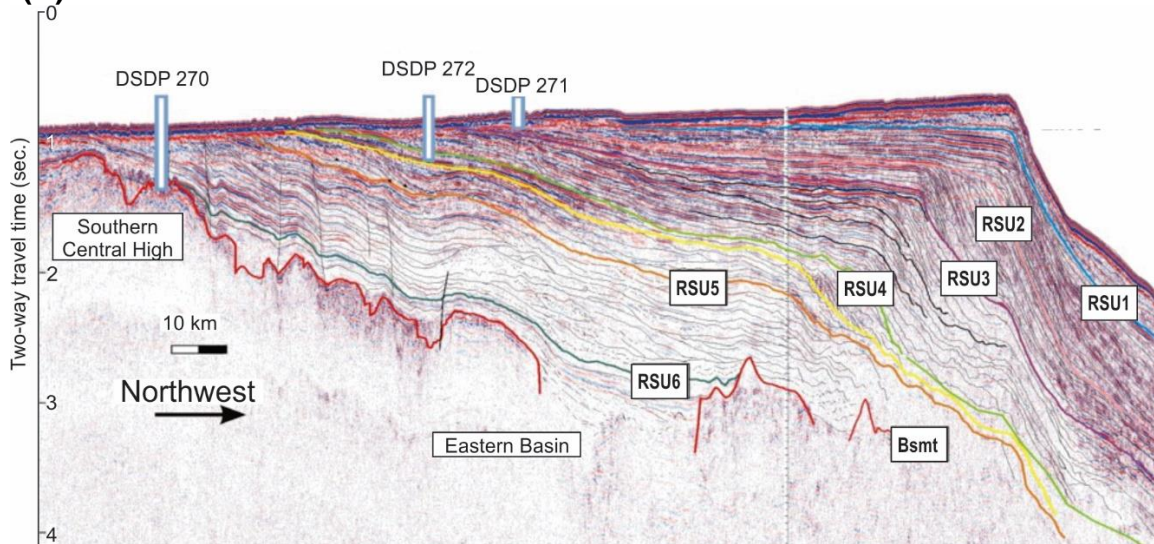
1.3 Age Model

This thesis makes use of a preliminary age model for the sediments recovered from DSDP Site 270, provided by Kulhanek et al. (in prep.). The preliminary age model (Fig. 1.5) is constrained by several datums:

1. The base of the glacimarine sediments, at ~380 mbsf, are dated at ~29.5 Ma based on the last occurrence datum of the dinoflagellate cyst *Lejeunecysta attenuata* (Kulhanek et al. in prep.). This is considered a more robust age than the K/Ar age of the glauconite (25.9 ± 1.45 Ma), because K/Ar ages of glauconite are typically up to 20% younger than the age of the sediments due to argon loss, and subsequent replacement by potassium (Hurley et al., 1960; Thompson and Hower, 1973). Using ^{40}Ar/^{39}Ar dating as an alternative to circumvent this problem is not suitable as there may be significant ^{39}Ar loss from recoil during irradiation due to the fine bladed mineral structure of glauconite (Foland et al., 1984).
2. The first appearance of *L. striata* (~24.1 Ma; Kulhanek et al. in prep.) at ~350 mbsf suggests a significantly younger age to the underlying sediments, and a likely hiatus between them.
3. Further up the core, at ~150 mbsf, the highest occurrence of the calcareous nannofossil *Dictyococcites bisectus*, dated at 23.13 Ma (Kulhanek et al., in prep.), provides a robust measure of the approximate depth of the Oligocene-Miocene boundary. Providing support to the interpretation that the Oligocene-Miocene boundary occurs not too far above 150 mbsf is the last occurrence of *D. bisectus* just below the Oligocene-Miocene boundary in the Cape Roberts cores (Naish et al., 2008).

Based on these dates, the base of the core (between 386 and 348 mbsf) is early to middle Oligocene in age, whilst the overlying sediments, separated by an inferred ~5-million-year hiatus, are late Oligocene to early Miocene in age. A significant unconformity is recorded at ~20 mbsf in the seismic data, but the strata bounding the unconformity were not recovered due to core breaks (Barrett, 1975b). Sediments above this are estimated to be Pliocene to recent in age (Leckie and Webb, 1983; The Shipboard Scientific Party, 1975b). Moreover, some biostratigraphic datums are not fully reconcilable with the magnetostratigraphy, raising the possibility of two age models: (1) one based solely on the biostratigraphy (black line in Fig. 1.5), which places the Oligocene-Miocene boundary between 150 and 100 mbsf, and (2) one which attempts to correlate the magnetostratigraphy to the geomagnetic polarity time scale (Ogg (2012); dashed line in Fig. 1.5), which places the Oligocene-Miocene boundary at ~170 mbsf. Future work, which will incorporate the strontium dating technique, will be able to further refine this age model.

Based on the aforementioned correlation of *D. bisectus* to the Cape Roberts cores, as well as the poor consistency of some of the paleomagnetic data below 230 mbsf (Allis et al., 1975), the age model based on a relatively linear sedimentation rate constrained solely by the biostratigraphy is favoured in this study. However, due to the ongoing nature of the age model refinement, and to remain unbiased, only the robust biostratigraphic datums are used in this study to constrain the ages of the sediments: the last occurrence of *L. attenuata*, the first occurrence of *L. striata*, and the highest occurrence of *D. bisectus*.
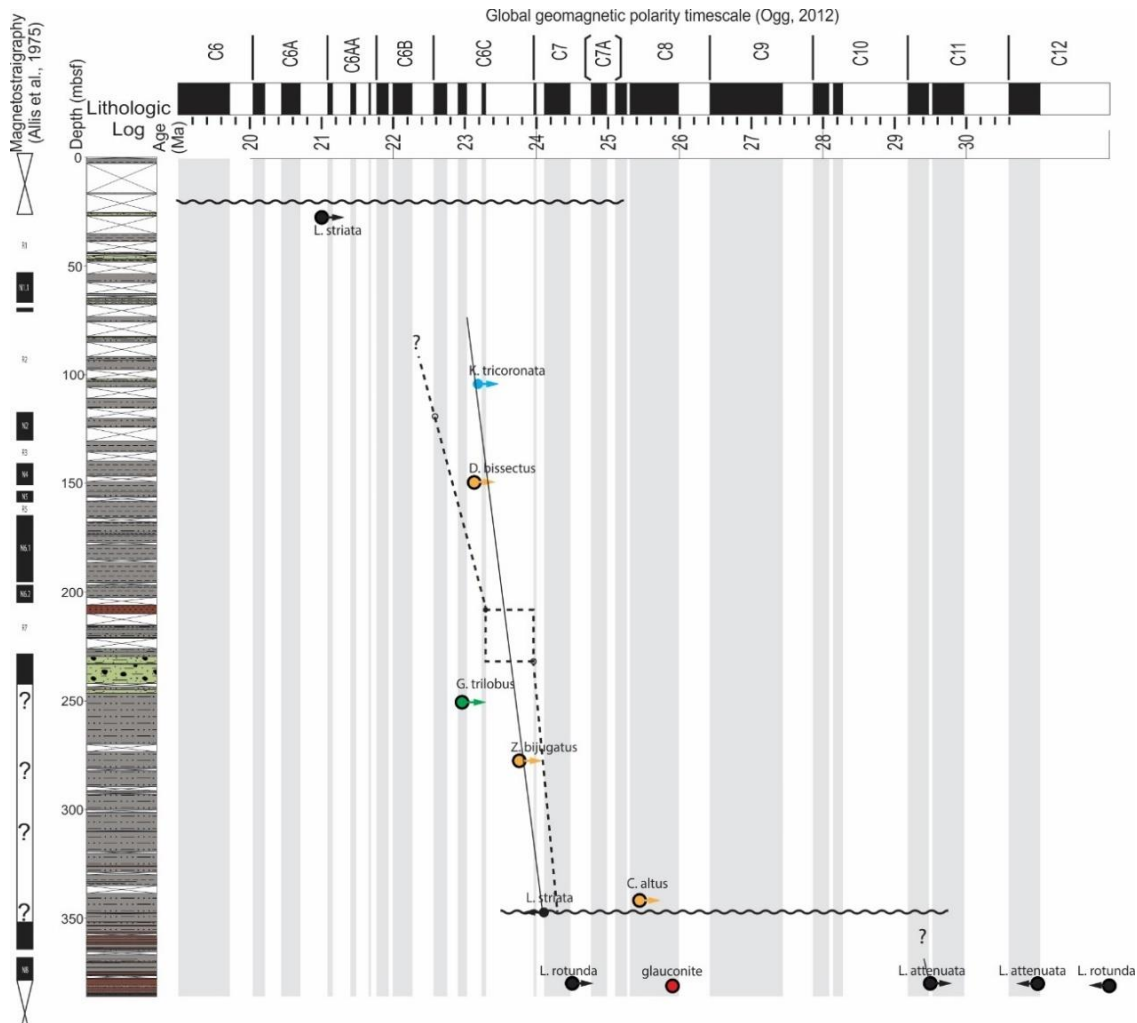
Fig. 1.5: Preliminary age model for DSDP Site 270 (Kulhanek et al., in prep.). The solid black line of correlation considers only the biostratigraphic data and ignores the magnetostratigraphy. The dashed line represents a correlation of the previously published magnetostratigraphy (Allis et al., 1975), with the global geomagnetic polarity timescale (Ogg, 2012), constrained by biostratigraphic datums.

1.4 Thesis aims and approach

This thesis aims to reconstruct the Oligocene to early Miocene glacial history of the central Ross Sea using: (1) a sedimentation model of ice-proximal records from the Ross Sea constructed on the basis of sedimentological data (visual core description, facies, and grainsize analysis), geochemical data (X-ray fluorescence (XRF), and inductively coupled mass spectrometry (ICP-MS)), and physical properties (magnetic susceptibility); and (2) geophysical (seismic) techniques to tie the results into the broader Ross Sea seismic framework. Central to this are two key aims, the answers to which will help constrain the sea level interpretations, as well as potentially advance our understanding of the sensitivity of marine-based ice sheets:

(1) Reconstruct the Oligocene to early Miocene glacial history of the central Ross Sea

By aiming to reconstruct the glacial history of the central Ross Sea during the Oligocene to early Miocene, this thesis is designed to test the following two hypotheses:
- Lowering of the West Antarctic bedrock topography and associated loss of West Antarctic ice contributed to the negative late Oligocene $\delta^{18}O$ isotope excursion.
- The Mi-1 represents the first advance of a marine-based WAIS to the edge of the continental shelf.

By testing these hypotheses, it is hoped novel insights into the early history of the marine-based ice sheets in West Antarctica, as well as insights into oceanic and climatic thresholds for marine-based ice sheet development and collapse during the geological past, will be gained. In particular, it will help assess the proposed CO_2 threshold of 400 ppm for the existence of marine-based ice sheets (Foster and Rohling, 2013), as CO_2 concentrations dropped below 400 ppm just prior to the Oligocene-Miocene boundary (Beerling and Royer, 2011; Kürschner et al., 2008; Pagani et al., 2011; Pagani et al., 2005; Zachos et al., 2001b; Zhang et al., 2013).

(2) Identify if there is evidence for orbital forcing of the glacimarine sedimentation during the late Oligocene to early Miocene

It has been demonstrated, based on ice sheet proximal evidence, as well as deep sea benthic stable isotopes, that large-scale ice volume changes during the Oligocene and early Miocene were regulated by orbital forcing, with major shift from obliquity (41 kyr) to eccentricity (400 and 100 kyr) cycles occurring across the Oligocene-Miocene boundary (Naish et al., 2001; Pälike et al., 2006b; Zachos et al., 1997; Zachos et al., 2001a; Zachos et al., 2001b). We anticipate that if the early WAIS or local ice caps fluctuated in volume at orbital-scale periods, this could be identified as cycles in the grainsize, facies, and chemical properties in DSDP Site 270. A direct, semi-continuous record of orbitally paced oscillations of the WAIS during the Oligocene-Miocene does not currently exist.

1.5 Additional contributors to the data presented in this thesis

This thesis was made possible with the contribution of collaborators:
- The original age model of the sediments recovered from DSDP Site 270 (Allis et al., 1975) is currently in the process of being updated by Kulhanek et al. (in prep.). This thesis uses their preliminary age model. Their published model is expected to have a higher in resolution.
- The XRF results, which were measured by myself and my supervisory team, were analysed with the help of Francisco Jiménez-Espejo (JAMSTEC), who normalised the dataset, and assessed the potential trends in the data using principle component analyses. Moreover, the ICP-MS samples were selected by me, and sent to Francisco Jiménez-Espejo who conducted the laboratory work and produced the results, which were analysed with his guidance. The interpretations of geochemical data in the context of the sedimentological evidence were conducted by myself and my supervisory team.
- Guidance on the interpretation of the available Ross Sea seismic data was provided by Laura De Santis (Istituto Nazionale di Oceanografia e di Geofisica Sperimentale). John

Anderson (Rice University) is acknowledged for collecting the seismic data shown in this thesis.

Chapter Two
BACKGROUND

2.1 Tectonic history of West Antarctica

As noted in the previous chapter, changes in the subaerial extent of West Antarctica during the Cenozoic have important implications on ice volume and sea level estimates. West Antarctica underwent several stages of intracontinental deformation in the Mesozoic-Cenozoic West Antarctic Rift System (WARS), which covers the area beneath the Ross Sea and Ice Shelf, Marie Byrd Land and parts of the WAIS, and is flanked by the Transantarctic Mountains on its western edge (Fig. 2.1; Siddoway (2008); Siddoway et al. (2005)). The Ross Sea lies within the central region of the WARS, and its deep continental shelf is ascribed largely to the combination of crustal thinning (Fitzgerald et al., 1986; Stern et al., 1992), glacial erosion, and sediment loading (Davey and Brancolini, 1995; ten Brink and Cooper, 1992).
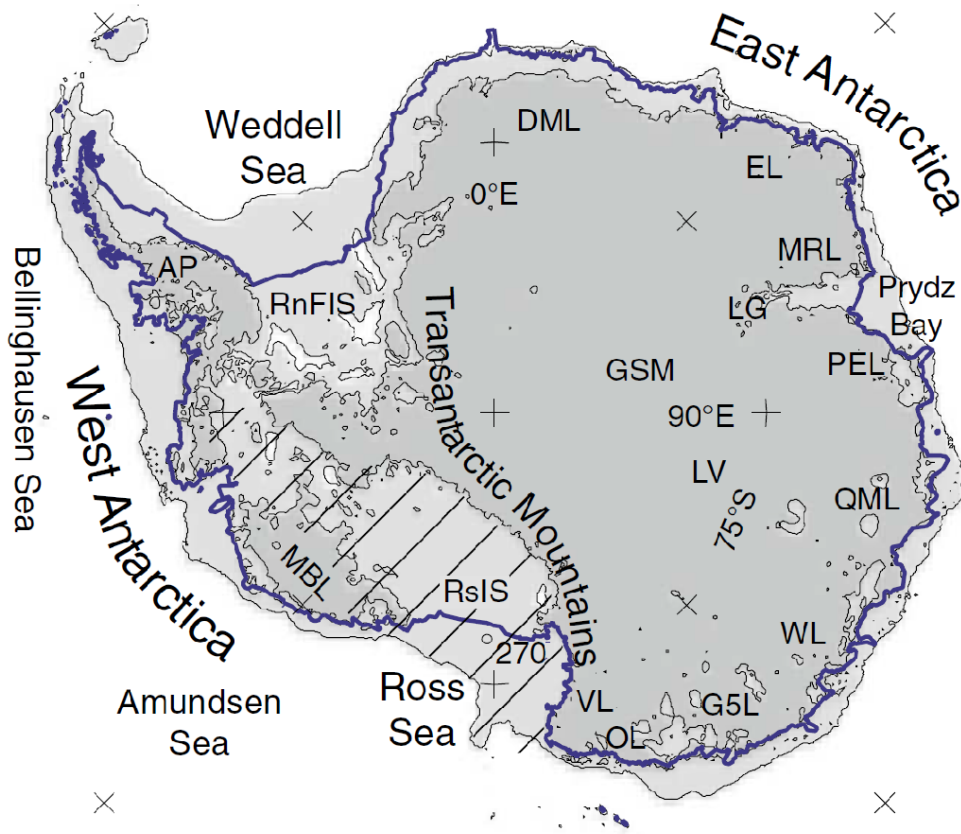
Fig. 2.1: Location of the WARS (diagonal lines), with respect to the rest of Antarctica and DSDP Site 270 (labelled 270). Dark (light) shading denotes areas above (below, down to -1000 m) present sea level, adjusted for ice load rebound. AP – Antarctic Peninsula; RnFIS – Ronne Filchner Ice Shelf; DML- Dronning Maud Land; EL – Enderby Land; MRL – Mac. Robertson Land; LG – Lambert Glacier; GSM – Gamburtsev Subglacial Mountains; PEL – Princess Elizabeth Land; LV – Lake Vostok; QML – Queen Mary Land; WL – Wilkes Land; G5L – George V Land; OL – Oates Land; VL – Victoria Land; RsIS – Ross Ice Shelf; MBL – Marie Byrd Land (Wilson et al., 2012).

2.1.1 Break-up of Gondwana and the initiation of the WARS

The extensional rifting of the WARS began in the Jurassic (Fig. 2.2; ~180 Ma), and was associated with the break-up of Gondwana, which involved right-lateral transtension between East (Antarctica, Australia, India, New Zealand) and West Gondwana (South America, Africa) (Davey and Brancolini, 1995; Fitzgerald, 2002). The separation of Gondwana resulted in four crustal blocks, which together comprise modern West Antarctica: The Antarctic Peninsula, Thurston Island, Ellsworth-Whitmore Mountains and Marie Byrd Land (Dalziel and Lawver, 2001). The break-up and rotating motion, centred in the Weddell Sea, was likely result of a mantle plume, and offshore ridge-crest subduction. This ultimately led to the production of significant areas of extended continental crust, which today forms the floors of the Ross and Weddell Seas (Dalziel and Lawver, 2001; Fitzgerald, 2002). Evidence for this initial stretching, and inception of the Ross Sea area is manifest in the emplacement of the tholeiitic Ferrar Dolerite and Kirkpatrick Basalt in the Transantarctic Mountains (Behrendt et al., 1991; Fitzgerald, 2002). The stress regime changed in the early Cretaceous from being north-south between the two Gondwanan parts, to being east-west (Fig. 2.2C), and by the middle to late Cretaceous Antarctica had assumed its polar position (Fitzgerald, 2002; Lawver et al., 1992).
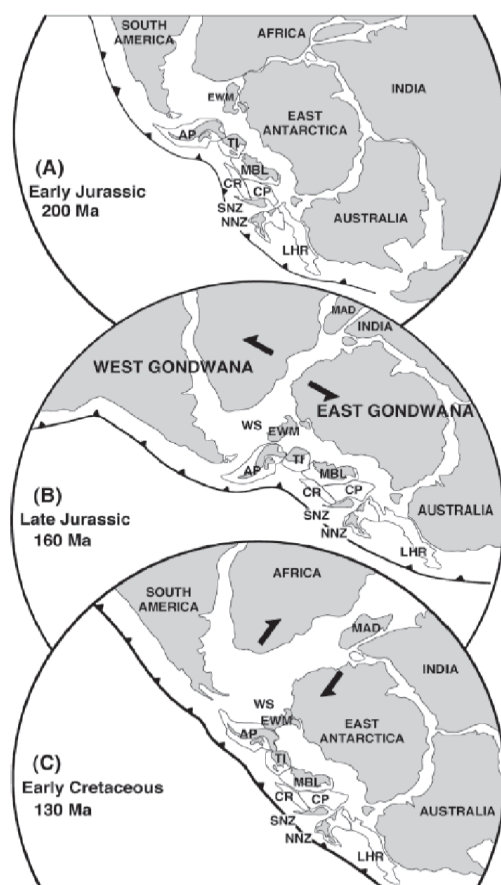
Fig. 2.2*: Model of the inception of the Gondwana break-up during Mesozoic times. AP – Antarctic Peninsula; TI – Thurston Island; MBL – Marie Byrd Land; CR – Chatham Rise; CP- Campbell Plateau; SNZ – southern New Zealand; NNZ – northern New Zealand; LHR – Lord Howe Rise; WS – Weddell Sea; EWM – Ellsworth-Whitmore Mountains (Fitzgerald (2002) and references therein).

2.1.2 Main stages of the WARS development

The rifting described above led to the initial opening of the Ross Sea area. However, the main phase of intracontinental extension and crustal thinning of the WARS is argued to have occurred in the Late Cretaceous (105-85 Ma; Fig. 2.3). As such, most of the development of the three sedimentary basins (western, central, and eastern) in the Ross Sea began ~105 Ma (Fitzgerald, 2002; Lawver and Gahagan, 1994, 1995; Luyendyk, 1995; Luyendyk et al., 2003; Siddoway, 2008; Siddoway et al., 2004). The evolution of the WARS through the key interval of 130-80 Ma (especially 100-80 Ma) is depicted and explained in Figure 2.3 (Siddoway, 2008). While the mechanism of rifting in the Ross Embayment through this time period is not entirely known, the regional crustal architecture, as well as the basement and breccia rocks recorded at DSDP 270 suggest that extension and exhumation during the middle to Late Cretaceous was, at least in part, accommodated by detachment faulting (Fitzgerald, 2002). Furthermore, the strike-slip faults which were initiated during the Early Cretaceous oblique convergence also accommodated some intracontinental extension of the WARS until 90 Ma (Siddoway, 2008). Siddoway (2008) points out that these fundamental differences in strain, arising from dextral strike-slip faults in the east, and normal faults in the central and western Ross Sea (e.g. DSDP 270), during the intense phase of intracontinental deformation between 100 and 90 Ma, is likely due to one of two reasons: Either, (1) the transition from oblique subduction of young lithosphere in the eastern WARS, to slow rifting of the mature continental crust of Australia-Antarctica in the western WARS (e.g. Cande and Mutter (1982)); or, (2) the geometry of the subducted lithosphere at the subduction zone to the north (e.g. Luyendyk (1995)). During this intense deformation in the Cretaceous large parts of the Ross Sea area were above sea level, before steadily subsiding during the Late Cretaceous and Cenozoic due to lithosphere cooling, and later glacial erosion and sediment loading (Luyendyk et al., 2001). Furthermore, no continental separation is thought to have occurred east of Marie Byrd Land, so that the Antarctic Peninsula and Thurston Island became tectonically inactive following the cessation of the convergent margin (~90 Ma; Mukasa and Dalziel (2000)).
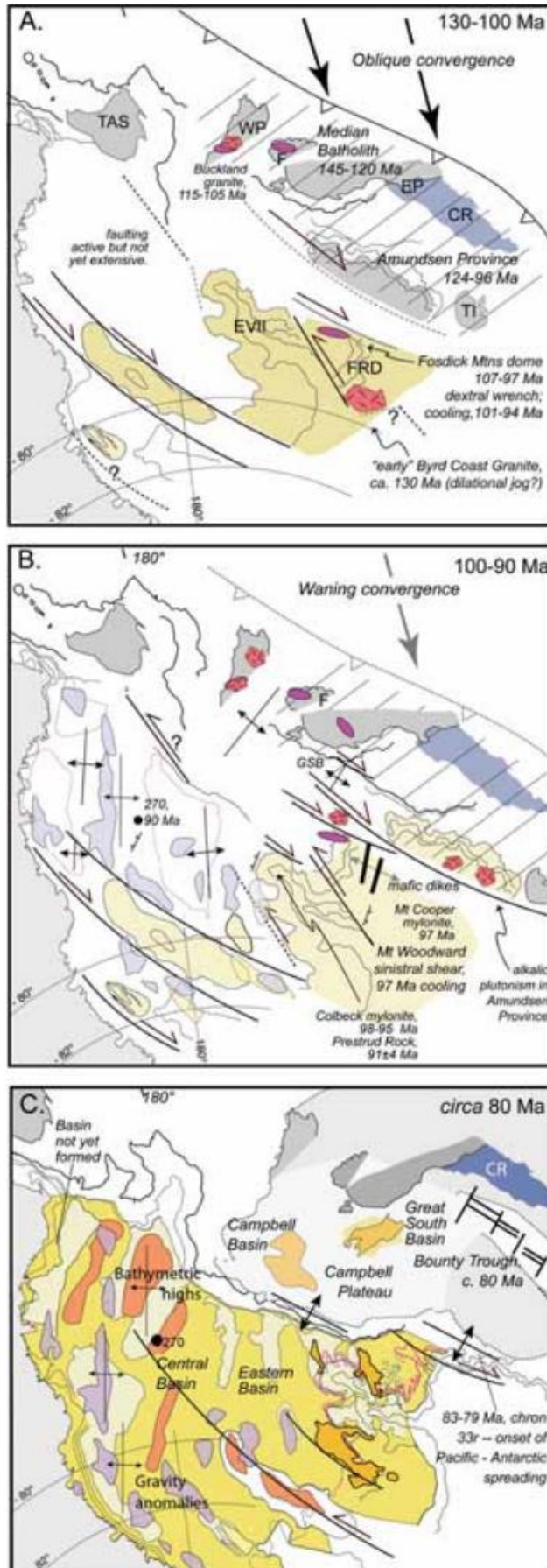
Fig. 2.3: Likely evolution of the WARS between 130 and 80 Ma (Siddoway (2008), and references therein).

A. Possible East Gondwanan margin, 130-100 Ma. Arc magmatism in the Western Province (WP) of New Zealand (NZ), Fiordland (F), and Fosdick Mountains in Marie Byrd Land, was coeval with metamorphism and crustal melt (ellipses). Diachronous plutons (Median Batholith; Amundsen province) may reflect the structure of offshore spreading ridges or the subducted slab geometry. TAS – Tasmania; EP – Eastern Province, NZ; CR – Chatham Rise; TI – Thurston Island.

B. 100-90 Ma was a significant phase of intracontinental deformation in the WARS: Dikes and plutons were emplaced, and the blue shading highlights high-density gravity anomalies along basin axes. The rapid cooling ages implied by their younging from SW (97 Ma) to NE (90 Ma) indicates differential movement on steep wrench zones. Wrench deformation is recorded in the Marie Byrd Land sector of the WARS, whilst normal faulting prevails in the western Ross Sea.

C. ~80 Ma, NZ and the Campbell Plateau began breaking free of West Antarctica. The continental extension across the WARS and Campbell Plateau was finished before the beginning of seafloor spreading, and exceeded 100%. Red (blue) polygons indicate bathymetric and basement highs (high-density gravity anomalies along basin axes). The break-up occurred at near right angles to those of the WARS opening, and pre-existing wrench fault structures were likely reactivated.

2.1.3 Cenozoic rifting in the WARS

The expression of the Cenozoic evolution of the WARS is different to that of the Mesozoic. The Victoria Land Basin, in the far western side of the Ross Sea is the only area where extension (~150-180 km) has occurred since the late Eocene (Cooper and Davey, 1985; Cande et al., 2000; Siddoway, 2008), consistent with the initiation of subsidence and sediment accumulation in the basin off Cape Roberts (Barrett, 2007). Although some minor uplift may have occurred sporadically since the Cretaceous, fission track data indicate that the most substantial uplift of the Transantarctic Mountains began in the Eocene (~55-50 Ma) (Fitzgerald, 2002; Fitzgerald, 1992, 1994; ten Brink et al., 1997), and offshore provenance studies suggest uplift was largely complete by ~34 Ma (Smellie, 2001). Moreover, it has been suggested that the unusually large height of the Transantarctic Mountains can be partially explained by isostatic rebound, as a result of glacial incision, and subsequent preservation of tall peaks due to a cold and arid climate (Stern et al., 2005).

On the eastern side of the WARS, the currently active intraplate volcanism and emplacement of plutons in Marie Byrd Land is argued to have been active since Oligocene times, and may be the consequence of a mantle hotspot (Hole and LeMasurier, 1994; LeMasurier and Rex, 1983; Lough et al., 2013; Rocchi et al., 2006; Winberry and Anandakrishnan, 2004). Since the local cessation of extensional tectonics, the central to eastern Ross Sea has been steadily subsiding due to cooling (Wilson and Luyendyk, 2009). After correcting for this thermal contraction due to earlier tectonic extension, as well as erosion and sedimentation since 34 Ma, topographic reconstructions show that much of West Antarctica (~20%) was subaerial at the Eocene-Oligocene boundary (Fig. 2.4; Wilson et al. (2012); Wilson et al. (2009)). This is independently supported by ~34 Ma exhumation ages of gabbro in Marie Byrd Land (Rocchi et al., 2006). This model also reconstructs DSDP 270 to between 30 and 120 m above sea level during the early Oligocene, in line with the terrestrial regolith recovered at the base of the core (Hayes and Frakes, 1975). Finally, the deepening in the central to eastern Ross Sea, such as that observed at DSDP 270 during the Oligocene to Miocene, was a consequence of glacial erosion, isostatic depression, and tectonic subsidence (Bart and De Santis, 2012; De Santis et al., 1995; De Santis et al., 1999).
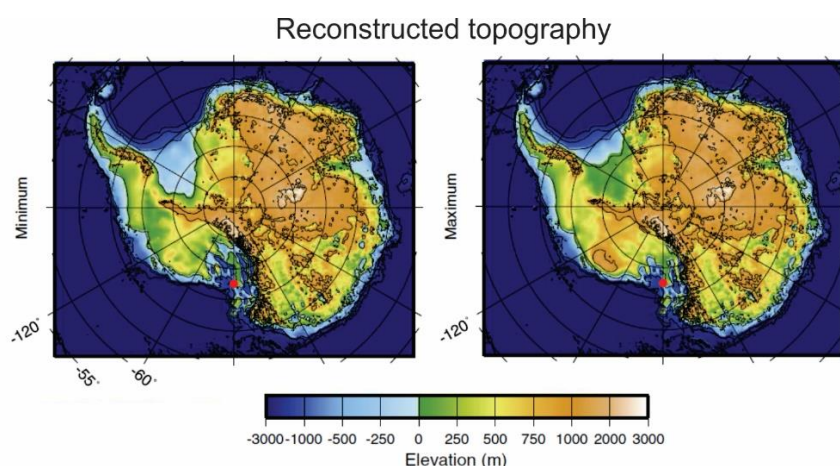
Fig. 2.4: Reconstructed topographies for the Eocene-Oligocene Transition based on (left) minimum erosion and (right) maximum erosion scenarios since ~34 Ma accounting for the effects of isostatic adjustment following ice removal, thermal contraction, erosion, sedimentation and West Antarctic plate motion. The red dot marks the location of DSDP 270 (modified from Wilson and Luyendyk (2009)).

2.2 The pacesetter of the climate: Orbital cycles and the Milankovitch Theory

Changes in the Earth's orbit are the dominant pacesetter of the higher-frequency (10^4 to 10^5 years) climatic changes (Zachos et al., 2001a). This is because the three parameters which characterise Earth's orbit (outlined below) control the amount and distribution of solar insolation received on the planet (Ruddiman, 2014; Zachos et al., 2001a).

2.2.1 The three orbital cycles

The three orbital parameters which define the geometry of Earth's orbit are (Fig. 2.5; Paillard (2010); Ruddiman (2014)):

(1) *Eccentricity* – the shape of Earth's orbit around the Sun, which is slightly elliptic. Thus, in its annual orbit around the Sun, one hemisphere's summer (presently the southern) receives more radiation than the other.

(2) *Obliquity* – the tilt of Earth's axis of rotation. This gives Earth its seasons by determining the latitudinal distribution of insolation (i.e. which hemisphere of Earth is tilted toward the Sun).

(3) *Precession* – there are two types of precession, which together cause the solstices and equinoxes to shift around Earth's orbit:
   a. Axial precession: the 'wobble' of Earth's axis of rotation. This is caused by the direction of tilt, rather than the amount of tilt. It can be envisaged as a circular rotation of Earth's axis.
   b. Precession of the ellipse: the rotation of the elliptical orbit of the Earth, where the long and short axes of the ellipse are turned.
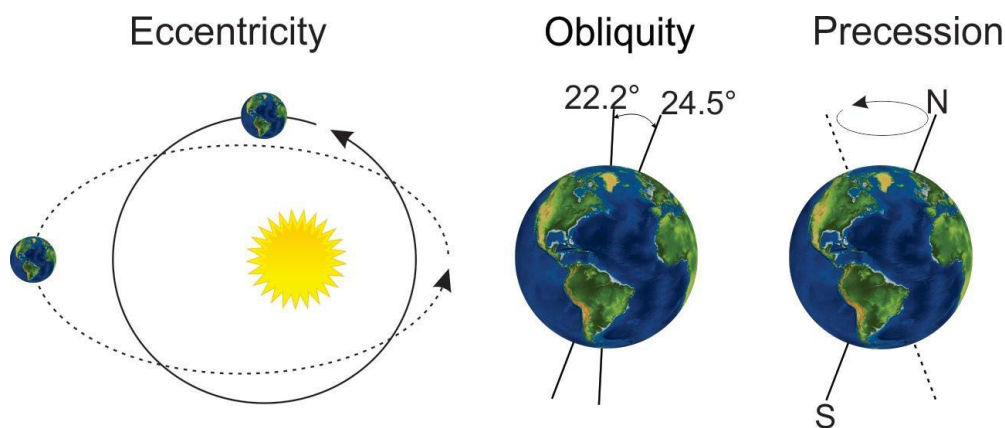
Fig. 2.5: Schematic depicting the changes in the orbital cycles of eccentricity, obliquity, and axial precession (re-drawn from Ruddiman (2014) and Zachos et al. (2001a)).

These parameters are not fixed in time, and instead vary in cyclic fashions. The tilt of Earth's axis of rotation varies between 22.2 and 24.5 ° at a period of ~41 thousand years (kyr) (Paillard, 2010; Ruddiman, 2014). Changes in tilt can amplify or suppress the strength of the seasons, an effect which is most readily observed at the high latitudes. This is due to increased tilt angles directing the polar regions more (less) toward the Sun during summer (winter), causing large seasonal differences. Meanwhile a lesser angle of tilt reduces the magnitude of seasonal differences (Paillard, 2010; Ruddiman, 2014).

Eccentricity varies between being more circular and more elliptic at periods of ~100 kyr (this parameter consists of 4 cycles, ranging in periods between 95 and 131 kyr), and ~400 kyr, although lower amplitude periods also exist (Paillard, 2010; Ruddiman, 2014).

The combined movement of the two types of precession, referred to as the precession of the equinoxes, varies at periods of 23 and 19 kyr, giving an average period of 21 kyr (Paillard, 2010; Ruddiman, 2014). Because Earth's orbit around the Sun is not constant (i.e. changes in eccentricity), changes in the position of the solstices and equinoxes cause long-term changes in the quantity of solar radiation received at Earth. As a result, eccentricity serves to modulate the amplitude of precession cycles, the result of which can be calculated as the precessional index (Fig. 2.6). Without this modulation, precession would cycle smoothly (Paillard, 2010; Ruddiman, 2014). The result of this is precession cycles with an average period of ~21 kyr, with cyclic modulations in its amplitude at the eccentricity periods of 100 and 400 kyr (Paillard, 2010; Ruddiman, 2014).
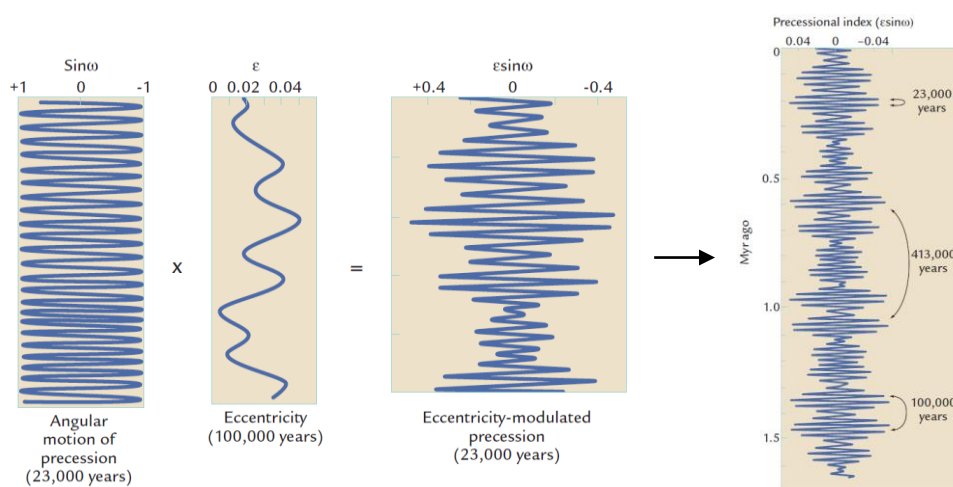
Fig. 2.6: The precessional index, product of precession and eccentricity. It has a main cycle periodicity of 23 kyr, which is amplitude modulated at the 100 and 413 kyr periods of eccentricity (modified from Ruddiman (2014)).

2.2.2 Milankovitch Theory

Milutin Milankovitch suggested that ice sheet growth in the Northern Hemisphere is favoured when northern summer insolation (65 °N) is low, thereby reducing summer melt (Milankovitch, 1941). This occurs when obliquity is low, the orbit is more elliptical, and the northern summer solstice occurs at aphelion (farthest from the Sun) (Ruddiman, 2014). Whilst early studies suggested a link between glacial-interglacial cyclicity in deep-sea oxygen isotope records and Northern Hemisphere changes in insolation (Emiliani, 1955), it was not until later that changes of astronomical periodicities in $\delta^{18}O$ were able to be unequivocally linked to changes in Earth's orbit (Hays et al., 1976). Since then, records have become of such high-resolution that orbital tuning of $\delta^{18}O$ records has, for example, revealed ice volume lags behind changes in atmospheric CO_2, and temperatures at the 100 kyr eccentricity period (Shackleton et al., 2000). Furthermore, large parts of the geological timescale have now been astronomically tuned, including the majority of the Cenozoic allowing for high resolution age models (i.e. up to ~0.02 Myr resolution) to be obtained from geological records (e.g. Hilgen (1991); Hinnov and Ogg (2007)).

2.3 Cenozoic climate history from far-field ocean sediment archives and models

Oxygen isotopes (δ^{18}O) have been the primary climate proxy in the endeavour to reveal the climate history of the Cenozoic (e.g. Emiliani (1954, 1961); Shackleton and Kennett (1975); Miller et al. (1987); Zachos et al. (2001a); Mudelsee et al. (2014)). The basis for oxygen isotope-based climate reconstructions is that ice preferentially sequesters the light ^{16}O over the heavier ^{18}O, so that the changes in global ice volume are recorded in the δ^{18}O of seawater (Miller and Mountain, 1996). Benthic foraminifera have been the key to this because they live at the water-sediment interface, thereby recording changes in bottom water conditions (δ^{18}O) in their calcite tests (Flower, 1999; Zachos et al., 2008; Zachos et al., 2001a). The Cenozoic Era (65 Ma to present) spans a first order cooling trend with Earth transitioning in a series of steps from a warm, largely ice free 'greenhouse' world, through progressive cooling to an 'icehouse' world characterised by ice sheets at both poles (Mudelsee et al., 2014; Zachos et al., 2008; Zachos et al., 2001a). These long-term changes are thought to have been caused by changes in key boundary conditions such as topography, atmospheric greenhouse gases, shifting continents, and the opening and closing of oceanic gateways, altering the way Earth responds to regulated periodic changes in Earth's orbital parameters (Beerling and Royer, 2011; Crowley and Burke, 1998; Haug and Tiedemann, 1998; Pearson and Palmer, 2000; Ruddiman, 1997; Scher et al., 2015; Zachos et al., 2001a; Zhang et al., 2013).

This first order shift can be observed in several records (Fig. 2.7; Masson-Delmotte, et al., 2013):

(1) δ^{18}O values are found to increase by ~4 ‰ over the past 50 Ma, with three distinct ~1 ‰ stepped increases reflecting ice volume expansion at ~34, ~14, and 2.6 Ma (Miller et al., 1987; Mudelsee et al., 2014; Zachos et al., 2001a).

(2) Atmospheric CO_2 shows a general declining trend over the course of the Cenozoic from >680 -1260 ppm during the Early Eocene Climatic Optimum (52-50 Ma) to less than pre-industrial levels (280 ppm) in the Pleistocene (Beerling and Royer, 2011; Zhang et al., 2013).

(3) Over the past 50 Ma average global temperatures decreased by ~12 °C, with declining CO_2 interpreted to be the primary cause (Beerling and Royer, 2011; Cramer et al., 2011). Significant cooling phases occurred during the early Middle Eocene, late Eocene to early Oligocene, the late middle Miocene and the Plio-Pleistocene (Cramer et al., 2011).

(4) Backstripped coastal sea level records, suggest a first order decrease in sea levels from the Eocene to Miocene. Superimposed on this are glacio-eustatic sea level variations of varying magnitudes (Kominz et al., 2008).
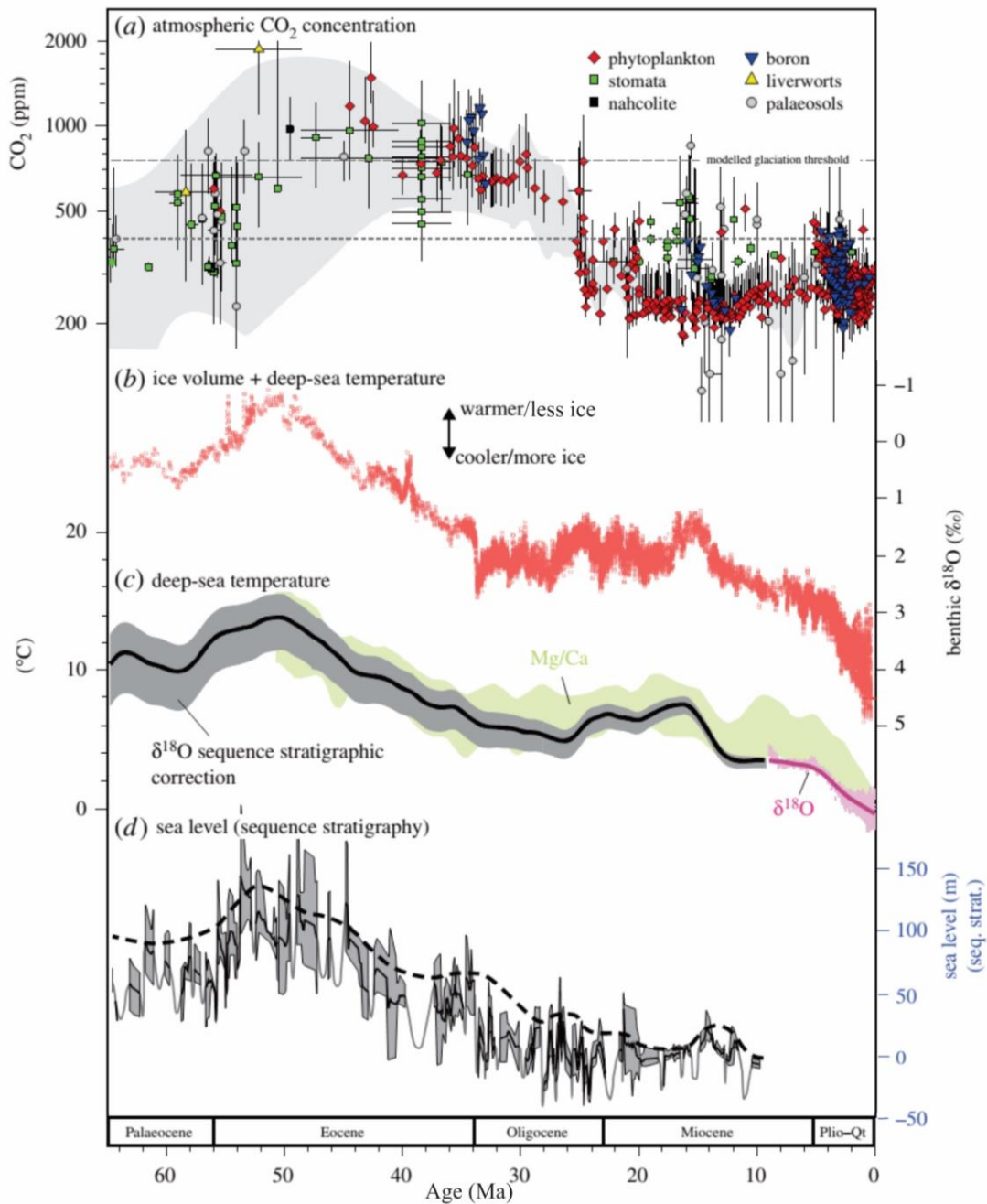
Fig. 2.7: Reconstruction of Cenozoic climate changes from a variety of proxies: (a) atmospheric CO_2 (Beerling and Royer, 2011); (b) composite deep-sea benthic $\delta^{18}O$ proxy of ice volume and deep-sea temperature (Zachos et al., 2008); (c) long-term deep sea temperatures from removal of the ice volume signature in $\delta^{18}O$ records using backstripped sea level estimates from passive margins (grey), benthic Mg/Ca (green; both from Cramer et al. (2011)), and scaled $\delta^{18}O$ of the past 10 Ma (pink; Miller et al. (2011)); (d) sea level estimates from backstripped passive continental margin records (Kominz et al., 2008). Figure modified from McKay et al. (2016).

Geological proxies of atmospheric CO_2 and records of sea level/ice volume through these periods of major Cenozoic climate change suggest a sigmoidal relationship between atmospheric CO_2 and sea level over the past 40 Ma. This indicates a fundamental control of atmospheric CO_2 on eustatic sea level over geologic time (Fig. 2.8; Foster and Rohling (2013)). The relationship found that CO_2 levels in excess of 1000 ppm prohibit any major

ice sheets from growing, causing sea levels up to 70 m above present. Between 650 and 1000 ppm, terrestrial Antarctic ice sheets appear to vary in size, and 600-650 ppm appears to be the threshold for permanent terrestrial Antarctic ice sheets. The relationship also dictates that the Greenland Ice Sheet and any Antarctic marine-based ice sheets did not persist above 400 ppm, and likewise the large Northern Hemisphere ice sheets (NHIS; Laurentide and Fennoscandian) cannot persist above pre-industrial CO_2 levels of 280 ppm (Foster and Rohling, 2013). This relationship is consistent with the modelled atmospheric CO_2 threshold of ~750 ppm for Antarctic glaciation (DeConto and Pollard, 2003). It is however noted that the atmospheric CO_2 threshold for glaciation of Antarctica is highly model dependant, and can vary between 560 and 920 ppm (Gasson et al., 2014), while uncertainties in geological proxies for both CO_2 and sea level remain large (Fig. 2.8).
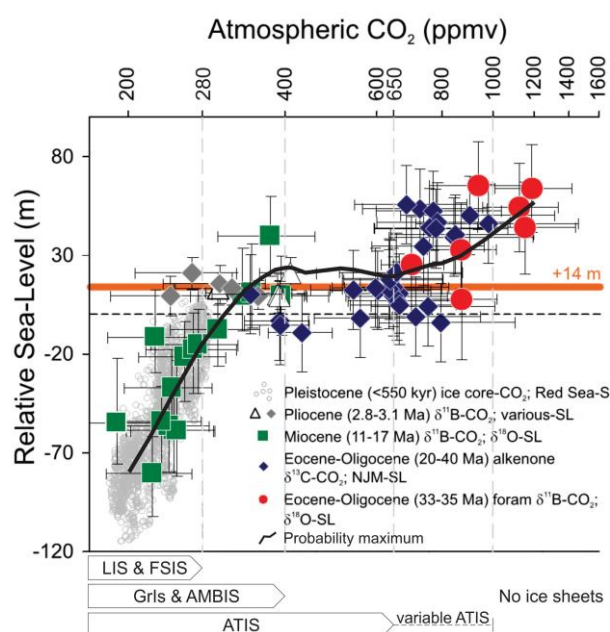
Fig. 2.8: Comparison of atmospheric CO_2 derived from various proxies with coeval estimates of sea level. The black line indicating the probability maximum highlights the sigmoidal relationship between the two datasets. Shown at the bottom are the proposed limits of the existence of the Laurentide Ice Sheet (LIS), Fennoscandian Ice Sheet (FIS), Greenland Ice Sheet (GrIs), Antarctic marine-based ice sheets (AMBIS), and Antarctic terrestrial ice sheets (ATIS). Figure modified from Foster and Rohling (2013).

2.3.1 Palaeocene to Eocene

The earliest Cenozoic witnessed a warming trend from the middle Palaeocene, which culminated in the Early Eocene Climatic Optimum (EECO; 54 to 49 Ma). However, during this warming, there were several short-term extreme warmings (4 to 5 °C amplitude, lasting for <200 ka), termed hyperthermals, the largest of which was the Palaeocene-Eocene Thermal Maximum, 55.76 Ma (Mudelsee et al., 2014; Zachos et al., 2008; Zachos et al., 2001a). The EECO is argued to have witnessed the warmest prolonged temperatures (12 °C warmer than present) during the Cenozoic (Hollis et al., 2012; Huber and Caballero, 2011; IPCC, 2013; Mudelsee et al., 2014), and was followed by a prolonged cooling until 38 Ma that was only briefly interrupted by a warming during the middle Eocene (Mudelsee et al., 2014). Furthermore, studies suggest that between 38 and 34 Ma, climate perturbations, involving both cooling and warming events, punctuated the long-term cooling trend (Pascher et al., 2015). Sea level records from stable isotope and backstripped

continental margin records displays variations >25 m over timescales <1 Myr, inferring temporary ice caps on highlands may have occurred during the colder periods of Palaeocene-Eocene (Cramer et al., 2011; Miller et al., 2008a; Miller et al., 2005a; Miller et al., 2005b; Tripati et al., 2005). This does not contradict model-based studies, and may be reconciled with the apparent warmth of coastal Antarctica and deep-waters as these ice sheets would have only grown inland during the coldest periods and not extended out toward the coast (DeConto and Pollard, 2003; Gasson et al., 2014; Miller et al., 2008a; Miller et al., 2005a; Miller et al., 2003; Miller et al., 2004; Miller et al., 2005b).

2.3.2 Transition from greenhouse to icehouse

Ephemeral ice sheets may have existed in the greenhouse world, but $\delta^{18}O$ records suggest that it was not until the Eocene-Oligocene transition (EOT; 33.8-33.5 Ma), that a continental-sized Antarctic ice sheet grew. The abrupt 1 ‰ increase in $\delta^{18}O$ at the EOT is argued to represent the rapid growth of a large (~25 x 10^6 km^3) ice sheet in Antarctica (Coxall et al., 2005; Cramer et al., 2011; Liu et al., 2009; Miller et al., 1987; Miller et al., 2008b; Mudelsee et al., 2014; Zachos et al., 2001a). From this point on, the Antarctic ice sheets became a driver of climatic change, resulting in increased latitudinal temperature gradients and a reorganisation of oceanic circulation and chemistry (Miller et al., 2008b). Furthermore, $\delta^{18}O$ and $\delta^{13}C$ data have revealed that latitudinal isotopic gradients in the oceans transitioned from homogeneity to heterogeneity at ~35 Ma, and this differentiation in isotopic values may indicate the isolation of the Southern Ocean (Cramer et al., 2009). The onset of the Antarctic Circumpolar Current is argued to have occurred ~5 Myr later at ~30 Ma, as indicated by neodymium isotopes (Scher et al., 2015)

The initial studies of benthic $\delta^{18}O$ data concluded that substantial ice did not exist beyond the middle Miocene, and instead interpreted the shift at the EOT as sea ice growth, cooling of the bottom waters by 5 °C, and the development of the thermohaline circulation (Kennett and Shackleton, 1976; Shackleton and Kennett, 1975). This notion was later revised in favour of the inception of continental-scale ice sheets at the EOT. The rationale for this was initially based on benthic $\delta^{18}O$ values exceeding 1.8 ‰ at the EOT, as ice-free conditions and $\delta^{18}O$ values >1.8 ‰ (in *Cibicidoides* spp.) are implausible because it would imply bottom waters, and high latitude surface waters, to be cooler than today (Miller and Fairbanks, 1983; Miller and Fairbanks, 1985).

Since then the models and far-field data have shown that the EOT represented a 300 kyr-long, two-step change, where a 40 kyr step of ocean temperature change was followed by a second 40 kyr step which heralded a change in ice volume. Moreover, both of these steps encompass minima in eccentricity and a node in obliquity (Coxall et al., 2005; DeConto and Pollard, 2003; Mudelsee et al., 2014; Zachos et al., 1996). Early Mg/Ca studies suggested that no temperature change occurred in the oceans across the EOT (e.g. Lear et al. (2004)), but the discovery of a secondary carbonate saturation state control on the Mg/Ca recorded in benthic foraminiferal tests by Elderfield et al. (2006) subsequently indicated a 2 to 3 °C cooling during the first step, with little to no concomitant ice volume change (Bohaty et al., 2012; Lear et al., 2008; Mudelsee et al., 2014). This is in line with the estimated 5 °C cooling of sea surface temperatures across the EOT using organic geochemistry proxies (Liu et al., 2009). The second step ('Oi-1 glaciation') solely represents an expansion of ice volume up to 125% of the modern Antarctic ice volume, causing a eustatic sea level fall on the order of 55-90 m. This represents the final step into the icehouse world (Cramer et al., 2009; Katz et al., 2008; Kominz and Pekar, 2001; Lear et al., 2008; Lear et al., 2004; Miller et al., 2008a; Miller et al., 2005a; Miller et al., 2008b;

Mudelsee et al., 2014; Pekar et al., 2002). Furthermore, a more terrestrial West Antarctic land mass at this time may have allowed the WAIS to also form, and as such the total Antarctic ice volume may have been as high as 35.9 million km^3 at the Oi-1 (Mudelsee et al., 2014; Wilson et al., 2013).

A ~0.8 ‰ increase in carbon isotope values at the EOT indicates that it was contemporaneous with a perturbation of the global carbon cycle (Zachos et al., 2001a). Consistent with this perturbation, atmospheric CO_2 decreased by 40%, from ~1100 to ~600 ppm, across the EOT, between 35.5 and 32.5 Ma (Beerling and Royer, 2011; Pagani et al., 2011; Zhang et al., 2013). By modelling the EOT with a closed and open Drake Passage, DeConto and Pollard (2003) inferred that this declining CO_2 and the orbital configuration (minima in eccentricity and a node in obliquity), rather than changes in oceanic heat transport due to the tectonic opening of gateways (e.g. Kennett (1977)), was the primary factor in the inception of continental-scale ice sheets. The model indicates the declining CO_2 first causes the formation of small isolated, highly dynamic ice caps on the high altitude sectors of Antarctica (e.g. Gamburtsev Mountains). Once a CO_2 threshold is crossed, positive ice sheet mass/height and snow/ice-albedo feedbacks cause dynamic ice caps to rapidly expand in concert with changes in the orbital configuration, before finally coalescing into a continental scale Antarctic ice sheet during favourable orbital configurations, and when the CO_2 threshold of ~750 ppm is crossed (DeConto and Pollard, 2003). Theories of an early bipolar glaciation at the EOT have also been disputed by models in favour of an Antarctic ice sheet which is less isotopically depleted than today, and 4 °C deep sea cooling (DeConto et al., 2008). Furthermore, the CO_2 at the time was well above the modelled threshold required for NHIS (280 ppm).

The Oi-1 glaciation appeared to end as a consequence of an overshoot behaviour, recovering to less glaciated and warmer conditions, which is represented by a subsequent 0.26 ‰ decrease in $\delta^{18}O$ (Coxall et al., 2005; Mudelsee et al., 2014; Zachos et al., 1996).

2.3.3 Oligocene to early Miocene

After the rapid expansion of ice at the Oi-1, the climate appears to have stabilised, and the sustained heavy isotope values (~2.5 ‰), as well as passive margin sea level records suggest continued and permanent ice cover equal to at least ~50% current volume, punctuated by glacial events (Kominz and Pekar, 2001; Liebrand et al., 2011; Miller and Fairbanks, 1985; Miller et al., 1987; Miller et al., 1991; Mudelsee et al., 2014; Pekar and Miller, 1996; Pekar and DeConto, 2006; Pekar et al., 2006; Zachos et al., 2001a). Sea levels are argued to have fallen ~30 m over the course of the Oligocene (Fig. 2.7), with intermittent eustatic sea level variations of 30 to 60 m, which can be explained by changes in Antarctic ice volume between 50 and 125% (Cramer et al., 2011; Kominz and Pekar, 2001; Lear et al., 2004; Miller et al., 2005a; Pinous et al., 1999; Wade and Pälike, 2004). Oligocene atmospheric CO_2 values are thought to have remained between 400 and 800 ppm which, based on the thresholds in the sea level-atmospheric carbon dioxide relationship of Foster and Rohling (2013), would preclude the formation of any marine-based ice sheets (Beerling and Royer, 2011; Pagani et al., 2005; Zhang et al., 2013).

Oligocene records from the equatorial Pacific have revealed that these changes in ice volume, as well as changes in the carbon cycle correspond to eccentricity (405, 127 and 96 kyr) cycles, as well as 1.2 Myr cycles in obliquity (Fig. 2.9; Pälike et al. (2006b); Wade and Pälike (2004)). To a first order, the fact that during the Oligocene more positive $\delta^{18}O$ values (glacial maxima) correspond with positive $\delta^{13}C$ excursions indicates that the

changes in Antarctic ice volume and high-latitude temperatures significantly affected the global carbon burial (Miller and Fairbanks, 1985; Wade and Pälike, 2004; Zachos et al., 1996; Zachos et al., 2001b)). This supports the notion that the carbon cycle and atmospheric CO_2 levels oscillated in conjunction with ice volume changes, whereby during glaciations enhanced biological productivity and an increased organic carbon burial rate resulted in significant variations in the $\delta^{13}C$ records (Wade and Pälike, 2004). More specifically, three observations have been made during the Oligocene: (1) a persistent 405 kyr eccentricity pacing of $\delta^{13}C$ records, and thus the carbon cycle; (2) large transient glaciations occurring every 1.2 Myr (via amplitude modulation of obliquity); and (3) higher amplitude variations in $\delta^{18}O$ during minima in both short and long eccentricity (96 and 126 kyr) (Pälike et al., 2006b). Together, these observations have been termed the 'heartbeat' of the Oligocene climate, and suggest a relationship between the carbon cycle, orbital forcing and glaciations (Pälike et al., 2006b). Furthermore, box modelling has indicated that deep ocean acidity and the burial of biomass are modulated by the interaction of orbital forcing and the carbon cycle. The 405 kyr cycle in $\delta^{13}C$ is further enhanced, due to the long residence time of carbon in the global oceans, which is the same reason for the frequency dependant lag of $\delta^{13}C$ with respect to $\delta^{18}O$ (Pälike et al., 2006b). Importantly, box modelling also showed that the beginning of a glaciation is not determined by the exact timing of a drop in CO_2, but rather by a favourable orbital configuration once CO_2 drops below a specific threshold value (Pälike et al., 2006b). Furthermore, the heaviest $\delta^{18}O$ values (largest glacial maxima) occur during 1.2 Myr nodes of obliquity and minimum eccentricity (near circular orbit), in the Oligocene and early Miocene (Pälike et al., 2006b; Wade and Pälike, 2004; Zachos et al., 2001b). This supports the hypothesis of Zachos et al. (2001b) who suggested that the absence of prolonged (Southern Hemisphere) warm summers and low seasonality are crucial to inhibiting summer melt, and expanding the ice mass.

As shown in Figure 2.9, the Oligocene can be broken down into four longer term phases (Pälike et al., 2006b):

1. The first 2.5 Myr represent the recovery warming phase after the Oi-1 glaciation. Smaller amplitude orbital changes, as well as the establishment of the longer term ~405 kyr climatic oscillations, which are typical of the Oligocene, characterise this phase.

2. Phase two begins with a $\delta^{13}C$ minimum, which is followed by a positive excursion and a subsequent 2 Myr long decrease in carbon isotope values. Meanwhile $\delta^{18}O$ values show enhanced variability at the higher frequency orbital cycles.

3. Stable isotopes values continue along similar baselines during phase 3 as before, with variations at orbital frequencies (especially at 405 kyr). During this phase, cycle 67 (Oi-2b; 26.8 Myr) contains the peak $\delta^{18}O$ values recorded in the equatorial Pacific. Based on these and other oxygen isotope data, as well as the sole Oligocene appearances of Arctic dinoflagellates at lower to middle-latitude sites in both hemispheres during Oi-2b, it is suggested that this may have been the strongest glaciation during the Oligocene (Pälike et al., 2006b; Van Simaeys et al., 2005; Wade and Pälike, 2004).

4. $\delta^{18}O$ values continue a multi-million-year trend toward lower values, with peak warmth/minimum ice volume at polarity chron C6Cr. Coevally, $\delta^{13}C$ values display high-amplitude shifts at the 405 kyr periodicity. Phase four is terminated with the Mi-1 glaciation.
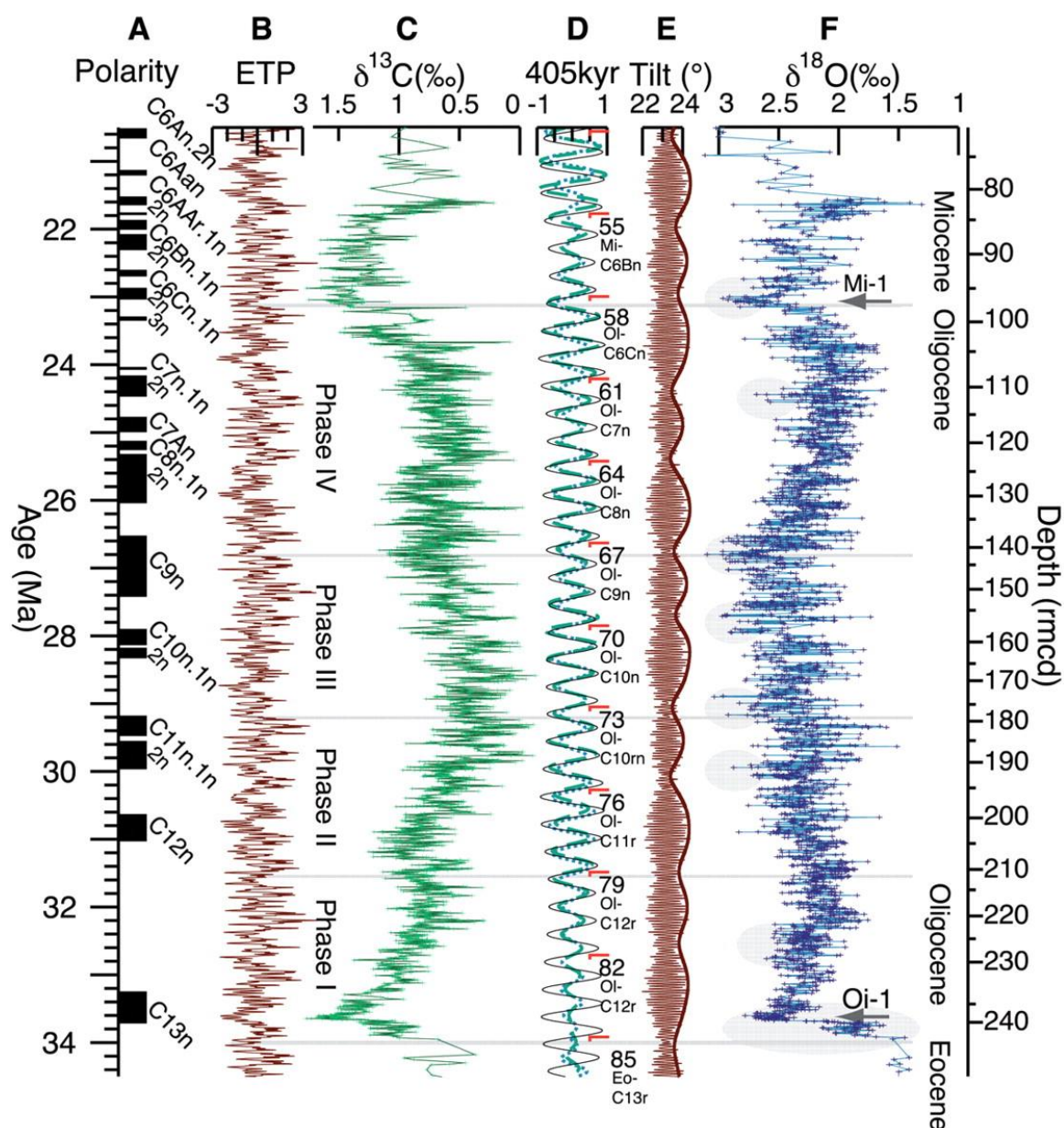
Fig. 2.9: Benthic stable isotope data from ODP Site 1218 (equatorial Pacific): (A) astronomically age-calibrated paleomagnetic record; (B) Calculated combination of all three orbital parameters; (C) $\delta^{13}C$ from benthic foraminifera; (D) 405 kyr eccentricity component extracted from astronomical eccentricity (sold line), benthic inverted $\delta^{13}C$ data (dashed line), and benthic inverted $\delta^{18}O$ data (dotted line) using bandpass filtering, the numbers represent the 405 kyr eccentricity cycle numbers, counted from present following the naming scheme of Wade and Pälike (2004); (E) obliquity and obliquity envelope; (F) $\delta^{18}O$ from benthic foraminifera. Horizontal lines mark the phase boundaries, grey ellipses mark the maximum $\delta^{18}O$ values at times of low obliquity amplitudes (Pälike et al., 2006b).

During phase four of the Oligocene, most benthic $\delta^{18}O$ records record a 1 ‰ decrease to values similar to those of the mostly ice free middle-late Eocene (Lear et al., 2004; Miller et al., 1987; Miller et al., 1991; Pekar et al., 2006; Zachos et al., 2001a). This decrease in oxygen isotope values has traditionally been interpreted as a warming of deep-sea temperatures and a partial deglaciation of Antarctica, and was therefore termed the 'late Oligocene warming' (Zachos et al., 2001a). However, this warming cannot be reconciled with ice proximal evidence from the western Ross Sea (Barrett, 2007), as these proximal

data suggest a cooling during the Oligocene and an Antarctic continent cold enough to sustain ice sheets at sea level. Moreover, the warming is also not reconcilable with the sustained decrease of late Oligocene atmospheric CO_2 values (Barrett, 2007; Zhang et al., 2013).

It has since been demonstrated that this decrease in $\delta^{18}O$ values is, at least in part, an artefact of the $\delta^{18}O$ compilation by Zachos et al. (2001a), due to a switch from sub-Antarctic to equatorial $\delta^{18}O$ data at 25 Ma (Cramer et al., 2009; Lear et al., 2004; Pälike et al., 2006a; Pälike et al., 2006b; Pekar et al., 2006). Conversely, single site data show that the decrease in $\delta^{18}O$ is in fact more gradual (over 4 Myr leading up to the Mi-1) and smaller in amplitude (Pälike et al., 2006b). Furthermore, contrasting the low $\delta^{18}O$ values of the Pacific and Atlantic sites, are data from the Southern Ocean which show sustained high $\delta^{18}O$ values during the late Oligocene (Pekar et al., 2006). Pekar et al. (2006) suggest that this conundrum of a glaciated Antarctica, and varying intrabasinal $\delta^{18}O$ values can be resolved if two deep-water masses, one sourced from Antarctica (proto-Antarctic Bottom Water; AABW) and another, warmer, bottom-water, sourced from lower latitudes, existed during the late Oligocene (Fig. 2.10). They argue that, beginning at 27 Ma, there was a divergence in $\delta^{18}O$ values between the Southern Ocean and other ocean basins, due to the Antarctic ice sheet causing high Southern Ocean $\delta^{18}O$ values. The coeval, but lower $\delta^{18}O$ values in other basins indicates that for much of the late Oligocene, the proto-AABW was not the dominant deep water. However, during the Oi-2b and Mi-1 glacial periods, the Antarctic ice sheets expanded to the coastline, thereby contributing to colder surface waters and expanded sea ice cover, and ultimately leading to enhanced deep water formation and a strengthening of the proto-AABW. The reverse is argued to have occurred during glacial minima, where the production of the proto-AABW was weakened (Pekar et al., 2006). As such, these authors suggest that the documented substantial $\delta^{18}O$ gradient between deep-sea sites during the late Oligocene was due to decreased production of proto-AABW, which was subsequently entrained by, and mixed into warmer deep-waters (Pekar et al., 2006).
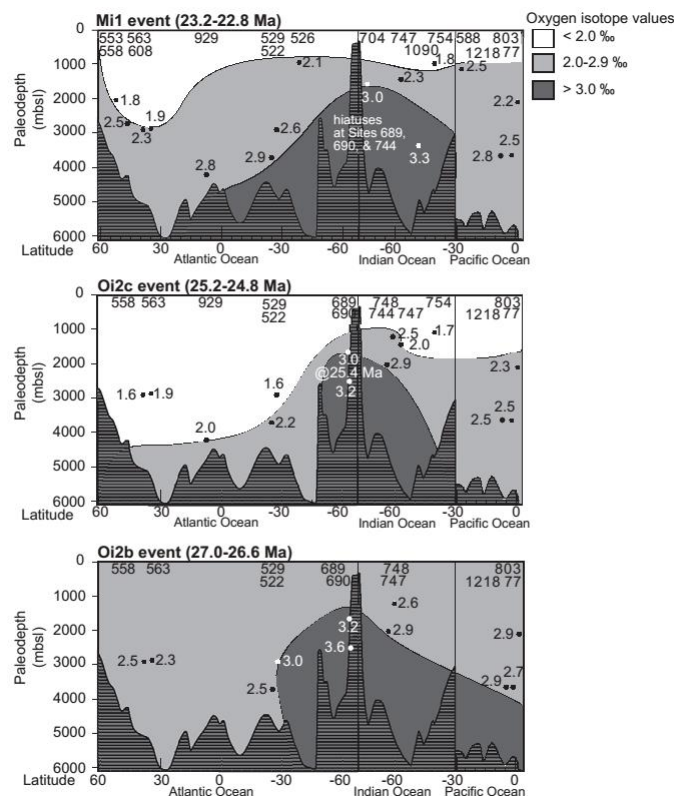
Fig. 2.10 (overleaf): Oxygen isotope transects for three events; Oi-2b, Oi-2c, and Mi-1. Labels at the top indicate DSDP and ODP sites used in this study, whilst numbers in the transect indicate $\delta^{18}O$ values at their paleodepths. The coldest deep-water (≥ 3 ‰) is generally confined to the Southern Ocean in all time slices, whilst warmer deep-water (<2 ‰), becomes a widespread water mass during Oi-2c. This reduction of proto-AABW offers an alternative explanation for the decreased $\delta^{18}O$ values during the late Oligocene (Pekar et al., 2006).

The late Oligocene was terminated by the second major glaciation of the Cenozoic, termed Mi-1 by Miller et al. (1991) at the Oligocene-Miocene boundary (23 Ma). The Mi-1 event occurred over ~300 kyr between 23.24 and 22.95 Ma, with maximum ice volume at 23.03 Ma (Mawbey and Lear, 2013; Mudelsee et al., 2014; Paul et al., 2000; Shevenell and Kennett, 2007; Zachos et al., 2001a). The comparison of low and high latitude records presented by Mudelsee et al. (2014) indicate that the Mi-1 had a $\delta^{18}O$ amplitude of 0.6 ‰, suggesting that the previous estimate of 1.0 ‰ (e.g. Miller et al. (1991); Shevenell and Kennett (2007)) may have been an overestimate. Ocean temperatures dropped by ~2 °C leading up to the Mi-1, in two cooling steps at 23.24 and 23.14, both of which were paced by ~100 kyr eccentricity (Billups and Schrag, 2002; Lear et al., 2004; Mawbey and Lear, 2013). It has been suggested that this cooling of ocean temperatures may have contributed to triggering the Mi-1 glaciation (Lear et al., 2004; Shevenell and Kennett, 2007). Furthermore, some studies, based on far-field $\delta^{18}O$ records, suggest that Antarctic ice volume expanded to 25% larger than the present day EAIS at the Mi-1, with a coeval ~80 m sea level drop (Liebrand et al., 2011; Miller and Mountain, 1996; Paul et al., 2000; Pekar and DeConto, 2006). It is however noted that this ice volume estimate may be smaller if the oxygen isotope excursion at the Mi-1 is smaller than the widely cited 1.0 ‰, as suggested by Mudelsee et al. (2014).

Notably, the aforementioned notion of a spatially restricted proto-AABW with expanded warmer deep-waters and large ice volume on Antarctica during the late Oligocene may also apply to the early Miocene given that high $\delta^{18}O$ values in the Southern Ocean continue to occur coevally to low $\delta^{18}O$ values in most other ocean basins during the early Miocene (Billups et al., 2002; Pekar and DeConto, 2006; Pekar et al., 2006). Only during glacial maxima, such as the Mi-1, was the proto-AABW production enhanced (Fig. 2.10). Pekar and DeConto (2006) draw support for this interpretation from deep-sea hiatuses in the sediments east of New Zealand during early Mi-events, interpreted to represent enhanced bottom-water formation (Carter et al., 2004).

The cause of the Mi-1 is partially ascribed to the coincidence of minima in the low frequency eccentricity (400 kyr) and in the amplitude of variability (node) of obliquity (1.2 Myr). Together this rare orbital configuration (four consecutive low-amplitude obliquity cycles during a low eccentricity) caused 200 kyr of low seasonality and cooler summers, which favours ice expansion on Antarctica (Pälike et al., 2006a; Paul et al., 2000; Zachos et al., 1997; Zachos et al., 2001a; Zachos et al., 2001b). However, the most recent astronomical solutions place the most extreme nodes of obliquity at 19.7, 20.7, 24.4 and 25.4 Ma (i.e. not at Mi-1). It has thus been suggested that glaciations are most readily recorded when the climate system is preconditioned by nodes in obliquity and then ultimately triggered by extremes in 110 and 405 kyr eccentricity cycles (Laskar et al., 2004; Pälike et al., 2006a; Wade and Pälike, 2004). Thus, the node in the 1.2 Myr amplitude of

obliquity during the Mi-1 is not of sufficient size to solely explain the extent of the glaciation and instead a further pre-conditioning, such as a drop in atmospheric CO_2 is required to enhance the climate sensitivity to orbital forcing (Pälike et al., 2006a; Zachos et al., 2001b). Furthermore, because the largest glaciations in the early Miocene are separated by several eccentricity cycles, non-linear mechanisms (e.g. the carbon cycle) are suggested (Liebrand et al., 2011).

The 400 kyr cycle is found to be dominant in the $\delta^{13}C$ and $\delta^{18}O$ records with additional peaks in shorter (95 and 125 kyr) eccentricity cycles, and to some extent at the 41 kyr obliquity cycle. Long-term eccentricity minima appear to coincide with maxima in $\delta^{18}O$ and $\delta^{13}C$, where $\delta^{13}C$ slightly lags $\delta^{18}O$, thereby implying a coupling between the carbon cycle and the climate system, possibly via a decrease in atmospheric CO_2 (Billups et al., 2002; Liebrand et al., 2011; Pälike et al., 2006b; Paul et al., 2000; Zachos et al., 1997; Zachos et al., 2001b). The coupling of increased ice volume and $\delta^{13}C$, as well as the coeval increases in U/Ca ratios (a proxy for enhanced carbon burial) across the Mi-1, may be explained by enhanced meridional temperature gradients leading to enhanced upwelling and subsequently more nutrients promoting export production via the biological pump (Diester-Haass et al., 2011; Paul et al., 2000; Zachos et al., 1997), and/or a control on the nutrients delivered from the shelf sediments to the oceans by changes in sea level (Liebrand et al., 2011). Both mechanisms are able to enhance carbon burial and thereby lower CO_2 through a positive feedback (Mawbey and Lear, 2013). Stomatal and alkenone data show that CO_2 records declined from ~600 to ~340 ppm leading up to the Mi-1, but remained invariant across it. This implies that at the Mi-1, CO_2 was below the threshold required to maintain a fully glaciated Antarctica (Kürschner et al., 2008; Zhang et al., 2013).

Similar to the EOT, the Mi-1 also appears to have ended with an overshoot behaviour followed by a recovery to $\delta^{18}O$ values similar to those prior to the glaciation, thereby pointing to similar mechanisms for both glaciations (Mudelsee et al., 2014; Zachos et al., 2001a). During this final recovery phase of Mi-1 (22.95-22.85 Ma), temperatures warmed by ~2 °C in two steps at 23.04 and 22.94 Ma paced by short eccentricity, and the Antarctic ice sheets reduced to ≥ 50% of modern day EAIS volume (Lear et al., 2004; Mawbey and Lear, 2013; Pekar and DeConto, 2006). It has been suggested that this recovery was aided by a late stage carbon dissolution event, where organic carbon which was being buried during the glaciation of Mi-1, was oxidised and subsequently released light carbon into the ocean-atmosphere system (Mawbey and Lear, 2013). This explanation supports the notion that orbital forcing alone was not strong enough to cause Antarctic deglaciation once the ice had expanded to its full extent around the continent (DeConto and Pollard, 2003; Zhang et al., 2013).

The Mi-1 showed that major expansions of ice on Antarctica occur during minima in 400 kyr eccentricity when the power of the 100 kyr cycle is suppressed, whilst termination phases of large glacial episodes appear to coincide with short (100 kyr) eccentricity cycles, indicating a higher sensitivity to shorter orbital cycles during the termination of glaciations (Liebrand et al., 2011; Zachos et al., 2001b). Furthermore, spectral analyses show that most of the variance in the $\delta^{18}O$ records leading up to the Mi-1 was concentrated in the obliquity (41 kyr) and long eccentricity (400 kyr) periods, while short and long eccentricity periods appear to pace the $\delta^{18}O$ records after the Mi-1, with little to no variance at periods relating to obliquity (Pälike et al., 2006b). The frequency, and large amplitude of these changes is argued to represent a more dynamic Antarctic cryosphere during the early Miocene (Pekar and DeConto, 2006).

2.3.4 Middle Miocene to present

A detailed middle Miocene to present climate history is outside the scope of this review, and as such is only briefly summarised. Following the early Miocene, several other glaciations followed during the Miocene (Miller et al., 1991; Mudelsee et al., 2014), but the general trend of the first half of the Miocene appears to have been warming, culminating in the middle Miocene climate optimum (MMCO; 17-14 Ma). This warming was terminated by the middle Miocene climate transition (MMCT; ~14 Ma), which is characterised by a persistent cooling trend and stronger glaciations (Cramer et al., 2011; Flower and Kennett, 1994; Mudelsee et al., 2014; Shevenell et al., 2004; Zachos et al., 2001a). Proxy data suggest that CO_2 rose to as much as 500 ppm during the MMCO and subsequently declined to ~300-400 ppm during the MMCT (Foster et al., 2012; Kürschner et al., 2008; Zhang et al., 2013). The MMCT marks the onset of more persistent Antarctic ice sheets and polar desert conditions in Antarctica (Miller et al., 2008b; Shackleton and Kennett, 1975; Shevenell et al., 2008).

Benthic oxygen isotopes values subsequently continued to increase, suggesting cooling and ice sheet expansion until the early Pliocene (6 Ma), before a slight decrease in oxygen isotope values suggests some warming during the Pliocene (Mudelsee et al., 2014; Zachos et al., 2001a). Between 3.6 and 2.4 Ma the continued increase in $\delta^{18}O$ values, and a major pulse of IRD in the Atlantic 2.6 Ma is argued to reflect the establishment of glaciations in the Northern Hemisphere, associated with sea level changes of up to 120 m (Mudelsee et al., 2014; Mudelsee and Raymo, 2005; Shackleton et al., 1988; Shackleton et al., 1984; Zachos et al., 2001a).

2.4 Cenozoic Antarctic glacial history from proximal geological records and models

While these distal proxy records discussed in the previous section have proven invaluable to understand the broad global trends, they remain subject to large uncertainties and assumptions regarding the location and extent of ice sheets in either hemisphere. To overcome some of these uncertainties, proximal records from the Antarctic continental margin (Fig. 2.11) are required to validate the previously discussed ice volume changes inferred from distal records. To provide context regarding these uncertainties, these proximal 'direct' records of Antarctic ice sheet variations and climate are discussed in further detail below, with a specific emphasis on the Oligocene to early Miocene.
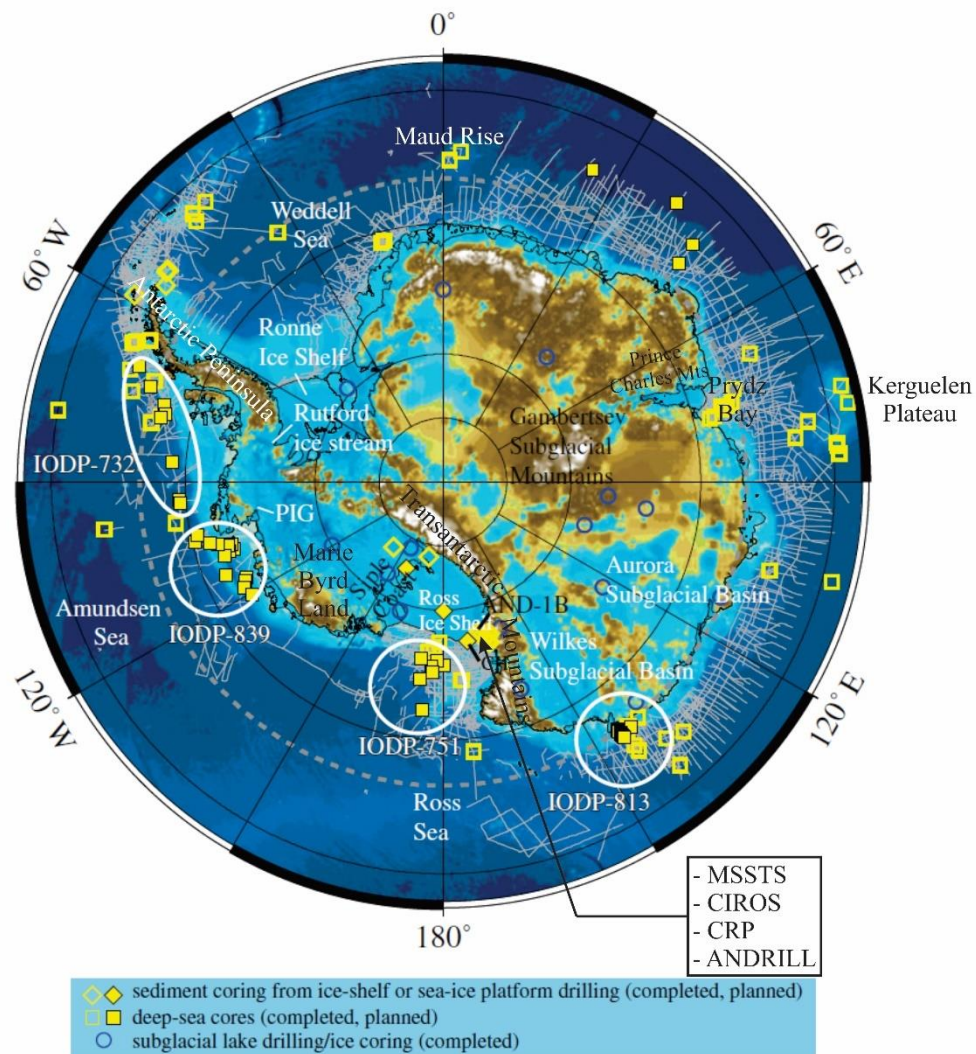
Fig. 2.11: Map (ice-free topography and bathymetry) of Antarctica, where darker blue shading indicates deeper bathymetry, and darker brown/white colours indicate higher topography. Open yellow squares and diamonds, as well as open blue circles, mark the locations of various completed drilling projects. Filled yellow squares and diamonds denote the locations of proposed future drilling, and grey lines mark the locations of where offshore seismic data was collected. All study locations referred to in the text are shown on this map (modified from McKay et al. (2016) and references therein).

2.4.1 Palaeocene to Eocene

Palynomorphs and fossil wood from Seymour Island (Antarctic Peninsula) indicate a transition from warm climates during the Late Cretaceous, to cool and wet climates with mean annual temperatures (MAT) of ~4.8 °C during the Palaeocene (Askin, 1989; Francis and Poole, 2002). Temperatures leading into the early Eocene were suggested to once again rise to MATs of 7 to 15 °C, with a subsequent deterioration of the climate during the later Eocene (Francis and Poole, 2002; Poole et al., 2005). Furthermore, biotic and organic geochemical climate proxies suggest that near-tropical forests grew in Wilkes Land (69 °S) during the early Eocene at MATs of ~16 °C, despite polar darkness. Local MATs later dropped to ~14 °C during the middle Eocene (Pross et al., 2012). Meanwhile, at Prydz Bay middle to late Eocene fluvial, deltaic and lagoonal deposits containing *Nothofagus* (southern beech) and other pollen, point to stunted rainforests and humid conditions, with

possibly some inland glaciers at the time (Cooper and O'Brien, 2004; Strand et al., 2003). In McMurdo Sound (77.5 °S), fossiliferous erratics suggest a cool, dry and temperate coastal climate, with *Nothofagus* trees growing during the Eocene (Francis, 2000; Harwood and Levy, 2000; Holmes, 2000; Pole et al., 2000). The absence of glacial facies in these erratics suggests that no ice extended to sea level in the McMurdo Sound at the time (Levy and Harwood, 2000). However, tills on King George Island, and drill cores recovered from the Antarctic Peninsula by SHALDRILL, suggest valley-type glaciers, surrounded by *Nothofagus* and podocarp conifer, existed on the Antarctic Peninsula from the middle Eocene (~45-41 Ma; Birkenmajer et al. (2005)), through to the late Eocene (Anderson et al., 2011).

In addition to this glacial evidence, Margolis and Kennett (1970) argued for the presence of Eocene-aged IRD in the South Pacific based on quartz grain microstructures, but doubt has been cast over the ice-rafted origin of these grains by more recent studies (Miller et al., 2008b). However, numerical models suggest that ice caps in the interior of the continent during the Eocene are physically plausible, and recent morphometric analyses of the Gamburtsev Subglacial Mountains indicates an alpine glacial landscape was present prior to the development of large ice sheets (DeConto and Pollard, 2003; Rose et al., 2013). Based on comparing paleo-equilibrium-line-altitude reconstructions to published pre- and post-EOT temperatures, they suggest local cirques were carved prior to the EOT, and remained fully glaciated ever since then (Rose et al., 2013). The preservation of this landscape also suggests that the core of the EAIS has been cold-based since the EOT (Rose et al., 2013). If ice masses such as this existed in the Antarctic interior prior to the EOT, then this could go some way to reconciling the variability in Eocene eustatic sea levels, as estimated from passive margins (Kominz et al., 2008; Miller et al., 2005a; Miller et al., 2005b). Alternatively, these passive-margin sea level variations may be explained by local dynamic mantle and topography processes causing changes in relative sea level (e.g. Moucha et al. (2008); Rowley et al. (2013)).

2.4.2 Transition from greenhouse to icehouse

Although Antarctica has been located in a polar position since the Late Cretaceous (Lawver et al., 1992), persistent ice sheets are widely considered not to have appeared until the transition from the 'greenhouse' to the 'icehouse' worlds at the EOT. Evidence for the inception of a continental-scale Antarctic ice sheet at the EOT can be found around all margins of Antarctica. The oldest unequivocal appearance of ice-rafted debris (IRD) in the Southern Ocean was identified at the Kerguelen Plateau (~1000 km north of Prydz Bay), with a sudden and contemporaneous ~100 kyr long spike in IRD and $\delta^{18}O$ (Fig. 2.12). This is argued to represent the first continental scale expansion of ice sheets in Antarctica, and thereby supported the aforementioned far-field data which suggested the onset of glaciation at the EOT (Breza and Wise Jr, 1992; Wise et al., 1992; Zachos et al., 1992). Zachos et al. (1992) linked the IRD to diamictites of similar age recovered from Prydz Bay. These prograding diamictites mark the advance of a grounded ice sheet extending to the continental shelf break at approximately the EOT, implying a continental-scale EAIS down to sea level, with periodic outbursts of meltwater (Barron and Larsen, 1989; Cooper and O'Brien, 2004; Hambrey et al., 1991; Strand et al., 2003). Coevally, siliceous biogenic facies replaced carbonate facies on the Maud Rise, reflecting the development of an upwelling regime related to an expanded Antarctic cryosphere (Kennett and Barker, 1990).
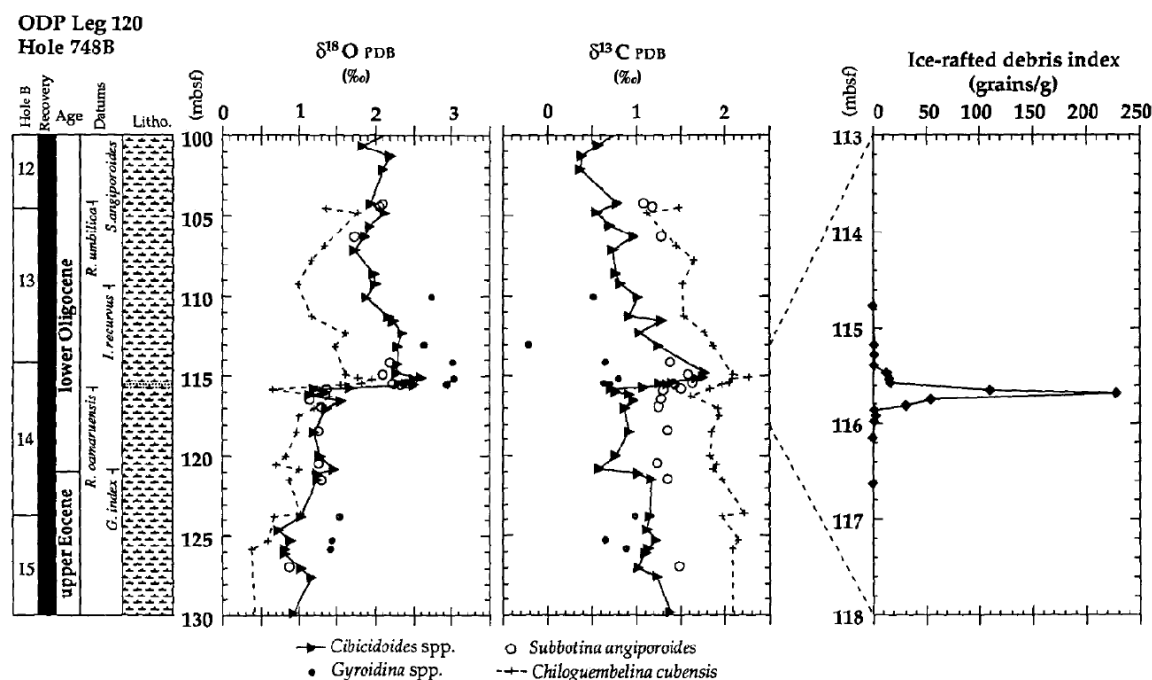
Fig. 2.12: Data from the Kerguelen Plateau, highlighting the coeval increase in benthic and planktonic $\delta^{18}O$ values, and IRD at the EOT (Zachos et al. (1992) and references therein).

Similar to Prydz Bay, IRD in the CIROS-1 cores (McMurdo Sound) and glacial strata at Seymour Island also record glaciers which extended to sea level at the EOT, draining the EAIS, and possibly WAIS, respectively, thereby also suggesting a continental scale glaciation (Barrett et al., 1989; Ivany et al., 2006). Moreover, sedimentological evidence from CIROS-1 suggest that the Antarctic ice sheet was wet-based and temperate (Barrett et al., 1989). At the Wilkes Land margin, the EOT is missing due to an unconformity, but the onset of glaciation is suggested by the presence of significant amounts of IRD in the overlying sediments (Escutia et al., 2014; Escutia et al., 2011).

Furthermore, clay minerals in sediments from the Kerguelen Plateau, Maud Rise, Wilkes Land as well as the Ross Sea (MSSTS-1, CIROS-1 and CRP drill cores) all indicate a shift from chemical weathering during relatively warmer, more humid climates (smectite-dominated), to physical weathering under cooler, drier climates (illite- and chlorite-dominated) across (or just prior to, in the case of Wilkes Land) the EOT. As such, these clays tell a consistent story of enhanced physical weathering linked to intensified glaciation across the EOT (Diester-Haass et al., 1996; Ehrmann, 1998; Ehrmann et al., 2005; Ehrmann and Mackensen, 1992; Escutia et al., 2014; Robert and Kennett, 1997). Similarly, geochemical analyses of East Antarctic sediments also suggest an abrupt aridification of East Antarctica at 34 Ma (Passchier et al., 2013).

The most detailed study of the EOT comes from the drill cores recovered by the CRP. These suggest an initial increase in glacial activity at 34 Ma through the appearance of striated clasts, followed by a significant increase in glacial activity at 33 Ma, with the appearance of diamictites indicating glaciers calving at sea level (Barrett, 2007; Ehrmann et al., 2005; Hannah et al., 2000; Hannah et al., 2001; Raine and Askin, 2001; Thorn, 2001). More recent analyses of the orbitally forced sedimentary cycles recovered between 34 and 31 Ma by the CRP suggest that the Oi-1 represents the onset of significant Antarctic glaciation, with an ice sheet which was highly dynamic in response to shorter period orbital forcing of precession and obliquity (Galeotti et al., 2016). However, it was not until 1 Myr later, at

the Oi-1a (32.8 Ma), when CO_2 dropped below 600 ppm during long term minima in eccentricity and obliquity (similar to the orbital configuration at the Oi-1), that a grounded, marine calving ice sheet first occurred in the Ross Embayment (Fig. 2.13), representing a larger, more stable Antarctic ice sheet (Galeotti et al., 2016; Laskar et al., 2004; Pagani et al., 2011; Pearson et al., 2009). Consequently, it is suggested that below 600 ppm, the EAIS becomes less sensitive to higher frequency orbital forcing, thereby enhancing its stability. These results are consistent with far field sea level estimates, modelled CO_2 thresholds, and the hypothesis that maximum glacial conditions are favoured by low seasonality and cooler summers (Bohaty et al., 2012; Coxall et al., 2005; DeConto and Pollard, 2003; Galeotti et al., 2016; Katz et al., 2008; Miller et al., 2005a).

However, even in light of all of this evidence of a continental-scale Antarctic expansion of ice, there was a problem of 'missing ice' at the EOT, as ice sheet models, such as that of DeConto and Pollard (2003), continue to fall short (by ~5 x 10^6 km^3) of the ice volume estimated for the EOT (125% that of present day). Although invoking some ice sheet advance in the northern hemisphere is supported by the presence of glacial dropstones in the North Greenland Sea and Arctic Ocean between 38-30 Ma (Eldrett et al., 2007), modelled climatic thresholds for bipolar glaciation contradict this idea (DeConto et al., 2008). However, this problem may be reconciled by reconstructing the paleotopography of Antarctica at the EOT. Modelled topographic reconstructions show that there was in fact up to 20% more land area, mostly in West Antarctica, at the time (Wilson et al., 2012). This implies that the WAIS may have formed much earlier than assumed, and that Antarctica may have supported an ice sheet larger than present, even under elevated CO_2. This is possible because the temperature threshold for the initiation of a terrestrial-based ice sheet is higher than a marine-based ice sheet which is more sensitive to oceanic temperature and circulation changes (DeConto et al., 2008; Foster and Rohling, 2013; Mercer, 1983; Wilson et al., 2013). If the WAIS did form at this time, an extra ~13 million km^3 of ice volume (~30 m sea level equivalent; Fig. 1.1) could have been harboured on Antarctica at the EOT (Wilson et al., 2013). Physical evidence in support of a WAIS during the Oligocene comes from the dissected volcanoes and hydrovolcanic eruptive deposits of this age (Rocchi et al., 2006).
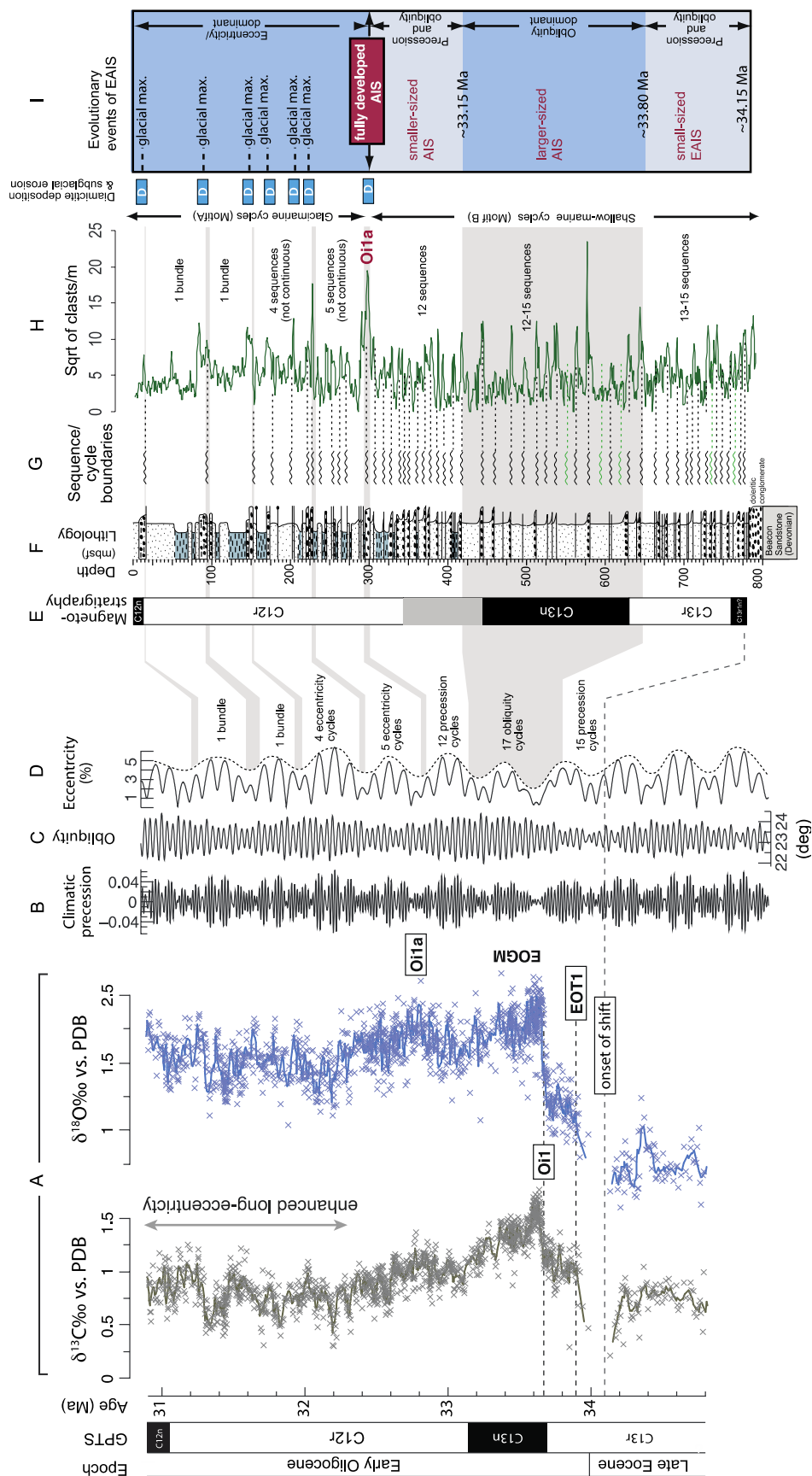
Fig. 2.13: Eocene-Oligocene deep-sea stable isotopes from the equatorial Pacific (A) and calculated orbital cyclicity (B-D) correlated to the magneto-, litho-, and sequence-stratigraphy (E-G), and the square-root of the abundance of clasts per metre (H) in the CRP cores. Sequence motif B contains 37 cycles of land-terminating glaciers, while the overlying motif A records 11 cycles of a more expansive marine-terminating ice sheet. A summary of inferred changes is given in (I). (Galeotti et al., 2016).

2.4.3 Oligocene to early Miocene

During the course of the Oligocene to early Miocene, 54 sedimentary cycles, which correlate with Oi- and Mi-glacials recorded in deep-sea sediments and continental shelves, were deposited at Cape Roberts, thereby highlighting the orbital pacing of an early EAIS at obliquity and eccentricity frequencies (Barrett, 2007; Dunbar et al., 2008; Fielding et al., 2000; Naish et al., 2008; Naish et al., 2001). During most of these cycles grounded ice extended into the Ross Sea, with significant unconformities at 29, 25 and 23 Ma likely representing substantial glacial erosion (Barrett, 2007). Similarly, the early to middle Oligocene MSSTS-1 cores from McMurdo Sound, recovered seven diamictite beds, which are argued to have been deposited beneath grounded ice (Barrett et al., 1987). It is suggested that during interglacials the coastline along the McMurdo Sound was largely ice free, with marine-calving polythermal glaciers at the edges (Dunbar et al., 2008; Powell et al., 2001). Furthermore, *Nothofagus*-dominated pollen assemblages, palynomorphs, and marine macrofossils recovered from the CRP drill cores, as well as a *Nothofagus* leaf found in an interglacial mud in the late Oligocene section of the CIROS core, all suggest a cool, temperate, Oligocene climate with mean summer temperatures of 4 to 12 °C (cf. -5 °C today) at sea level in the McMurdo Sound. These pollen data indicate that trees and shrubs grew around the foothills of the Transantarctic Mountains, and persisted through several Oligocene glacial cycles (Barrett et al., 1989; Prebble et al., 2006; Raine and Askin, 2001; Taviani and Beu, 2003; Thorn, 2001). Coevally, at DSDP Site 270, glacimarine sediments containing IRD and *Nothofagus*-dominated pollen assemblages provide evidence for the contemporaneous presence of ice masses and vegetation during the Oligocene (Kemp and Barrett, 1975). Moreover, the high Oligocene-early Miocene sedimentation rates at DSDP 270 have been interpreted to reflect wet-based, temperate glaciers or ice sheets calved into an open Ross Sea, without an ice shelf (Kemp and Barrett, 1975). Similar to this evidence from the Ross Sea, the *Nothofagus*- and conifer-dominated vegetation on the Antarctic Peninsula occurred coeval with the presence of marine calving wet-based, polythermal ice caps and tidewater glaciers during much of the Oligocene, in a subpolar environment with MATs of ~10 °C (Anderson et al., 2011; Troedson and Smellie, 2002). Meanwhile, Oligocene to Miocene aged (29-27, and 27-15 Ma) pyroclastic deposits with sub-ice eruption textures, and coeval exhumation ages of gabbro, both from Marie Byrd Land, are suggested to provide evidence of a continental ice sheet or ice cap over West Antarctica (LeMasurier and Rex, 1983; LeMasurier and Rocchi, 2005; Rocchi et al., 2006; Wilch and McIntosh, 2000). In addition to the evidence of Antarctic glaciation, a cooling trend is noted throughout the Oligocene to early Miocene in the Ross Embayment by an increase in the percent of illite-chlorite clays (indicating more physical weathering) in glacimarine sediments to >40% from 32 to 25 Ma, and to 70% between 23 and 17 Ma (Ehrmann et al., 2005). Over the same time period, palynomorphs indicate a progressive decrease in fresh meltwater and intensifying glacial conditions (Barrett, 2007; Ehrmann et al., 2005; Hannah et al., 2000; Hannah et al., 2001; Raine and Askin, 2001; Thorn, 2001). Furthermore, foraminifera from DSDP Site 270 indicate increasingly cooler conditions, culminating with the enhanced appearance of significant ice masses at sea level during the early Miocene (Leckie and Webb, 1983).

Seismic data reveals glacial troughs and moraines during the Oligocene, implying grounded ice cap advances from Marie Byrd Land. These features are only observed in the eastern Ross Sea, and it is conceivable that the WAIS may have been confined to Marie Byrd Land during this time (Sorlien et al., 2007). Elsewhere in the Ross Sea, mid-late Oligocene seismic data indicate that the climate had not cooled sufficiently for widespread expansion of a marine-based ice sheet onto the outer Ross Sea shelf (Bart and De Santis, 2012; De

Santis et al., 1999). Instead small till tongues suggest that glaciers and ice caps drained from local highs (e.g. Central High, Coulman High) of the Ross Sea, and advanced slightly into shallow marine areas at the time (Bart and De Santis, 2012; Brancolini et al., 1995; De Santis et al., 1995). On the western side of the Ross Sea, the late Oligocene to early Miocene section of the CIROS-1 core recovered seven advances and retreats of the ice sheet (Barrett et al., 1989), but unfortunately no sediments of similar age were recorded at Prydz Bay due to a major unconformity, likely the result of an expanded middle Miocene ice sheet (Cooper and O'Brien, 2004; Hambrey et al., 1991). However, glacial sediments in the Prince Charles Mountains, along the western margin of the Lambert graben in Prydz Bay, indicate dynamic, wet-based polythermal glaciers extending into a fjordal style setting during the late Oligocene to early Miocene (Hambrey and McKelvey, 2000a, b). Fluctuations of the EAIS' volume caused orbitally controlled eustatic sea level changes the order of 10-40 m (i.e. 15-40% present day ice volume) during the late Oligocene based on the isostatically and tectonically adjusted sedimentary sea level record from Cape Roberts (Dunbar et al., 2008; Naish et al., 2008). As such, the Cape Roberts records (Barrett, 2007; Dunbar et al., 2008; Naish et al., 2008; Naish et al., 2001) are consistent with far-field late Oligocene to early Miocene ice volume estimates of between 50 and 125% of the present-day EAIS volume (Pekar and DeConto, 2006; Pekar et al., 2006).

Significantly, all of this evidences supports the view of Barrett (2007), who pointed out that the aforementioned data from the CRP cores do not indicate a significant loss of ice or warming during the late Oligocene, as has been suggested by compilations of deep-sea benthic $\delta^{18}O$ data (Zachos et al., 2001a). Instead, he suggests that the hypothesis of reduced Antarctic deep-water and strengthening of northern warm deep waters, resulting in a warming of deep waters in many ocean basins (Pekar et al., 2006), is more in line with the data recovered from Cape Roberts.

Subsequent to the late Oligocene, sediments recovered from the western Ross Sea suggest that the Mi-1 glaciation likely represents the first major advance of marine-based ice in the Ross Sea. The Mi-1 glaciation is marked by a 3 Myr erosional unconformity in CRP and CIROS (Naish et al., 2008; Wilson et al., 2009). Furthermore, CRP records show an orbitally paced EAIS, whose changes match observed deep sea $\delta^{18}O$ pattern of ice volume, leading up to Mi-1 (Naish et al., 2008). Eustatic sea level estimates from Cape Roberts also suggest an expansion to 125% of the modern EAIS during the Mi-1, equivalent to a eustatic sea level fall of ~50 m, also in agreement with far-field data (Kominz et al., 2008; Miller et al., 2005a; Pekar and DeConto, 2006). The changes across Mi-1, as observed at Cape Roberts can be summarised as follows (Fig. 2.14; Wilson et al. (2009)):

(1) Sedimentary cycles are 55-60 m thick in the late Oligocene versus being only 10-20 m thick and commonly truncated during the early Miocene.
(2) The chemical index of alteration (CIA) suggests a slight shift to more physical weathering and mechanical erosion immediately after the Oligocene-Miocene boundary (Passchier and Krissek, 2008).
(3) Marine palynomorphs indicate cooler climates and a reduction in meltwater production across the Oligocene-Miocene boundary (Barrett, 2007).
(4) Pollen indicate the persistence of *Nothofagus* in the Victoria Land Basin into the early Miocene (Askin and Raine, 2000; Mildenhall, 1989; Raine and Askin, 2001; Thorn, 2001), suggesting that truly polar conditions were not reached until well after the Mi-1 glaciation (Roberts et al., 2003).
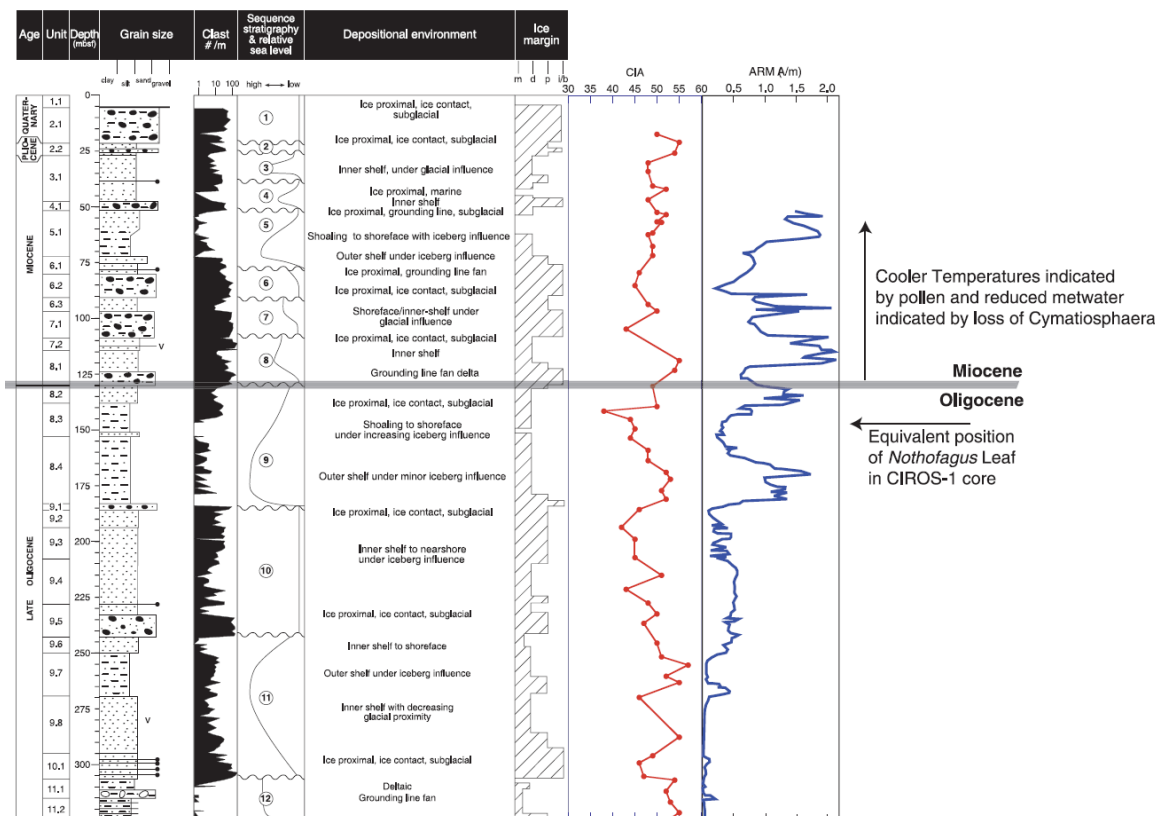
Fig. 2.14: The Oligocene-Miocene section of the CRP sediments, showing the litho- and sequence-stratigraphy, clasts per metre (IRD), depositional environments, ice proximity curve, CIA index and anhysteric remanent magnetisation data. In the sequence stratigraphy one glacial cycle of advance and retreat is represented as: an initial erosional surface is followed by a diamictite and sandstone, which are in turn overlain by bioturbated muds with sparse fossils (Wilson et al., 2009).

The Ross Sea seismic data contain large, thick till deltas with foreset heights of ~250 m, deposited close to grounding line zones, suggesting that the first marine-based ice sheets advanced at some point during the early Miocene. This indicates that temperate to subpolar style grounded ice sheets with abundant meltwater advanced into a relatively shallow marine realm across large areas of the continental shelf during the early Miocene (Anderson and Bartek, 1992; Bart and De Santis, 2012; De Santis et al., 1995). Similarly, early Miocene diamictites on the Antarctic Peninsula also suggest the first known local expansion of temperate marine-based ice with episodic meltwater discharge, onto the continental shelf (Dingle and Lavelle, 1998; Troedson and Riding, 2002). These diamictites, linked to Mi-1, contain local as well as far-field (e.g. Transantarctic Mountains, and the mountains fringing the Weddell Sea) ice-rafted clasts, suggesting significant ice coverage at the time (Troedson and Riding, 2002). Meanwhile, ice-rafting across the Mi-1 was also noted as far away as at Maud Rise (Barker and Kennett, 1990), but did not reach the Kerguelen Plateau (cf. at the EOT) (Schlich et al., 1992). At the Wilkes Land margin, sediments of the early Miocene lack the debris flow deposits which characterised the late Oligocene sediments. This is suggested to represent the change from mass transport processes resulting from the EAIS expansion leading up to Mi-1, to a return to hemipelagic and bottom current deposition (Escutia et al., 2014; Salabarnada et al., 2015). Seismic data at Wilkes Land also show that Oligocene to early Miocene strata appear to be dominated by low angle prograding foresets characteristic of temperate glaciation with dynamic ice sheets (Escutia et al., 2005).

Meanwhile, in the Transantarctic Mountains, fossiliferous (e.g. insects and vegetation such as *Nothofagus*) fluvial and lacustrine deposits suggest interglacial summer temperatures of 6-7 °C during the early Miocene (Lewis and Ashworth, 2015). Furthermore, early to middle Miocene (20.5-14 Ma) drill cores recovered from ANDRILL suggest that during this time the Antarctic Ice Sheet was highly variable and very sensitive to small changes in CO_2 (Levy et al., 2016). They show that the ice sheet expanded across the Ross Sea at times of low CO_2 (~280 ppm). Meanwhile, during times of elevated CO_2 (~500 ppm), substantial ice retreat occurred to inland areas, coastal air temperatures were relatively warm (6-10 °C), and vegetation was growing around the foothills of the Transantarctic Mountains (Levy et al., 2016).

2.4.4 Middle Miocene to present

Subsequent to the early Miocene a period of global warmth developed (MMCO, 17-14.5 Ma), which is inferred to be associated with large ice volume changes (e.g. Holbourn et al. (2015)). This inference is supported by highly variable margins of the Antarctic ice sheets (Fielding et al., 2011; Gasson et al., 2016; Levy et al., 2016; Passchier et al., 2011; Warny et al., 2009). Additional evidence for a warmer glacial regime is provided by bedrock channels and scoured terrain in the Transantarctic Mountains which suggest major subglacial floods draining the EAIS (Lewis et al., 2006), abundant seismic data images of meltwater channels in the Ross Sea (Bart and De Santis, 2012), and sedimentological evidence for lakes with tundra vegetation in the Transantarctic Mountains (Lewis and Ashworth, 2015; Lewis et al., 2008).

The MMCO was terminated by the MMCT, when more persistent, cold-based ice sheets developed, temperatures dropped significantly and Antarctic conditions intensified to an increasingly polar environment (Bart and De Santis, 2012; Hannah, 2006; Lewis et al., 2008; Lewis et al., 2007). After longstanding debates, there is now a consensus that the central regions of the EAIS have remained stable since ~14 Ma, but with variable marine-based margins during the Miocene to Pliocene (Barrett, 2013). Mid-Pliocene sea level estimates, computer models, and ice proximal data all imply losses of the West Antarctic and Greenland ice sheets, as well as retreat of some marine-based sectors of the EAIS during interglacials (Cook et al., 2013; DeConto and Pollard, 2016; McKay et al., 2016; Miller et al., 2012; Patterson et al., 2014; Pollard and DeConto, 2009; Pollard et al., 2015). The WAIS became more persistent after 3.3 Ma, and evidence exists for a major ice expansion in the Ross Sea between 3.3 and 2.5 Ma (McKay et al., 2012a). Ice proximal geological data show that orbital variations in Antarctic ice sheet volumes continued throughout the Miocene and Plio-Pleistocene, and to the present day (e.g. McKay et al. (2012b); Naish et al. (2009); Patterson et al. (2014)).

Chapter Two - *Background*

Chapter Three
METHODOLOGY

3.1 Core recovery

The sediment cores at DSDP Site 270 (77° 26.48' S, 178° 30.19' W) were retrieved in 1972 and 1973 aboard the *Glomar Challenger* on DSDP Leg 28 using a rotary drilling method (Hayes and Frakes, 1975; The Shipboard Scientific Party, 1975a, b). The hole at DSDP Site 270 penetrated 422.5 m into the continental shelf, coring marble bedrock at 413.3 metres below sea floor (mbsf). An average of 62% of sediment was recovered at this site, with higher recovery in the lower half of the core (The Shipboard Scientific Party, 1975b). The depths of samples in subsequent analyses outlined below were calculated based on the core top depths provided by the initial reports of The Shipboard Scientific Party (1975b). However, a mistake in core top depths was noted in cores 41 and 42, and corrected for all data as outlined in Table 3.1 below.

Table 3.1: Core top depth correction, with original core log top depths from The Shipboard Scientific Party (1975b).

Core	Section	Original core log top depth (mbsf)	Corrected top depth (mbsf)
41	1	367.0	365.5
41	2	368.5	367.0
41	3	370.0	368.5
42	1	370.0	370.0
42	2	371.5	371.5
42	3	373.0	373.0
42	4	374.5	374.5

3.2 Visual core description and clast counts

The visual core descriptions were initially recorded manually by me and my supervisory team using visual core description sheets before being digitised by me using the PSICAT computer programme (http://portal.chronos.org/psicat-site/). The digitised stratigraphic logs are attached in Appendix 2. In order to be compared with younger stratigraphic records recovered in the Ross Sea, the sediments were described following the ANDRILL scientific logistics and implementation plan (Naish et al., 2006). Fine grained sediments which did not contain any terrigenous gravel sized (>2mm) material were classified according to the Mazzulo and Graham (1988) classification scheme (Fig. 3.1), while those sediments which did contain terrigenous sediment in the gravel fraction were classified according to the Moncrieff (1989) classification scheme for poorly sorted sediments (Table 3.2).

During the visual description process clasts exceeding 2 mm in diameter (argued to represent ice-rafted debris) exposed in the split core face (6.6 cm core width) of the archive half of the core were counted, and recorded in 10 cm bins (attached in Appendix 3),

following the methodologies of previous ship- and land-based investigations of Antarctic continental margin sediments (Expedition 318 Scientists, 2011; Naish et al., 2006).
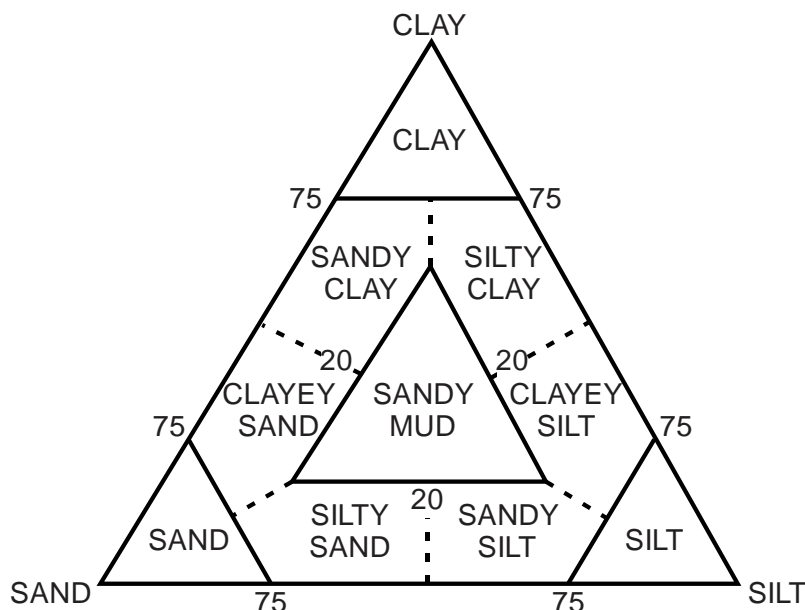
Fig. 3.1: Classification scheme for terrigenous sediments lacking gravel sized clasts (re-drawn from Naish et al. (2006), modified from Mazzulo and Graham (1988)).

Table 3.2: Classification scheme for poorly sorted terrigenous clastic sediments containing gravel sized clasts (re-drawn from Naish et al. (2006), modified from Moncrieff (1989)).

	PERCENT GRAVEL (> 2 mm) IN WHOLE ROCK ESTIMATED FROM CORE					
	Trace (< 1 %)	1 - 5 %	5 - 30 %	30 - 80 %	> 80 %	
FINE-GRAINED SEDIMENTS	**MUDSTONE** with dispersed clasts	**MUDSTONE** with common clasts	**MUDSTONE** with abundant clasts	Muddy **CONGLOMERATE / BRECCIA**	CONGLOMERATE / BRECCIA	
	Sandy **MUDSTONE** with dispersed clasts	Clast-poor muddy **DIAMICTITE**	Clast-rich muddy **DIAMICTITE**	Sandy muddy **CONGLOMERATE / BRECCIA**		
	Muddy **SANDSTONE** with dispersed clasts	Clast-poor sandy **DIAMICTITE**	Clast-rich sandy **DIAMICTITE**	Muddy sandy **CONGLOMERATE / BRECCIA**		
	SANDSTONE with dispersed clasts	**SANDSTONE** with common clasts	**SANDSTONE** with abundant clasts	Sandy **CONGLOMERATE / BRECCIA**		

(Left axis: PERCENT SAND IN MATRIX — 0, 10, 50, 90. Right axis: PERCENT SAND IN MATRIX — 0, -10, -50, -90)

3.3 Grainsize analysis

In order to characterise changes in grainsize down core, 462 samples were requested from the International Ocean Discovery Program (IODP) core repository at Texas A&M University. The upper part of the core (16.90 m to 232.70 m) was sampled approximately every metre, while the lower part of the core (234.14 to 385.45 m) was sampled at a higher

resolution, approximately every 40 cm. The different sampling resolutions are due to the poorer recovery rate in the upper part of the core, and to allow for spectral analysis of the sediments further downcore where the recovery rate was greater. Of the samples requested, 18 of the 462 requested samples were not analysed due 11 some samples not being received and the rest because of cementation.

3.3.1 Separation into grainsize fractions

In order to calculate the weight percentages of various grainsize fractions (< 125 μm, 125 - 250 μm, 250 μm - 2 mm, >2 mm) the following steps were taken. All weighing was either repeated or conducted using two separate scales to ensure correctness.

Approximately 10 cm^3 of dry sample were initially carefully crushed using paper wrapped around a wooden block until they were able to pass through a 2 mm sieve to appropriately reduce the size of the sample. Clasts exceeding 2 mm in diameter were separated from the rest of the sample and weighed. The rest of the sample was also weighed, and the total sample weight was recorded. Approximately 150 to 200 mL of 1 g/L calgon ($Na_6P_6O_{18}$) was subsequently added to the sample, which was then placed into an ultrasonic bath and gently stirred. If a sample was strongly calcite cemented, ~20 mL of 10% HCl was added to the sample before adding the calgon, to aid disaggregation. Following disaggregation, samples were wet sieved at 125 μm, and the >125 μm and <125 μm fractions were treated to the following procedures:

(1) The >125 μm fraction was dried in the oven at 40 °C overnight. Once dried, the sample was dry sieved at 250 μm and 125 μm. Each fraction (250 μm - 2 mm, 125 - 250 μm, and <125 μm) was weighed and bagged separately. Note that the 250 μm - 2 mm fraction in this case is argued to represent ice-rafted detritus, and as such was weighed in order to provide an additional measure of ice-rafting, complementing the aforementioned >2 mm clast counts. Furthermore, it is worth noting that the <125 μm fraction was usually very small and only designed to capture any grains which did not penetrate the sieve during the previous wet sieving.

(2) Sediments <125 μm were cleaned of the calgon by diluting them with milli-Q water, and centrifuging them a minimum of three times at 4700 rpm for ten minutes each. The fine fractions were subsequently left to settle out. Once settled, the water was pipetted off, and the sediment was put into the freezer. The frozen samples were subsequently freeze-dried at -56 °C and 0.001 mbar. Dried sediments were weighed, and the total weight of the <125 μm fraction (i.e. sum of this size fraction left after wet and dry sieving) was calculated. The fractions were bagged and added to their respective samples.

All size fractions of each sample were visually checked under a stereo microscope to ensure disaggregation was complete and no diagenetic material was present. The grainsize data gathered from the sieving procedure are attached in Appendix 4. Please also note that the percentage difference in the before and after weights (Appendix 4) is ascribed to salts or gypsum which grew on the core, or cements (e.g. carbonate), as no sample loss occurred during the processing.

3.3.2 Grainsize analysis of the fine fraction (<125 µm)

In order to characterise the background sedimentation, the grainsize distribution of the fine fraction (here defined as <125 µm) was carried out. In order to do so, the previously freeze-dried <125 µm sample fractions were first sub-sampled (~1 g) using the cone-and-quartering method. Using this method ensures representative sub-sampling as the entire sample is heaped and evenly divided into smaller quantities, each containing a representative range of grainsizes. The sub-samples were then submersed in 20 mL of 10% hydrochloric acid (HCl) for approximately one to two hours to dissolve any carbonate. The remaining HCl and reaction product was subsequently removed from the sub-samples by adding milli-Q water to the samples and centrifuging them three times for ten minutes each at 4700 rpm. Organic matter was removed next by adding ~20 mL of 27% hydrogen peroxide (H_2O_2) to the sub-samples for a 72-hour period, whilst heating them in a boiling bath to 70 °C and stirring them occasionally (Lewis and McConchie, 1994). The sub-samples were subsequently washed in milli-Q water and centrifuged three times for ten minutes each at 4700 rpm. The sub-samples were then freeze-dried and weighed to calculate an estimate of the percentage organic and carbonate matter (i.e. initial sub-sample weight minus the final dry weight). Although McCollum (1975) reported a complete lack of diatoms in our sampled range, the initial reports did note a very minor presence of diatoms in cores 23 to 16 (The Shipboard Scientific Party, 1975b), as well as the presence of cristobalite, attributed to the opaline tests of diatoms, between 160 and 35 mbsf (Cook et al., 1975; The Shipboard Scientific Party, 1975b). Nevertheless, sodium hydroxide treatment to dissolve biogenic silica was not deemed necessary as it is unlikely that the minor presence (and complete absence in parts), of diatoms in either form would have had a significant impact on the analyses.

Before being analysed using a Beckman Coulter LS 13 320 laser diffraction particle size analyser (LPS; with the aqueous liquid module), the sub-samples were again sub-sampled (~0.1 to ~0.2 g depending on lithology) to gain an adequate obscuration (6 to 14%) of the laser. Following this, the sub-samples were immersed in ~80 mL of 0.5 g/L calgon and stirred whilst being agitated in an ultrasonic bath for a minimum of 20 minutes. The samples were then analysed for 60 seconds on the LPS. The laser was re-aligned and the background measured before every sample, and the unit was automatically rinsed for 3 minutes after each run. The offset was measured every 30 minutes. Measurements were calibrated using the 'quartz natural' model. 68 µm glass bead standards were run at the beginning and end of every day to ensure the accuracy of the machine.

Due to the small sample size (<0.1 g) required for mud-rich sediments in the LPS, and the poorly sorted nature of the 270 sediments, 106 repeat samples were run throughout the core which showed good reproducibility (Fig. 3.2). A comparison of the mud content of repeat samples and the original measurements displays a very strong correlation ($r^2 = 0.85$ Fig. 3.3), providing confidence in the precision of the subsampling and reproducibility of the results. Moreover, every tenth sample was measured three times to check reproducibility and the internal consistency of the instrument. The precision of the instrument was consistent (Fig. 3.2), further providing confidence in the reproducibility. As the LPS requires the proper obscuration to be obtained prior to analysis, some samples had to be drained and diluted in order to achieve this obscuration. If a sample had to be drained to reduce obscuration values, a new sub-sample of the same sample was run to ensure the reproducibility of the data. For example, in sample 270-256, the first subsample's obscuration was too high, and needed to be drained and diluted to achieve proper

obscuration on the LPS (270-256_A, Fig. 3.2). The subsequent sub-samples (270-256_B, 270-256_C, Fig. 3.2) were run with a lower sample concentration and did not require draining. The difference in the grainsize frequency distribution in this sample highlighted the importance of repeat runs for poorly sorted sediments with the correct volume of sample to attain an appropriate obscuration level for accuracy without draining and dilution, if draining for the first sample run was required. However, despite some exceptions (e.g. 270-256_A), it was generally found that in most other cases where draining was required, there was no significant difference between subsequent sample splits that were run with the appropriate volume and obscuration.

Finally, the data gathered from the LPS was statistically analysed using the GRADISTAT programme (Blott, 2010; Blott and Pye, 2001). The mud content (<63 µm) of each sample was then calculated by multiplying the percentage mud in the fine fraction (<125 µm; derived from the laser particle size analysis), by the percentage of each sample which was smaller than 125 µm (derived from the sieving process). The results of the grainsize analysis of the fine fraction are available in Appendix 5, and combined grainsize data which provides the sample statistics for the whole sample (i.e. fine and coarse fraction combined) is available in Appendix 6.
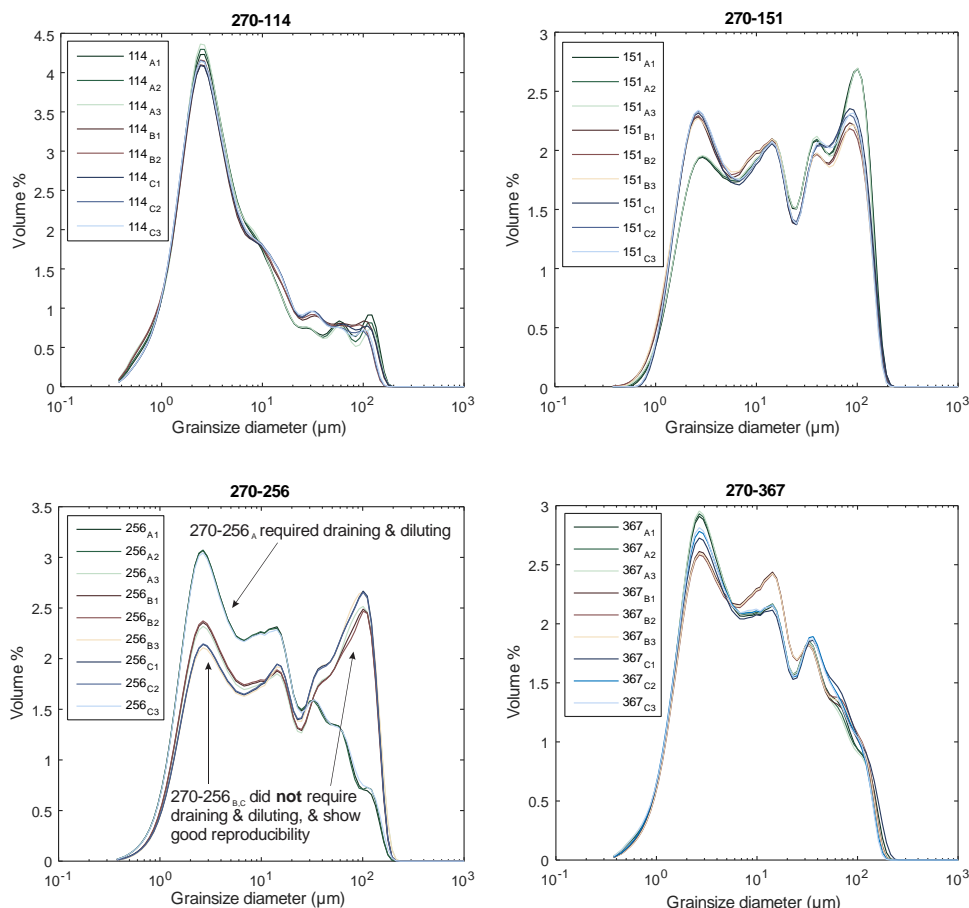
Fig. 3.2: Four representative examples of samples that were subsampled and measured three times (A, B, and C) to test the precision of the subsampling technique. Furthermore, each subsample was measured three times (1, 2, and 3) to test the precision of the LPS. Note that the comparison of 270-256_A to 270-256_{B,C} highlights the importance of measuring additional subsamples (here 270-256_{B,C}) if a sample had to be drained and diluted to acquire the correct obscuration on the LPS unit (here 270-256_A).
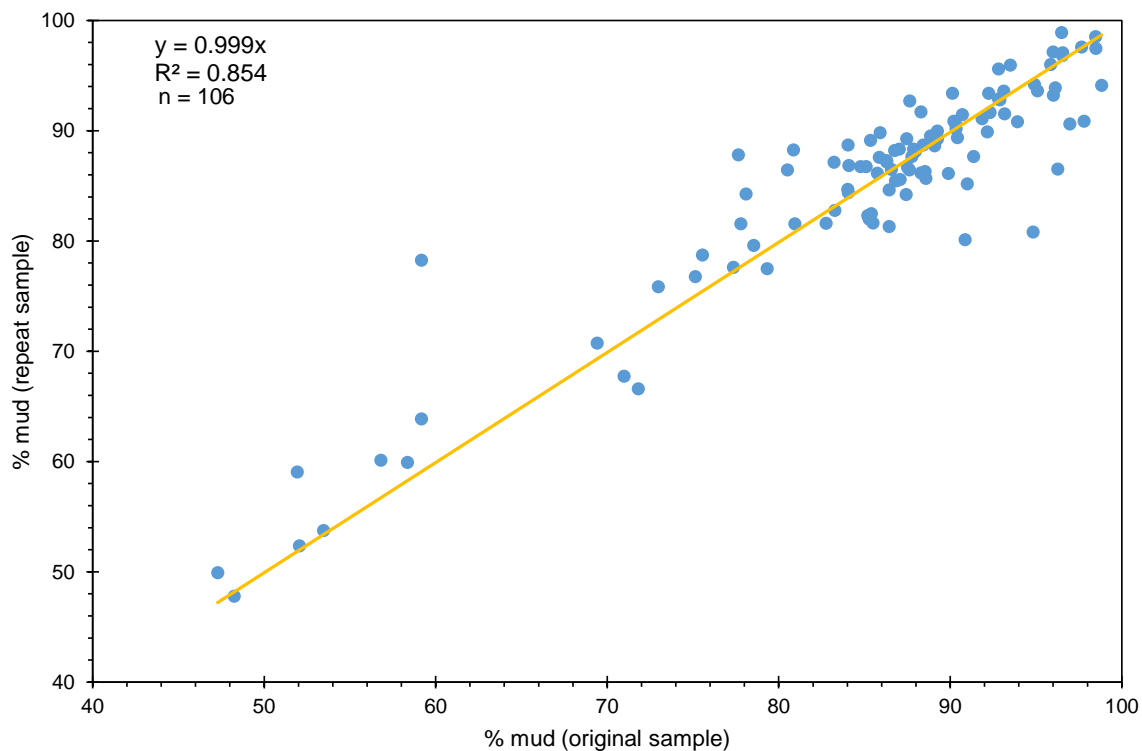
Fig. 3.3: Comparison of the mud content of the original measurements and repeat samples (blue dots). The linear trend (yellow line) with a slope of 0.999 indicates the consistency of results for all analyses, with limited spread of points about the regression line indicating good reproducibility.

3.4 Lithofacies analysis

Lithofacies were defined on the basis of identifying common characteristic noted in the visual descriptions of the lithology, thickness and contact of beds, sedimentary texture (including IRD) and structures, fossil content, and bioturbation. This method for defining lithofacies has previously been successfully used for Antarctic sediments in the Cape Roberts (CRP) and Antarctic Drilling (ANDRILL) projects (Fielding et al., 2000; Krissek et al., 2007; McKay et al., 2009), and the facies schemes from those studies were used a guide to define the facies in DSDP 270.

3.5 Geochemical data

3.5.1 Corescan X-ray fluorescence

Core sections were scanned by me, my supervisory team, and Denise Kulhanek using a third generation Avaatech x-ray fluorescence (XRF) core scanner at the IODP facilities at Texas A&M University, College Station. The core sections were removed from the refrigerated (at 4 °C) core repository several hours prior to being scanned, allowing the core sections to warm to room temperature before XRF scanning. Prior to scanning the core face surface was cleaned of any gypsum and salts which had precipitated during storage.

The core sections were subsequently covered using 4 µm thick Ultralene plastic film in order to protect the sensor of the scanner becoming contaminated with sediment during the scans. Moreover, this also prevents water condensation building up on the inside of the film, which could cause the light element peaks to reduce in amplitude due to the low-energy X-rays being absorbed by condensation (Lyle et al., 2012). To mitigate the chance of false results due to inhomogeneities on the core surface being scanned, the sampled surfaces were carefully adjusted manually to form an even surface prior to analysis.

Scans were conducted at 10 kV and 800 µA, with 20 second contact times, analysing for Fe, Al, Si, P, S, Cl, Ar, K, Ca, Ti, Cr, Mn, Rh and Ba. Due to the drilling disturbance (brecciation) for many parts of the core face, we chose to spot sample (average spacing of ~15 cm) rather than scan the section continuously. Moreover, sediments above 73 mbsf, and between 150 and 230 mbsf were not scanned due to time constraints, as the interval below 230 mbsf held a greater potential to statistically identify Milankovitch scale variability due to its higher recovery rates. The intensities of the elements were measured in total counts. During the scans and subsequent post-processing, peaks of Ar (>300 counts) were used as indicators of air rather than sediments being measured (Helling and Kuhn, 2007). Furthermore, negative Al measurements were taken as indicative of erroneous measurements, and as such all data from these runs were deleted (F. Jiménez-Espejo, pers. comm.). All XRF data of each measurement point were subsequently normalised to the total counts (i.e. all elements) at that point in the core by Dr Francisco Jiménez-Espejo (JAMSTEC). This alleviates the issue of reduced XRF signals due to coarser lithologies, rough surface, porosity, and the formation of a water film due to condensation beneath the foil (Weltje and Tjallingii (2008); F. Jiménez-Espejo, pers. comm.). In order to express the compositional data analysis of the XRF core scanner data, the element counts are plotted as log ratios, which give the statistically most robust record of relative changes in chemistry (Weltje et al., 2015; Weltje and Tjallingii, 2008). Discrete XRF measurements, which would allow the XRF scan data to be converted to absolute figures, were not taken because for this study only the relative changes in element intensities down core were of interest. Finally, principle component analyses (PCA) on the XRF dataset were carried out by Dr Francisco Jiménez-Espejo (JAMSTEC) in order to identify trends in the data and identify possible factors influencing the data. The PCA were carried out following standard, previously employed methods (e.g. Bahr et al. (2014)). The normalised XRF data are attached in Appendix 8.

3.5.2 ICP-MS

40 sediment samples (~5 g each), representing an average sample spacing of ~9.5 m between 16.8 and 384.7 mbsf, were obtained from the DSDP 270 material stored at GNS Science, and were sent to the Japan Agency for Marine-Earth Science and Technology (JAMSTEC), where they were analysed by Dr Francisco Jiménez-Espejo as follows: Visually identifiable IRD was first removed from the sediments so that it does not bias the results. Each sample was then weighed before being digested with a mixture of nitric acid (HNO_3) and hydrofluoric acid (HF) at 120 °C overnight. After drying, each sample was then treated with HNO_3 several times to dissolve by-products such as calcium fluoride (CaF_2). Samples were then re-dissolved in diluted HNO_3, and trace element compositions were measured by external calibration method with a Thermo Scientific iCAP quadropole inductive coupled plasma-mass spectrometry (ICP-MS) at JAMSTEC. The procedural blank was nearly negligible for all elements presented in this study. The trace element data is attached in Appendix 9.

3.6 Magnetic susceptibility

The magnetic susceptibilities (κ) of the sediments were measured by me at the IODP facilities at Texas A&M University, using a Bartington MS2 magnetic susceptibility meter loop (Bartington MS2C sensor), mounted atop a core linescanner. The magnetic susceptibility meter was zeroed before each core. Measurements were taken every 2.5 cm; however, it is noted that each measurement integrates over a 20 cm area (i.e. 10 cm either side of the loop). Core void measurements were removed from the data set, although due to the aforementioned spatial integration of data voids may still have affected other measurements by reducing their amplitude (Nowaczyk, 2001). The magnetic susceptibility data are attached in Appendix 10.

3.7 Spectral analysis

In order to conduct spectral analyses of the sediments recovered from DSDP Site 270, the mud (<63 µm) and coarse sand (250 µm – 2 mm) content of the sediments between 348 and 250 mbsf were sampled every 40-45 cm. This results in a temporal resolution of ~2-2.5 kyr based on the initial age model (Kulhanek et al., in prep.; see Results chapter), which is high enough to avoid aliasing the signal of orbital variability. These two datasets were investigated separately for orbital frequencies using the astrochron package in the computer programme R (Meyers, 2014). The methodology presented here follows that of a previous study where the resolution of the independent age control was also coarser than that of the orbital periods (Meyers et al., 2012). Using this method, the results of this study are largely independent of the age model, which is yet to be fully completed. The codes used for the spectral analyses are available in Appendices 11 and 12.

The data were first linearly interpolated and any existing linear trends were removed. The multitaper method (MTM; Thomson (1982)), modified by Meyers et al. (2012) to incorporate the noise estimation of Mann and Lees (1996), was then used to identify significant frequencies in the depth domain of the data. The MTM analyses were run from 0 cycles/m to the Nyquist frequency of 1.25 cycles/m.

Following this, the orbital target frequencies to which the frequencies identified in the datasets recovered from DSDP 270 will be tuned for the approximate age of the sampled interval (23 to 24.5 Ma) had to be identified. This was done by applying the MTM to existing theoretical astronomical models for the late Oligocene: the time domain models of Laskar et al. (2004) and Laskar et al. (2011), as well as the frequency domain model of Berger et al. (1992). The resultant periods are listed in Table 3.3.

Table 3.3: Orbital target periods identified using MTM analysis of 0.5 Ma intervals for the model of Berger et al. (1992), and 1.5 Ma intervals for the 2004 (La04) and 2011 (La11) models of Laskar (Laskar et al., 2011; Laskar et al., 2004). Notations for the orbital periods are: E - eccentricity, O - obliquity, P – precession.

Orbital period	Berger					La04	La11	Laskar
	23 Ma	23.5 Ma	24 Ma	24.5 Ma	Mean	23-24.5 Ma	23-24.5 Ma	Mean
E1	N/A	N/A	N/A	N/A	N/A	395.053	417.917	406.485
E2	N/A	N/A	N/A	N/A	N/A	136.473	120.843	128.658
E3	N/A	N/A	N/A	N/A	N/A	92.667	93.738	93.203
O1	53.126	53.107	53.088	53.069	53.098	52.490	N/A	N/A
O2	40.494	40.483	40.472	40.461	40.478	39.714	N/A	N/A
P1	22.816	22.812	22.808	22.804	22.810	23.383	N/A	N/A
P2	18.908	18.906	18.904	18.902	18.905	18.672	N/A	N/A

Subsequently, evolutive harmonic analyses (EHA) were conducted on the two detrended and linearly interpolated datasets from DSDP Site 270 to investigate the stability of the sedimentation rate, as a change in sedimentation rate over the course of the sampling interval could skew the data. The EHA was conducted using window sizes of 34 m in steps of 0.2 m. The results were normalised, and padded with zeroes to 1000 points, a standard procedure to enhance the clarity of the signal without affecting the integrity of the data.

After assuring that the sedimentation rate was constant, average spectral misfit (ASM) analyses were conducted on each dataset. The ASM is an inverse method, which based on a given set of possible sedimentation rates, calculates the alignment between measured spectral peaks (frequencies) in a stratigraphic dataset and a set of targeted orbital periods (Meyers and Sageman, 2007; Meyers et al., 2012). The ASM represents the average distance from the targeted and measured peaks, and is measured in cycles per thousand years (cycles/ka). As part of these calculations the ASM calculates the most plausible sedimentation rate, which has to surpass the critical significance level of 0.5%, and thereby reject the null hypothesis (H_o) of no orbital periods being present in the dataset (Meyers et al., 2012).

The ASM analysis requires several key inputs: the frequencies obtained from the data, the orbital frequencies to be tuned to, the Rayleigh and Nyquist frequencies, and plausible sedimentation rates. Given the two plausible orbital models (Berger et al., 1992; Laskar et al., 2011; Laskar et al., 2004), two ASM analyses were conducted per dataset in this study:

(1) between the (a) frequencies identified as significant in the MTM analyses, and (b) the tuning targets for obliquity and precession derived from Berger et al. (1992), as well as the mean values for eccentricity derived from the work of Laskar (Laskar et al., 2011; Laskar et al., 2004); and

(2) between (a) the frequencies identified as significant in the MTM analyses, and (b) the averaged data from Laskar and others (Laskar et al., 2011; Laskar et al., 2004).

Note that the tuning targets always involved the mean periodicities spanning the plausible time frame of deposition of the sediments following the methodology of Meyers et al. (2012). The frequencies were then simply derived by dividing one by each of these periods. The Rayleigh and Nyquist frequencies used in the analyses were those identified during the

earlier MTM analyses of the percent mud and coarse sand datasets. Based on the preliminary age model (Kulhanek et al., in prep), the sedimentation rate for the sampled interval can be constrained to between 10 and 35 cm/ka (see Results chapter). As such, the ASM analyses for each dataset were performed for 100 different sedimentation rates between 10 and 35 cm/ka. Moreover, 100000 Monte Carlo simulations were run per ASM analysis in order to test the significance of the data. Finally, using the sedimentation rates derived from the ASM analyses, the spectra were calibrated to determine a relative timescale.

3.8 Photographic line-scan

All core sections between 0 and 389 mbsf were photographed in high resolution using a Nikon 60 mm camera lens mounted on a custom built linescanner at the IODP facilities at Texas A&M University, College Station. Based on these linescan images, red-green-blue (RGB) data were recorded at a 1 cm resolution. RGB data of core voids were rejected. Photographs of the core sections can be found in Appendix 1.

Chapter Four
RESULTS

4.1 Lithostratigraphy

The initial shipboard description of the core described a 3 m thick sequence, between 385 and 388 mbsf, of sandstones that pass downward from glauconitic greensand into a calcareous sandstone and a carbonaceous sandstone. These sandstones overly a buried terrestrial regolith and breccia, which in turn rest unconformably on top of metamorphic basement rocks at the base of the core (Fig. 4.1; The Shipboard Scientific Party (1975b)). The sandstones were described to be overlain by a 365 m thick sequence of glacimarine mudstones containing macro- and microfossils, as well as IRD. Diamictites were judged to have only been deposited above 100 mbsf (The Shipboard Scientific Party, 1975b).
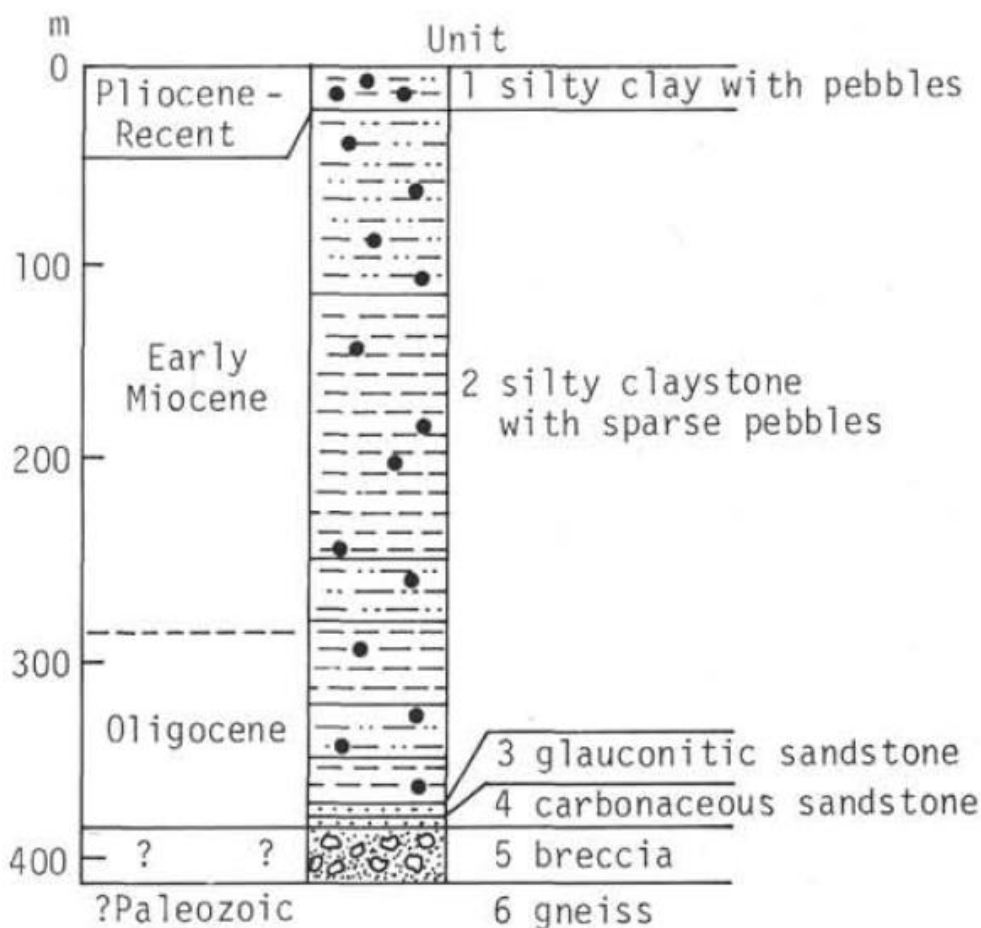
Fig. 4.1: Summarised version of the original lithostratigraphic logs, divided into six units, where the ages are based on the initial age model (Barrett, 1975b). For the original detailed lithostratigraphic logs refer to The Shipboard Scientific Party (1975b).

The new high-resolution stratigraphic logs in this study focused on the glacimarine interval overlying the 1 m thick glauconite bearing sandstone at 385 mbsf. As such, the stratigraphy below 386 mbsf in the new lithostratigraphic log (Fig. 4.2) was adopted from The Shipboard Scientific Party (1975b). The stratigraphy above 385 mbsf can be broadly divided into six intervals, as is described below:

(1) Overlying the glauconitic sandstone at 385 mbsf is a bioturbated, organic-rich, massive claystone with a sharp basal contact. Resting on top of the claystone is a ~30 m repetitive sequence of fine sandstones of varying thickness (centimetre to decimetre scale) with sharp bases grading up into decimetre-scale siltstones, containing variable amounts of IRD. The sandstones, as well as mudstones, can be bioturbated, and the most intense bioturbation occurs between 377 and 384 mbsf. Any shells present were usually fragmented.

(2) Between ~348 and 252 mbsf, these interstratified sandstones and siltstones are replaced by a sequence of predominantly massive siltstones containing dispersed to abundant IRD of metasedimentary and igneous lithologies, and rare shell fragments.

(3) The siltstones are overlain by a ~30 m thick sequence of sandy to muddy diamictites, with very rare interbeds (<1.5 m) of siltstones. The diamictites are predominantly massive, but weak stratification is noted in places on the basis of grainsize changes. The clasts are predominantly metasedimentary and igneous in lithology, and many contain striations. Shells are rarely present, but if so are fragmented. Moreover, no bioturbation is noted in the diamictites. Where the diamictites are interbedded with mudstones the contacts are gradational. The diamictites are in turn conformably overlain by IRD bearing siltstones, similar to those found below the diamictites, and ~5 m of millimetre-scale rhythmic couplets of sandstone and siltstone. The couplets have distinct sharp bases, and are composed of fine sandstones and siltstones grading into finer mudstones. Moreover, they lack bioturbation or macrofossils.

(4) Clayey mudstones form the dominant lithology over the next ~70 m of the core, with occasional interbeds of siltstones and very rare diamictites. The basal contacts of the siltstone interbeds are usually gradational, while those of diamictites are sharp. The clayey siltstones are predominantly massive, but weak stratification is noted in places based on changes in grainsize. Their clast (IRD) content is very low compared to other sediments recovered from DSDP 270, however, they contain abundant millimetre- to centimetre-scale carbonaceous stringers and lenses. Furthermore, rare articulated bivalves can be found in addition to shell fragments.

(5) Separated by a 5 m core break is a 100 m thick interval of clast-bearing siltstone deposits, which are again similar to those found between 252 and 348 mbsf. However, their clast content is lower compared to the previous siltstones further downcore, but the clasts did not display an obvious change in lithologies. Shell fragments are again rare in these siltstones, which are predominantly massive. This sequence of siltstones is commonly interbedded by diamictites, which are primarily less than 1 m thick, and characterised by gradational lower and upper contacts.

(6) The upper 20 m of the core are composed of significantly younger mudstones (Kulhanek et al., in prep.; The Shipboard Scientific Party, 1975b), and the top 3 m of the core are characterised by the sole appearance of diatom-rich clays.

Fig. 4.2 (overleaf): Lithostratigraphic log of the sediments recovered at DSDP Site 270 and re-described in this thesis. The width of the column is based on visual observations. Lithologic abbreviations are: Cl – clay, Slt – silt, Sd – sand, Grv – gravel. The stratigraphy below 386 mbsf is adapted from The Shipboard Scientific Party (1975b). Facies numbers refer to the glacimarine facies described in detail in section 4.3. Facies numbers represent the following facies: 1 – mudstone; 2 – mudstone with dispersed to common clasts; 3 – sandstone (interbedded with mudstone); 4; rhythmically interlaminated sandstone/siltstone with mudstone; 5 – massive diamictites; 6 – stratified diamictites; 7 – glauconitic sandstone. Facies were not assigned to sediments above 20 mbsf, as these sediments are significantly younger than the rest, or below 385 mbsf, as these units are not glacimarine. Lithostratigraphic units (LSU) are shown for reference and are discussed in section 5.1. Original units refer to the units described by The Shipboard Scientific Party (1975b).
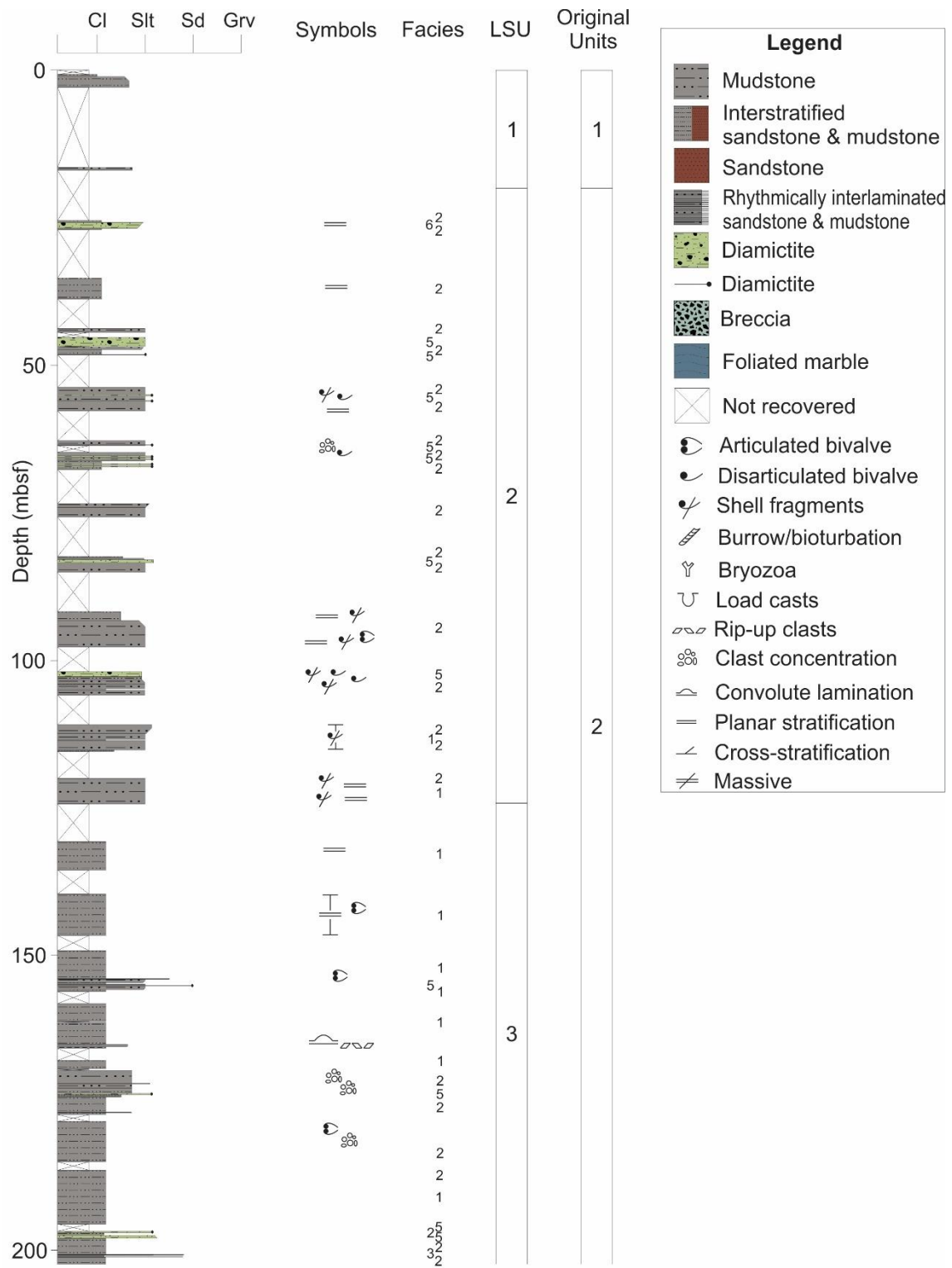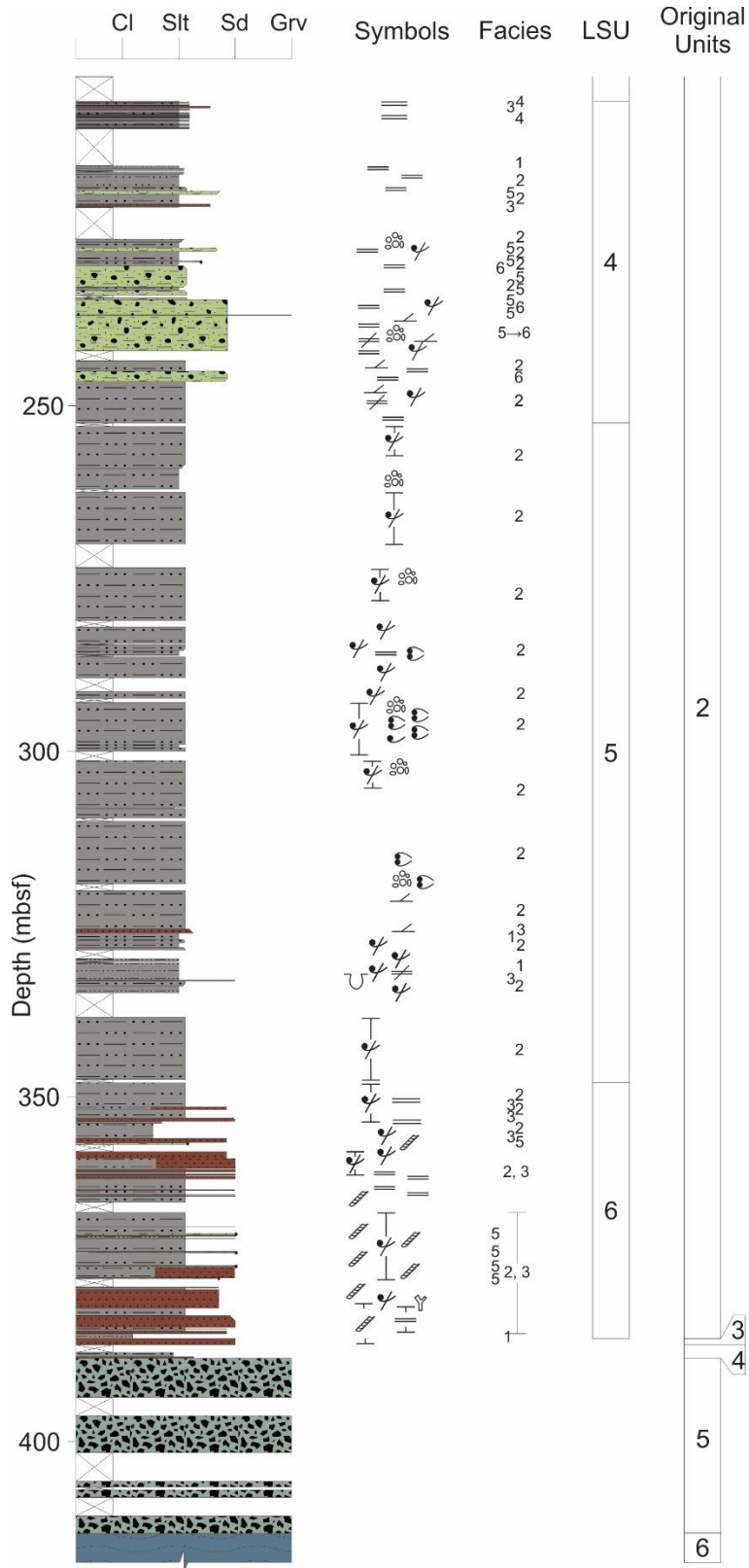
4.2 Grainsize

4.2.1 Ice-rafted debris (visual clast count and coarse sand fraction)

Two independent proxies of IRD were utilised in the effort to characterise changes in ice volume over time: (1) visual counts of extraformational clasts exceeding 2 mm in diameter, which are exposed in the cut core face of the archive half of the core, binned into 10 cm intervals; and (2) the weight percent of the 250 µm to 2 mm grainsize fraction, following the methodology of Naish et al. (2006). As shown in Figure 4.4, both proxies are largely consistent, and can be grouped into five distinct intervals (from bottom to top): (1) from the base of the glacimarine sediments up to ~350 mbsf, the IRD content is highly variable (0.2 - 7 wt% coarse sand; 0 - 26 clasts/10 cm), but generally increasing. This is followed by (2) an increase in baseline values (~4 weight percent (wt%) coarse sand; ~5 clasts/10 cm), which remain fairly constant until ~250 mbsf. Interestingly, the visual clast count appears to show more variability throughout this interval than the coarse sand fraction. (3) The interval between 250 and 220 mbsf is characterised by a large increase (up to 20 wt% coarse sand, and 51 clasts/10 cm) in ice-rafted debris. (4) The IRD subsequently decreases significantly to extremely low baseline values (~0.5 wt% coarse sand; ~2 clasts/10 cm) between 220 and 125 mbsf; and (5) the amount of IRD present increases again above ~125 mbsf, but never recovers to the previous baselines (here baseline values are ~2 wt% coarse sand; ~3 clasts/10 cm). These findings are broadly consistent with the previous coarse resolution estimates of IRD using clast counts and weight percentages of the coarse sand fraction (Balshaw, 1981; Barrett, 1975b). An IRD mass accumulation rate was not calculated because the exact sedimentation rates in each interval cannot yet be determined based on the present status of the age model (Kulhanek et al., in prep.), and diagenesis of the lithified sediment compromises the use of dry bulk density in determining mass changes resulting from variable sedimentation. Thus only constant values for linear sedimentation rates and dry bulk density could be assumed, which would result in an identical curve shape to that of the values of the weight percent of coarse sand (Fig. 4.4).

4.2.2 Interpretation of coarse sand as IRD

The coarse sand fraction can either be interpreted as being of ice-rafted origin, or as a lag deposit following the winnowing of the fine fraction by currents. Previous studies have suggested that should a peak in IRD coincide with well-sorted fine grained terrigenous material (<125 µm), then the IRD peak would reflect a lag deposit of coarse sand after currents winnowed the finer grained sediments, rather than ice-rafting (Passchier, 2011; Patterson et al., 2014). To ensure the correct interpretation of the records, the sorting of the fine fraction was calculated using the Folk and Ward method (Folk and Ward, 1957) in the GRADISTAT programme (Blott, 2010; Blott and Pye, 2001). The results of this analysis show that there is a complete absence of well-sorted fine fractions in the DSDP 270 sediments (Fig. 4.4C). It can therefore be assumed with relative confidence that the changes in the coarse sand fraction in the glacimarine sediments reflect an ice-rafted origin. Furthermore, similarly to Patterson et al. (2014), the lack of any fine-grained sediment which is moderately or well sorted, in combination with the largely massive (or very weakly bedded) structure of the glacimarine sediments indicates that bottom currents likely were never strong enough for erosion to have been greater than deposition. The suggested absence of strong bottom currents is consistent with the interpretations by The Shipboard Scientific Party (1975b), who also described an absence of sedimentary structures expected

from bottom currents. In addition, the foraminiferal assemblages suggest that the water column was deep enough, and the sedimentation rates high enough to mask bottom currents (Leckie and Webb, 1983). Furthermore, Barrett (1975b) described the grainsize in the glacimarine sequence as being similar to subglacially derived tills in Ohio (USA). This comparison suggests that the sediments at Site 270 were likely eroded and transported by grounded ice sheets with little to no subsequent modification in grainsize distribution during glacimarine deposition. This implies that shear stress on the sea floor was at or below the lower limits for the movement of sediment. He does however note that weak traction currents may have acted in places, citing occasional weak stratification as evidence.

4.2.3 Grainsize characteristics of the fine fraction (<125 µm)

The results show that the fine fraction is predominantly polymodal (Fig. 4.3), and poorly to very poorly sorted (Fig. 4.4C). Changes in the mud content (Fig. 4.4D) can be grouped into five distinct intervals that broadly overlap with the distinct IRD intervals discussed in section 4.2.1: (1) a highly variable mud content, ranging between 83% and 30%, between 385 and 348 mbsf; (2) a more consistent baseline percentage of mud, of ~70 to 75%, between 350 and 250 mbsf; (3) a drastically decreased mud content to values as low as 22% between ~250 and 200 mbsf; (4) a renewed baseline increasing up to 85% mud content between 200 and 150 mbsf; (5) above 150 mbsf, there is again a slight decrease in mud content, marked by a ~5-10% drop in baseline values. As expected, the percent mud co-varies with the mean grainsize of the fine fraction (Fig. 4.4E). Furthermore, the mean grainsize of the fine fraction (<125 µm) remains well below the sand-silt boundary (63 µm) throughout the core, varying primarily between 5-15 µm, and is coarsest (up to ~40 µm) in intervals dominated by diamictites, or sandier beds (Fig. 4.4E).
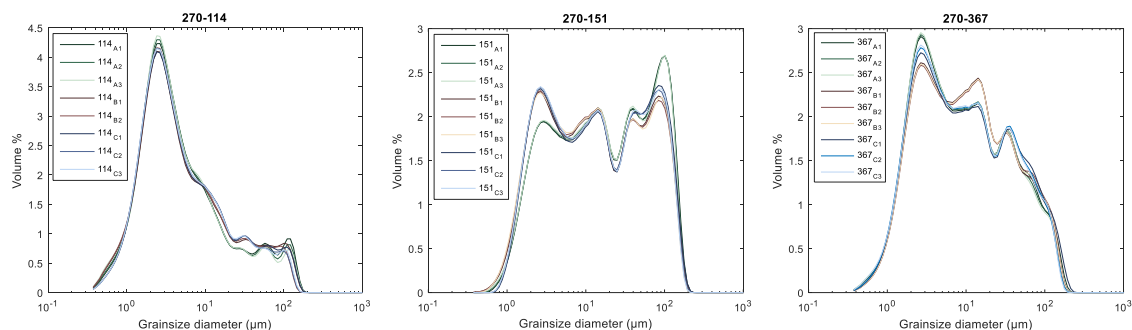
Fig. 4.3: Representative examples of the polymodal grainsize distributions of the fine fraction. Three subsamples (A, B, C) of each of three samples graphed (270-114, -161, -367) were measured, and each subsample was again measured three times (1, 2, 3). This was done to show the precision of the subsampling technique and the LPS unit, respectively.

Fig. 4.4 (overleaf): Summary of the grainsize analysis results plotted against a simplified lithologic log (A). The variation of clasts >2 mm in diameter, and the weight percentage of the coarse sand fraction are shown in (B). The dashed lines in (B) show the five intervals of IRD deposition which have been identified. (C) shows the sorting of the fine fraction, classified according to the definitions of Folk and Ward (1957). Note that all samples were poorly to very poorly sorted. The total volume percent mud of each sample is depicted in (D). (E) shows the mean grainsize (in µm) of the fine fraction.
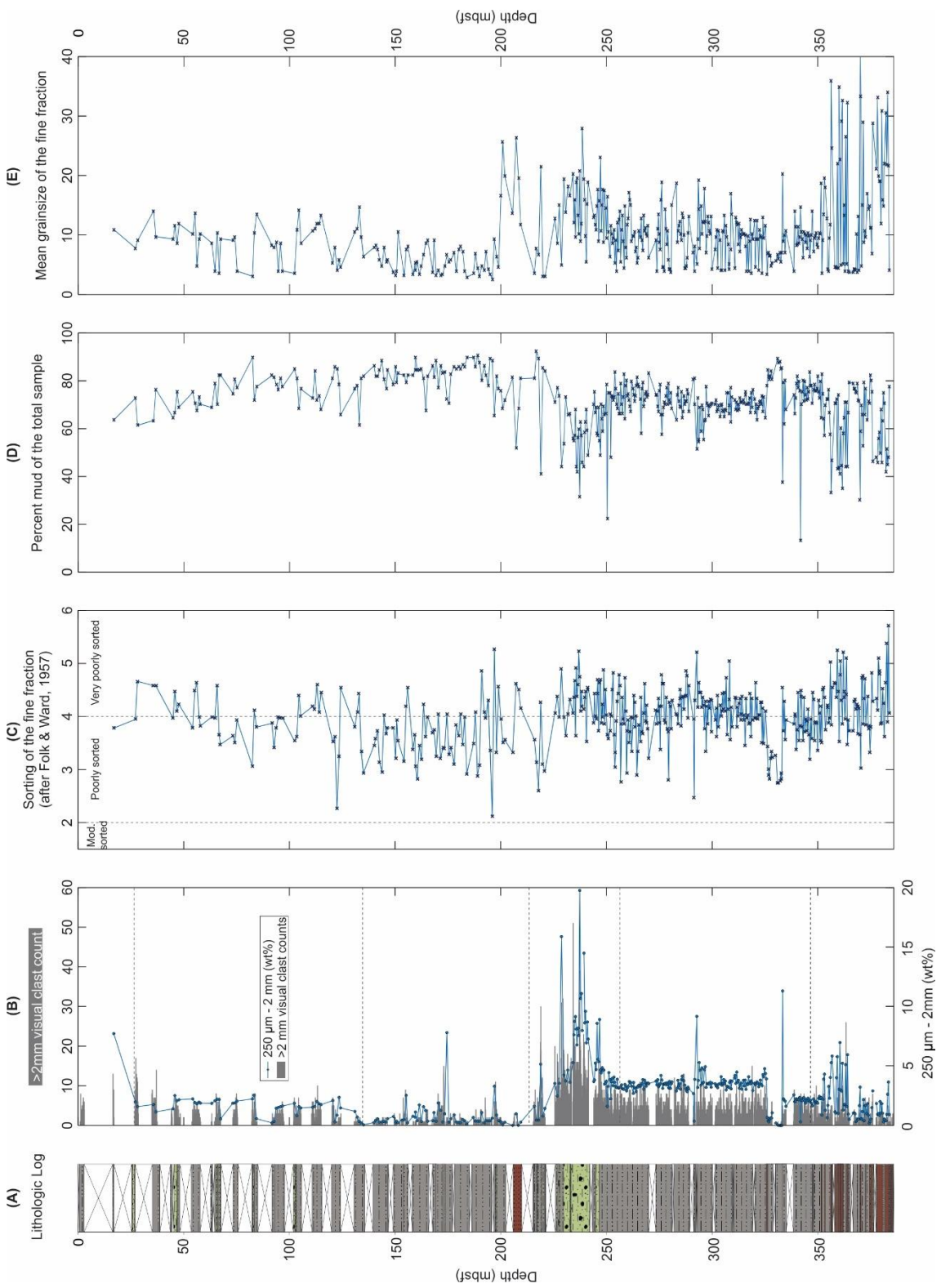
4.3 Lithofacies analysis

Six lithofacies were recognised between 385 and 20 mbsf in the cores recovered at Site 270 (Table 4.1). The facies classified here represent environments influenced by a combination of glacial proximity, as well as water depth. The facies are described below, and a range of possible depositional environments they may represent is outlined based on previous studies of high-latitude glacimarine records and environments. Each facies description and interpretation is concluded with a preferred interpretation of its depositional environment. These depositional environments are all interpreted to be glacimarine, and range from distal to very proximal to the ice front. Notably no subglacial facies are thought to have been deposited between 385 and 20 mbsf at DSDP 270. Each of the facies also has characteristic grainsize distributions of the fine fraction, which are plotted in Figure 4.5.

Table 4.1: Summary of the glacimarine facies recognised between 20 and 385 mbsf (Unit 2 of the Initial Reports (The Shipboard Scientific Party, 1975b)) at DSDP Site 270. Note that the sum of the total thickness does not equal 365 m because the sum of unrecovered intervals is not listed. The facies proportions are calculated based on recovered sediments only (i.e. excluding core voids). The full data are available in Appendix 7.

Facies Code	Simplified Description	Preferred interpretation	Thickness (m)	Prop. (%)
1	Mudstone	Hemipelagic settling, with distal ice rafting	48.85	20.29
2	Mudstone with dispersed to common clasts	Hemipelagic settling, with proximal ice rafting	145.04	60.24
3	Sandstone (interbedded with mudstone)	Turbidity currents and suspension settling	22.90	9.51
4	Rhythmically interlaminated sandstone/siltstone with mudstone	Proximal proglacial sediment plumes	3.57	1.48
5	Massive diamictite	Proximal ice rafting, re-deposition	11.53	4.79
6	Stratified diamictite	Proximal ice rafting, re-deposition	8.87	3.68
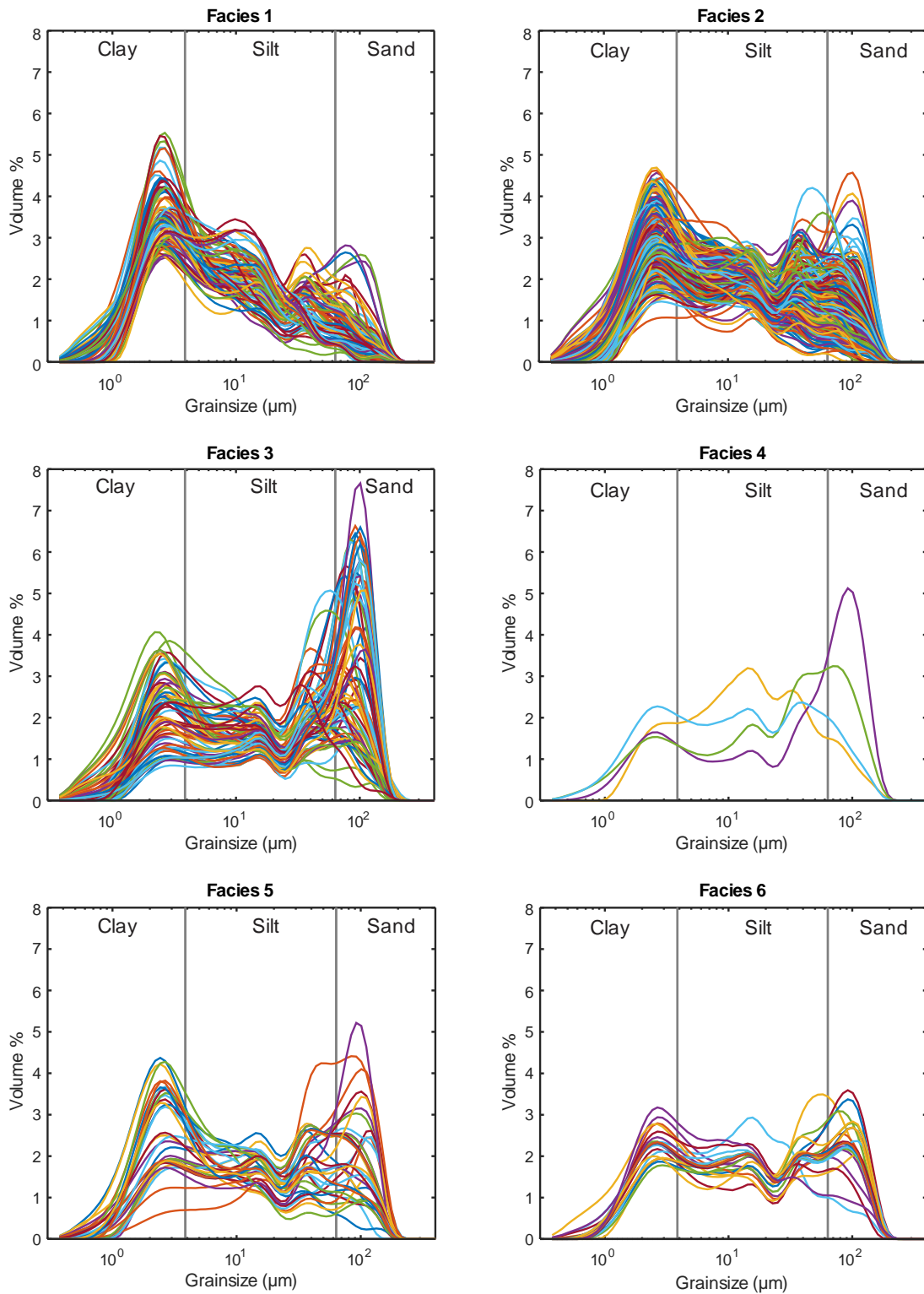
Fig. 4.5: Grainsize distributions of the fine fractions of each of the six glacimarine facies. Grey bars mark the changes between clay and silt (3.9 µm), as well as silt and sand (63 µm).

4.3.1 Facies 1 – mudstone

Description

This facies is composed of light grey, silty claystones to sandy siltstones (Fig. 4.6). It is predominantly massive, although weak horizontal stratification and very rare convolute laminations can be observed on the basis of changes in grainsize. Extraformational clasts are absent to rare, but when present consist of igneous (gabbro, diorite) and metasedimentary (quartzite, marble) lithologies, are sub-rounded to angular, and are up to 50 mm in diameter. Concentrations of clasts are observed sporadically, but are also extremely rare. Sandy and clay-rich lenses occur in places, although the latter are less common. Extremely rarely mud intraclasts are also recorded. Shell material is usually absent, although rare fragments, and very rare articulated bivalves are found. Carbonaceous fragments (cm-scale) in the form of stringers and lenses are common. Toward the base of the core this facies is often bioturbated and more organic rich, which is reflected in a more purple colour of the sediments. Very rare (e.g. at 154.92 – 154.94 mbsf) interbeds of facies 6 (stratified diamictite) can also be observed.

Possible interpretations

Deposits such this facies may be distal or proximal to grounded ice. The dominant mudstone lithology, with rare to absent outsized clasts and low contents of sand, suggests an environment dominated by hemipelagic suspension settling, with occasional sediment input from ice rafting (Fielding et al., 2000; Krissek et al., 2007; McKay et al., 2009).

Generally high-latitude studies agree that the combination of fine-grained mudstones and low IRD contents are likely representative of low energy, ice distal environments (Dowdeswell et al., 1998; Eyles and Eyles, 1992; Fielding et al., 2000; Ó Cofaigh and Dowdeswell, 2001). In these cases, the fine-grained sediment may be derived from high sediment input from meltwater plumes, which emanated from the ice front (Dowdeswell et al., 1998; Elverhøi et al., 1980; Evans et al., 2002; Eyles and Eyles, 1992; Sexton et al., 1992; Svendsen et al., 1992). Where these mudstones are most bioturbated, and/or more massive they are generally interpreted as being most ice distal (Dowdeswell et al., 1998; Eyles and Eyles, 1992; Krissek et al., 2007; McKay et al., 2009; Ó Cofaigh and Dowdeswell, 2001). This is because sedimentation rates are higher in more grounding line proximal settings, inhibiting benthic organisms from thriving.

Weak horizontal and convolute stratification may reflect the distal parts of sediment gravity flows (Krissek et al., 2007; Ó Cofaigh et al., 2001). Alternatively, laminations in fine grained mudstones have also been taken as indicative of bottom currents, or submarine outwash winnowing the fine fraction, or of suspension settling of turbid plumes, indicating the presence of subglacial meltwater. Lenses of silt and sand may be the distal component of turbidity flows, or are potentially wind-blown/sea ice rafted debris (Krissek et al., 2007). Organic matter, such as the carbonaceous stringers and lenses observed in this facies, have been recorded in other mudstones lacking clasts in other glacimarine environments, where they indicate discharge of terrestrial organic material (Fielding et al., 2000; Powell and Molnia, 1989).

Silty claystones lacking IRD have also been interpreted as being deposited below an ice shelf, which lacks subglacial debris, in a polar glacial regime at a significant distance from any basal debris (Domack et al., 1999; McKay et al., 2008). In such a setting laminations

and bioturbation may be present. Similarly, mudstones lacking outsized clasts have also been interpreted to have been deposited beneath sediment-poor shore-fast sea ice in some glacimarine environments (Ó Cofaigh and Dowdeswell, 2001).

Preferred interpretation

The preferred interpretation is that facies 1 represents an ice distal environment, with sedimentation primarily derived from hemipelagic settling and only very occasional ice-rafting. A sub-ice shelf setting for facies 1 seems less likely, as the evidence (e.g. sedimentation rate) does not suggest that it was deposited in a polar glacial regime (section 5.1.6).

Fig. 4.6: Facies 1 – mudstone (core 17, section 3). Note the lack of clasts. Stratigraphic top is to the left, and the scale bar is 5 cm long.

4.3.2 Facies 2 – mudstone with dispersed to common clasts

Description

Facies 2 consists of light olive, to light or dark grey, silty claystones to sandy mudstones which contain dispersed (<1%) to common (1-5%) clasts (Fig. 4.7). Clasts are predominantly less than 10 mm in diameter, but can reach up to 30 mm across. These clasts are angular to sub-rounded, and composed of a variety of lithologies, including plutonic igneous (diorite, dolerite, granodiorite, granite, gabbro), metasedimentary (marble, quartzite) and metavolcanics. Centimetre-scale concentrations of these clasts (Fig. 4.7C), as well as sand lenses can be observed in places. Weak to moderate horizontal stratification up to decimetre scale can be observed on the basis of matrix grainsize changes, clast alignment or bedding related fractures. Moreover, high-angle cross-stratification can also be found when interstratified with diamictites between 225 and 250 mbsf (Fig. 4.7A). Shell fragments are often sparse, but can be common in places, and disarticulated and articulated bivalves may be found. Bioturbation is also evident throughout this facies. Locally this facies can be interbedded with facies 6 (diamictite) on a centimetre to decimetre scale. Furthermore, this facies frequently coarsens into muddy diamictites (facies 5 and 6) at its base, while in some places an upward fining is also observed. The mudstones are carbonate cemented in places and occasionally contain mudstone intraclasts. This is the most abundant facies at DSDP 270.

Possible interpretations

The depositional environment is generally similar to facies 1, where sedimentation is dominated by hemipelagic settling of muds derived from a pro-grounding line marine environment. The extraformational clasts point to rainout from floating ice (ice shelf or icebergs), but where clast concentrations are present they indicate deposition beneath

icebergs tipping over, causing an instant dumping of sediment (Krissek et al., 2007; McKay et al., 2009; Powell and Cooper, 2002).

The increased IRD content of this facies, relative to other mudstone facies (e.g. facies 1), is interpreted to reflect a more proximal setting to the ice front (Evans et al., 2002; Krissek et al., 2007; McKay et al., 2009; Powell et al., 2000; Powell et al., 2001). Increased amounts of IRD are often related to deposition during an advance or retreat of the ice front (Dowdeswell et al., 1998). However, the IRD content may also change as a result of: the type of glacier front, debris content of ice, drift patterns of icebergs, the presence of an ice shelf, water temperatures, and the basal condition of the ice mass from which the floating ice was derived (frozen or melting/freezing) (Ó Cofaigh and Dowdeswell, 2001). Thus the higher IRD content of this facies does not necessarily reflect a more ice proximal environment.

Bedding, especially when combined with an upward fining sequence, may be the result of distal sediment gravity flows, and/or indicate an increased proximity to an ice sheet grounding line (Ó Cofaigh and Dowdeswell, 2001; Ó Cofaigh et al., 2001; Stow and Piper, 1984). Some studies also suggest that where ice proximal sediments are laminated, the ice mass probably discharged significant volumes of subglacial meltwater, and therefore likely had a polythermal or warm-based basal regime (Ó Cofaigh and Dowdeswell, 2001). However, this does not strictly imply a temperate glacial regime as it only implies the base of a glacier is at the pressure melting point, which also occurs in subpolar glacial regimes.

Where bioturbation, and/or articulated bivalves are present, the depositional environment is likely more ice-distal and less turbid in order to allow for a benthic community (Benn and Evans, 2010; Eyles and Eyles, 1992; Krissek et al., 2007; McKay et al., 2009; Ó Cofaigh and Dowdeswell, 2001).

Alternatively, when this facies is interbedded with diamictite facies (5 and 6), they may represent deposition in a subglacial environment, especially where bioturbation is absent (Krissek et al., 2007; McKay et al., 2009). The high-angle cross stratification (Fig. 4.7A) found in these interbeds may be the result of glacitectonic deformation (e.g. Benn and Evans, 2010) and therefore support the notion of a subglacial origin, however, it may also be the result of submarine sliding/re-deposition (e.g. Krissek et al., 2007).

Preferred interpretation

Facies 2 was most likely deposited more proximal to the ice front than facies 1. This is based on the higher IRD content, which usually, though not always, indicates a more ice-proximal location. Moreover, the silt/sand content (Fig. 4.5) is also greater in facies 2 than 1, further suggesting a more energetic/turbid environment (e.g. closer to a grounding line), where the finer particles cannot settle out.

Based on the absence of substantial sedimentological and structural features indicative of subglacial deposition (see section 4.3.5), with the possible exception of the cross-stratification, a subglacial origin for deposits of facies 2 which are interbedded with diamictites is tentatively precluded.
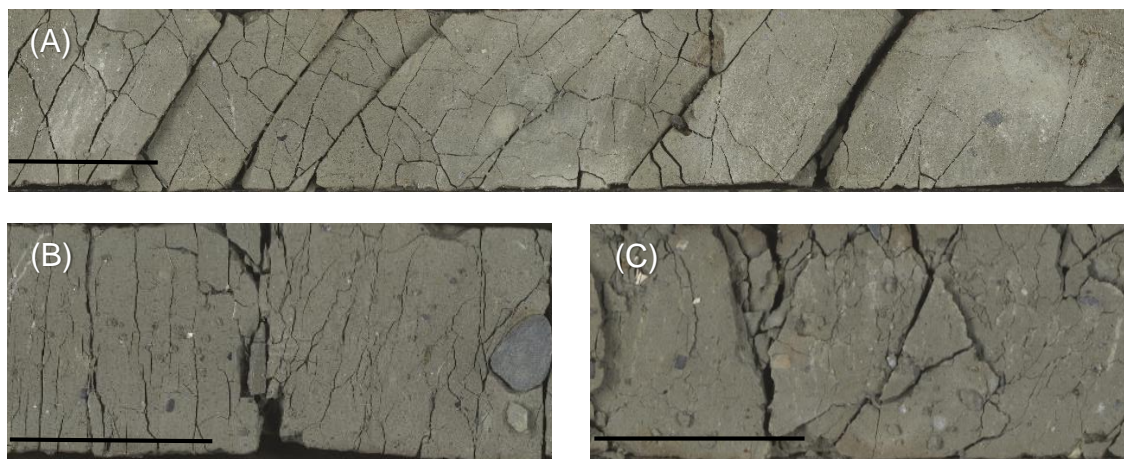
Fig. 4.7: Three examples of Facies 2 – mudstone with dispersed to common clasts (A – core 28 section 1; B – core 32, section 3; C – core 35, section 3). Note the high-angle cross stratification in (B), and the large clast at the bottom of (A). (C) shows a clast concentration within the mudstone. Stratigraphic top is to the left, and the scale bars is 5 cm long in all images.

4.3.3 Facies 3 – sandstone (interbedded with mudstone)

Description

This facies consists of centimetre (Fig. 4.8A, B) to decimetre-scale (Fig. 4.8C) muddy to very fine sandstone beds, with sharp and irregular basal contacts fining upwards into mudstones (up to 1 m thick). Both the sandstone and mudstone beds display weak to moderate (in mud), millimetre to centimetre scale stratification, as defined by clast and granule alignment. The sandstone beds are frequently carbonate cemented, contain soft sediment deformation features, such as contorted bedding, and sometimes occur as alignments of lenses. Diffuse sand lenses and dikes (Fig. 4.8D), as well as rare to dispersed angular to sub-rounded extraformational clasts, can also be observed. Rare shell fragments and burrows up to 10 cm in length can be observed in places (Fig. 4.8C), and bryozoans are found toward the base of the glacimarine section of the core. Bioturbation is strongest below 375 mbsf. Facies 3 is found exclusively below 200 mbsf in the core.

Possible interpretations

Normally graded sandstones with sharp erosive basal contacts are often interpreted as turbidites, with additional diagnostic features including: planar and/or convolute lamination, ripples, lateral changes or discontinuity in stratification, variable bed and laminae thicknesses, as well as injection (e.g. dikes) and deformation structures (Ó Cofaigh et al., 2001; Stow and Piper, 1984; Stow, 1979; Stow and Shanmugam, 1980; Walker, 1992).

The depositional environment of turbidites in glacimarine sequences can vary from ice distal to ice proximal. The soft-sediment deformation features and clastic lenses/dykes are evidence of rapid emplacement of the sediments (Powell et al., 2001), while the occasional presence of extraformational clasts in mudstones draping the turbidites are evidence of floating ice crossing the site (Fielding et al., 2000; Ó Cofaigh et al., 2001). The depositional

mechanism for turbidites in glacimarine settings could include turbid overflow plumes initiated by sediment-laden meltwater, meltwater coming direct from subglacial conduit forming underflows (uncommon), and failure and re-sedimentation of unstable sediment accumulations (very common in ice proximal where high sedimentation rates from turbid overflow plumes cause quick accumulation of thick sedimentary packages). Where mass failures are the causal factors, failure may be initiated by oscillations of the ice margin, glacitectonic deformation, waves, oversteepening of the sediment, icebergs during calving, or earthquakes (Eyles and Eyles, 1992; Fielding et al., 2000; Krissek et al., 2007; McKay et al., 2009; Ó Cofaigh and Dowdeswell, 2001; Ó Cofaigh et al., 2001; Powell et al., 2000; Powell et al., 2001; Powell, 1984).

More proximal flows generally have thicker medium to coarse sand beds, while more ice distal deposits tend to be finer grained, and usually only record the muddier units (Krissek et al., 2007; McKay et al., 2009; Ó Cofaigh and Dowdeswell, 2001). Moreover, the more ice proximal deposits are usually more stratified and lack macrofauna and bioturbation, as colonisation is inhibited by the high sedimentation rates (Fielding et al., 2000; Ó Cofaigh and Dowdeswell, 2001; Ó Cofaigh et al., 2001).

Preferred interpretation

Facies 3 is interpreted to represent turbidite deposition, with the sediment being delivered below wave base. Outsized clasts in the mudstones draping the sands are indicative of concurrent ice-rafting during the waning of the flows, while rare outsized clasts in the sandstone beds were likely entrained during the turbidity flow. Moreover, at DSDP 270 the general lack of medium to coarse sands at the base of the turbidites, and the presence of bioturbation, suggests that the turbidites were not deposited immediately ice proximal.
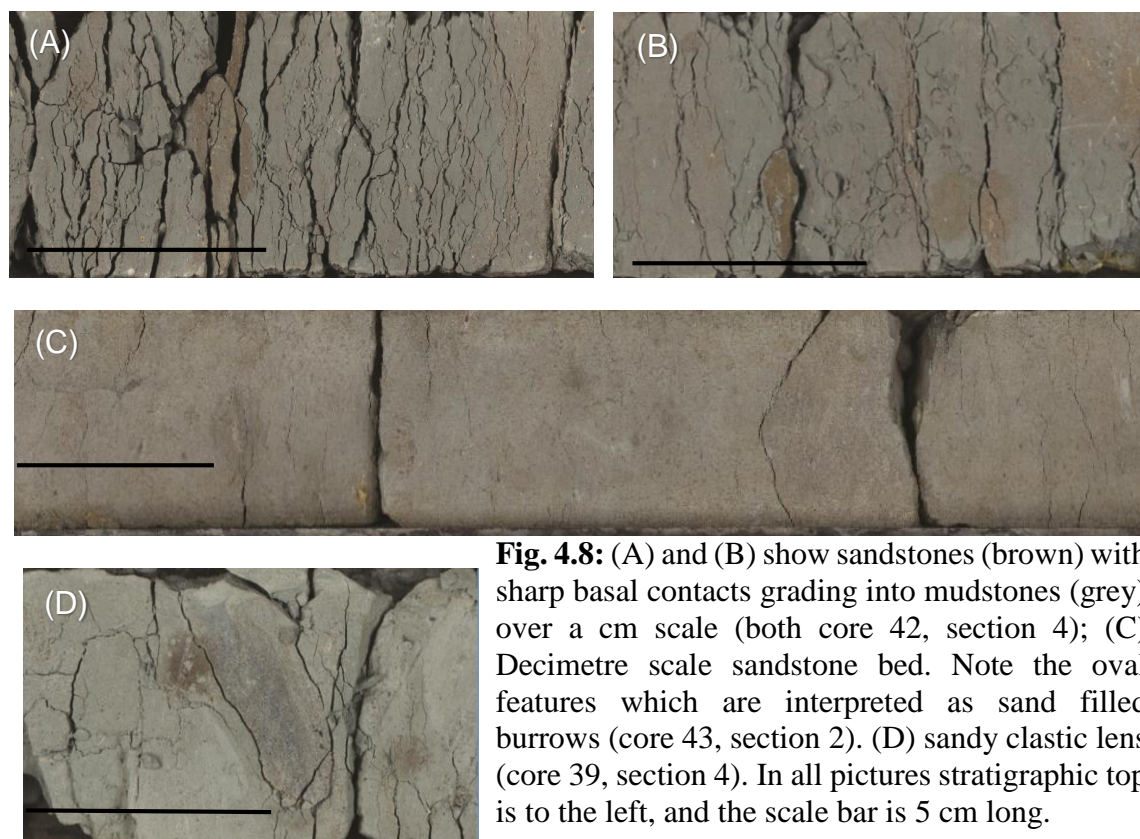
Fig. 4.8: (A) and (B) show sandstones (brown) with sharp basal contacts grading into mudstones (grey) over a cm scale (both core 42, section 4); (C) Decimetre scale sandstone bed. Note the oval features which are interpreted as sand filled burrows (core 43, section 2). (D) sandy clastic lens (core 39, section 4). In all pictures stratigraphic top is to the left, and the scale bar is 5 cm long.

4.3.4 Facies 4 – rhythmically interlaminated sandstone/siltstone with mudstone

Description

Facies 4 consists of rhythmically interlaminated couplets of siltstone to very fine sandstone laminae (Fig. 4.9). The couplets are characterised by very fine sandstones or siltstones with sharp bases, which grade up into mudstones (siltstone or claystone). The fine sandstone and siltstone beds are up to 3 mm thick, while the overlying mudstones can be as thick as 5 mm. A slight upward fining is apparent where the fine sandstone beds are replaced by siltstones, and the thickness of the rhythmic couplets is slightly reduced (millimetre- to sub-millimetre scale). Dispersed sub-rounded to angular extraformational clasts can be observed, but shells and bioturbation are absent. This facies occurs exclusively between 205 and 210 mbsf, and a 10 cm thick interbed, with sharp contacts, of facies 3 (sandstone) was recorded.

Possible interpretations

Rhythmically interlaminated sandstones/siltstones and mudstones are likely derived from suspension settling of sediment-laden turbid plumes which originate from the glacier's terminus in an ice proximal environment. The rhythmicity results from sediment, sourced from turbid proglacial sediment plumes, interacting with tidal currents near top of water column, which regulate the release of the suspended sediment (Mackiewicz et al., 1984; Cowan et al., 1999; Powell et al., 2000; McKay et al., 2009). These rhythmic sand/mud couplets have been termed cyclopels (silt/mud) for ice distal, and cyclopsams (sand/mud) for more proximal, deposits (Mackiewicz et al., 1984). Studies have suggested that both cyclopels and cyclopsams are deposited within a few kilometres of the marine terminating grounded ice mass (Benn and Evans, 2010; Mackiewicz et al., 1984; Ó Cofaigh and Dowdeswell, 2001).

Dropstones indicate the contribution of ice-rafted sediment (Krissek et al., 2007; McKay et al., 2009; Ó Cofaigh and Dowdeswell, 2001), and the absence of bioturbation and macrofossils indicates high sedimentation rates, which inhibited faunal colonisation (Ó Cofaigh and Dowdeswell, 2001). Interbedding with facies 3 (turbidites) may occur due to the ice proximal nature (Ó Cofaigh and Dowdeswell, 2001). The laminated nature of these ice proximal sediments imply deposition by a polythermal or warm-based ice mass with ample sediment-laden meltwater input (Ó Cofaigh and Dowdeswell, 2001).

Preferred interpretation

The nature of rhythmically interlaminated sandstones/siltstones with mudstones in high-latitude glacimarine environments is fairly well documented, and therefore the preferred interpretation is that facies 4 represents cyclopels/cyclopsams which were deposited in relative proximity to the grounding line.

Fig. 4.9: Rhythmically interlaminated mudstones with silt-/sandstones. Brown coloured beds are the fine sandstones, and grey beds are the mudstones (core 24, section 2). Stratigraphic top is to the left, and the scale bar is 5 cm long.

4.3.5 Facies 5 – massive diamictite

Description

Facies 5 consists of massive, sandy and muddy diamictites (Fig. 4.10). Both sharp and gradational contacts are recorded, as well as some fining upward sequences from a sandy to a muddier diamictite. Rare shell fragments can be observed in places, and very rare disarticulated bivalves may be found. Bioturbation is absent. The diamictites range from clast-rich to clast-poor, and numerous clasts are faceted and striated. Clasts commonly do not exhibit a preferred orientation, are predominantly metasedimentary and igneous, are sub-rounded to angular, and up to pebble grade ($\leq$ 15 mm) in size. Facies 5 commonly grades into, or is interbedded with, facies 2 (mudstone with dispersed to common clasts). It is also more common than facies 6 (stratified diamictite).

Possible interpretations

Massive diamictites may form in a variety of depositional environments, but irrespective of the exact deposition mechanism (possibilities outlined below) this facies can generally be regarded as an indicator of turbid, relatively ice proximal sediments (Krissek et al., 2007; McKay et al., 2009), a notion supported by the lack of *in situ* macrofauna and bioturbation, because the high sedimentation rates are not favourable for faunal colonisation (Benn and Evans, 2010; Eyles and Eyles, 1992; Ó Cofaigh and Dowdeswell, 2001).

Where massive diamictites contain sharp basal contacts, they have commonly been interpreted as being of subglacial origin. In addition to sharp basal contacts, characteristic features which point to a subglacial origin include: a lack of bioturbation, discontinuous units, folds, faults, augens and pressure shadows, boudins, shear planes and décollement surfaces, tectonic lamination, banding inclusions, load injection structures, oriented clasts, broken fauna, as well as rip-up clasts (Domack et al., 1999; Hart and Roberts, 1994; Krissek et al., 2007; McKay et al., 2009; Ó Cofaigh and Dowdeswell, 2001).

Moreover, massive diamictites containing sharp basal contacts and a fining upward trend may also be interpreted as having formed by one or more debris flows arising from oversteepening near the grounding line (Dowdeswell et al., 1998; Elverhøi et al., 1983; Evans et al., 2002; Eyles and Eyles, 1992; Hambrey et al., 1991; Krissek et al., 2007; McKay et al., 2009; Nam et al., 1995; Ó Cofaigh et al., 2001; Powell et al., 2000).

Conversely, where massive diamictites are bounded by gradational upper and lower contacts, and contain clasts displaying no systematic orientation, they have been argued to

have resulted from the rain-out of debris beneath icebergs, as the gradational contacts imply continued sedimentation (Evans et al., 2002; Eyles and Lagoe, 1990; Krissek et al., 2007; McKay et al., 2009; Ó Cofaigh et al., 2001; Powell et al., 2000). Moreover, where present, concentrations of clasts, as well as sand lenses support an iceberg-rafted origin, as these features are indicative of iceberg tipping events (Dowdeswell et al., 1994). Iceberg rain-out derived massive diamictites can contain abundant micro- and macro-fauna, and may have also been subject to keeling of these icebergs, as this would homogenise the sediment (Ó Cofaigh and Dowdeswell, 2001).

Alternatively, where ice shelves are present, icebergs calving from their front usually carry little debris as most debris is melted out close to the grounding line. In such an environment massive diamictites are more likely to be deposited near the grounding line (Anderson et al., 1983; Anderson et al., 1991; Hambrey et al., 1991; McKay et al., 2008; Ó Cofaigh and Dowdeswell, 2001; Powell, 1984).

Preferred interpretation

The favoured interpretation for the massive diamictite facies is that it was deposited in very close proximity to the grounding line, with sedimentation likely resulting from a combination of mass flows, and ice-rafting. A subglacial origin for facies 5 is here deemed unlikely due to the lack of the previously discussed evidence for subglacial deposition. Where facies 5 is interstratified with facies 1 or 2, and the contacts are gradational, the preferred interpretation is that these diamictites resulted from the rainout of IRD.

Fig. 4.10: Facies 5 – massive diamictite (core 27, section 3). Stratigraphic top is to the left and the scale bar is 5 cm long.

4.3.6 Facies 6 – stratified diamictite

Description

Facies 6 consists of a clast-poor, muddy to sandy diamictite (Fig. 4.11). The diamictite is very weakly to moderately stratified on centimetre to decimetre scales, as defined by clast concentrations, and matrix grainsize (i.e. muddy and sandy diamictite interbeds). The sub-rounded to angular clasts, some of which are striated, are up to pebble grade ($\leq$ 10 mm), composed of metasedimentary and igneous lithologies, and not usually oriented in a preferred manner. Basal contacts were often not recovered by the drilling, but both gradational and sharp lower contacts are present. The bed orientation, though predominantly horizontal, can be inclined up to 30°, and rare cross-bedding is observed. Rare shell fragments are recovered in some units, and the diamictite also contains calcareous intervals. Rare solitary intraclasts of mud can be observed. Facies 6 can be found to be interstratified with, or grade into, facies 2 (mudstone with dispersed to common clasts) and 5 (massive diamictite).

Possible interpretations

Similar to facies 5, stratified diamictites are seen as indicators of proximity to the grounding line, and the plausible depositional environments are the same as those listed for facies 5. The stratification may be a result of: traction currents winnowing fine material (indicated by cross bedding and a sandier matrix), sediment laden meltwater plumes emanating from grounding line cavity (indicated by laminations of silt clay and fine sand), individual or stacked mass flow deposits resulting from re-sedimentation of unstable deposits near the grounding line (indicated by sharp bases, convolute lamination, normal grading), or by fall sorting by currents during rainout of IRD (indicated by gradational contacts and random orientation of clasts) (Domack et al., 1999; Eyles and Eyles, 1992; Fielding et al., 2000; Ó Cofaigh et al., 2001; Powell et al., 2000; Powell, 1984). Beds of stratified diamictites resulting from rain-out of IRD are usually thinner, and associated with comparatively more distal facies, such as facies 1 and 2 (Krissek et al., 2007; McKay et al., 2009). Moreover, when stratification becomes finer it may indicate enhanced meltwater input (Fielding et al., 2000; Ó Cofaigh et al., 2001; Powell et al., 2000).

Stratified diamictites may also represent subglacial deposition, with sedimentological and structural evidence being the same as those listed for massive diamictites (facies 5). An example of such evidence could be the inclined bedding found between 250 and 230 mbsf, which may be evidence of glacitectonic deformation (e.g. Benn and Evans, 2010), or alternatively mass flows/slumping. Some studies have however suggested that stratified diamictites are less commonly associated with subglacial origin than massive ones (Fielding et al., 2000; Krissek et al., 2007; McKay et al., 2009).

Preferred interpretation

Similar to facies 5, facies 6 was most likely deposited very proximal to the grounding line, but not subglacially. This interpretation is based on the lack of the aforementioned (section 4.3.5) sedimentological and structural evidence for subglacial deposition, with the possible exception of some inclined bedding. Where conformably interbedded within facies 1 or 2, the deposition of a stratified diamictite is interpreted as resulting from rainout of IRD.

Fig. 4.11: Facies 6 – weakly to well-stratified diamictite. Here weak stratification is indicated by occasional alignment of clasts (core 27, section 3). Stratigraphic top is to the left, and the scale bar is 5 cm long.

4.4 Geochemistry

4.4.1 X-ray fluorescence

Point X-ray fluorescence measurements were undertaken on the split core during the core description phase as part of this thesis, and the results were sent to collaborator F. Jiménez-Espejo (JAMSTEC) to identify different geochemical trends and associations in the data using principle component analyses (PCA). F. Jiménez-Espejo provided some guidance on how XRF data can be broadly interpreted in marine sediments, but the interpretations of the XRF results in the context of the broader stratigraphic constraints of the DSDP Site 270 core were conducted by myself.

One PCA was done on the whole core dataset (73 – 385.5 mbsf), in addition to individual analyses being conducted on four selected intervals (1: 73 – 145 mbsf; 2: 234 – 256.5 mbsf; 3: 256.5 – 379 mbsf; 4: 379 – 385.5 mbsf), which were distinguished based on baseline shifts in the elemental abundances. All PCA results (Table 4.2; Fig. 4.12) show that in each interval, as well as the whole core, the most significant principle component, which in these cases accounts for more than half of the variance of elemental counts, is the correlation between Ca and S, versus all other elements. This is interpreted to reflect gypsum ($CaSO_4$) growth on the core face during storage. As such, despite efforts to clean the core faces of gypsum, the XRF signal was dominated by it, thereby compromising all Ca and S measurements. Furthermore, in all analyses, apart from interval four, the second principle component, explaining between ~15 to 20% of the variance, was the covariance of Ba and Cl versus all other elements. This again is ascribed to salts (Cl) and barite (Ba) growth on the core faces, explaining why the Ba neither correlated with a biogenic source (i.e. not correlated with Ca), nor with detrital elements. As such, Ba and Cl were also compromised and not used. A correction factor to account for the gypsum, barite, and salt growth was not applied because even in discrete samples it would have been very difficult to distinguish what proportion of the Ca, S, Cl, and Ba measurements resulted from the post-recovery mineral growth, versus the original sediment composition. Even though Ca, S, Ba, and Cl could not be used, the other elements were still useful, despite their lower signal (F. Jiménez-Espejo, pers. comm.). Apart from the fourth interval, all PCA showed an anti-correlation between Mn and S as their third principle component. Mn is not regarded as being compromised and, the significance of the Mn signal is described below.

The growth of gypsum, barite and salts on the core face means that elemental ratios used as proxies of terrigenous (IRD) input (e.g. Fe/Ca, Al/Ca, Ti/Ca, K/Ca, where Al, Ti, K and Fe are primarily derived from detrital sources, while Ca reflects changes in $CaCO_3$), the chemical index of alteration (CIA), proxy ratios of organic productivity (e.g. Ba/Al, Ba/Ti), and some indicators of redox conditions (e.g. Fe/S) could not be employed in this study because they incorporate one of the compromised elements. However, as stated before, changes in the other elements are still meaningful. Changes in the log-ratios of Mn/Al, Mn/Ti, and Mn/Fe (Fig. 4.13) have been attributed to changes in bottom water oxygenation and sediment redox conditions by a number of studies, where constant Mn/Fe values are taken to represent oxic conditions, while higher Mn/Ti and Mn/Al ratios indicate oxygenated waters (Hepp et al., 2009; Marsh et al., 2007; Rothwell and Croudace, 2015; Spofforth et al., 2008). At DSDP 270, the Mn/Al, Mn/Ti and Mn/Fe ratios all show the same trends: elevated values at the base of the core that decline steadily until ~365 mbsf, followed by little to no significant changes in baseline values to the top of the core. However, positive and abrupt excursions are noted, for example at ~282 mbsf.

Furthermore, changes in the log ratios of Si/Ti and Si/Al (Fig. 4.14) have been attributed to changes in biogenic silica, where higher values in both ratios indicate the increased presence of siliceous microfossils (Dickson et al., 2010; Marsh et al., 2007; Rothwell and Croudace, 2015). Si/Ti values appear to be slightly higher at the base of the core, but baseline values overall remain largely invariant as shown by the linear trendline. Baseline values of Si/Al on the other hand show an overall increase upcore, in addition to the higher values at the base of the core.

Table 4.2: Principle component analysis results of the XRF dataset. Numbers corresponding to elements for each principle component (PC) of each interval are the loadings graphed in Figure 4.12.

Element	Whole core			Interval 1			Interval 2			Interval 3			Interval 4			
	PC1	PC2	PC3	PC1	PC2	PC3	PC1	PC2	PC3	PC1	PC2	PC3	PC1	PC2	PC3	PC4
Al	0.38	-0.23	0.06	0.36	-0.09	-0.18	0.35	-0.29	0.00	0.37	-0.30	0.06	0.39	0.27	-0.14	0.14
Si	0.39	-0.12	0.08	0.36	-0.04	-0.10	0.37	-0.14	0.03	0.40	-0.13	0.13	0.39	0.26	-0.12	-0.02
S	-0.36	0.03	-0.36	-0.37	-0.07	0.14	-0.34	0.07	-0.28	-0.31	0.01	-0.60	-0.36	0.03	0.03	0.52
Cl	0.04	0.70	0.15	0.07	0.69	0.11	0.16	0.72	0.08	0.03	0.65	0.19	0.12	0.09	0.73	-0.15
K	0.40	-0.12	-0.01	0.36	-0.13	-0.12	0.37	-0.19	-0.01	0.42	-0.11	0.03	0.41	0.00	-0.13	0.21
Ca	-0.39	-0.08	0.18	-0.37	-0.09	-0.03	-0.37	-0.01	0.17	-0.42	-0.12	0.20	-0.39	0.29	0.02	0.04
Ti	0.30	-0.04	-0.02	0.37	-0.08	-0.07	0.38	0.00	-0.04	0.25	0.00	-0.05	0.39	0.13	-0.08	0.29
Mn	-0.11	-0.13	0.89	0.22	-0.14	0.95	-0.04	-0.13	0.92	-0.21	-0.14	0.72	0.00	0.62	0.10	-0.50
Fe	0.36	0.04	-0.08	0.36	-0.08	-0.02	0.36	-0.04	-0.11	0.36	0.13	-0.11	0.20	-0.59	-0.05	-0.47
Ba	0.17	0.63	0.10	0.11	0.67	0.03	0.25	0.57	0.14	0.11	0.63	0.10	0.20	-0.15	0.63	0.30
Eigenvalue	5.70	2.00	1.09	6.95	1.88	1.71	6.84	1.48	1.10	5.02	1.95	1.16	5.37	1.68	1.52	0.84
% variance	51.81	18.27	9.90	69.55	18.81	7.06	68.37	14.80	11.03	50.18	19.52	11.57	53.76	16.80	15.20	8.42
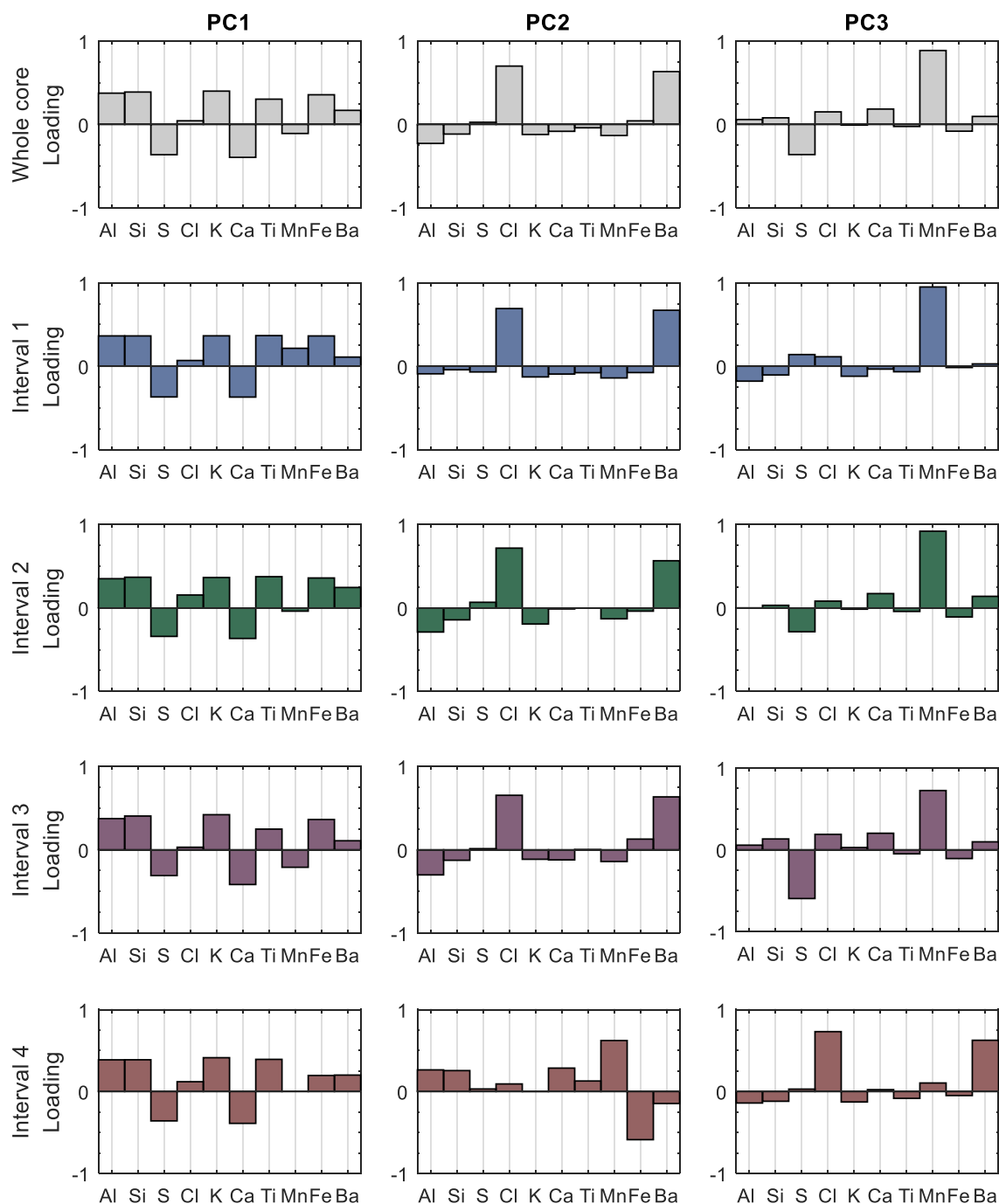
Fig. 4.12: Results of the PCA of the whole core and four intervals. Shown are the three principle components which account for most of the variance in each interval. Note that PC4 of interval 4 (see Table 4.2) is not plotted because it only explains a very low amount of the variance.
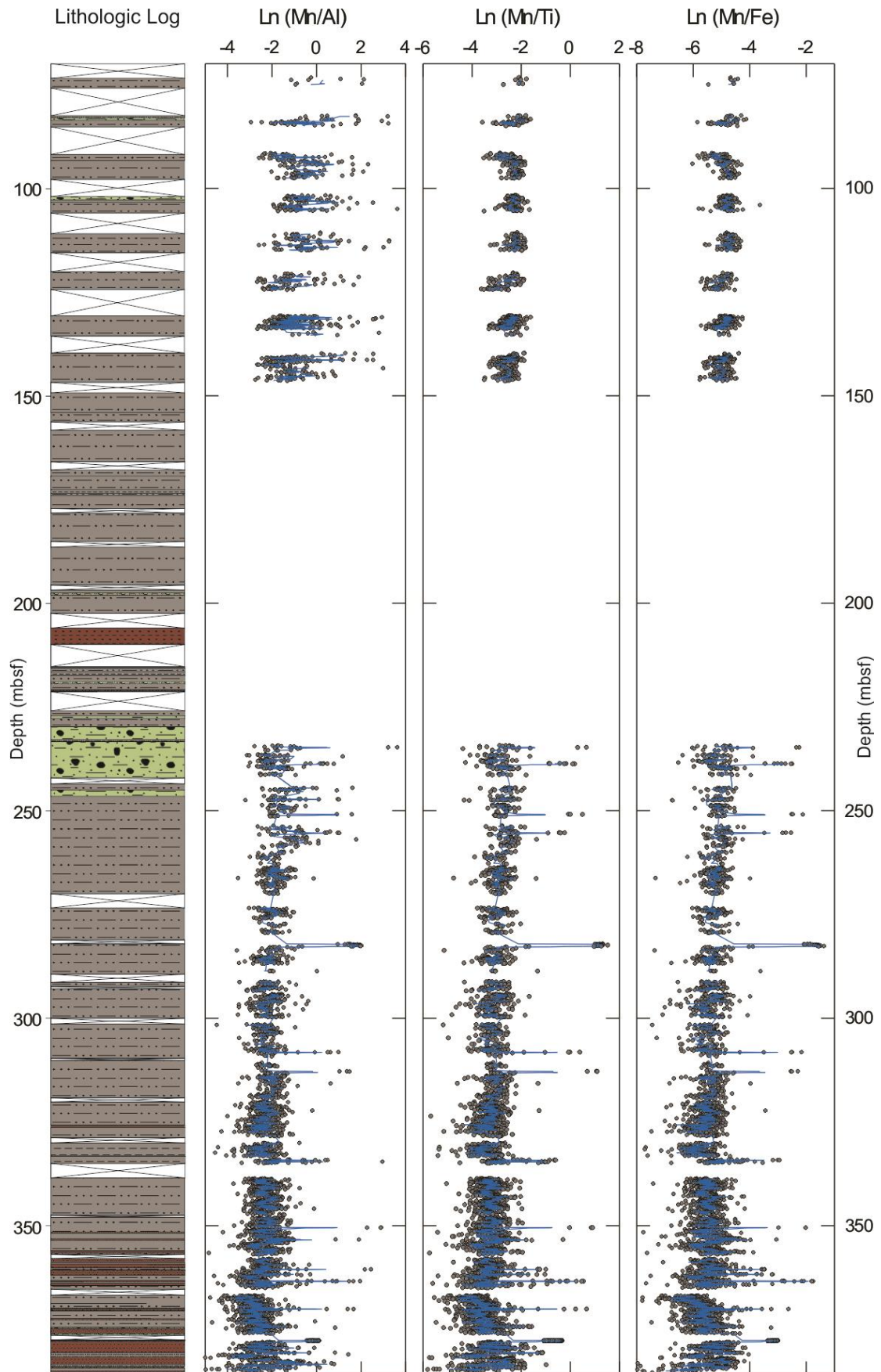
Fig. 4.13: Graphs of elemental log ratios indicative of variations in reduced oxidation conditions, referenced to a simplified lithologic log. Blue lines represent 5-point moving averages of the data (grey dots).
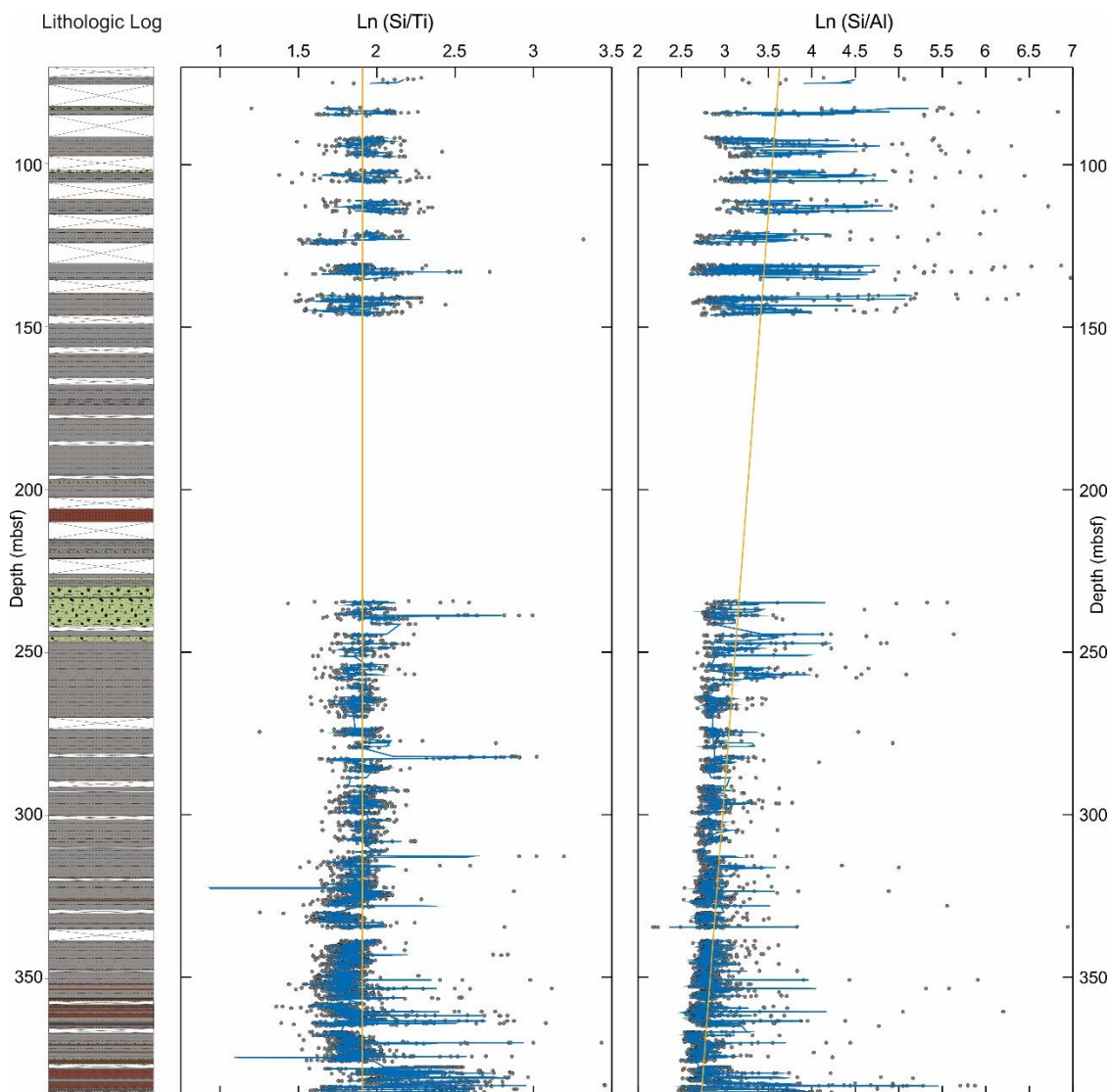
Fig. 4.14: Changes in the proxy ratios of biogenic silica (Si/Al, Si/Ti) throughout the core, referenced to a simplified lithologic log (left). Blue lines are a 5-point moving average of the data (grey dots), and the yellow line is a linear fit to the data.

4.4.2 ICP-MS

In addition to the XRF data, further geochemical data was collected by means of ICP-MS by F. Jiménez-Espejo (JAMSTEC). Again, the results are displayed as ratios, the most relevant of which are plotted in Figure 4.15. Three different Eu anomaly (Eu*) values were calculated for each sample, using Equation 4.1 and the three commonly-used normalisation values: CI chondrite, upper continental crust (UCC), and North American Shale Composite (NASC).

$$\text{Eu*} = \frac{\text{(Eu sample/Eu normalising value)}}{\text{(Sm sample/Sm normalising value)}} \tag{4.1}$$

The Eu anomaly is a proxy sensitive to changes in detrital input, while La/Lu and La/Yb have been often used as indicators of the provenance of the sediments (Gaiero et al., 2004;

Jiménez-Espejo et al., 2014; Levitan et al., 2007; Shigemitsu et al., 2007). Th/Sc can also serve as a continental provenance proxy, where a higher Th/Sc ratio indicates a more felsic source, as Th is more abundant in felsic than basic minerals (Levitan and Lavrushin, 2009; Levitan et al., 2007; Rollinson, 1993). Alternatively, Th-enriched sediments have also been associated with the abundant presence of kaolinite clays (Ruffell et al., 2002). At DSDP 270, Th/Sc records appear quite variable below 305 mbsf, followed by relatively uniform values of ~1.2 between 305 and 200 mbsf (Fig. 4.15). At 200 mbsf there is a marked increase in Th/Sc values to ~1.5. Above 125 mbsf, the Th/Sc data begin a slowly decreasing trend, however, values generally remain above those found between 305 and 200 mbsf (with the exception of two very low data points at 83 and 104 mbsf). Meanwhile, the Eu anomaly values do not change significantly throughout the core, and the La/Yb and La/Lu ratios both show changes scattered about a uniform baseline of ~12 and 80, respectively (Fig. 4.15). As such, no major shifts appear to have occurred in detrital input or sources sensitive to La/Lu or La/Yb.

Furthermore, U/Th ratios have been used as a proxy for bottom-water oxygenation, where values of 0.75-1.25 and >1.25 represent dysoxia and anoxia, respectively (Gallego-Torres et al., 2007). This is because fluctuations from oxic to anoxic conditions cause uranium to shift from being soluble to being immobile (Anderson, 1982; Barnes and Cochran, 1990; Mangini et al., 2001). In the DSDP 270 records, with the exception of slightly elevated ratio values at the base of the core, and one data point just above 100 mbsf, U/Th values remain below 0.75 (oxic), and show little to no variation (Fig. 4.15).
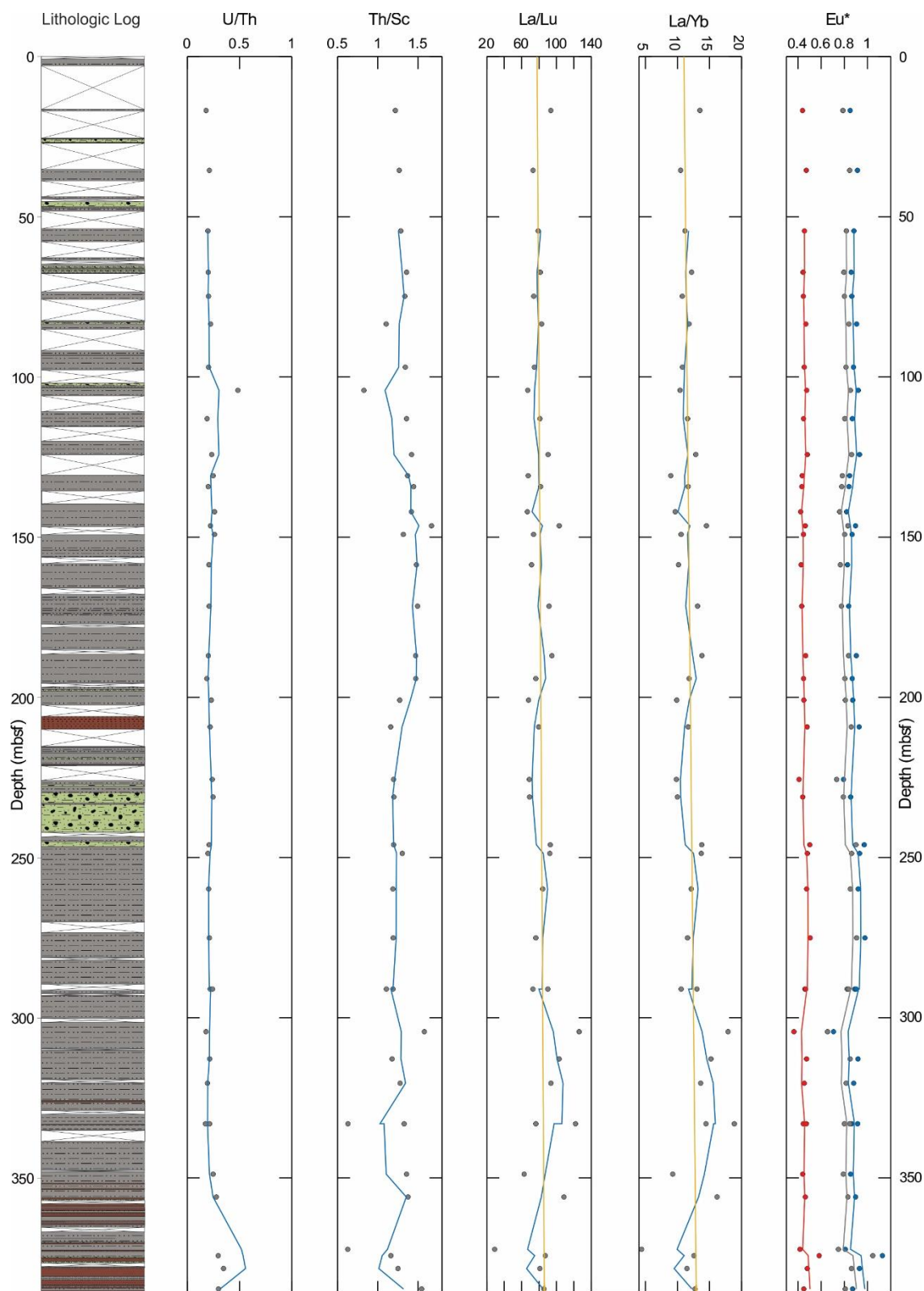
Fig. 4.15: Graphs of the downcore variations of the most significant elemental ratios derived from the ICP-MS measurements, referenced to a simplified lithologic log (left). In all graphs, except the Eu*, blue lines indicate 3-point moving averages of the data (grey dots), and where graphed, linear trendlines are drawn in yellow. For the Eu anomaly, red dots indicate data normalised to CI chondrites, grey to NASC, and blue to UCC; the 3-point moving averages are coloured according to this scheme also.

4.5 Magnetic susceptibility

The magnetic susceptibility, which reflects the response of the minerals in the sediments to an external magnetic field (Hunt et al., 1995) and is expressed in dimensionless SI units, shows several distinct changes downcore (Fig. 4.16). From the base of the glacimarine sediments, the magnetic susceptibility varies along a similar baseline (~9 SI units), until an abrupt increase, to values as high as 120 SI units, is recorded between ~235 and 215 mbsf, followed by a return to previous baseline values. Subsequently, from ~183 to 150 mbsf, the baseline increases again, and the amplitude of variations (between ~8 and ~293 SI units) becomes substantially larger. Above 150 mbsf, variations then return to lower amplitudes along a similar, or lower, baseline as before, all the way to the top of the core. The exception to this are two abrupt increases in magnetic susceptibility (to as much as 100 SI units) between 135 and 123 mbsf.
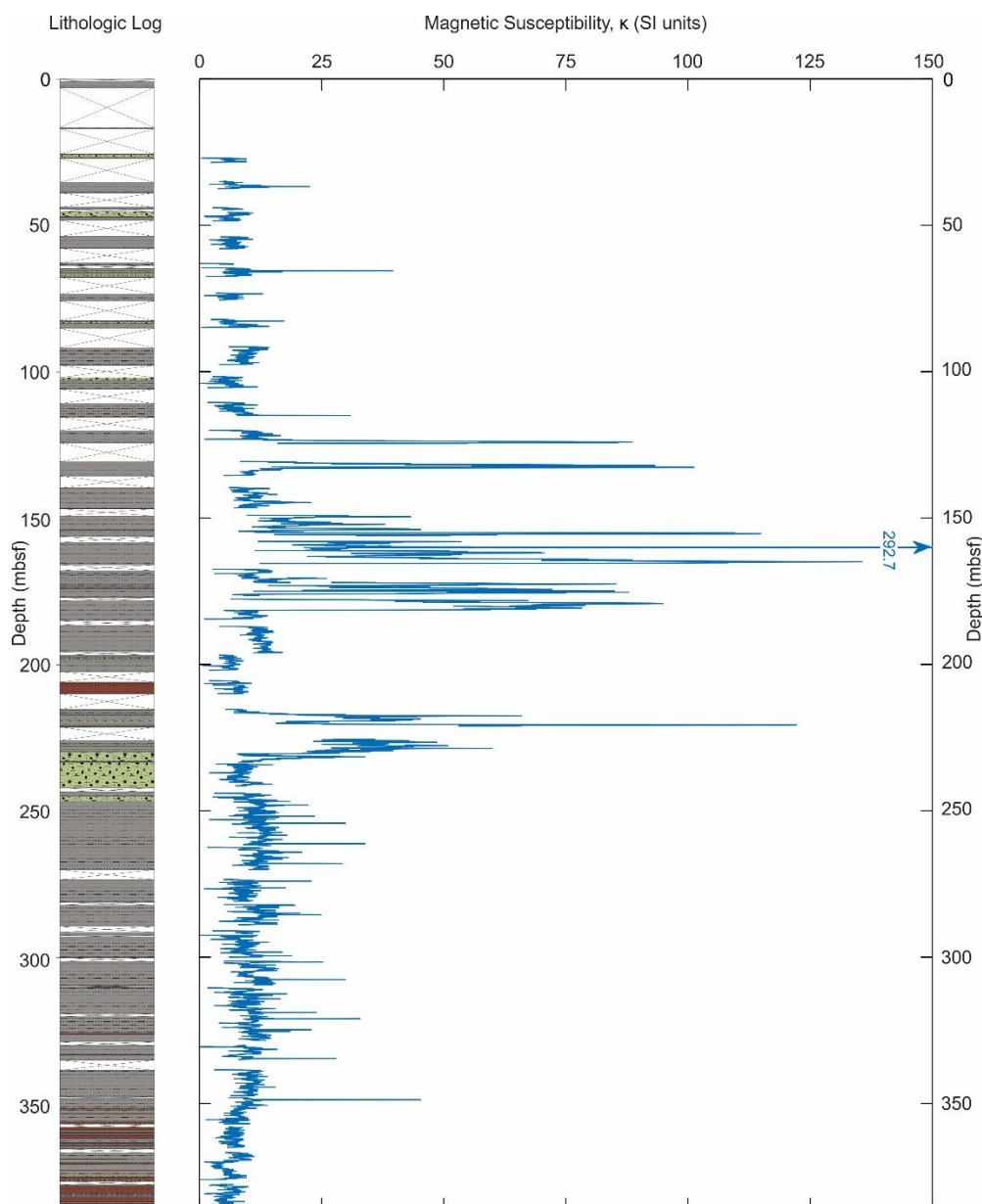
Fig. 4.16: Variations in magnetic susceptibility of the sediments recovered at DSDP 270 (right), plotted next a simplified lithostratigraphic log for reference (left). Note that one data point (292.7 SI units) is off the chart as indicated by the arrow.

4.6 Spectral analysis

The results of the ASM analysis are very consistent (Table 4.3, Fig. 4.17, 4.18). In all analyses (i.e. both, percent mud (<63 µm) and percent coarse sand (250 µm – 2 mm) datasets, and both, Laskar and Berger orbital targets) a sedimentation rate of approximately 17 cm/ka provided the optimal fit between the measured and targeted data (Fig. 4.17i, ii(a), Fig. 4.18i, ii(a)). The ASM (i.e. the distance between the target and measured spectrum) is very small in all datasets, suggesting a good fit between the target and the measured data, and providing confidence in the results (Table 4.3). It is noted that the ASM is smaller in the percent mud data than in the coarse sand, suggesting a better fit to the tuning target. Furthermore, this sedimentation rate consistently rejects the null hypothesis, with all H_o significance levels substantially below the required threshold of 0.5% (Table 4.3; Fig. 4.17i(b), 4.17ii(b), 4.18i(b), 4.18ii(b)). In all analyses seven astronomical terms were able to be fitted to the data using the calculated sedimentation rates (Fig. 4.17i, ii(c), 4.18i, ii(c)). Thus, the ASM analyses show that in both datasets orbital frequencies are clearly present. Furthermore, using this sedimentation rate, the orbital frequencies captured by the sampled data become apparent (Fig. 4.17i, ii(d), 4.18i, ii(d)). All three eccentricity cycles (E1, E2, and E3) are captured by the coarse sand dataset, but only two are recovered in the percent mud data (E1, E2). Conversely, the coarse sand data only records the strongest obliquity period (O2), while percent mud picks up both, the strong (O2) and subordinate (O1) obliquity periods. Both datasets pick up the two periods of precession (P1, P2). Furthermore, one period of noise was identified in each dataset, marked by the question marks in Figures 4.19B and 4.20B.

Table 4.3: Results from the ASM analyses, depicted in Figures 4.17 and 4.18. H_o-SL stands for the significance level of the null hypothesis.

	Coarse sand		Percent mud	
	Laskar target	Berger target	Laskar target	Berger target
ASM (cycles/ka)	7.85×10^{-4}	8.21×10^{-4}	3.51×10^{-4}	3.59×10^{-4}
Sed. rate (cm/ka)	17.014	17.231	17.451	17.231
H_o-SL (%)	0.027	0.039	0.015	0.026
Astronomical terms	7	7	7	7
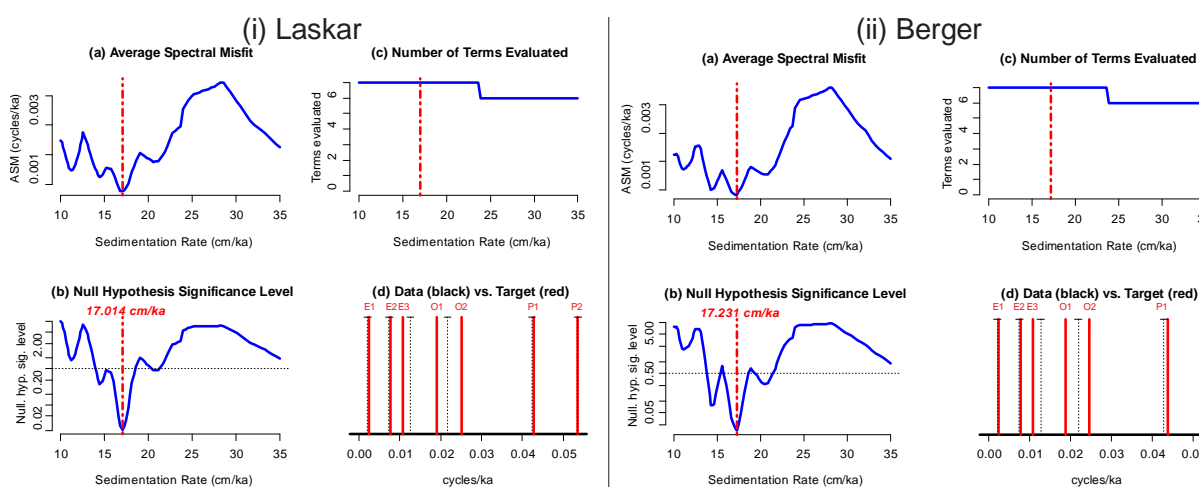
Fig. 4.17 (overleaf): ASM results for the coarse sand dataset, using the (i) Laskar tuning solutions, and (ii) Berger tuning solutions. In each result (a) is the average spectral misfit, where the red dashed line denotes the optimal fit; (b) the sole sedimentation rate (red dashed line) which surpasses the significance level, and thus rejects the null hypothesis; (c) the number of orbital periods evaluated, where the dashed red line is the sedimentation rate; and (d) comparing the frequencies present in the data (black dotted line) against the tuning targets (red solid line) labelled using the same abbreviations as in Table 3.3.
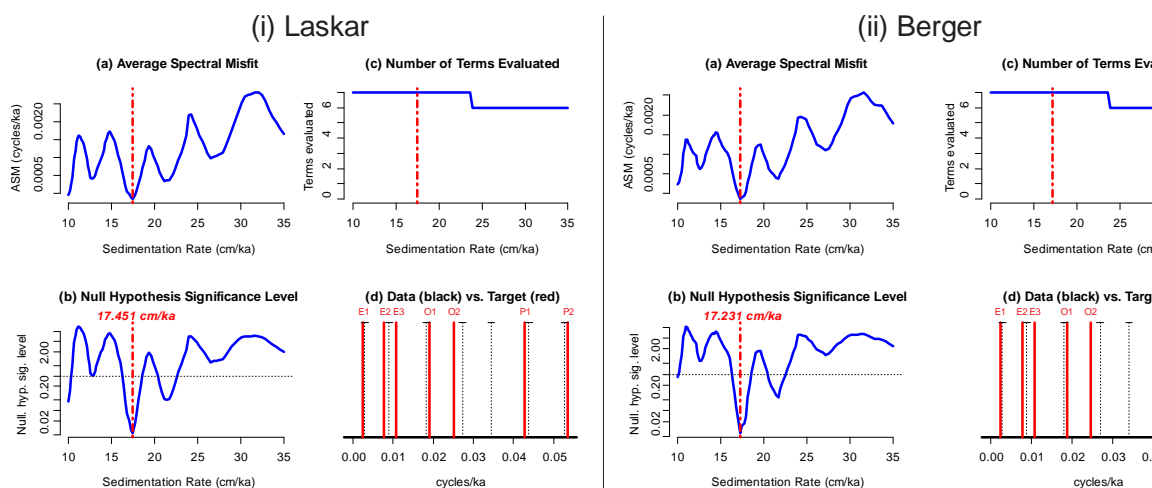
Fig. 4.18: ASM results for the percent mud dataset, using the (i) Laskar tuning solutions, and (ii) Berger tuning solutions. In each result (a) is the average spectral misfit, where the red dashed line denotes the optimal fit; (b) the sole sedimentation rate (red dashed line) which surpasses the significance level, and thus rejects the null hypothesis; (c) the number of orbital periods evaluated, where the dashed red line is the sedimentation rate; and (d) comparing the frequencies present in the data (black dotted line) against the tuning targets (red solid line) labelled using the same abbreviations as in Table 3.3.

The ASM results allowed the calibration of the MTM and EHA data, shown in Figures 4.19 and 4.20. The results of the MTM analyses for both datasets, the percent mud and percent coarse sand, indicate that most of the power is concentrated in frequencies below 0.4 cycles per metre (Fig. 4.19C, 4.20C). Seven frequencies (labelled 1-7 in Figures 4.19B, C and 4.20B, C) were judged as being significant in the MTM analyses, based on surpassing the 90% confidence interval in the harmonic F-tests (Fig. 4.19B, 4.20B), and displaying significant power (Fig. 4.19C, 4.20C). It is acknowledged that some orbital frequencies are approximately at noise level (Fig. 4.19C, 4.20C), however, they were still regarded as significant by the MTM analyses. The EHA analyses (Fig. 4.19D, 4.20D) show that the coarse sand displays a high amplitude frequency corresponding to eccentricity throughout the sampled interval. Meanwhile frequencies corresponding to obliquity and precession only gain significant amplitude between 310 and 275 mbsf. The percent mud dataset records reduced amplitudes in eccentricity frequencies between 310 and 280, and higher amplitude frequencies corresponding to obliquity beginning at 310 mbsf. Frequencies of precession appear strongest between 310 and 290 mbsf in both datasets.
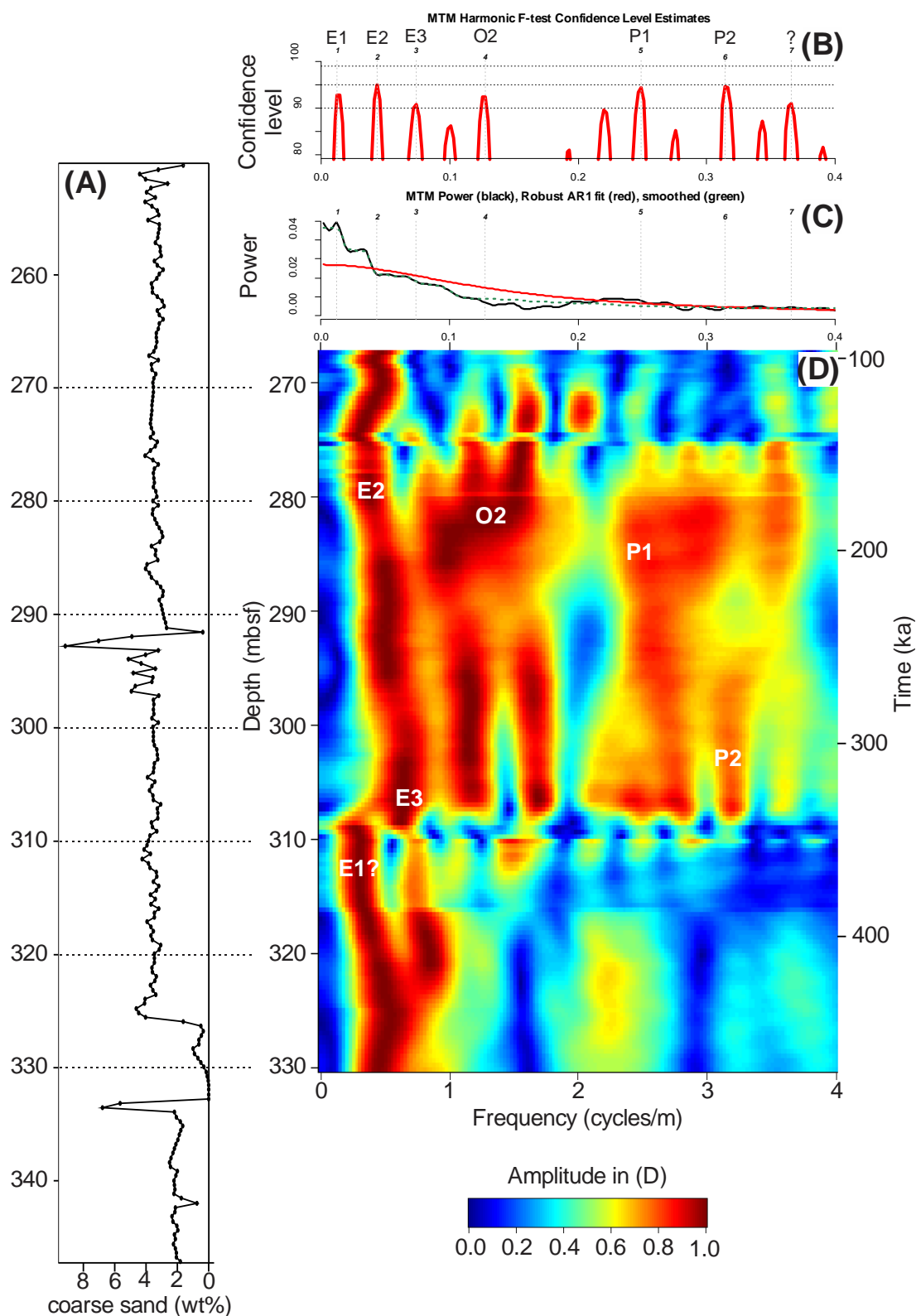
Fig. 4.19: Calibrated MTM (B and C) and EHA (D) results for the coarse sand dataset (A). E, O, and P notations in (B) and (D) refer to orbital cycles as noted in Table 3.3, while the question mark in (B) denotes a frequency which corresponds to noise. Digits (1-7) in (B) and (C) refer to significant frequencies identified using the MTM analysis. Estimated noise levels using the conventional autoregressive-1 (AR1, red line) and the robust AR1 approach of Mann and Lees (1996) (green dashed line) are shown in (C). The floating timescale is based on the ASM-derived sedimentation rate of ~17 cm/ka.
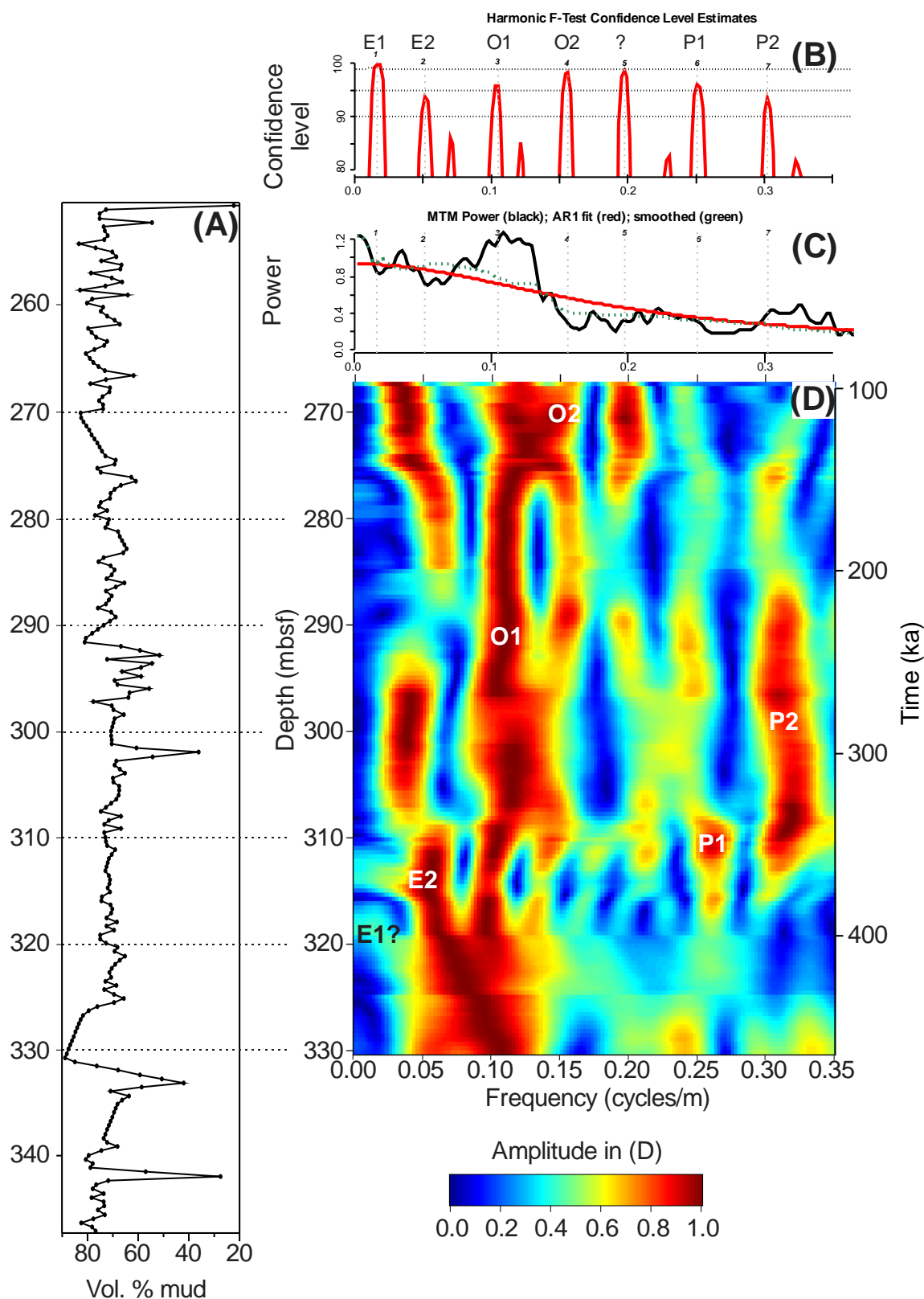
Fig. 4.20: Calibrated MTM (B and C) and EHA (D) results for the percent mud dataset (A). E, O, and P notations in (B) and (D) refer to orbital cycles as noted in Table 3.3, while the question mark in (B) denotes a frequency which corresponds to noise. Digits (1-7) in (B) and (C) refer to significant frequencies identified using the MTM analysis. Estimated noise levels using the conventional autoregressive-1 (AR1, red line) and the robust AR1 approach of Mann and Lees (1996) (green dashed line) are shown in (C). The floating timescale is based on the ASM-derived sedimentation rate of ~17 cm/ka.

Chapter Four – *Results*

Chapter Five
DISCUSSION

5.1 Facies analysis for DSDP 270

By a process of comparison to modern glacial depositional settings, glacially-derived sediments allow the evaluation of the glacial history of an area, including the identification of past expansions and retreats of an ice sheet over a drill site, and changing climatic and glacial boundary conditions. This approach was adopted by the ANDRILL programme and Cape Roberts Project, for Miocene to recent, and Eocene to Miocene glacimarine deposits, respectively. The identification of characteristic lithofacies, lithostratigraphic units (or motifs where associations were repetitive in nature), and sedimentation rates allowed the identification of different glacial regimes and extent under changing climatic conditions (Dunbar et al., 2008; Krissek et al., 2007; Levy et al., 2016; McKay et al., 2009; Naish et al., 2009; Naish et al., 2008). For example, the comparison of modern analogue glacial settings with geological deposits can allow for the identification of warmer-than-present glacial regimes (e.g. subpolar) where ablation was dominated by meltwater process (cf. motifs 2b and 3 of McKay et al. (2009)), and glacial regimes where meltwater processes decrease and iceberg calving processes increasingly dominated ice sheet mass loss (cf. motifs 1 and 2a of McKay et al. (2009)). It is important to note that while individual facies (section 4.3) alone may be poor indicators of specific paleo-environments, their stacking patterns have proven useful in identifying systematic changes in grounding line proximity (e.g. expansions and retreats of the ice sheet across the continental shelf), and/or relative water-depth changes (e.g. Levy et al. (2016); Naish et al. (2009); Naish et al. (2008)).

In this section, six lithostratigraphic units (LSU; Table 5.1) are defined based on the previously described glacimarine facies, and guided by facies schemes used in Cape Roberts and ANDRILL (Fielding et al., 2000; Krissek et al., 2007; Levy et al., 2016; McKay et al., 2009; Naish et al., 2009; Naish et al., 2008; Naish et al., 2001). Of these six LSUs, only five are described here, as LSU 1 is significantly younger than the other LSUs and outside the scope of this study. Additionally, these interpretations are augmented by trends in the geochemical and magnetic susceptibility data, as well as previously published information on the palynology and foraminifera (Kemp and Barrett, 1975; Leckie and Webb, 1983). These lithostratigraphic units provide insights into Oligocene to early Miocene West Antarctic glacial regime, as well as significant shifts in water depth and the glacial proximity of ice masses to DSDP Site 270. The lithostratigraphic units and their interpretations are described from oldest to youngest.

Table 5.1: Lithostratigraphic units (LSU) for sediments between 0 and 385 mbsf at DSDP 270, with facies proportions (%) for each lithostratigraphic unit. Note that facies proportion calculations excluded core voids. The full data are available in Appendix 7.

LSU (Depth, mbsf)	Main facies	Facies proportions (%)					
		F1	F2	F3	F4	F5	F6
1 (0 – 20)	N/A	N/A	N/A	N/A	N/A	N/A	N/A
2 (20 – 124)	Mudstone with clasts	7.94	79.29	0.00	0.00	10.22	2.55
3 (124 – 202)	Mainly massive mudstone	69.56	29.07	0.00	0.00	1.37	0.00
4 (202 – 252)	Diamictite with mudstone	0.94	45.35	2.00	10.50	18.06	23.15
5 (252 – 348)	Mudstone with clasts	4.85	94.99	0.15	0.00	0.00	0.00
6 (348 – 385)	Sandstone and mudstone	7.85	22.21	68.06	0.00	1.88	0.00

5.1.1 Lithostratigraphic unit 6

Lithostratigraphic unit (LSU) 6 is characterised by sandstones (facies 3) interbedded at the centimetre to decimetre scale with mudstones containing very rare (facies 1) to dispersed to common clasts (facies 2), and occurs exclusively in the early Oligocene interval of the core (385 to 348 mbsf). The sandstone beds range in thickness from 0.02 to 2 m, have sharp wavy and basal contacts, and grade up into the mudstone facies. The sandstone beds become finer and decrease in thickness up-core, and the mudstone facies become more prevalent. Both facies are characterised by highly variable contents of ice-rafted debris, however, the highest clast contents are recorded in the sandstone facies, indicating that these clasts were possibly introduced as part of the turbidity currents. *Nothofagus*, podocarp, *Protaceae*, and *Myrtaceae* pollen, as well as degraded tissues, leaf cuticles and vascular fragments are very abundant in this lithostratigraphic unit, especially in the mudstone immediately overlying the glauconitic sandstone, suggesting nearby vegetation (Kemp and Barrett, 1975). Geochemically, lithostratigraphic unit 6 deposits are characterised by slightly elevated U/Th values, lower Mn/element ratios and a lack of correlation between Ti and Fe ($r^2 = 0.13$). This may point to more reduced, possibly suboxic conditions, which have previously been noted in other turbidite deposits (e.g. Robinson (2001); Rosenthal et al. (1995)). Moreover, the presence of glauconite in the sandstone (385 - 386 mbsf) underlying this lithostratigraphic unit also supports the interpretation of high organic matter input, and suboxic to anoxic conditions (Carson and Crowley, 1993; Cloud Jr, 1955). Meanwhile, Th/Sc values appear to be quite variable, and magnetic susceptibility values remained low (averaging 7 SI units) during lithostratigraphic unit 6.

Lithostratigraphic unit 6 is thus interpreted as turbidites (with the exception of the organic rich mudstone at the base) based on their characteristic sharp bases, with fine sandstones or coarse siltstones grading up into mudstones, as well as other evidence diagnostic of reworking such as fragmented shells, which are compatible with the models of turbidites in glacimarine environments (e.g. Powell et al., 2001). The turbidity currents were likely initiated by various triggers (e.g. earthquakes, calving icebergs, or sediment overloading) causing re-sedimentation of unstable sediment, which was supplied by glacial outwash and accumulated at the ice front, and/or they may also have been caused by rapid sediment input from meltwater-rich plumes discharging from a marine-terminating ice sheet/cap into this rapidly deepening basin (Eyles and Eyles, 1992; Fielding et al., 2000; Krissek et al., 2007; McKay et al., 2009; Ó Cofaigh and Dowdeswell, 2001; Ó Cofaigh et al., 2001; Powell et al., 2000; Powell et al., 2001; Powell, 1984). The rapid deepening is ascribed to the ongoing post-rift subsidence (De Santis et al., 1999), and about 70 m of deepening is recorded by the foraminifera during lithostratigraphic unit 6 (Leckie and Webb, 1983). The presence of IRD points to marine terminating glaciers discharging icebergs into the central Ross Sea during this transgression, with the pollen and vegetation fragments indicating a coastal region that was well vegetated. Moreover, there was likely a glaciofluvial component to this terrigenous sediment input. The increasingly finer turbidites up-core suggest that the DSDP 270 became more distal to the sediment source (i.e. ice front or river mouths) with time (Krissek et al., 2007; McKay et al., 2009; Ó Cofaigh and Dowdeswell, 2001; Stow and Piper, 1984).

5.1.2 Lithostratigraphic unit 5

Lithostratigraphic unit 5 consists almost exclusively (95%) of mudstones with dispersed to common clasts, and infrequent clast concentrations (facies 2). Rare interbeds (<1 m thick) of mudstones lacking clasts (facies 1) are found. The IRD content is fairly constant in lithostratigraphic unit 5, averaging 3 wt% for the coarse sand fraction, and 4 clasts greater than 2 mm per 10 cm in the visual count. The dominance of mudstone facies in LSU 5 is reflected in a higher mud content (up to 89%) than in the lithostratigraphic units bounding it. Magnetic susceptibility values are higher than in LSU 6, averaging ~11 SI units. The redox sensitive elemental ratios show no significant changes during LSU 5, with the exception of a large spike in all three ratios at ~282 mbsf. Geochemical ratios indicative of biogenic silica, and the ICP-MS also do not show significant changes during the deposition of lithostratigraphic unit 5. It is worth noting that while the elemental ratios indicative of provenance changes do not show a change a baseline shift during LSU 5, they do show considerable scatter around the baseline. Vegetation may have still existed in both depositional sequences, but the pollen in this lithostratigraphic unit are intermixed with older, recycled pollen, implying that the plant matter cannot be guaranteed to be *in situ* (Kemp and Barrett, 1975).

The high mud content suggests that sedimentation is dominated by hemipelagic settling, while the periodic clast concentrations and absence of diamictites or sharp contacts between beds suggest that the coarse fraction of the sediments was likely derived from the rain-out of ice-rafted debris (Krissek et al., 2007; McKay et al., 2009; Ó Cofaigh et al., 2001; Powell et al., 2000). The high and constant IRD content, when compared to lithostratigraphic units 1, 4, and 5, and the monolithologic nature of LSU 5 together suggest that lithostratigraphic unit 5 was deposited in a relatively ice proximal environment with a fairly stable ice mass providing a fairly uniform supply of sediment.

5.1.3 Lithostratigraphic unit 4

Lithostratigraphic unit 4 (202 – 252 mbsf) is composed of a sequence of stratified and massive diamictites (41% of LSU 4), mudstones containing dispersed to common clasts (45% of LSU 4), and the only occurrence in the core of sandstones/siltstones which are rhythmically interlaminated with mudstones (10% of LSU 4). The base of this lithostratigraphic unit is characterised by mudstones with dispersed clasts conformably grading in and out of a 4.5 m thick, weakly stratified diamictite (facies 6), as well as a steadily increasing IRD content. Separated by a core break is a 13 m thick sequence of stratified and massive diamictites (facies 5 and 6), containing the highest IRD content (up to 20 wt% coarse sand, and up to 51 clasts >2 mm per 10 cm) recorded in the core. The mud content is low compared to the rest of the core in these diamictites, between 22 and 73%. The diamictites are conformably overlain by interbedded mudstones with common clasts (facies 2), diamictites (facies 5, 6), and a single, 1 m thick, turbidite deposit (facies 3). The interbeds of diamictites display gradational upper and lower contacts, and are up to 50 cm thick. Separated by another core break is a 5 m thick sequence of rhythmically interlaminated sandstones/siltstones and mudstones (facies 4), interbedded with a 20 cm thick sandstone (facies 3) deposit. Magnetic susceptibility readings vary along baseline values similar to those of lithostratigraphic unit 5, with the exception of an increase to several times that of the normal baselines values between 216 and 235 mbsf. Moreover, no significant geochemical variations are noted in lithostratigraphic unit 4, and the presence of vegetation is unsure for the same reasons as those outlined in lithostratigraphic unit 5

(Kemp and Barrett, 1975). Foraminifera (e.g. *Elphidiidae magellanicum*, and *Trochoelphidiella* spp.) during this lithostratigraphic unit indicate continued subsidence, with water depths ranging between 300 and 500 m (Leckie and Webb, 1983).

Some parts of the diamictite sequence show millimetre to centimetre scale stratification, defined by grainsize changes and clast alignment, as well as upward fining trends, which suggests that they were derived from mass flows proximal to the grounding line (Dowdeswell et al., 1998; Elverhøi et al., 1983; Evans et al., 2002; Eyles and Eyles, 1992; Hambrey et al., 1991; Krissek et al., 2007; McKay et al., 2009; Nam et al., 1995; Ó Cofaigh et al., 2001; Powell et al., 2000). Alternatively, the diamictites may also have been derived from the rain-out of debris from icebergs, given the random orientations of clasts and, where recorded, gradational contacts (Evans et al., 2002; Eyles and Lagoe, 1990; Krissek et al., 2007; McKay et al., 2009; Ó Cofaigh et al., 2001; Powell et al., 2000). Moreover, facies 4, which overlies the diamictites, is interpreted as cyclopels and cyclopsams based on the rhythmically laminated nature of the sandstones and mudstones, suggesting turbid subglacial plume deposition within a few kilometres of the grounded ice (Cowan et al., 1997; Cowan et al., 1999; Fielding et al., 2000; Krissek et al., 2007; Mackiewicz et al., 1984; McKay et al., 2009; Powell et al., 2000). Lithostratigraphic unit 4 therefore suggests an increase in ice proximity at the base, becoming most proximal during the deposition of the diamictites (facies 5, 6). This is followed by the increasingly more distal deposits of interbedded mudstones (facies 2) and diamictites (facies 5), and the overlying cyclopels/cyclopsams (facies 4). This sequence is broadly consistent with an established facies model for glacial maximum conditions and subsequent retreat (Fig. 5.1; Powell and Cooper (2002)). The key difference is that peak glacial conditions at DSDP 270 were likely not marked by ice contact or subglacial deposits, but rather by very ice proximal glacimarine diamictites. Although subglacial deposition of the diamictite sequence cannot be ruled out because the basal contact was not recovered, the random orientation of the clasts and lack of macromorphologic sedimentological or structural evidence of overriding ice (see section 4.3.5) suggest this was not the case. Micromorphological analysis would however be needed to further confirm this interpretation. As such lithostratigraphic unit 4 is interpreted as a high-energy, very ice proximal environment, where the presence of laminated ice proximal sediments indicates that the ice mass responsible for these deposits was likely wet-based with significant volumes of subglacial meltwater (Ó Cofaigh and Dowdeswell, 2001).
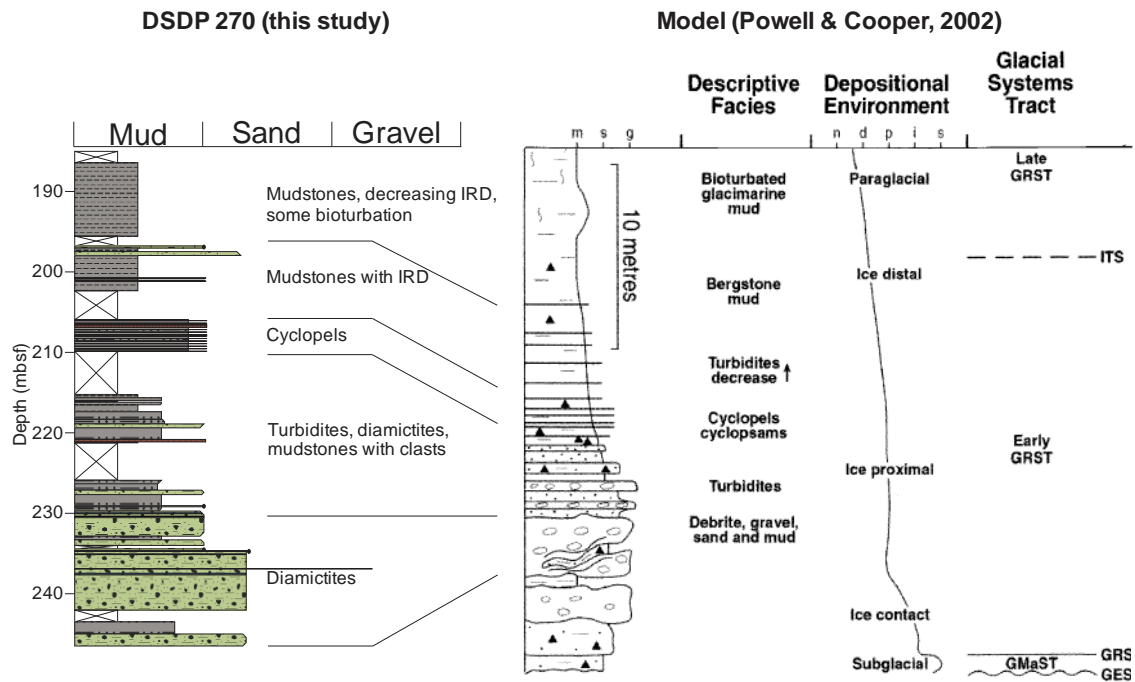
Fig. 5.1: Comparison of the glacial retreat sequence recorded at DSDP 270 to the glacial retreat model of temperate ice masses on continental shelves by Powell and Cooper (2002). Notations in the modelled sequence (left to right): m – mud; s – sand; g – gravel; s – subglacial, i - ice contact; p – ice proximal; d – ice distal; n – non-glacial; GES – glacial erosion surface; GMaST – glacial maximum systems tract; GRS – grounding line retreat surface; GRST – glacial retreat systems tract; ITS – iceberg-rafting termination surface. Note that the GES and GRS were not recovered at DSDP 270 due to the interpreted lack of ice contact, and therefore the diamictites represent the glacial maximum in this case.

5.1.4 Lithostratigraphic unit 3

The dominant sedimentation pattern of lithostratigraphic unit 3 (124 – 202 mbsf) are massive mudstones with absent to rare clasts (facies 1; ~70% of LSU 3). These mudstones can be interbedded on a decimetre scale with siltstones containing common to dispersed clasts (facies 2; 29% of LSU 3), and massive diamictites (facies 5; 1% of LSU 3). Interbeds of either lithology usually have sharp bases and fine upward again into massive mudstones. IRD contents are characteristically low in lithostratigraphic unit 3, and sporadic increases are generally confined to the interbeds of siltstones and diamictites. Magnetic susceptibility values display high amplitude variations, and include the peak values recorded at DSDP 270. An increase in foraminifera affiliated with polar regions (*Haplophragmoides* spp., *Trifarina* spp., *Cibicides* spp.) is taken to suggest the onset of the cooling of bottom waters in the latter stages of this lithostratigraphic unit (Leckie and Webb, 1983). Th/Sc is higher during this interval than during the lithostratigraphic units below it, which may suggest a higher input of felsic material into the sediments, resulting from either a change in the location of, or spatial increase in, the source area of the sediments, and/or a switch in clay mineralogy (Rollinson, 1993; Ruffell et al., 2002). Again, the presence of vegetation remains uncertain due to the presence of some recycled pollen species (Kemp and Barrett, 1975).

In glacimarine environments, mudstones lacking IRD are often ascribed to ice-distal environments (e.g. Dowdeswell et al. (1998); Fielding et al. (2000); Sexton et al. (1992)).

The same is suggested for this lithostratigraphic unit, especially when seen in the context of overlying the increasingly distal deposits of lithostratigraphic unit 4. Furthermore, occasional clast concentrations, characteristic of iceberg tipping events, also suggest deposition in an open marine environment rather than below an ice-shelf (cf. Domack et al. (1999); McKay et al. (2008)). Moreover, mudstones in an ice distal environment are likely the result of the hemipelagic settling of fine-grained debris, derived from sediment-laden meltwater plumes emanating from the grounding line. The massive nature of the some of the mudstones in this lithostratigraphic unit may also be indicative of an ice distal setting, as it could be the result of pervasive bioturbation (Ó Cofaigh and Dowdeswell, 2001). Outsized clasts, sand lenses, and the aforementioned clast concentrations are indicative of continued, albeit at a lesser frequency, ice-rafting across the drill site. The interbeds of sharp-based, coarser units grading upwards are interpreted to represent distal end-members of debris flows (Dowdeswell et al., 1998; Krissek et al., 2007; Ó Cofaigh et al., 2001). Thus, in accord with previous high-latitude studies (Dowdeswell et al., 1998; Powell and Cooper, 2002), this lithostratigraphic unit is interpreted as an ice distal environment and the culmination of a deglaciation sequence, where the increasing dominance of fine grained material is interpreted to suggest meltwater input during the retreat of the ice across the shelf and into the terrestrial realm.

5.1.5 Lithostratigraphic unit 2

Lithostratigraphic unit 2 is similar in character to lithostratigraphic unit 5, as mudstones with dispersed to common clasts (facies 2) form the dominant facies in both. As opposed to lithostratigraphic unit 5, however, lithostratigraphic unit 2 contains only one interbed of mudstones lacking clasts (facies 1), and instead encompasses several interbeds (<1 m thick) of clast-poor diamictites (facies 5 and 6). The upper and lower contacts of interbedded diamictites, where recovered, are gradational, and none of the previously discussed (section 4.3.5) macro-scale sedimentological or structural features characteristic of subglacial deformation are recorded. The IRD content in lithostratigraphic unit 2 varies between 0.2 and 2.5 wt% for the coarse sand fraction, and 0-17 clasts greater than 2 mm per 10 cm in the visual count. Furthermore, due to the dominant mudstone facies in this lithostratigraphic unit, the mud content is fairly high, with an average of 75%. Magnetic susceptibility values are fairly low, averaging 7.6 SI units. No significant geochemical changes appear to occur during the deposition of lithostratigraphic unit 2, with the exception of a slight decrease in Th/Sc values, and a slight increase in Si/Al values in the lower part of LSU 2. The foraminifera indicate that LSU 2 was deposited in the deepest waters (≤500 m water depth) of the studied section (385 – 20 mbsf; Leckie and Webb, 1983). Moreover, between 124 and 20 mbsf, this lithostratigraphic unit includes foraminifera (*Epistominella vitrea, Elphidium magellanicum, Nonionella iridea, Cibicides* spp., and *Melonis* spp.) which indicate significantly cooler conditions than previously at DSDP 270 (Leckie and Webb, 1983). As is the case in the underlying units, the existence of vegetation during the deposition of LSU 2 is unclear because recycled pollen are observed in these sediments (Kemp and Barrett, 1975).

The gradational contacts of the diamictite interbeds suggest that the coarse fraction of the sediments was likely derived from the rain-out of iceberg-rafted debris (Evans et al., 2002; Eyles and Lagoe, 1990; Krissek et al., 2007; McKay et al., 2009; Ó Cofaigh et al., 2001; Powell et al., 2000). This is superimposed on the dominant hemipelagic settling of fine grained sediments, which is indicated by the high mud contents (up to ~90%). Furthermore, the high mud content and occasional laminated sediments suggest significant amounts of

meltwater were being introduced to the environment (Ó Cofaigh and Dowdeswell, 2001). The exact ice proximity is difficult to determine, but based on the renewed increase in the amount of IRD and simultaneous decrease in mud content, lithostratigraphic unit 2 is interpreted to represent a more ice-proximal environment than lithostratigraphic unit 3. The higher Si/Al values, compared to those further downcore, may indicate increased biogenic content (Rothwell and Croudace, 2015).

5.1.6 Facies evidence for a subpolar glacial regime throughout the Oligocene to Miocene

The absence of biosiliceous content in mudstones below ~160 mbsf, and the complete lack of diatomites in ice distal environments point towards a warmer-than-present glacial regime in the central Ross Sea during the Oligocene to early Miocene. This lack of diatoms, which is characteristic of temperate and some subpolar glacial regimes, is interpreted as being the consequence of large quantities of glacial outwash prohibiting the distribution of diatoms (McKay et al. (2009), and references therein). However, while diatoms were judged to be mostly absent in DSDP 270 sediments (McCollum, 1975), the presence of cristobalite and tridymite clays above ~160 mbsf (Cook et al., 1975) suggests that some diatoms were likely present in sediments above ~160 mbsf before the onset of diagenesis (Harwood, 2010). This may be reconciled with a slight positive shift in the biogenic silica proxy ratio Si/Al upcore (Fig. 4.14). Together these observations may suggest there was some reduction in water column turbidity and meltwater input above 160 mbsf. An additional line of evidence for a subpolar glacial regime that is dominated by sediment laden glacial meltwater, is the high long-term sedimentation rates (up to ~18 cm/kyr; perhaps even more rapid during the deposition of the very proximal LSU 4 sediments) between the two hiatuses at 348 and 20 mbsf. The presence of stratified ice proximal sediments in lithostratigraphic unit 4 is particularly important in this context, as cyclopels/cyclopsams in relation to turbid meltwater are almost entirely absent in the modern polar regime of Antarctica, but they are common in subpolar and temperate settings, and can be 10s of metres thick (Cowan et al., 1997; Cowan et al., 1999; Evans et al., 2002; Mackiewicz et al., 1984; McKay et al., 2009; Ó Cofaigh and Dowdeswell, 2001). This sedimentological evidence for a subpolar glacial regime is congruent with the palynology, as well as the micro- and macro-fossil assemblages at DSDP 270, which all suggest that climatic boundary conditions in the Oligocene to early Miocene allowed the development of flora and fauna which today are found in more temperate-style environments (Dell and Fleming, 1975; Kemp and Barrett, 1975; Leckie and Webb, 1983).

5.1.7 Sediment provenance

Previous studies of glacially derived pebbles at DSDP 270 were unable to accurately determine their source area, but based on their lack of affiliation with Transantarctic Mountains and coastal Marie Byrd Land lithologies, a provenance source located between the two was surmised (Barrett, 1975a). However, given that other than the marble and gneiss observed at the base of DSDP 270 (Ford and Barrett, 1975) the lithologies present on the Central High are unknown, it cannot be ruled out that some of the pebbles may have originated from local ice caps on the Central High. This would be consistent with the seismic data (discussed in the next section) which suggests that the sediments at DSDP 270 were derived from ice caps on the Central High during glacial periods (De Santis et al., 1995). Furthermore, Barrett (1975a) reported no significant change in provenance with

time, and textural studies suggested that all glacimarine sediments are very poorly sorted, and are indicative of extensive ice interaction (Barrett, 1975b).

5.2 Oligocene-Miocene central Ross Sea seismic data

The broader regional implications of these facies changes can be reassessed by integrating these new results and interpretations with the existing Ross Sea seismic stratigraphic framework (Fig. 5.2). The sediments at Site 270 were deposited as part of Ross Sea Seismic Sequence (RSS) 2, which overlies Ross Sea Unconformity (RSU) 6 (De Santis et al., 1995). It is important to note that RSU6 onlaps the Central High, and therefore the sediments at DSDP 270 do not directly overlie the unconformity. Seismic evidence suggests that prior to the late Oligocene, significant parts of the present continental shelf were subaerial, and occupied by glaciers which carved the U-shape valleys, such as the one on whose flank DSDP 270 is located (Line 33 in figure 5.2; De Santis et al. (1995)). This is supported by the presence of talus deposits overlain by a paleosol at the base of DSDP 270 (below ~388 mbsf). These glacially eroded, U-shape valleys occur around the Central High, and the heads of these valleys are topographically above RSU6, which onlaps the Central High (De Santis et al., 1995; De Santis et al., 1999).

Overlying the pre-glacial sediments is seismic facies C, which has been interpreted as an ice proximal facies based on a mixture of sub-horizontal reflectors and chaotic lenses. This facies generally downlaps onto lower strata, and is solely deposited on the flanks of basement highs in the Ross Sea, and as such has previously been interpreted to be sourced from ice caps and glaciers centred on the Central High (De Santis et al., 1995). As is shown in Figure 5.3, the lower seismic facies C of De Santis et al. (1995) can be further subdivided into three subsections based on the lithostratigraphic units described in this study: (1) a shallower ice proximal setting where sediment delivery is dominated by the turbidites of lithostratigraphic unit 6. This is overlain by an unconformity (brown reflector in Figure 5.3), which is correlated to the aforementioned 5-Myr hiatus between lithostratigraphic units 6 and 5. The reflector correlating to this unconformity truncates the underlying strata and is fairly flat above the strata overlying the Central High, but matches the dip of the strata as it moves further offshore. Above the unconformity (2) moderately stratified strata within the bounds of seismic facies C are correlated to the slightly more distal setting of lithostratigraphic unit 5 of this study. Finally, (3) the upper part of seismic facies C, which displays somewhat clearer stratification, is suggested to represent an even more proximal setting, and is correlated to the sediments recovered in lithostratigraphic unit 4.

Stratified sediments covering facies C have previously been interpreted as ice distal, where the Central High was submerged and sediment was onlapping basement highs (seismic facies B). This seismic facies corresponds to lithostratigraphic unit 3 presented here, which is also interpreted as ice distal (Fig. 5.3). Above ~120 mbsf, another ice proximal facies (seismic facies C), similar in character to the one lower down in the core, was recognised (De Santis et al., 1995), and is correlated to lithostratigraphic unit 2 at DSDP 270 (Fig 5.3). It is noted that stratification in this interval is not as distinct as in the lower seismic facies C. This may be due to the increased water depth and distance from source, resulting in a more homogenous structure of the deposit.

The Oligocene to early Miocene seismic sequence boundaries are associated with minimal erosion on the outer continental shelf surrounding the basement highs, as indicated by their low angle truncation surfaces, as well as the lack of troughs and other features characteristic of large scale erosion in seismic images (De Santis et al., 1995). Furthermore, the absence of erosional features produced by grounded ice masses has been suggested to preclude a major, long lasting advance of an ice sheet to the continental shelf during RSS-2 (De Santis et al., 1999). As such, it has been proposed that the Central High remained a bathymetric high which periodically hosted ice caps during sea level lowstands, until a combination of tectonic subsidence, glacial erosion and eustatic changes caused the Central High to permanently submerge beneath sea level at some point during the early to middle Miocene (Bart and De Santis, 2012; De Santis et al., 1995; De Santis et al., 1999).

Fig. 5.2 (overleaf): Structure contour map of RSU6, overlain with the distribution of seismic facies during the deposition of RSS-2. Also shown are three previously interpreted seismic lines across DSDP Site 270. Each line is noted by a colour, corresponding to the title of each interpreted seismic section on the right (modified from De Santis et al. (1995))
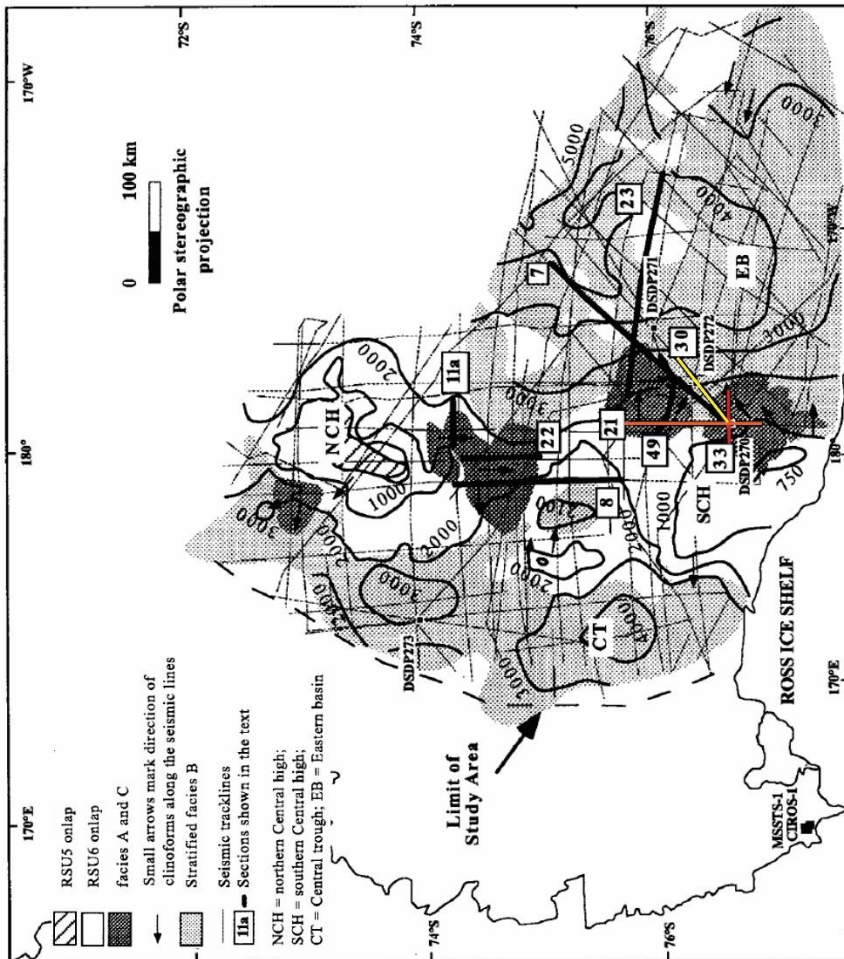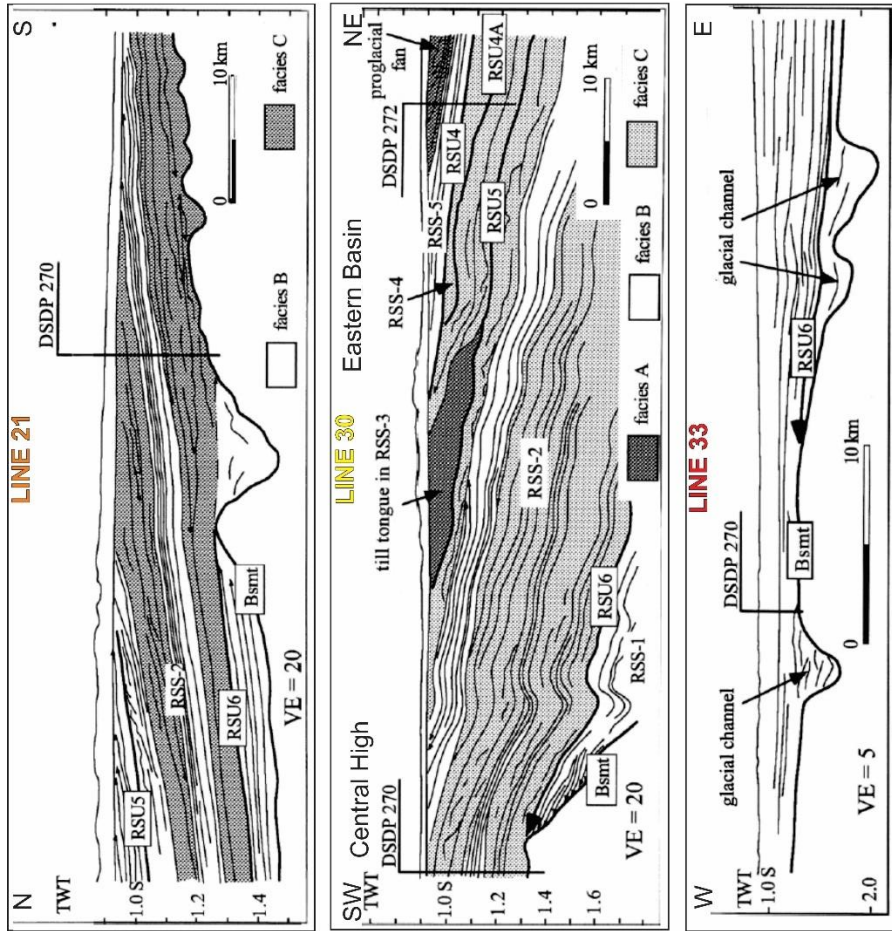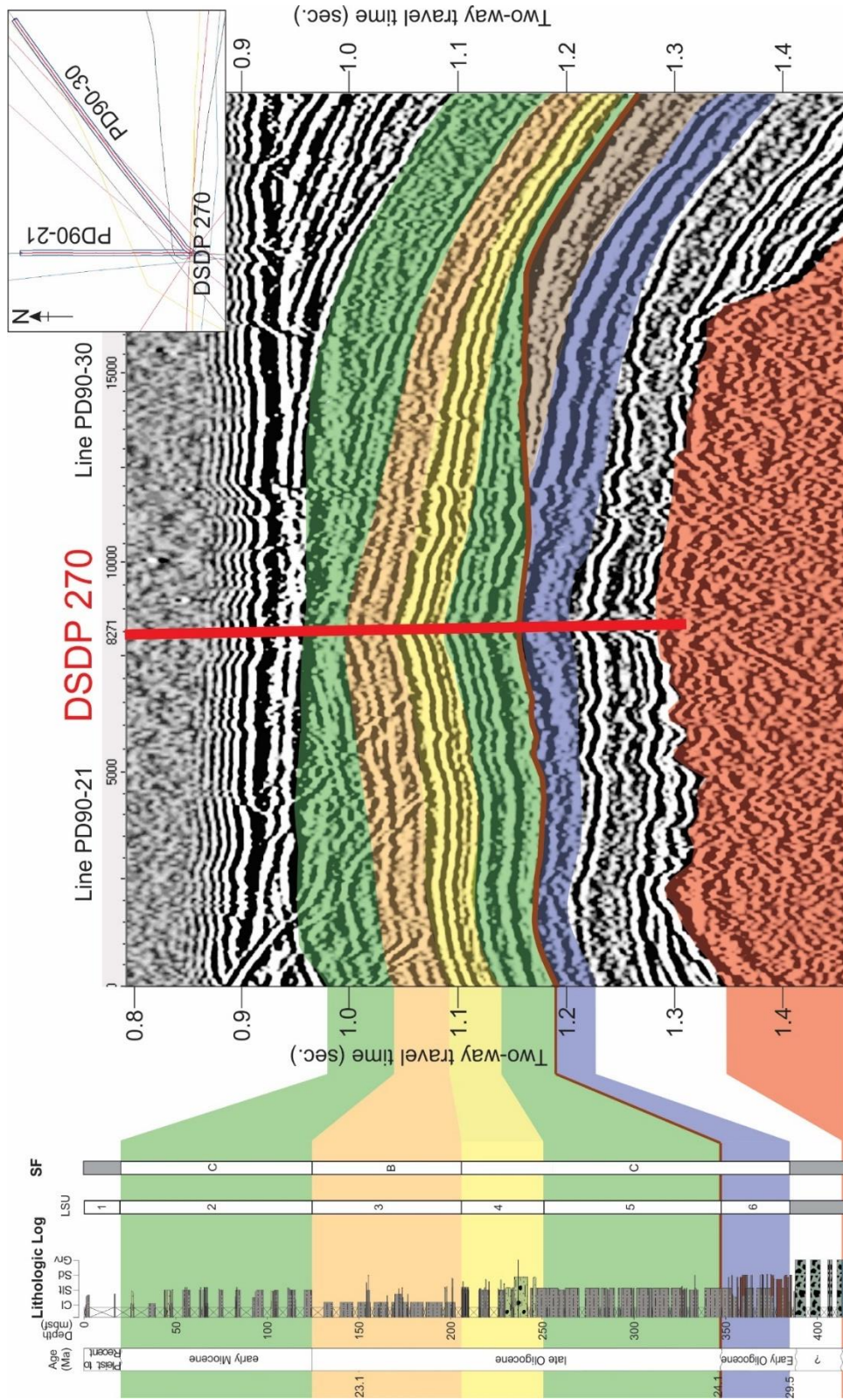
Fig. 5.3: Correlation of the lithostratigraphy and lithostratigraphic units (LSU) to the seismic facies (SF) of De Santis et al. (1995), and two seismic lines (PD90-21, PD90-30). The colours in the seismic correlate to the LSUs. The brown line is the newly identified reflector which likely correlates to the hiatus at 348 mbsf (L. De Santis, pers. comm.). The inset map shows the location of the seismic lines and DSDP 270. This figure was produced with the help of L. De Santis, and an uninterpreted version of this seismic image is available in Appendix 13.

5.3 Integrated Oligocene-early Miocene central Ross Sea glacial history

By combining the data and interpretations of the sediments recovered from DSDP 270 with several far-field records (Fig. 5.4), a broad Oligocene to early Miocene glacial history of the central Ross Sea can be constructed. A cartoon summarising this history (Fig. 5.5) is provided at the end of this section.

5.3.1 Early Oligocene – marine transgression

The base of the core is characterised by a pre-glacial sequence which records the initial transgression from subaerial brecciated talus deposits and a paleosol, to estuarine calcareous sands and shallow water (≤30 m) glauconitic sands (Barrett, 1975b). This sedimentation pattern, from terrestrial deposits to the organic-rich, marine mudstone overlying 1 m of glauconitic sandstone, broadly matches the modelled stacking pattern of transgressive shelf deposits (Galloway and Hobday, 1983). This organic-rich mudstone between 385 and 384 mbsf (~29.5 Ma), is the first marine sediment that bore witness to ice interaction, as evidenced by the presence of outsized clasts which are interpreted as IRD. Previous studies have found that this interval of the core also contains the highest abundance of pollen, as well as abundant degraded tissues, leaf cuticles and vascular fragments. Together with the lack of recycled pollen, these plant remains suggest that they were deposited very proximal to the contemporaneous vegetation source (Kemp and Barrett, 1975). This implies that *Nothofagus* dominated vegetation coexisted with glaciers in the remaining subaerial exposures on the Central High during the early Oligocene, a phenomenon also witnessed elsewhere in Antarctica at this time (Anderson et al., 2011; Barrett et al., 1989; Kemp and Barrett, 1975; Prebble et al., 2006). It is not possible to determine when the vegetation ceased to exist, as pollen further upcore yield similar assemblages in very lower abundance to those lower in the core, but also included extensively reworked older assemblages (Kemp and Barrett, 1975). The reduced supply of pollen further upcore may have been the consequence of a diminished, or more ice covered, landmass on the Central High by the late Oligocene (which is congruent with further evidence presented in the following sections). Overlying the organic-rich mudstone, which is also part of LSU 6, are turbidites which are interpreted to be the result of slope instabilities associated with the rapid sediment input from marine terminating glaciers and/or rapid transgression, where foraminifera indicate a deepening down to inner shelf depths of ≤100 mbsf (Leckie and Webb, 1983). The sediment supply for these turbidites was likely derived from sediment-laden meltwater emanating from marine terminating glaciers (as evidenced by the presence of IRD) and glaciofluvial systems. The rapid input of glacial sediment, some of which was delivered via subglacial meltwater conduits to below wave base, into this subsiding basin likely led to slope instabilities at the grounding line of marine terminating glaciers, which are known to have been present. Other factors which possibly caused the re-sedimentation of pro-glacial deposits include iceberg calving and earthquakes.
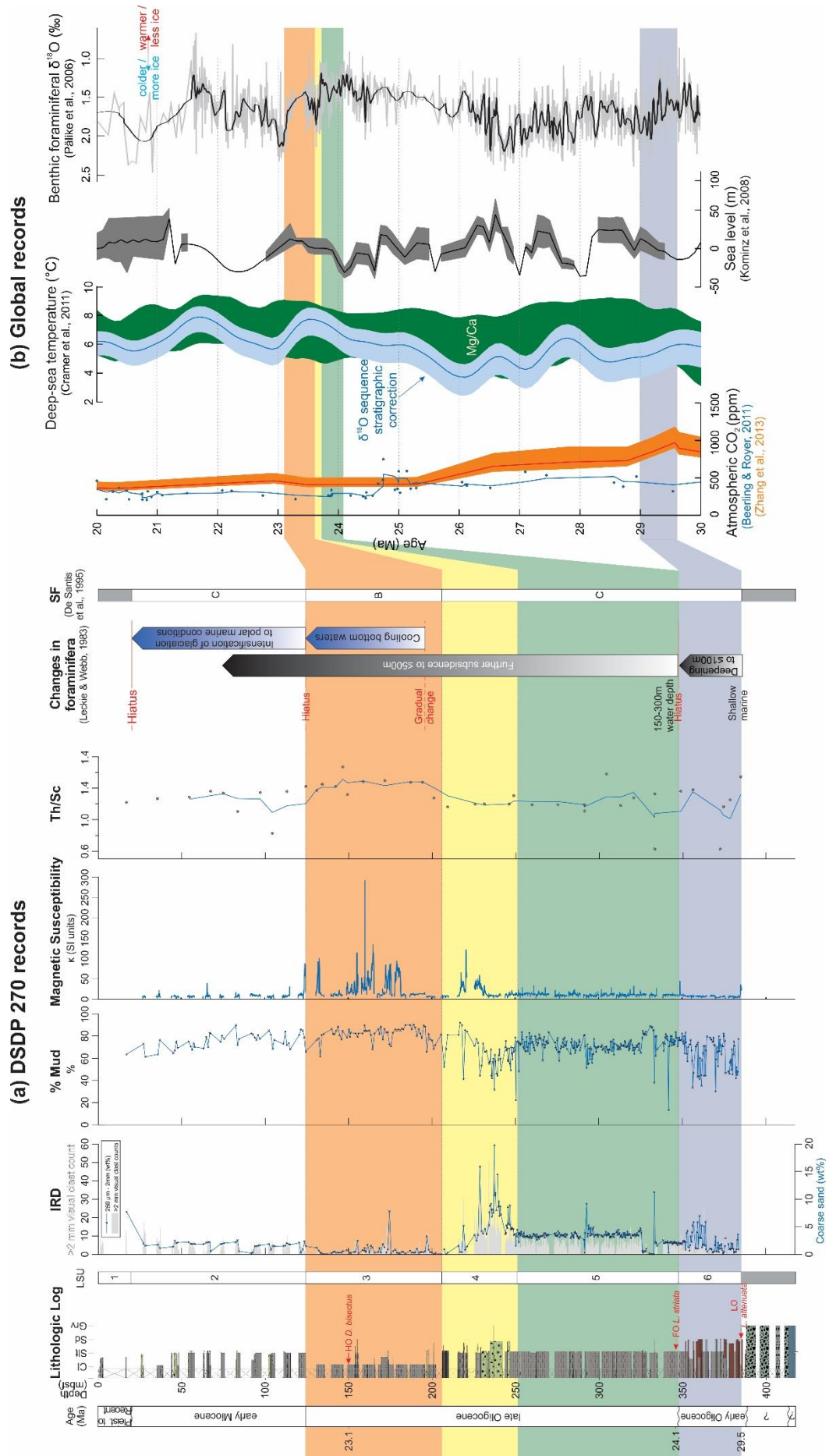
Fig. 5.4 (overleaf): (a) Records recovered from DSDP 270. Shown are the revised lithologic log from this study, the lithostratigraphic units (LSU) described in the text, the two IRD proxies (number clasts >2 mm in the core face, and % coarse sand (250 µm – 2mm), mud, magnetic susceptibility, and the Th/Sc ratio (with a 3-point moving average). The changes recorded in the foraminifera are adapted from Leckie and Webb (1983), and the seismic facies (SF) from De Santis et al. (1995). The ages are based of the biostratigraphic datums (in red) of the preliminary age model by Kulhanek et al. (in prep.), and allow a tentative correlation to the global records (b) including: benthic foraminiferal $\delta^{18}O$ proxy of ice volume and temperature (black line is a 20-point robust loess smoothing; Pälike et al., 2006b); far-field passive margin sea level estimates, where the black line indicates the best fit with estimated sea-level lowstands bounded by maximum and minimum estimates in grey (Kominz et al., 2008); deep ocean temperatures derived from removing the ice volume component from benthic $\delta^{18}O$ records using passive margin backstripped sea level records (blue), and low resolution Mg/Ca records (green) (Cramer et al., 2011); atmospheric CO_2, compiled from several sites using various proxies (blue dots, with a 3-point moving average) (Beerling and Royer (2011), and references therein), as well as from a single site using alkenone-based reconstructions (ODP 925; orange) (Zhang et al., 2013). Shown on the far right of the graph is an expanded section of the oxygen isotope curve between 24.1 and 22.5 Ma, with a 15-point moving average (red line) of the data.

The temperate-style climatic conditions suggested by the pollen and foraminifera are consistent with the high terrigenous sedimentation rates suggested by the preliminary age model (up to 18 cm/kyr). As previously mentioned, this suggests a wet-based, subpolar-style glaciation, where the presence of IRD indicates glaciers likely calved into an open sea, and the high mud percentage indicates the presence of large volumes of sediment-rich glacial meltwater. Terrestrial run-off from glaciofluvial systems is indicated by the high amounts of contemporaneous pollen, which suggest surface temperatures were high enough to allow surface meltwater and a co-existing vegetation (Kemp and Barrett, 1975). Ice-rafted debris is fairly variable over this interval, but steadily increasing through time, suggesting the presence of at least a local marine terminating glacier calving into the sea. Such a glacier likely drained from the Central High judging by the proximity implied by the coarse sands in the turbidite deposits, which are most likely derived from the nearest topographic high (i.e. the Central High). The fact that these turbidite deposits immediately overlie the shallow marine and terrestrial deposits further supports the interpretation that these turbidites were deposited in relatively close proximity to a terrestrial margin. Moreover, this is supported by the proximal seismic facies, which have been interpreted as being sourced form an ice cap on the Central High (facies C; De Santis et al. (1995)). As previously discussed (section 5.2), seismic facies C can be subdivided into three sections, and this slightly less stratified interval below the unconformity corresponds to the turbidite sequence of lithostratigraphic unit 6. However, the aforementioned provenance of the IRD (section 5.1.7; Barrett (1975a)) implies that some sediment was also derived from Marie Byrd Land, a location where seismic data of significant glacial offshore troughs and ridges also suggests contemporaneous marine terminating glaciers of substantial size (Sorlien et al., 2007). Furthermore, studies of the textures of volcanic deposits, and of the exhumation rates of intruded gabbros suggest that there was also an ice cap in Marie Byrd Land during

the Oligocene, consistent with the data presented here (LeMasurier and Rex, 1983; LeMasurier and Rocchi, 2005; Rocchi et al., 2006).

Furthermore, the higher than average U/Th data during lithostratigraphic unit 6 (Fig. 4.15) suggest that the waters were less well oxygenated, possibly dysoxic in places, during the early Oligocene. A lack of correlation between Fe and Ti ($r^2 = 0.13$), the sole appearance of hematite clays (Cook et al., 1975), as well as lower Mn/element values (Fig. 4.14), indicative of reducing conditions and suboxic waters (Rothwell and Croudace, 2015), appear to confirm this view. Suboxic waters may have been the result of increased productivity, or sluggish water circulation, possibly resulting from a highly stratified water column due to nearby freshwater runoff (Gallego-Torres et al., 2007; Karstensen et al., 2008; Keeling et al., 2009). However, lithostratigraphic unit 6 was likely the only extended period of reduced oxygenation, as sediments further upcore consistently record stable to slightly increasing Mn/element values, and U/Th values which remain in the oxic field (<0.75). As such, it is suggested that waters were well oxygenated for most of the late Oligocene to early Miocene at DSDP 270, which may be the combined consequence of the deeper water environment, a more distal environment to terrestrial freshwater runoff (reducing the stratification of the water column), and greater mixing with oceanic waters (Keeling et al., 2009).

The ~5-million-year disconformity at 348 mbsf had previously been suggested based on the foraminiferal assemblages (Leckie and Webb, 1983), but was not noted in the initial age model (Allis et al., 1975). The hiatus appears to correspond to a distinct seismic reflector at ~1.2 seconds two-way travel time in seismic lines PD90-21 and PD90-30 at DSDP 270 (brown line in Figure 5.3; L. De Santis, pers. comm.). Furthermore, this unconformity between ~29 and 24.1 Ma at DSDP 270 may be associated with an unconformity observed in the Cape Roberts Project drillcores at ~25 Ma (e.g. Barrett (2007)), which is attributed to a glacial period, coincident with a lower $\delta^{18}O$ values (Pälike et al., 2006b). However, there is no direct evidence of glacial overriding associated with this hiatus at DSDP 270. Therefore, if this hiatus is associated with glacial expansion, it was either associated with non-depositional glacial erosion or the glacimarine sedimentary depocentre was shifted, or a combination of both. Evidence for a shift in depocentre may be found in the seismic data, which shows a seismic unit (brown shading in Figure 5.3) onlapping the early Oligocene sequence and pinching out into the unconformity, causing it to not be recorded at DSDP 270.

5.3.2 Late Oligocene – continued subsidence and distal glacimarine sedimentation

Above the hiatus, benthic foraminifera suggest a 100 m deepening of the water depth at DSDP 270, down to 300 m. Furthermore, foraminifera suggest this subsidence gradually continued into the early Miocene interval of the core (Leckie and Webb, 1983). Between 348 and 252 mbsf (~24.1 to ~23.6 Ma), mudstones containing significant amounts of IRD (lithostratigraphic unit 5), and the relatively uniform distribution of IRD are interpreted as a steady supply of icebergs, and relatively stable ice masses without large shifts in dynamic ice discharge. The provenance of pebbles suggest icebergs sourced from Marie Byrd Land continued to drift over DSDP 270 (Barrett, 1975a), while this section of the ice proximal seismic facies C, albeit slightly more distal than before (see section 5.2), also suggests continued sedimentation derived from an ice cap on the Central High (De Santis et al., 1995). Studies of gabbros, exhumed through block faulting and dome uplift, in Marie Byrd

Land do indeed confirm the continued presence of ice caps in that region during the late Oligocene and early Miocene (Rocchi et al., 2006). Based on the results presented here, and the aforementioned studies, it is suggested that ice masses of substantial size continued to calve at sea level during this part of the late Oligocene. Moreover, the presence of marine-terminating ice masses in West Antarctica through this time period is consistent with other coeval ice proximal records in Antarctica. For example, the Oligocene section of the CRP cores in the western Ross Sea record shallow marine, ice proximal glacimarine cycles which provide direct evidence of orbitally-paced expansions of EAIS outlet glaciers across the continental shelf (Barrett, 1989; Naish et al., 2008). These oscillations, indicated by cyclic changes in lithofacies (e.g. diamictites during glacial lowstands, and bioturbated massive mudstones during interglacial highstands) of the outlet glaciers appear to have been paced largely by obliquity in the time leading up to the Mi-1 (Naish et al., 2008; Naish et al., 2001), a similar result to that found in this study (section 5.4).

5.3.3 Late Oligocene – marine ice sheet expansion and retreat

Lithostratigraphic unit 4 is characterised by the presence of both stratified and massive diamictites (facies 5, 6) between ~250 and 220 mbsf, passing up into the rhythmically laminated mud and silt/sandstone, which are interpreted as ice proximal glacimarine rhythmites (cyclopels/cyclopsams; facies 4), and then into mudstones with an up-core decrease in clast abundance (i.e. grading into lithostratigraphic unit 3; Fig. 5.1). As pointed out earlier, there is no evidence that these diamictites were deposited subglacially. A subglacial depositional environment can be confidently identified from drillcores by evidence of glacial surfaces of erosion, in the form of sharp facies dislocations, and evidence of brittle and ductile deformation features across these facies boundaries (Fielding et al., 2000; McKay et al., 2009; McKay et al., 2012b; Naish et al., 2009; Naish et al., 2001). However, the basal contact of the diamictite at 252 mbsf in DSDP 270 was not recovered, and so it cannot be conclusively determined if these diamictites were deposited subglacially. Moreover, diamictites can be deposited in a range of proximal, and occasionally distal, glacimarine environments (Anderson et al., 1980; Domack et al., 1999; Dowdeswell et al., 1994; Fielding et al., 2000; Krissek et al., 2007; McKay et al., 2012b; Powell and Molnia, 1989), but the facies stacking pattern which overlies the diamictites – cyclopels/cyclopsams (facies 4) passing up into mudstones with decreasing IRD content (facies 1, 2 in lithostratigraphic unit 3) – is highly indicative of a diamictite which was deposited proximal to an ice sheet grounding line. This overall facies stacking pattern is nearly identical to that of the conceptual retreat sequence of temperate-subpolar ice masses on continental shelves (Fig. 5.1; Powell and Cooper (2002)), with the exception that the glacial maximum is not represented by ice contact, but by glacimarine diamictites. Consequently, the diamictites at the base of lithostratigraphic unit 4 are argued to reflect the expansion of a partly marine-based ice sheet/cap on the Central High, expanding close to the site, but not necessarily overriding it. This ice advance may be coeval with a low in oxygen isotope values at ~23.6 Ma (Fig. 2.9, 5.4; Pälike et al. (2006b)). Moreover, it is important to note that these sediments indicate that substantial ice masses not only existed in West Antarctica during the late Oligocene, but also advanced during certain periods in this time interval which had previously been suggested to be characterised by a warming (Cramer et al., 2011; Zachos et al., 2008; Zachos et al., 2001a). The cyclopels/cyclopsams overlying the diamictites and mudstones were deposited in an ice proximal glacimarine sediment within a few kilometres of an ice sheet grounding line (Cowan et al., 1999; Mackiewicz et al., 1984; Ó Cofaigh and Dowdeswell, 2001), and represent the initiation of glacial retreat away from DSDP 270. The overlying mudstones with an upcore decline in

IRD (lithostratigraphic unit 3) are indicative of a continuation of this grounding line retreat (section 5.3.4).

Furthermore, an increase in the magnetic susceptibility between 215 and 235 mbsf, which occurs immediately above the diamictite, indicates a shift in the fine grained provenance, and is tentatively interpreted as being the consequence of a widespread discharge in sediment laden meltwater during the initiation of glacial retreat, as opposed to the more localised erosional source (e.g. Central High) during the glacial maxima.

5.3.4 Latest Oligocene – distal glacimarine sedimentation

The subsequent deposition of IRD-poor, ice distal mudstones containing centimetre-scale carbonaceous stringers (lithostratigraphic unit 3) points to an extended period of higher relative sea level, and possibly lower ice volumes, at least locally, during the latest Oligocene. This interpretation of the stratigraphy is congruent with other ice proximal studies from subpolar glacial regimes which have also interpreted bioturbated mudstones with rare to absent clasts as being distal to a grounding line, and thus representing a minimum in ice volume (e.g. Dowdeswell et al. (1998); Fielding et al. (2000); McKay et al. (2009)). A notable increase in magnetic susceptibility occurs between 180 and 150 mbsf (Fig. 5.4), and as with the earlier spike in magnetic susceptibility at 215-235 mbsf, is interpreted to reflect a provenance shift related to a change in glacial discharge processes, such as enhanced meltwater input during a pulsed retreat of the ice. The meltwater input may have been derived from an increased glaciofluvial discharge into the embayment along a more deglaciated coastline. Conversely, glacial advances are also characterised by enhanced dynamic ice discharge processes, and can result in an increased areal extent of the zone of glacial erosion, thereby possibly causing increases in magnetic susceptibility (Golledge et al., 2013; Levy et al., 2016). However, the retreat scenario is favoured as IRD are at their lowest values in the core, and an increase in IRD is expected if advance towards the site was occurring (but see alternative explanation below). This peak in magnetic susceptibility may represent part of a long-term retreat after the glacial advance observed in lithostratigraphic unit 4 between 252 and 202 mbsf. Previous studies in southern Greenland have found a similar pattern to the one observed in this study, where the initial deglaciation is marked by a large positive excursion in IRD, and as deglaciation progressed further inland, the IRD content of the sediments decreased significantly whilst magnetic susceptibility measurements increased drastically. This is argued to reflect enhanced meltwater output during the later stages of deglaciation and the course of the interglacial (Carlson et al., 2008; Stoner et al., 1995). In the Ross Sea, the low IRD values suggest glacial termini had largely retreated onland and glaciofluvial discharge was dominating the terrigenous sedimentary input into the central Ross Sea. Moreover, this interval contains the sole occurrence of carbonaceous stringers and lenses, which had previously also been reported in ice distal mudstones in other glacimarine environments (e.g. Fielding et al. (2000); Powell and Molnia (1989)). This may indicate that the glaciofluvial meltwater discharge into the Ross Sea was carrying terrestrially-derived organic matter into the marine realm, consistent with the continued presence of pollen in the sediments (Kemp and Barrett, 1975). Furthermore, a coeval positive shift is recorded in the Th/Sc ratio, which can either point to an increase in felsic material in the sediments (Cullers, 1988; Rollinson, 1993), or a relative increase in kaolinite over illite and chlorite clays (Ruffell et al., 2002). The former would indicate a change in, or wider range of, provenance, possibly associated with deglaciation of different parts of West Antarctica, while the latter would suggest more humid conditions. As low-resolution X-ray diffraction data of the clay mineralogy have

only identified the presence of kaolinite below 360 mbsf (Cook et al., 1975), the interpretation of a relative increase in felsic material appears more likely. Either way, both possible interpretations of the Th/Sc data, as well as the elevated magnetic susceptibility of the sediments, are consistent with the interpretation of continued deglaciation during lithostratigraphic unit 3.

Some studies have suggested that increased magnetic susceptibility measurements such as those observed during this interval can be the result of the formation of secondary magnetic minerals during diagenesis (Hatfield and Stoner, 2013). Multiple lines of evidence suggest that this is not the case here. Firstly, higher magnetic susceptibility values were measured, at the very top, and directly above, the sequence of diamictites. This points to magnetic signals which reflect terrigenous input rather than authigenic minerals. Secondly, Fe and Ti are strongly correlated above 348 mbsf ($r^2 = 0.91$) which suggests that Fe was not affected by reducing conditions, decreasing the likelihood of the presence of secondary magnetic mineral growth. It is however noted that no Fe and Ti measurements are available for the interval of higher magnetic susceptibility. Elevated magnetic susceptibility measurements due to sediment being introduced by bottom-waters (e.g. Moros et al. (1997); Richter et al. (2006)) cannot be ruled out, but given the aforementioned lack of evidence of significant bottom current activity at DSDP 270, this option appears less likely.

The switch from lithostratigraphic unit 4 to lithostratigraphic unit 3, during the proposed deglaciation sequence following a glacial maximum, is contemporaneous with the sudden shift from ice-proximal to ice-distal facies in the seismic data (Fig. 5.3; De Santis et al. (1995)), and consistent with deglaciation and higher (local) sea levels during the latest Oligocene (~23.4 Ma). Providing further support to this interpretation of reduced ice volume is the sole occurrence of a macrofossil (*Chlamys* n. sp. aff. *natans*) at DSDP 270 which suggests open rocky shores during this interval (Dell and Fleming, 1975). Moreover, widespread glacial retreat is broadly consistent with low resolution far-field passive margin sea level estimates, which suggest a coeval period of rising sea levels (Fig. 5.4; Kominz et al. (2008)). As, such this deglaciation may have contributed to a decrease in benthic $\delta^{18}O$ during the latest Oligocene, representing the culmination of a long-term decrease in $\delta^{18}O$ values during the late Oligocene (e.g. Zachos et al. (2001a)). Although it has been shown that the magnitude of this long-term change was exaggerated due to a switch in sampling sites from vastly differing latitudes around that time (e.g. Cramer et al. (2009); Pekar et al. (2006)), single site $\delta^{18}O$ records have also recorded a decrease in $\delta^{18}O$ during the late Oligocene, albeit of smaller magnitude, with minimum ice volume and/or maximum temperatures during magnetochron C6Cr (~24-23 Ma; Fig. 5.4; Pälike et al. (2006b)). Due to the apparent contradiction of long-term deglaciation with ice proximal data from East Antarctica (e.g. Barrett (2007)), decreases in Antarctic Bottom Water production had been proposed to explain the lighter $\delta^{18}O$ values during the late Oligocene (Pekar et al., 2006). In agreement with Barrett (2007), the results presented here suggest that leading up to the latest Oligocene significant ice volumes persisted in West Antarctica (i.e. lithostratigraphic units 6, 5, and 4). Only in the latest Oligocene does there appear to be a period of (local) reduced ice volume. Therefore, it is suggested here that some of the reduction in $\delta^{18}O$ values during the latest Oligocene (i.e. not covering the entire 'late Oligocene warming') may reflect a decrease in ice volume, at least in parts of West Antarctica.

Two possible causes of this deglaciation and period of low ice volumes are considered here. Firstly, the ablation of ice on the Central High, and presumably other areas of West Antarctica, at the culmination of warming temperatures during the latest Oligocene (Zachos

et al., 2001a). Supporting this interpretation are the comparatively warm deep-sea temperatures during the latest Oligocene (Fig. 5.4; Cramer et al. (2011)). However, CO_2 measurements during this interval of the late Oligocene appear to be invariant, with a baseline value between 300 and 400 ppm, depending on the proxy used (Fig. 5.4; Beerling and Royer (2011); Zhang et al. (2013)). This implies that either, some mechanism of radiative forcing other than CO_2 would have to be invoked to cause the warming, or the lack of change is an artefact of low sampling density or uncertainties with the CO_2 proxies during this interval.

Alternatively, the deglaciation may also have been a result of the ongoing rapid subsidence indicated by the foraminifera (Leckie and Webb, 1983). Marine terminating ice-sheets and ice-caps could have persisted in the shallower water (~300 m water depth) of the earlier part of the record, as they were dominated by ice masses that were largely terrestrially-based and only extended slightly into the marine realm. However, the increased subsidence would have decreased the terrestrial area where most of the ice volume was accumulating, and the latest Oligocene ocean temperatures may have been too warm (Cramer et al., 2011) to support marine-based ice in the deeper marine settings (McKay et al., 2016; Levy et al., in prep.). Providing support for a deglaciation due to rapid subsidence is the fact that no significant ice loss is recorded in East Antarctica (Barrett, 2007), and periodic coastal expansions of EAIS outlet glaciers appear to have continued during this interval (Naish et al., 2008), as well as the lack of a significant change in CO_2 forcing to drive the warming (Beerling and Royer, 2011; Zhang et al., 2013).

Unfortunately, given the data presented in this study, it cannot be confidently determined whether the interpreted ice loss during the latest Oligocene was due to the rapid subsidence of the Central High, warming temperatures, or a combination of both. Future work incorporating organic geochemistry and stable isotopes as proxies of changes in temperature and the hydrological regime may be able to determine the causal factor of the deglaciation (Duncan et al., in prep.).

An additional alternative explanation to that of a deglaciation, is that the latest Oligocene sediments of lithostratigraphic unit 3 may be associated with ice sheet expansion. While a relative sea level rise leading up to a major glaciation such as the Mi-1 may appear to be contradictory with the usual facies models for glacial cycles (Dunbar et al., 2008; Naish et al., 2008), recent modelling efforts have shown that a significant local sea level rise, on the order of several tens, to more than one hundred of metres, can occur at ice proximal sites leading into, and across a large scale expansion of ice on Antarctica (Stocchi et al., 2013). For example, a 70-80 m rise in relative sea level is proposed around Antarctica during the EOT, where sediments recovered at Cape Roberts indicated a transgressive trend with a steady decline in the frequency of maximum abundances of IRD (Galeotti et al., 2012; Stocchi et al., 2013). This effect occurs due to the local depression of the lithosphere caused by the loading of a large ice mass, in addition to the gravitational attraction of the water to the ice mass. Low IRD contents, such as those observed in lithostratigraphic unit 3 at DSDP 270, are not inconsistent with this theory as enhanced IRD discharges are usually inferred to occur during the deglaciation (e.g. Patterson et al. (2014); Weber et al. (2014)). Such a scenario is also potentially reconcilable with the seismic data, as the seismic facies B, interpreted as ice distal by De Santis et al. (1995), would still reflect deposition distal to the ice front due to the relative sea level rise. Curiously, the seismic strata in the central Ross Sea display gently undulating strata, and could be interpreted in the context orbitally paced shifts in bathymetry due to effects such as repetitive glacio-isostatic loading and unloading

(L. De Santis, pers. comm.). This hypothesis could be tested through further modelling studies, which is beyond the scope of this thesis. As noted earlier, elevated magnetic susceptibility measurements, such as those recorded in lithostratigraphic unit 3, have also been previously identified during glacial periods in the Ross Sea and the Antarctic Peninsula as a result of changes in provenance due to glacial expansion (e.g. Hepp et al. (2009); Levy et al. (2016); Lucchi et al. (2013); Pudsey (2000)). As such, together with the shift in Th/Sc, the increased magnetic susceptibility could also be interpreted as an enhanced zone of glacial erosion resulting from the expansion of the WAIS. However, on the weight of evidence from far-field proxy data and the underlying facies stacking pattern showing a retreat sequence, the notion of an extended period of low ice volumes during the late Oligocene is currently favoured (Fig. 5.4).

5.3.5 Early Miocene – renewed intensification of marine-based glaciation at the Mi-1 event

The highest occurrence of *D. bisectus* (23.13 Ma) occurs at ~150 mbsf in DSDP 270, and immediately below the Mi-1 in the Cape Roberts cores (Kulhanek et al. (in prep.); Naish et al. (2008)). As such, the Mi-1 glaciation is interpreted to lie above 150 mbsf in DSDP Site 270, making it less likely that larger ice volumes were attained prior to, but not sustained during the Mi-1 (i.e. providing further support for the interpretation of lithostratigraphic unit 3 as a deglaciation), which is suggested to have experienced maximum ice volume at 23.03 Ma (Mudelsee et al., 2014). Furthermore, a significant shift in the assemblage of benthic foraminifera, suggested to be representative of the intensification of glaciation (Leckie and Webb, 1983), is coincident with a shift from ice distal (B) to proximal (C) seismic facies (De Santis et al., 1995). These transitions occur approximately at the transition from lithostratigraphic unit 3 to lithostratigraphic unit 2 (~120 mbsf), which is manifest by a renewed increase in IRD and a decrease in mud content. The combination of these changes makes this transition a likely candidate for the location of Mi-1 at DSDP 270. The onset of cooling bottom-waters at some point during lithostratigraphic unit 3 in the latest Oligocene, implied by the relative increase in species of benthic foraminifera with polar affinities (Leckie and Webb, 1983), are reconcilable with far-field data which suggest a cooling of bottom waters leading up to the Mi-1 glaciation (Billups et al., 2002; Lear et al., 2004; Mawbey and Lear, 2013).

The foraminifera also indicate that the subsidence of the area ceases at some point during this period, at outer shelf to bathyal water depths (300 – 500 m) (Leckie and Webb, 1983). Although Mi-1 presents the largest glaciation since the EOT (Mudelsee et al., 2014), the facies do not indicate an environment as proximal to the ice front as during lithostratigraphic unit 4. However, this does not necessarily imply lesser ice volume, and may instead reflect the deeper setting of DSDP 270 during the Mi-1, which would also cause the site to be laterally further from source. Furthermore, because subsidence was the likely factor for very ice proximal sediments, such as those deposited further downcore in lithostratigraphic unit 4, not being recorded at DSDP 270 during the Mi-1, this may suggest that the previous deglaciation (lithostratigraphic unit 3) may be attributed to subsidence also (section 5.3.4). The IRD source during this period was likely again mixed between Marie Byrd Land, and from the Central High, as seismic evidence suggests that the latter hosted ice caps each time an ice proximal seismic facies was deposited until the early to middle Miocene (De Santis et al., 1995), and no change in the pebble lithologies was noted (Barrett, 1975a).

Moreover, the presence of cristobalite and tridymite clays above ~160 mbsf, becoming more pervasive above 120 mbsf (Cook et al., 1975), suggests that diatoms were present during the deposition of the sediments (Harwood, 2010). This may be reconciled with the sparse, but apparently slightly elevated Si/Al ratios. It is however noted that the Si/Ti ratio does not appear to show significant changes (Fig. 4.14). Diatoms are generally indicative of ice distal deposits in a cooling glacial regime as the terrigenous sediment supply becomes increasingly starved (McKay et al., 2009). Thus the presence of these clays, together with the change in foraminifera species, may indicate a trend toward a cooling West Antarctic glacial regime, during, and subsequent to, the Mi-1 glaciation. These changes can be reconciled with the coeval Cape Roberts records, which detected trends toward lower CIA values, higher percentages of illite-chlorite clays in the sediments (both indicate more physical weathering), as well as decreasing meltwater input (Barrett, 2007; Ehrmann et al., 2005; Wilson et al., 2009).

Although conditions may have deteriorated, the lack of sedimentary textures characteristic of subglacial diamictites (e.g. Hart and Roberts (1994); Ó Cofaigh and Dowdeswell (2001)) indicates that, not only at the Mi-1, but most likely at no point during the late Oligocene to early Miocene did the grounding line of the WAIS override DSDP Site 270. This is consistent with seismic evidence which suggests that late Oligocene to early Miocene sequence boundaries are associated with minimal erosion on the outer continental shelf of the central Ross Sea surrounding the basement highs (De Santis et al., 1995; De Santis et al., 1999). Furthermore, foraminifera also do not support the notion of large-scale glacial stripping (Leckie and Webb, 1983). As such, the initial hypothesis that the Mi-1 represents the first marine-based, continental shelf wide, advance of ice sheets is not supported by this study. The evidence presented here does suggest an intensification of glaciation during Mi-1, but the WAIS did not advance across DSDP Site 270. The possibility of a subglacial diamictite at Mi-1 not being recorded due to the poor recovery above 150 mbsf, is tentatively rejected due to the aforementioned seismic evidence. Moreover, this record thus indicates that the large ice volumes of up to 125% of the modern EAIS, estimated for the Mi-1 using near- and far-field sea level records (Naish et al., 2008; Pekar and DeConto, 2006), were likely not a result of an expansion of this sector of the WAIS to the continental shelf margins. Therefore, it is here suggested that if these ice volume estimates are correct, the ice was likely stored elsewhere on Antarctica, or the Northern Hemisphere. Alternatively, the oxygen isotope shift at the Mi-1 may be reconciled with an isotopically less depleted ice sheet, implying a smaller ice volume than the previously suggested 125% of the modern EAIS (Pekar and DeConto, 2006). A recent study incorporating isotope-enabled models (i.e. allowing the oxygen isotope composition of the ice sheets to vary) has suggested that by invoking an Antarctic ice sheet with different isotopic composition during the Miocene, substantial ice volume changes (30-36 m sea level equivalent) can still be achieved, even under low atmospheric CO_2 variability (Gasson et al., 2016). Furthermore, Gasson et al. (2016) suggest a modelled seawater oxygen isotope signal greater than the commonly used 0.01 ‰ per 1 m of sea level, allowing a smaller ice volume change to achieve the same oxygen isotope shift. Applying such a scenario to the Mi-1 (i.e. just prior to the aforementioned modelling study), where changes isotopic composition of the ice and different seawater oxygen isotope signals allow for a smaller ice sheet, would be reconcilable with our records of DSDP 270 which reflect a renewed intensification of glaciation, but no overriding event. Either way, the absence of a grounded ice sheet across DSDP 270 suggests that this record is the first in the Ross Sea to recover the Mi-1 glaciation without a major multi-million-year unconformity, such as that in the CRP cores (e.g. Naish et al. (2008)).

The increasing occurrence of diamictites above ~68 mbsf, may represent later transient glaciation events in the Miocene (Miller et al., 1991), but the very poor recovery rate and poor age model does not allow any firm sedimentological interpretations above ~100 mbsf.
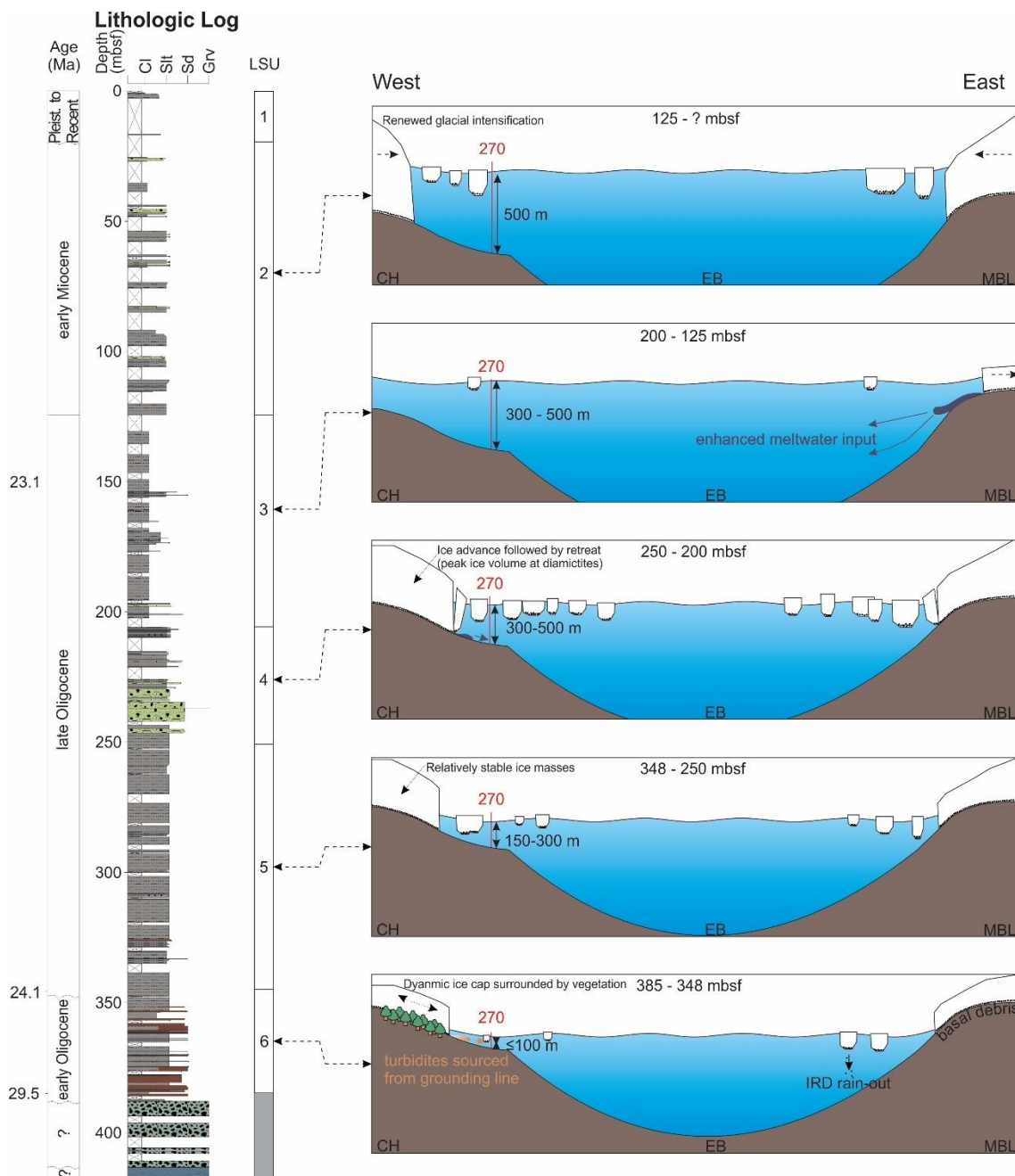
Fig. 5.5: Simplified cartoon of the sedimentation model of the Oligocene to early Miocene glacial history of the central to eastern Ross Sea, correlated to the appropriate sediments in the core. Drawn is a schematic west to east cross-section from the Central High (CH), across the Eastern Basin (EB), to Marie Byrd Land (MBL). Note that the schematic is not to scale, and the shoaling of the EB due to sediment input is not depicted.

5.4 Orbital pacing of West Antarctic ice volumes during the Oligocene

In order to compare the orbital cyclicity identified at DSDP 270 to other coeval records, the floating timescale was anchored in time at the base of the sampled interval, dated at ~24.1 Ma based on the first occurrence of *L. striata* at ~348 mbsf (Kulhanek et al., in prep.). Given the timeframe of the sampled interval, calculated to be 500 kyr using the sedimentation rate of 17 cm/ka, it is estimated that the interval was deposited between 24.1 and 23.6 Ma.

As noted in the results, there appears to be a switch from eccentricity to obliquity dominated frequencies in the percent mud dataset at 310 mbsf (Fig. 4.20D). Using the timescale anchored at 24.1 Ma, this corresponds to a switch in frequencies at about 23.9 Ma (Fig. 5.6). Moreover, while the coarse sand data retains an eccentricity imprint throughout (cf. percent mud data), the obliquity signal only appears at 310 mbsf (Fig. 4.19D). Therefore, it is observed that in both datasets obliquity increases in amplitude at ~23.9 Ma. These changes at DSDP Site 270 are congruent with the findings of far-field studies and the theoretical models of the studied time interval (Fig. 5.6; Laskar et al. (2004); Pälike et al. (2006b)). Theoretical solutions of orbital parameters (Laskar et al., 2004) suggest that the two short eccentricity frequencies weaken significantly between ~24 and 23.4 Ma, coeval with a stronger obliquity signal. A similar result was found in the coeval benthic $\delta^{18}O$ data recovered from the equatorial Pacific at ODP Site 1218 (Pälike et al., 2006b), where short eccentricity frequencies are almost absent, but obliquity is present.

Based on the identification of orbital frequencies in the sediments at DSDP 270, and the tentative positive correlation to spectra of theoretical orbital models and previously published oxygen isotope data, it is suggested that West Antarctic ice volume fluctuations during the late Oligocene were paced by orbital frequencies. As such, this record provides the first evidence of orbital pacing of West Antarctic ice during the Oligocene. East Antarctic ice volume fluctuations at orbital periodicities during the late Oligocene had previously been identified in sediment cores recovered by the Cape Roberts Project from the Ross Sea (Naish et al., 2008; Naish et al., 2001). Two cycles of ice margin advance and retreat onto the continental shelf of ~40 kyr duration between 24 and 23.5 Ma were recognised in these records (using the age model which was recalibrated by Naish et al. (2008)). The dominance of obliquity in both DSDP 270 and CRP cores implies that Antarctica's marine-based ice margins were dynamic, and responded to higher frequency orbital forcing during the late Oligocene. A similar pattern of orbital response has been described for the climate warmth during the Early Pliocene in ice proximal geological drillcore records from the Ross Sea (Naish et al., 2009), and the Wilkes Land margin (Patterson et al., 2014). Both of these records show that between 4.6 and 3.3 Ma marine margins of the Antarctic ice sheet oscillated in response to obliquity. Following the subsequent cooling after 3.3 Ma, summer sea-ice develops, and the ice sheet stabilises and is less responsive to obliquity forcing. Thus the obliquity pacing of ice volumes may be the signature of more dynamic ice sheets during warmer-than-present climates.

Finally, the identification of orbital frequencies and correlation to other records provides confidence in the accuracy of the age model. By extension this also provides confidence in the temporal accuracy of comparisons between sedimentological and geochemical interpretations of this study and other coeval near- and far-field records.
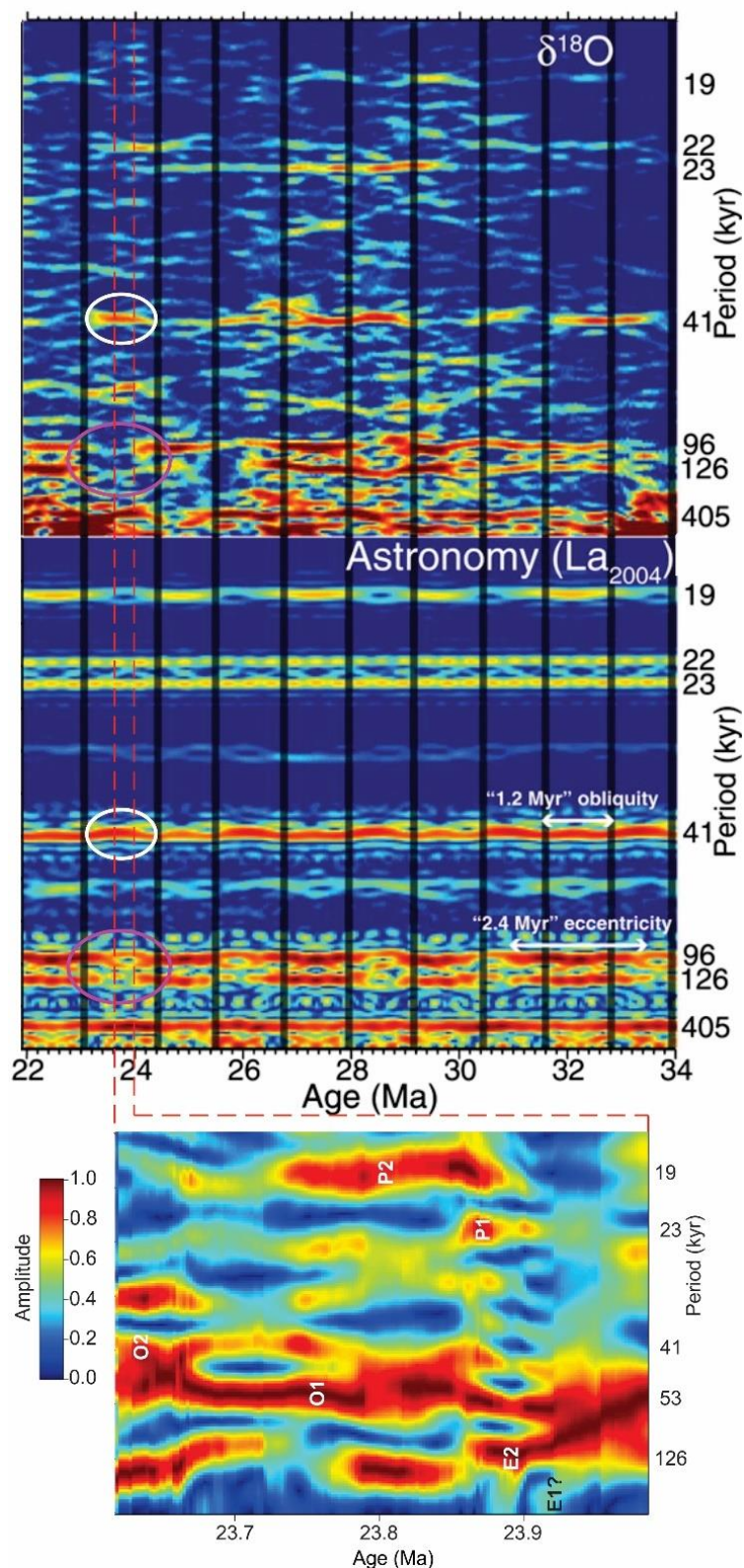
Fig. 5.6: Spectra of $\delta^{18}O$ data from ODP Site 1218, and the theoretical model of Laskar et al. (2004), both analysed by Pälike et al. (2006b). The time interval between 24 and 23.6 Ma (orange dashed lines) is compared to the spectral analysis of the mud percentage between 348 and 250 mbsf at DSDP 270. White (purple) ellipses draw attention to increases (decreases) in the amplitudes of obliquity (eccentricity). Note that only the percent mud dataset is here used to compare to the previous records because it is less noisy than the coarse sand dataset (Fig. 4.19C versus 4.20C).

Chapter Six

CONCLUSIONS AND FUTURE WORK

6.1 Conclusions

Given the improvements in analytical techniques, as well as advances in our scientific understanding since the original work conducted on cores from DSDP Site 270, this study re-examined these sediment cores with the specific aim of better understanding the glacial evolution of West Antarctica through the Oligocene and early Miocene. The sediments were first re-described using the approaches applied to Cape Roberts and ANDRILL cores (Naish et al., 2006), and were subsequently analysed for their IRD content at higher resolution than previous studies. Two proxies of IRD, visual counts of clasts exceeding 2 mm in diameter, and the sieved weight percentage of the coarse sand fraction, were used. Furthermore, the fine fraction of the sediments was analysed at a resolution matching that of the coarse sand IRD proxy, using laser particle size analysis. The sediments were also geochemically characterised using X-ray fluorescence scanning and inductively coupled mass spectrometry on discrete samples. The magnetic susceptibility of the sediments was logged using the magnetic loop line scanning method.

The XRF data of Ca, S, Ba and Cl had to be discarded as they were compromised by the growth of gypsum, barite and salts during core storage. This highlights the importance of correctly identifying, and only interpreting the data representative of the sediments themselves when scanning old legacy cores.

Based on the high-resolution visual core descriptions and the content of ice-rafted debris, the sediments between 20 and 385 mbsf were divided into six glacimarine lithofacies. When the glacimarine lithofacies were integrated with the geochemical and magnetic susceptibility datasets, as well as the existing information on the palynology and foraminiferal content (Kemp and Barrett, 1975; Leckie and Webb, 1983), five lithostratigraphic units were used to describe the large scale changes downcore. These lithostratigraphic units, which were interpreted based on previous studies of past and modern glacimarine environments, were then correlated with the seismic strata, and the regional stratigraphic framework of the Ross Sea (De Santis et al., 1995).

The glacimarine sediments are interpreted to reflect a subpolar glacial regime, consistent with the previous studies of the palynology, as well as macro- and micro-fossils in the core, which all suggested a more temperate-style climate (Dell and Fleming, 1975; Kemp, 1975; Kemp and Barrett, 1975; Leckie and Webb, 1983). The source of the sediments remains somewhat enigmatic, with seismic evidence suggesting a local source from ice caps on the Central High (De Santis et al., 1995), and pebble lithologies which point to an inland Marie Byrd Land source (Barrett, 1975a). As such it is suggested that the sediments were likely derived from both areas.

By matching the integrated lithostratigraphic units and seismic data to an updated preliminary age model (Kulhanek et al., in prep.), a sedimentation model of the glacial history of the central Ross Sea during the Oligocene to Miocene was developed. This glacial history, superimposed on an overall marine transgression to water depths of ~500 m (Leckie and Webb, 1983), is summarised as follows:

- The initial glacimarine sediments, overlying terrestrial and shallow marine deposits, are interpreted as being ice proximal, in less well oxygenated waters, dominated by turbidite deposits. The sediments likely represent a fluctuating ice cap on the Central High which calved at sea level, surrounded by *Nothofagus* dominated vegetation during the early Oligocene.

- Biostratigraphic data have led to the interpretation that the bottom ~30 m of the glacimarine section are significantly older than the overlying sediments. This suggests an unconformity, which may be matched to a strong reflector in the seismic data, spanning up to ~5 million years. The unconformity may be coeval with other unconformities mapped in the Ross Sea region, coincident with a glacial maximum at ~25 Ma (Barrett, 2007; Pälike et al., 2006b). Above the hiatus, the facies were interpreted to suggest an extended period of relatively stable marine terminating ice masses on the Central High and in Marie Byrd Land without significant change during this part of the late Oligocene. This is consistent with sedimentary records which reflect changes in the EAIS at the time (Barrett, 2007).

- This stable period was terminated by a sequence of diamictite deposits, overlain by increasingly ice distal deposits of relatively proximal cyclopels/cyclopsams, and more distal mudstones. When compared to previous studies and facies models, this sequence was interpreted to reflect peak ice volume, followed by a steady deglaciation. An absence of structural and sedimentological features characteristic of subglacial deposition suggests that the ice mass responsible for the deposit came close to, but did not override DSDP Site 270. However, the basal contact of the diamictites was not recovered, and as such overriding cannot be ruled out. Importantly, these sediments indicate that marine calving ice masses not only existed during this interval of the late Oligocene (~23.6 Ma), but also displayed periodic advances. This is again congruent with the sediments recovered at Cape Roberts (Barrett, 2007).

- The subsequent deposition of the predominantly ice distal mudstones of lithostratigraphic unit 3 suggest a continuation of the deglaciation which began after the glacial maximum in lithostratigraphic unit 4. Furthermore, the increases in magnetic susceptibility and the Th/Sc ratio in the sediments of lithostratigraphic unit 3 are interpreted to reflect periods of significant meltwater input during the deglaciation. Therefore, these sediments suggest a period of retreat reduced ice volume during the latest Oligocene (~23.4 Ma). This may account for some of the widely documented reduction in benthic foraminiferal $\delta^{18}O$ values during the latest Oligocene (e.g. Pälike et al. (2006b)). Moreover, the culmination of warming climates, as well as tectonic subsidence have been discussed as potential mechanisms for the deglaciation, however, based on the proxies employed in this study a causal mechanism unfortunately could not be determined. Furthermore, during the latter stages of lithostratigraphic unit 3 the foraminifera indicate a cooling of bottom-waters leading into the Mi-1 glaciation (Leckie and Webb, 1983), which is consistent with the cooling of ocean temperatures recorded at far-field sites (e.g. Mawbey and Lear, 2013).

- The major $\delta^{18}O$ excursion at the Mi-1 glaciation is correlated with ~125 mbsf at DSDP 270 on the basis of the biostratigraphically-constrained preliminary age model, and is marked by a renewed increase in IRD, coarsening of the fine fraction,

and upcore transition from lithostratigraphic unit 3 to 2. This is also coincident with a shift from ice-distal to ice-proximal seismic facies, and a change to a benthic foraminiferal assemblage which suggests a significant build-up of ice at sea level (De Santis et al., 1995; Leckie and Webb, 1983). Moreover, the higher Th/Sc values compared to lower down in the core may point to a wider provenance area. The increased presence of cristobalite and tridymite clays, derived from the diagenetic alteration of silicic microfossils, above ~120 mbsf (Cook et al., 1975) may further point to the development of a more polar glacial regime. It is important to note however that while the records at DSDP 270 suggest a renewed intensification of glaciation, again no sedimentological or seismic data characteristic of subglacial deposition were recorded. Thus, because no subglacial deposits were recorded at DSDP 270 during the Mi-1, the hypothesis that the Mi-1 represents the first marine-based WAIS advance to the edge of the continental shelf is not supported by this study. However, this does not preclude the coeval development of a marine-based ice sheet in other sectors of Antarctica. Furthermore, if the suggested ice volume of 125% of the modern EAIS for the Mi-1 (Pekar and DeConto, 2006) are correct, then the ice has to have been stored elsewhere in Antarctica. Alternatively, different oxygen isotope compositions (e.g. Gasson et al. (2016)) may be able to explain the oxygen isotope shift with a lesser ice volume. As such, unfortunately no firm conclusion can be drawn as to whether 400 ppm represents the CO_2 threshold for the existence of marine-based ice sheets. However, because the area was not overridden by an ice sheet, this record provides the first relatively continuous late Oligocene to early Miocene record which captures the Mi-1 in the Ross Sea without a major unconformity. Furthermore, the fact that DSDP 270 was not overridden by an ice sheet during the Mi-1 provides an important constraint to any future modelling efforts.

Finally, spectral analysis of the weight percent of coarse sand and mud content between 348 and 250 mbsf was conducted largely independently of the age model using MTM, ASM, and EHA analyses, as the age model is not yet complete. The analyses consistently revealed a uniform sedimentation rate of ~17 cm/ka during this interval. Moreover, eccentricity, obliquity and precession were recovered in both datasets, although not all periodicities of the orbital parameters were present. An apparent decrease in the amplitude of eccentricity, matched by a coeval increase in the amplitude of obliquity at 310 mbsf is correlated to a similar pattern occurring in coeval $\delta^{18}O$ records from the equatorial Pacific (Pälike et al., 2006b), and a theoretical model of variations in Earth's orbital parameters (Laskar et al., 2004). As such these results provide the first evidence of orbitally-paced ice volume fluctuations in West Antarctica during the Oligocene. It is also important to note that coeval cyclic glacimarine sediments from East Antarctica also record a dominant obliquity control (Naish et al., 2008; Naish et al., 2001). Furthermore, by comparison to other ice proximal sediments which record a dominant obliquity control during warmer-than-present climates, it is tentatively suggested that more dynamic, obliquity-paced ice sheets may be characteristic of these climates.

6.2 Future work

The results of this study will form part of a broader work programme being carried out on the Oligocene-Miocene ice sheet variability, especially the PhD work of Bella Duncan (Victoria University of Wellington), who is using organic geochemical proxies and stable isotopes to provide reconstructions of temperature and changes in the hydrological regime of the Ross Sea during the Oligocene and Miocene.

Future sedimentological work should focus on identifying the lithologies present in the coarse sand IRD fractions at equally high resolutions to those of this study in order to ground truth the results suggested by the changes in magnetic susceptibility and geochemistry. Moreover, such detail would potentially identify long and/or short term changes in provenance. Furthermore, high-resolution provenance studies using modern geochemical techniques such as neodymium and strontium isotope compositions (e.g. Cook et al. (2013)), as well as radiogenic dating of hornblendes in IRD (e.g. Williams et al. (2010)), could also further aid the interpretations. Finally, a higher resolution study of the clay mineralogy, palynology and foraminifera may be useful for developing further insights into detailed changes.

Future work will also attempt to reduce the noise levels in the spectral analyses using a variety of data processing tools available in the astrochron package (Meyers, 2014). Moreover, the availability of a completed age model (Kulhanek et al., in prep.), will allow a more detailed analysis of orbital forcing, and the possibility of astronomically tuning the age model where the recovery is adequate.

REFERENCES

Allis, R., Barrett, P., and Christoffel, D., 1975, A paleomagnetic stratigraphy for Oligocene and early Miocene marine glacial sediments at Site 270, Ross Sea, Antarctica: Initial Reports of the Deep Sea Drilling Project, v. 28, p. 879-884.

Anderson, J. B., and Bartek, L. R., 1992, Cenozoic glacial history of the Ross Sea revealed by intermediate resolution seismic reflection data combined with drill site information: The Antarctic Paleoenvironment: A Perspective on Global Change: Part One, American Geophysical Union, p. 231-264.

Anderson, J. B., Brake, C., Domack, E., Myers, N., and Wright, R., 1983, Development of a polar glacial-marine sedimentation model from Antarctic Quaternary deposits and glaciological information, Glacial-marine sedimentation, Springer, p. 233-264.

Anderson, J. B., Kennedy, D. S., Smith, M. J., and Domack, E. W., 1991, Sedimentary facies associated with Antarctica's floating ice masses: Geological Society of America Special Papers, v. 261, p. 1-26.

Anderson, J. B., Kurtz, D., Domack, E., and Balshaw, K., 1980, Glacial and glacial marine sediments of the Antarctic continental shelf: Journal of Geology, p. 399-414.

Anderson, J. B., Warny, S., Askin, R. A., Wellner, J. S., Bohaty, S. M., Kirshner, A. E., Livsey, D. N., Simms, A. R., Smith, T. R., Ehrmann, W., Lawver, L. A., Barbeau, D., Wise, S. W., Kulhanek, D. K., Weaver, F. M., and Majewski, W., 2011, Progressive Cenozoic cooling and the demise of Antarctica's last refugium: Proceedings of the National Academy of Sciences, v. 108, no. 28, p. 11356-11360.

Anderson, R. F., 1982, Concentration, vertical flux, and remineralization of particulate uranium in seawater: Geochimica et Cosmochimica Acta, v. 46, no. 7, p. 1293-1299.

Askin, R., and Raine, J., 2000, Oligocene and Early Miocene terrestrial palynology of the Cape Roberts Drillhole CRP-2/2A, Victoria Land Basin, Antarctica: Terra Antartica, v. 7, p. 493-501.

Askin, R. A., 1989, Endemism and heterochroneity in the Late Cretaceous (Campanian) to Paleocene palynofloras of Seymour Island, Antarctica: implications for origins, dispersal and palaeoclimates of southern floras: Geological Society, London, Special Publications, v. 47, no. 1, p. 107-119.

Bahr, A., Jiménez-Espejo, F. J., Kolasinac, N., Grunert, P., Hernández-Molina, F. J., Röhl, U., Voelker, A. H. L., Escutia, C., Stow, D. A. V., Hodell, D., and Alvarez-

References

Zarikian, C. A., 2014, Deciphering bottom current velocity and paleoclimate signals from contourite deposits in the Gulf of Cádiz during the last 140 kyr: An inorganic geochemical approach: Geochemistry, Geophysics, Geosystems, v. 15, no. 8, p. 3145-3160.

Balshaw, K., 1981, Antarctic glacial chronology reflected in the Oligocene through Pliocene sedimentary section in the Ross Sea, Unpublished PhD thesis: Rice University, 140 p.

Bamber, J. L., Riva, R. E. M., Vermeersen, B. L. A., and LeBrocq, A. M., 2009, Reassessment of the Potential Sea-Level Rise from a Collapse of the West Antarctic Ice Sheet: Science, v. 324, no. 5929, p. 901-903.

Barker, P., and Kennett, J., 1990, Proceedings of the Ocean Drilling Program, Scientific results Leg 113: Ocean Drill. Program, College Station, TX, p. 937-960.

Barnes, C., and Cochran, J., 1990, Uranium removal in oceanic sediments and the oceanic U balance: Earth and Planetary Science Letters, v. 97, no. 1, p. 94-101.

Barrett, P. J., 1975a, Characteristics of pebbles from Cenozoic marine glacial sediments in the Ross Sea (DSDP Sites 270-274) and the South Indian Ocean (Site 268): Initial Reports of the Deep Sea Drilling Project, v. 28, p. 769-784.

Barrett, P. J., 1975b, Textural characteristics of Cenozoic preglacial and glacial sediments at Site 270, Ross Sea, Antarctica: Initial Reports of the Deep Sea Drilling Project, v. 28, p. 757-767.

Barrett, P. J., 1989, Antarctic Cenozoic history from the CIROS-1 drillhole, McMurdo Sound, Wellington, DSIR Publishing, DSIR Bulletin 245, 254 pp.

Barrett, P. J., 1999, Antarctic Climate History over the Last 100 Million Years: Terra Antarctica, v. 3, p. 53-72.

Barrett, P. J., 2007, Cenozoic climate and sea level history from glacimarine strata off the Victoria Land coast, Cape Roberts Project, Antarctica, *in* Hambrey, M. J., Christoffersen, P., Glasser, N., and Hubbard, B., eds., Glacial sedimentary processes and products, Volume 39: Oxford, Blackwell Publishing, p. 259-287.

Barrett, P. J., Elston, D., Harwood, D., McKelvey, B., and Webb, P.-N., 1987, Mid-Cenozoic record of glaciation and sea-level change on the margin of the Victoria Land basin, Antarctica: Geology, v. 15, no. 7, p. 634-637.

Barrett, P., Hambrey, M. J., Harwood, D., Pyne, A., and Webb, P.-N., 1989, Synthesis, *in* Barrett, P., ed., Antarctic Cenozoic history from the CIROS-1 drillhole, McMurdo Sound, Wellington, DSIR Publishing, DSIR Bulletin 245, p. 241-251.

References

Barrett, P. J., 2013, Resolving views on Antarctic Neogene glacial history – the Sirius debate: Earth and Environmental Science Transactions of the Royal Society of Edinburgh, v. 104, no. 01, p. 31-53.

Barron, J., and Larsen, B., 1989, Initial Report: Kerguelen Plateau-Prydz Bay, College Station, TX, Ocean Drilling Program, Proceedings of the Integrated Ocean Drilling Program, 942 p.

Bart, P. J., and De Santis, L., 2012, Glacial Intensification During the Neogene: A Review of Seismic Stratigraphic Evidence from the Ross Sea, Antarctica, Continental Shelf: Oceanography, v. 25, no. 3, p. 166-183.

Beerling, D. J., and Royer, D. L., 2011, Convergent Cenozoic CO_2 history: Nature Geoscience, v. 4, no. 7, p. 418-420.

Behrendt, J., LeMasurier, W., Cooper, A., Tessensohn, F., Trehu, A., and Damaske, D., 1991, Geophysical studies of the West Antarctic rift system: Tectonics, v. 10, no. 6, p. 1257-1273.

Benn, D. I., and Evans, D. J. A., 2010, Glaciers & glaciation, London, Hodder Education, 802 pp.

Berger, A., Loutre, M. F., and Laskar, J., 1992, Stability of the Astronomical Frequencies Over the Earth's History for Paleoclimate Studies: Science, v. 255, no. 5044, p. 560-566.

Billups, K., Channell, J. E. T., and Zachos, J., 2002, Late Oligocene to early Miocene geochronology and paleoceanography from the subantarctic South Atlantic: Paleoceanography, v. 17, no. 1, p. 4-1-4-11.

Billups, K., and Schrag, D. P., 2002, Paleotemperatures and ice volume of the past 27 Myr revisited with paired Mg/Ca and $^{18}O/^{16}O$ measurements on benthic foraminifera: Paleoceanography, v. 17, no. 1, p. 3-1-3-11.

Bindschadler, R., 2006, The environment and evolution of the West Antarctic ice sheet: setting the stage: Philosophical Transactions of the Royal Society of London A: Mathematical, Physical and Engineering Sciences, v. 364, no. 1844, p. 1583-1605.

Birkenmajer, K., Gazdzicki, A., Krajewski, K. P., Przybycin, A., Solecki, A., Tatur, A., and Yoon, H. I., 2005, First Cenozoic glaciers in West Antarctica: Polish Polar Research, v. 26, no. 1, p. 3-12.

Blott, S. J., 2010, GRADISTAT: A Grainsize Distribution and Statistics Package for the Analysis of unconsolidated Sediments by Sieving or Laser Granulometer: Berkshire, UK, Kenneth Pye Associates Ltd. Computer Programme.

References

Blott, S. J., and Pye, K., 2001, GRADISTAT: a grainsize distribution and statistics package for the analysis of unconsolidated sediments: Earth Surface Processes and Landforms, v. 26, no. 11, p. 1237-1248.

Boggs Jr, S., 2011, Siliciclastic Marine Environments, Principles of Seimentology and Stratigraphy: Upper Saddle River, New Jersey, Pearson Prentice Hall, p. 280-307.

Bohaty, S. M., Zachos, J. C., and Delaney, M. L., 2012, Foraminiferal Mg/Ca evidence for Southern Ocean cooling across the Eocene–Oligocene transition: Earth and Planetary Science Letters, v. 317, p. 251-261.

Brancolini, G., Cooper, A. K., and Coren, F., 1995, Seismic facies and glacial history in the western Ross Sea (Antarctica): Geology and Seismic Stratigraphy of the Antarctic Margin, p. 209-233.

Breza, J. R., and Wise Jr, S. W., 1992, Lower Oligocene ice-rafted debris on the Kerguelen Plateau: Evidence for East Antarctic continental glaciation, *in* Wise Jr, S. W., Schlich, R., and et al., eds., Proc. ODP Sci. Res., Volume 120: College Station, TX, ODP, p. 161-178.

Cande, S. C., and Mutter, J. C., 1982, A revised identification of the oldest sea-floor spreading anomalies between Australia and Antarctica: Earth and Planetary Science Letters, v. 58, no. 2, p. 151-160.

Cande, S. C., Stock, J. M., Muller, R. D., and Ishihara, T., 2000, Cenozoic motion between East and West Antarctica: Nature, v. 404, no. 6774, p. 145-150.

Carlson, A. E., Stoner, J. S., Donnelly, J. P., and Hillaire-Marcel, C., 2008, Response of the southern Greenland Ice Sheet during the last two deglaciations: Geology, v. 36, no. 5, p. 359-362.

Carson, G. A., and Crowley, S. F., 1993, The glauconite-phosphate association in hardgrounds: examples from the Cenomanian of Devon, southwest England: Cretaceous Research, v. 14, no. 1, p. 69-89.

Carter, L., Carter, R., and McCave, I., 2004, Evolution of the sedimentary system beneath the deep Pacific inflow off eastern New Zealand: Marine Geology, v. 205, no. 1, p. 9-27.

Cloud Jr, P. E., 1955, Physical limits of glauconite formation: AAPG Bulletin, v. 39, no. 4, p. 484-492.

References

Cook, C. P., van de Flierdt, T., Williams, T., Hemming, S. R., Iwai, M., Kobayashi, M., Jimenez-Espejo, F. J., Escutia, C., Gonzalez, J. J., Khim, B.-K., McKay, R. M., Passchier, S., Bohaty, S. M., Riesselman, C. R., Tauxe, L., Sugisaki, S., Galindo, A. L., Patterson, M. O., Sangiorgi, F., Pierce, E. L., Brinkhuis, H., Klaus, A., Fehr, A., Bendle, J. A. P., Bijl, P. K., Carr, S. A., Dunbar, R. B., Flores, J. A., Hayden, T. G., Katsuki, K., Kong, G. S., Nakai, M., Olney, M. P., Pekar, S. F., Pross, J., Rohl, U., Sakai, T., Shrivastava, P. K., Stickley, C. E., Tuo, S., Welsh, K., and Yamane, M., 2013, Dynamic behaviour of the East Antarctic ice sheet during Pliocene warmth: Nature Geoscience, v. 6, no. 9, p. 765-769.

Cook, H. E., Zemmels, I., and Matti, J., 1975, X-ray mineralogy data, austral-Antarcic region, Leg 28, Deep Sea Drilling Project: Initial Reports of the Deep Sea Drilling Project, v. 28, p. 981-998.

Cooper, A. K., and Davey, F., 1985, Episodic rifting of Phanerozoic rocks in the Victoria land Basin, western Ross Sea, Antarctica: Science, v. 229, no. 4718, p. 1085-1087.

Cooper, A. K., and O'Brien, P. E., Leg 188 synthesis: transitions in the glacial history of the Prydz Bay region, East Antarctica, from ODP drilling, *in* Proceedings Proc. ODP, Sci. Results, 2004, Volume 188, College Station Texas, p. 1-42.

Cowan, E. A., Cai, J., Powell, R. D., Clark, J. D., and Pitcher, J. N., 1997, Temperate glacimarine varves: an example from Disenchantment Bay, southern Alaska: Journal of Sedimentary Research, v. 67, no. 3, p. 536-549.

Cowan, E. A., Seramur, K. C., Cai, J., and Powell, R. D., 1999, Cyclic sedimentation produced by fluctuations in meltwater discharge, tides and marine productivity in an Alaskan fjord: Sedimentology, v. 46, no. 6, p. 1109-1126.

Coxall, H. K., Wilson, P. A., Palike, H., Lear, C. H., and Backman, J., 2005, Rapid stepwise onset of Antarctic glaciation and deeper calcite compensation in the Pacific Ocean: Nature, v. 433, no. 7021, p. 53-57.

Cramer, B., Toggweiler, J., Wright, J., Katz, M., and Miller, K., 2009, Ocean overturning since the Late Cretaceous: Inferences from a new benthic foraminiferal isotope compilation: Paleoceanography, v. 24, no. 4.

Cramer, B. S., Miller, K. G., Barrett, P. J., and Wright, J. D., 2011, Late Cretaceous–Neogene trends in deep ocean temperature and continental ice volume: Reconciling records of benthic foraminiferal geochemistry (δ^{18}O and Mg/Ca) with sea level history: Journal of Geophysical Research: Oceans, v. 116, no. C12.

Crowley, T. J., and Burke, K., 1998, Tectonic boundary conditions for climate reconstructions, Oxford Monographs on Geology and Geophysics, v.39, Oxford University Press, 285 pp.

References

Cullers, R., 1988, Mineralogical and chemical changes of soil and stream sediment formed by intense weathering of the Danburg granite, Georgia, U.S.A: Lithos, v. 21, no. 4, p. 301-314.

Dalziel, I. W. D., and Lawver, L. A., 2001, The Lithospheric Setting of the West Antarctic Ice Sheet, *in* Alley, R. B., and Bindschadler, R. A., eds., The West Antarctic Ice Sheet: Behavior and Environment, Antarctic Research Series, v. 77, American Geophysical Union, Washington, D. C., p. 29-44.

Davey, F., and Brancolini, G., 1995, The Late Mesozoic and Cenozoic structural setting of the Ross Sea region: Geology and seismic stratigraphy of the Antarctic margin, *in* Cooper, A. K., Barker, P. F., and Brancolini, G., eds., Geology and Seismic Stratigraphy of the Antarctic Margin, Antarctic Research Series, v. 68, American Geophysical Union, Washington, D. C., p. 167-182.

De Man, E., and Van Simaeys, S., 2004, Late Oligocene Warming Event in the southern North Sea Basin: benthic foraminifera as paleotemperature proxies: Netherlands Journal of Geosciences/Geologie en Mijnbouw, v. 83, no. 3, p. 227-239.

De Santis, L., Anderson, J. B., Brancolini, G., and Zayatz, I., 1995, Seismic record of late Oligocene through Miocene glaciation on the central and eastern continental shelf of the Ross Sea, *in* Cooper, A. K., Barker, P. F., and Brancolini, G., eds., Geology and Seismic Stratigraphy of the Antarctic Margin, Antarctic Research Series, v. 68, American Geophysical Union, Washington, D. C., p. 235-260.

De Santis, L., Prato, S., Brancolini, G., Lovo, M., and Torelli, L., 1999, The Eastern Ross Sea continental shelf during the Cenozoic: implications for the West Antarctic ice sheet development: Global and Planetary Change, v. 23, no. 1–4, p. 173-196.

DeConto, R. M., and Pollard, D., 2003, Rapid Cenozoic glaciation of Antarctica induced by declining atmospheric CO2: Nature, v. 421, no. 6920, p. 245-249.

DeConto, R. M., and Pollard, D., 2016, Contribution of Antarctica to past and future sea-level rise: Nature, v. 531, no. 7596, p. 591-597.

DeConto, R. M., Pollard, D., and Harwood, D., 2007, Sea ice feedback and Cenozoic evolution of Antarctic climate and ice sheets: Paleoceanography, v. 22, no. 3.

DeConto, R. M., Pollard, D., Wilson, P. A., Palike, H., Lear, C. H., and Pagani, M., 2008, Thresholds for Cenozoic bipolar glaciation: Nature, v. 455, no. 7213, p. 652-656.

Dell, R., and Fleming, C., 1975, Oligocene-Miocene bivalve mollusca and other macrofossils from Sites 270 and 272 (Ross Sea), DSDP, Leg 28: Initial Reports of the Deep Sea Drilling Project, v. 28, p. 693-703.

References

Dickson, A. J., Leng, M. J., Maslin, M. A., and Röhl, U., 2010, Oceanic, atmospheric and ice-sheet forcing of South East Atlantic Ocean productivity and South African monsoon intensity during MIS-12 to 10: Quaternary Science Reviews, v. 29, no. 27–28, p. 3936-3947.

Diester-Haass, L., Billups, K., and Emeis, K., 2011, Enhanced paleoproductivity across the Oligocene/Miocene boundary as evidenced by benthic foraminiferal accumulation rates: Palaeogeography, Palaeoclimatology, Palaeoecology, v. 302, no. 3–4, p. 464-473.

Diester-Haass, L., Robert, C., and Chamley, H., 1996, The Eocene-Oligocene preglacial-glacial transition in the Atlantic sector of the Southern Ocean (ODP Site 690): Marine Geology, v. 131, no. 3–4, p. 123-149.

Dingle, R., and Lavelle, M., 1998, Antarctic Peninsular cryosphere: Early Oligocene (c. 30 Ma) initiation and a revised glacial chronology: Journal of the Geological Society, v. 155, no. 3, p. 433-437.

Domack, E. W., Jacobson, E. A., Shipp, S., and Anderson, J. B., 1999, Late Pleistocene–Holocene retreat of the West Antarctic Ice-Sheet system in the Ross Sea: Part 2—sedimentologic and stratigraphic signature: Geological Society of America Bulletin, v. 111, no. 10, p. 1517-1536.

Dowdeswell, J., Elverhfi, A., and Spielhagen, R., 1998, Glacimarine sedimentary processes and facies on the Polar North Atlantic margins: Quaternary Science Reviews, v. 17, no. 1, p. 243-272.

Dowdeswell, J. A., Whittington, R. J., and Marienfeld, P., 1994, The origin of massive diamicton facies by iceberg rafting and scouring, Scoresby Sund, East Greenland: Sedimentology, v. 41, no. 1, p. 21-35.

Dunbar, G. B., Naish, T., Barrett, P. J., Fielding, C. R., and Powell, R., 2008, Constraining the amplitude of late Oligocene bathymetric changes in Western Ross Sea during orbitally-induced oscillations in the East Antarctic Ice Sheet:(1) Implications for glacimarine sequence stratigraphic models: Palaeogeography, Palaeoclimatology, Palaeoecology, v. 260, no. 1, p. 50-65.

Ehrmann, W., 1998, Implications of late Eocene to early Miocene clay mineral assemblages in McMurdo Sound (Ross Sea, Antarctica) on paleoclimate and ice dynamics: Palaeogeography, Palaeoclimatology, Palaeoecology, v. 139, no. 3–4, p. 213-231.

Ehrmann, W., Setti, M., and Marinoni, L., 2005, Clay minerals in Cenozoic sediments off Cape Roberts (McMurdo Sound, Antarctica) reveal palaeoclimatic history: Palaeogeography, Palaeoclimatology, Palaeoecology, v. 229, no. 3, p. 187-211.

References

Ehrmann, W. U., and Mackensen, A., 1992, Sedimentological evidence for the formation of an East Antarctic ice sheet in Eocene/Oligocene time: Palaeogeography, Palaeoclimatology, Palaeoecology, v. 93, no. 1, p. 85-112.

Elderfield, H., Yu, J., Anand, P., Kiefer, T., and Nyland, B., 2006, Calibrations for benthic foraminiferal Mg/Ca paleothermometry and the carbonate ion hypothesis: Earth and Planetary Science Letters, v. 250, no. 3, p. 633-649.

Eldrett, J. S., Harding, I. C., Wilson, P. A., Butler, E., and Roberts, A. P., 2007, Continental ice in Greenland during the Eocene and Oligocene: Nature, v. 446, no. 7132, p. 176-179.

Elverhøi, A., Liestol, O., and Nagy, J., 1980, Glacial erosion, sedimentation and microfauna in the inner part of Kongsfjorden, Spitsbergen: Norsk Polarinstitutt Skrifter, v. 172, p. 33-58.

Elverhøi, A., Lønne, Ø., and Seland, R., 1983, Glaciomarine sedimentation in a modern fjord environment, Spitsbergen: Polar Research, v. 1, no. 2, p. 127-150.

Emiliani, C., 1954, Temperatures of Pacific bottom waters and polar superficial waters during the Tertiary: Science, v. 119, no. 3103, p. 853-855.

Emiliani, C., 1955, Pleistocene temperatures: Journal of Geology, p. 538-578.

Emiliani, C., 1961, The temperature decrease of surface sea-water in high latitudes and of abyssal-hadal water in open oceanic basins during the past 75 million years: Deep Sea Research (1953), v. 8, no. 2, p. 144-147.

Escutia, C., Brinkhuis, H., and The Expedition 318 Scientists, 2014, From Greenhouse to Icehouse at the Wilkes Land Antarctic Margin: IODP Expedition 318 Synthesis of Results, *in* Ruediger Stein, D. K. B. F. I., and Hans-Christian, L., eds., Developments in Marine Geology, Volume 7, Elsevier, p. 295-328.

Escutia, C., Brinkhuis, H., Klaus, A., and IODP Expedition 318 Scientists, 2011, IODP Expedition 318: From Greenhouse to Icehouse at the Wilkes Land Antarctic Margin: Scientific Drilling, v. 12, p. 15-23.

Escutia, C., De Santis, L., Donda, F., Dunbar, R., Cooper, A., Brancolini, G., and Eittreim, S., 2005, Cenozoic ice sheet history from East Antarctic Wilkes Land continental margin sediments: Global and Planetary Change, v. 45, no. 1, p. 51-81.

Evans, J., Dowdeswell, J., Grobe, H., Niessen, F., Stein, R., Hubberten, H.-W., and Whittington, R., 2002, Late Quaternary sedimentation in Kejser Franz Joseph Fjord and the continental margin of east Greenland: Geological Society, London, Special Publications, v. 203, p. 149-179.

References

Expedition 318 Scientists, 2011, Methods, *in* Escutia, C., Brinkhuis, H., Klaus, A., and Expedition 318 Scientists, eds., Proceedings of the Integrated Ocean Drilling Program, Volume 318: Tokyo, Integrated Ocean Drilling Program Management International, Inc.

Eyles, C. H., and Lagoe, M. B., 1990, Sedimentation patterns and facies geometries on a temperate glacially-influenced continental shelf: the Yakataga Formation, Middleton Island, Alaska: Geological Society, London, Special Publications, v. 53, no. 1, p. 363-386.

Eyles, N., and Eyles, C. H., 1992, Glacial depositional systems: Facies Models: response to sea level change, Walker, RG and James, NP (eds) St. John's: Geological Association of Canada, p. 73-100.

Fahnestock, M. A., Scambos, T. A., Bindschadler, R. A., and Kvaran, G., 2000, A millennium of variable ice flow recorded by the Ross Ice Shelf, Antarctica: Journal of Glaciology, v. 46, no. 155, p. 652-664.

Fielding, C. R., Browne, G. H., Field, B., Florindo, F., Harwood, D. M., Krissek, L. A., Levy, R. H., Panter, K. S., Passchier, S., and Pekar, S. F., 2011, Sequence stratigraphy of the ANDRILL AND-2A drillcore, Antarctica: A long-term, ice-proximal record of Early to Mid-Miocene climate, sea-level and glacial dynamism: Palaeogeography, Palaeoclimatology, Palaeoecology, v. 305, no. 1–4, p. 337-351.

Fielding, C. R., Naish, T., Woolfe, K., and Lavelle, M., 2000, Facies analysis and sequence stratigraphy of CRP-2/2A, Victoria Land Basin, Antarctica: Terra Antartica, v. 7, no. 3, p. 323-338.

Fitzgerald, P., 2002, Tectonics and landscape evolution of the Antarctic plate since the breakup of Gondwana, with an emphasis on the West Antarctic Rift System and the Transantarctic Mountains: Royal Society of New Zealand Bulletin, v. 35, p. 453-469.

Fitzgerald, P. G., 1992, The Transantarctic Mountains of southern Victoria Land: The application of apatite fission track analysis to a rift shoulder uplift: Tectonics, v. 11, no. 3, p. 634-662.

Fitzgerald, P. G., 1994, Thermochronologic constraints on post-Paleozoic tectonic evolution of the central Transantarctic Mountains, Antarctica: Tectonics, v. 13, no. 4, p. 818-836.

Fitzgerald, P. G., Sandiford, M., Barrett, P. J., and Gleadow, A. J., 1986, Asymmetric extension associated with uplift and subsidence in the Transantarctic Mountains and Ross Embayment: Earth and Planetary Science Letters, v. 81, no. 1, p. 67-78.

References

Flower, B., 1999, Cenozoic deep-sea temperatures and polar glaciation: the oxygen isotope record: Terra Antarctica Reports, v. 3, p. 27-42.

Flower, B., and Kennett, J. P., 1994, The middle Miocene climatic transition: East Antarctic ice sheet development, deep ocean circulation and global carbon cycling: Palaeogeography, Palaeoclimatology, Palaeoecology, v. 108, no. 3–4, p. 537-555.

Foland, K. A., Linder, J. S., Laskowski, T. E., and Grant, N. K., 1984, ^{40}Ar/^{39}Ar dating of glauconites: Measured ^{39}Ar recoil loss from well-crystallized specimens: Chemical Geology, v. 46, no. 3, p. 241-264.

Folk, R. L., and Ward, W. C., 1957, Brazos River bar: a study in the significance of grainsize parameters: Journal of Sedimentary Research, v. 27, no. 1, p. 3-26.

Ford, A., and Barrett, P., 1975, Basement rocks of the South-Central Ross Sea, Site 270, DSDP Leg 28: Initial Reports of the Deep Sea Drilling Project, v. 28, p. 861-868.

Foster, G. L., Lear, C. H., and Rae, J. W. B., 2012, The evolution of pCO$_2$, ice volume and climate during the middle Miocene: Earth and Planetary Science Letters, v. 341–344, p. 243-254.

Foster, G. L., and Rohling, E. J., 2013, Relationship between sea level and climate forcing by CO$_2$ on geological timescales: Proceedings of the National Academy of Sciences, v. 110, no. 4, p. 1209-1214.

Francis, J. E., 2000, Fossil Wood from Eocene High Latitude Forests: McMurdo Sound, Antarctica, *in* Stilwel, J. D., and Feldman, R. M., eds., Paleobiology and Paleoenvironments of Eocene Rocks: McMurdo Sound, East Antarctica: Washington, DC, American Geophysical Union, p. 253-260.

Francis, J. E., and Poole, I., 2002, Cretaceous and early Tertiary climates of Antarctica: evidence from fossil wood: Palaeogeography, Palaeoclimatology, Palaeoecology, v. 182, no. 1, p. 47-64.

References

Fretwell, P., Pritchard, H. D., Vaughan, D. G., Bamber, J. L., Barrand, N. E., Bell, R., Bianchi, C., Bingham, R. G., Blankenship, D. D., Casassa, G., Catania, G., Callens, D., Conway, H., Cook, A. J., Corr, H. F. J., Damaske, D., Damm, V., Ferraccioli, F., Forsberg, R., Fujita, S., Gim, Y., Gogineni, P., Griggs, J. A., Hindmarsh, R. C. A., Holmlund, P., Holt, J. W., Jacobel, R. W., Jenkins, A., Jokat, W., Jordan, T., King, E. C., Kohler, J., Krabill, W., Riger-Kusk, M., Langley, K. A., Leitchenkov, G., Leuschen, C., Luyendyk, B. P., Matsuoka, K., Mouginot, J., Nitsche, F. O., Nogi, Y., Nost, O. A., Popov, S. V., Rignot, E., Rippin, D. M., Rivera, A., Roberts, J., Ross, N., Siegert, M. J., Smith, A. M., Steinhage, D., Studinger, M., Sun, B., Tinto, B. K., Welch, B. C., Wilson, D. S., Young, D. A., Xiangbin, C., and Zirizzotti, A., 2013, Bedmap2: improved ice bed, surface and thickness datasets for Antarctica: The Cryosphere, v. 7, no. 1, p. 375-393.

Gaiero, D. M., Depetris, P. J., Probst, J.-L., Bidart, S. M., and Leleyter, L., 2004, The signature of river- and wind-borne materials exported from Patagonia to the southern latitudes: a view from REEs and implications for paleoclimatic interpretations: Earth and Planetary Science Letters, v. 219, no. 3–4, p. 357-376.

Galeotti, S., DeConto, R., Naish, T., Stocchi, P., Florindo, F., Pagani, M., Barrett, P., Bohaty, S., Lanci, L., Pollard, D., Sandroni, S., Talarico, F., and Zachos, J., 2016, Direct evidence for Antarctic Ice-Sheet variability across the Eocene-Oligocene boundary climate transition: Science, v. 352, no. 6281, p.76-80.

Galeotti, S., Lanci, L., Florindo, F., Naish, T. R., Sagnotti, L., Sandroni, S., and Talarico, F. M., 2012, Cyclochronology of the Eocene–Oligocene transition from the Cape Roberts Project-3 core, Victoria Land basin, Antarctica: Palaeogeography, Palaeoclimatology, Palaeoecology, v. 335–336, p. 84-94.

Gallego-Torres, D., Martínez-Ruiz, F., Paytan, A., Jiménez-Espejo, F. J., and Ortega-Huertas, M., 2007, Pliocene–Holocene evolution of depositional conditions in the eastern Mediterranean: Role of anoxia vs. productivity at time of sapropel deposition: Palaeogeography, Palaeoclimatology, Palaeoecology, v. 246, no. 2–4, p. 424-439.

Galloway, W. E., and Hobday, D. K., 1983, Terrigenous Shelf Systems, Terrigenous Clastic Depositional Systems, Springer US, p. 143-165.

Gasson, E., DeConto, R. M., Pollard, D., and Levy, R. H., 2016, Dynamic Antarctic ice sheet during the early to mid-Miocene: Proceedings of the National Academy of Sciences, v. 113, no. 13, p. 3459-3464.

Gasson, E., Lunt, D. J., DeConto, R., Goldner, A., Heinemann, M., Huber, M., LeGrande, A. N., Pollard, D., Sagoo, N., Siddall, M., Winguth, A., and Valdes, P. J., 2014, Uncertainties in the modelled CO2 threshold for Antarctic glaciation: Clim. Past, v. 10, no. 2, p. 451-466.

References

Golledge, N. R., Fogwill, C. J., Mackintosh, A. N., and Buckley, K. M., 2012, Dynamics of the last glacial maximum Antarctic ice-sheet and its response to ocean forcing: Proceedings of the National Academy of Sciences, v. 109, no. 40, p. 16052-16056.

Golledge, N. R., Kowalewski, D. E., Naish, T. R., Levy, R. H., Fogwill, C. J. and Gasson, E. G., 2015, The multi-millennial Antarctic commitment to future sea-level rise: Nature, v. 526, no. 7573, p. 421-425.

Golledge, N. R., Levy, R. H., McKay, R. M., Fogwill, C. J., White, D. A., Graham, A. G. C., Smith, J. A., Hillenbrand, C.-D., Licht, K. J., Denton, G. H., Ackert Jr, R. P., Maas, S. M., and Hall, B. L., 2013, Glaciology and geological signature of the Last Glacial Maximum Antarctic ice sheet: Quaternary Science Reviews, v. 78, p. 225-247.

Hambrey, M. J., Ehrmann, W., and Larsen, B., 1991, Cenozoic glacial record of the Prydz Bay continental shelf, East Antarctica: In: Barron, J; Larsen, B, et al.(eds.), Proc. ODP, Sci. Results, College Station, TX.(Ocean Drilling Program), 119, 77-132, v. 119, p. 77-132.

Hambrey, M. J., and McKelvey, B., 2000a, Major Neogene fluctuations of the East Antarctic ice sheet: Stratigraphic evidence from the Lambert Glacier region: Geology, v. 28, no. 10, p. 887-890.

Hambrey, M. J., and McKelvey, B., 2000b, Neogene fjordal sedimentation on the western margin of the Lambert Graben, East Antarctica: Sedimentology, v. 47, no. 3, p. 577-607.

Hannah, M., Wilson, G., and Wrenn, J., 2000, Oligocene and Miocene marine palynomorphs from CRP-2/2A, Victoria Land Basin, Antarctica: Terra Antarctica, v. 7, no. 4, p. 503-511.

Hannah, M., Wrenn, J., and Wilson, G., 2001, Preliminary report on early Oligocene and ?latest Eocene marine palynomorphs from CRP-3 drillhole, Victoria Land Basin, Antarctica: Terra Antarctica, v. 8, no. 4, p. 383-388.

Hannah, M. J., 2006, The palynology of ODP site 1165, Prydz Bay, East Antarctica: A record of Miocene glacial advance and retreat: Palaeogeography, Palaeoclimatology, Palaeoecology, v. 231, no. 1–2, p. 120-133.

Hart, J. K., and Roberts, D. H., 1994, Criteria to distinguish between subglacial glaciotectonic and glaciomarine sedimentation, I. Deformation styles and sedimentology: Sedimentary Geology, v. 91, no. 1, p. 191-213.

Harwood, D., 2010, Diatomite, *in* Smol, J., and Stoermer, F., eds., The Diatoms: Applications for the Environmental and Earth Sciences: Cambridge, Cambridge University Press, p. 570-574.

References

Harwood, D. M., and Levy, R. H., 2000, The McMurdo Erratics: Introduction and Overview, *in* Stilwel, J. D., and Feldman, R. M., eds., Paleobiology and Paleoenvironments of Eocene Rocks: McMurdo Sound, East Antarctica, Volume 76: Washington, DC, American Geophysical Union, p. 1-18.

Hatfield, R., and Stoner, J. S., 2013, Magnetic proxies and susceptibility, *in* Elias, S., ed., Encyclopedia of Quaternary Science, Volume 2: Amsterdam, Elsevier, p. 884-898.

Haug, G. H., and Tiedemann, R., 1998, Effect of the formation of the Isthmus of Panama on Atlantic Ocean thermohaline circulation: Nature, v. 393, no. 6686, p. 673-676.

Hayes, D., and Frakes, L., 1975, General synthesis, deep sea drilling project leg 28: Initial Reports of the Deep Sea Drilling Project, v. 28, p. 919-942.

Hays, J. D., Imbrie, J., and Shackleton, N. J., 1976, Variations in the Earth's Orbit: Pacemaker of the Ice Ages: Science, v. 194, no. 4270, p. 1121-1132.

Helling, D., and Kuhn, G., 2007, Geochemical variations detected with continuous XRF measurements on ANDRILL AND-1B core-preliminary results, *in* Cooper, A., Raymond, C, and the 10th ISAES Editorial Team, eds., Antarctica: A Keystone in a Changing World—Online Proceedings for the 10th International Symposium on Antarctic Earth Sciences, USGS Open-File Report 2007-1047, Extended Abstract 129, 4 p.

Hepp, D. A., Mörz, T., Hensen, C., Frederichs, T., Kasten, S., Riedinger, N., and Hay, W. W., 2009, A late Miocene–early Pliocene Antarctic deepwater record of repeated iron reduction events: Marine Geology, v. 266, no. 1, p. 198-211.

Hilgen, F., 1991, Extension of the astronomically calibrated (polarity) time scale to the Miocene/Pliocene boundary: Earth and planetary science letters, v. 107, no. 2, p. 349-368.

Hinnov, L. A., and Ogg, J. G., 2007, Cyclostratigraphy and the astronomical time scale: Stratigraphy, v. 4, no. 2-3, p. 239-251.

Holbourn, A., Kuhnt, W., Kochhann, K. G. D., Andersen, N., and Sebastian Meier, K. J., 2015, Global perturbation of the carbon cycle at the onset of the Miocene Climatic Optimum: Geology, v. 43, no. 2, p. 123-126.

Hole, M., and LeMasurier, W., 1994, Tectonic controls on the geochemical composition of Cenozoic, mafic alkaline volcanic rocks from West Antarctica: Contributions to Mineralogy and Petrology, v. 117, no. 2, p. 187-202.

References

Hollis, C. J., Taylor, K. W., Handley, L., Pancost, R. D., Huber, M., Creech, J. B., Hines, B. R., Crouch, E. M., Morgans, H. E., and Crampton, J. S., 2012, Early Paleogene temperature history of the Southwest Pacific Ocean: Reconciling proxies and models: Earth and planetary science letters, v. 349, p. 53-66.

Holmes, M. A., 2000, Clay Mineral Composition of Glacial Erratics, Mcmurdo Sound, *in* Stilwel, J. D., and Feldman, R. M., eds., Paleobiology and Paleoenvironments of Eocene Rocks: McMurdo Sound, East Antarctica, Volume 76: Washington, DC, American Geophysical Union, p. 63-72.

Huber, M., and Caballero, R., 2011, The early Eocene equable climate problem revisited: Clim. Past, v. 7, no. 2, p. 603-633.

Hunt, C. P., Moskowitz, B. M., and Banerjee, S. K., 1995, Magnetic Properties of Rocks and Minerals, *in* Ahrens, T., ed., Rock Physics & Phase Relations, American Geophysical Union, p. 189-204.

Hurley, P. M., Cormier, R. F., Hower, J., Fairbairn, H., and Pinson Jr, W., 1960, Reliability of glauconite for age measurement by K-Ar and Rb-Sr methods: AAPG Bulletin, v. 44, no. 11, p. 1793-1808.

IPCC, 2013, Climate Change 2013: The Physical Science Basis. Contribution of Working Group I to the Fifth Assessment Report of the Intergovernmental Panel on Climate Change, Cambridge, United Kingdom and New York, NY, USA, Cambridge University Press, 1535 p.:

Ivany, L. C., Van Simaeys, S., Domack, E. W., and Samson, S. D., 2006, Evidence for an earliest Oligocene ice sheet on the Antarctic Peninsula: Geology, v. 34, no. 5, p. 377-380.

Jiménez-Espejo, F., García-Alix, A., Jiménez-Moreno, G., Rodrigo-Gámiz, M., Anderson, R., Rodríguez-Tovar, F., Martínez-Ruiz, F., Giralt, S., Huertas, A. D., and Pardo-Igúzquiza, E., 2014, Saharan aeolian input and effective humidity variations over western Europe during the Holocene from a high altitude record: Chemical Geology, v. 374, p. 1-12.

Joughin, I., Smith, B. E., and Medley, B., 2014, Marine Ice Sheet Collapse Potentially Under Way for the Thwaites Glacier Basin, West Antarctica: Science, v. 344, no. 6185, p. 735-738.

Karstensen, J., Stramma, L., and Visbeck, M., 2008, Oxygen minimum zones in the eastern tropical Atlantic and Pacific oceans: Progress in Oceanography, v. 77, no. 4, p. 331-350.

Katz, M. E., Miller, K. G., Wright, J. D., Wade, B. S., Browning, J. V., Cramer, B. S., and Rosenthal, Y., 2008, Stepwise transition from the Eocene greenhouse to the Oligocene icehouse: Nature Geoscience, v. 1, no. 5, p. 329-334.

References

Keeling, R. F., Körtzinger, A., and Gruber, N., 2009, Ocean Deoxygenation in a Warming World: Annual Review of Marine Science, v. 2, no. 1, p. 199-229.

Kemp, E. M., 1975, Palynology of Leg 28 drill sites, Deep Sea Drilling Project: Initial Reports of the Deep Sea Drilling Project, v. 28, p. 599-623.

Kemp, E. M., and Barrett, P. J., 1975, Antarctic glaciation and early Tertiary vegetation: Nature, v. 258, no. 5535, p. 507-508.

Kennett, J., and Shackleton, N., 1976, Oxygen isotopic evidence for the development of the psychrosphere 38 Myr ago: Nature, v. 260, no. 5551, p. 513-515.

Kennett, J. P., 1977, Cenozoic evolution of Antarctic glaciation, the circum-Antarctic Ocean, and their impact on global paleoceanography: Journal of geophysical research, v. 82, no. 27, p. 3843-3860.

Kennett, J. P., and Barker, P. F., Latest Cretaceous to Cenozoic climate and oceanographic developments in the Weddell Sea, Antarctica: an ocean-drilling perspective, *in* Proceedings Proceedings of the Ocean Drilling Program, Scientific Results, 1990, Volume 113, Ocean Drilling Program College Station, TX, p. 937-960.

Kominz, M. A., Browning, J. V., Miller, K. G., Sugarman, P. J., Mizintseva, S., and Scotese, C. R., 2008, Late Cretaceous to Miocene sea-level estimates from the New Jersey and Delaware coastal plain coreholes: an error analysis: Basin Research, v. 20, no. 2, p. 211-226.

Kominz, M. A., and Pekar, S. F., 2001, Oligocene eustasy from two-dimensional sequence stratigraphic backstripping: Geological Society of America Bulletin, v. 113, no. 3, p. 291-304.

Krissek, L., Browne, G., Carter, L., Cowan, E., Dunbar, G., McKay, R., Naish, T., Powell, R., Reed, J., Wilch, T., and ANDRILL-MIS Science Team, 2007, Sedimentology and Stratigraphy of the AND-1B Core, ANDRILL McMurdo Ice Shelf Project, Antarctica: Terra Antartica, v. 14, no. 3, p. 185-222.

Kürschner, W. M., Kvaček, Z., and Dilcher, D. L., 2008, The impact of Miocene atmospheric carbon dioxide fluctuations on climate and the evolution of terrestrial ecosystems: Proceedings of the National Academy of Sciences, v. 105, no. 2, p. 449-453.

Lacis, A. A., Schmidt, G. A., Rind, D., and Ruedy, R. A., 2010, Atmospheric CO_2: Principal Control Knob Governing Earth's Temperature: Science, v. 330, no. 6002, p. 356-359.

References

Laskar, J., Fienga, A., Gastineau, M., and Manche, H., 2011, La2010: a new orbital solution for the long-term motion of the Earth: Astronomy & Astrophysics, v. 532, p. A89.

Laskar, J., Robutel, P., Joutel, F., Gastineau, M., Correia, A. C. M., and Levrard, B., 2004, A long-term numerical solution for the insolation quantities of the Earth: Astronomy & Astrophysics, v. 428, no. 1, p. 261-285.

Lawver, L., and Gahagan, L., 1994, Constraints on timing of extension in the Ross Sea region: Terra Antartica, v. 1, p. 545-552.

Lawver, L., and Gahagan, L., 1995, Revised plate reconstructions and implications for extension in the Ross Sea region, in Proceedings Proceedings, VII International Symposium on Antarctic Earth Sciences: Siena, Italy, Universita di Siena, p. 239.

Lawver, L. A., Gahagan, L. M., and Coffin, M. F., 1992, The development of paleoseaways around Antarctica, in Kennett, J. P., and Warnke, D. A., The Antarctic Paleoenvironment: A Perspective on Global Change: Part One, Antarctic Research Series, v. 56, American Geophysical Union, Washington, D.C,, p. 7-30.

Lear, C. H., Bailey, T. R., Pearson, P. N., Coxall, H. K., and Rosenthal, Y., 2008, Cooling and ice growth across the Eocene-Oligocene transition: Geology, v. 36, no. 3, p. 251-254.

Lear, C. H., Rosenthal, Y., Coxall, H. K., and Wilson, P. A., 2004, Late Eocene to early Miocene ice sheet dynamics and the global carbon cycle: Paleoceanography, v. 19, no. 4.

Leckie, R. M., and Webb, P.-N., 1983, Late Oligocene–early Miocene glacial record of the Ross Sea, Antarctica: Evidence from DSDP site 270: Geology, v. 11, no. 10, p. 578-582.

LeMasurier, W. E., and Rex, D. C., 1983, Rates of uplift and the scale of ice level instabilities recorded by volcanic rocks in Marie Byrd Land, West Antarctica, in Oliver, R., James, P., and Jago, J., eds., Antarctic Earth Science: New York, Cambridge University Press, p. 663-670.

LeMasurier, W. E., and Rocchi, S., 2005, Terrestrial Record of Post-Eocene Climate History in Marie Byrd Land, West Antarctica: Geografiska Annaler. Series A, Physical Geography, v. 87, no. 1, p. 51-66.

Levitan, M., and Lavrushin, Y. A., 2009, Seas of the Eastern Subarctic, in Levitan, M., and Lavrushin, Y. A., eds., Sedimentation History in the Arctic Ocean and Subarctic Seas for the Last 130 kyr: Heidelberg, Springer, p. 301-329.

References

Levitan, M., Luksha, V., and Tolmacheva, A., 2007, History of sedimentation in the northern Sea of Okhotsk during the last 1.1 Ma: Lithology and Mineral Resources, v. 42, no. 3, p. 203-220.

Levy, R., Harwood, D., Florindo, F., Sangiorgi, F., Tripati, R., von Eynatten, H., Gasson, E., Kuhn, G., Tripati, A., DeConto, R., Fielding, C. R., Field, B., Golledge, N. R., McKay, R., Naish, T., Olney, M. P., Pollard, D., Schouten, S., Talarico, F., Warny, S., Willimott, V., Acton, G., Panter, K., Paulsen, T., Taviani, M., and SMS Science Teams, 2016, Antarctic ice sheet sensitivity to atmospheric CO_2 variations in the early to mid-Miocene: Proceedings of the National Academy of Sciences, v. 113, no. 13, p. 3453-3458.

Levy, R., Naish, T., Harwood, D., Gebhardt, C., Florindo, F., Suganuma, Y., McKay, R., Lee, J., Bohaty, S., Jovane, L., DeConto, R., Kulhanek, D., Paulsen, T., Rack, F., Shevenell, A., Wellner, J., and Wilson, D., 2014, The Coulman High Project - Drilling beneath the Ross Ice Shelf to understand Antarctic Ice Sheet sensitivity to climatic, tectonic, and environmental forcing in a high CO_2 world, unpublished IODP Proposal, 99 pp.

Levy, R. H., and Harwood, D. M., 2000, Sedimentary Lithofacies of the Mcmurdo Sound Erratics, *in* Stilwel, J. D., and Feldman, R. M., eds., Paleobiology and Paleoenvironments of Eocene Rocks: McMurdo Sound, East Antarctica, Volume 76: Washington, DC, American Geophysical Union, p. 39-61.

Lewis, A. R., and Ashworth, A. C., 2015, An early to middle Miocene record of ice-sheet and landscape evolution from the Friis Hills, Antarctica: Geological Society of America Bulletin, v. 128, no. 5-6, p. 719-738.

Lewis, A. R., Marchant, D. R., Ashworth, A. C., Hedenäs, L., Hemming, S. R., Johnson, J. V., Leng, M. J., Machlus, M. L., Newton, A. E., Raine, J. I., Willenbring, J. K., Williams, M., and Wolfe, A. P., 2008, Mid-Miocene cooling and the extinction of tundra in continental Antarctica: Proceedings of the National Academy of Sciences, v. 105, no. 31, p. 10676-10680.

Lewis, A. R., Marchant, D. R., Ashworth, A. C., Hemming, S. R., and Machlus, M. L., 2007, Major middle Miocene global climate change: Evidence from East Antarctica and the Transantarctic Mountains: Geological Society of America Bulletin, v. 119, no. 11-12, p. 1449-1461.

Lewis, A. R., Marchant, D. R., Kowalewski, D. E., Baldwin, S. L., and Webb, L. E., 2006, The age and origin of the Labyrinth, western Dry Valleys, Antarctica: Evidence for extensive middle Miocene subglacial floods and freshwater discharge to the Southern Ocean: Geology, v. 34, no. 7, p. 513-516.

Lewis, D. W., and McConchie, D., 1994, Analytical sedimentology, New York, Chapman & Hall, 197 p.:

References

Liebrand, D., Lourens, L., Hodell, D., De Boer, B., Van de Wal, R., and Pälike, H., 2011, Antarctic ice sheet and oceanographic response to eccentricity forcing during the early Miocene: Climate of the Past, v. 7, no. 3, p. 869-880.

Liu, Z., Pagani, M., Zinniker, D., DeConto, R., Huber, M., Brinkhuis, H., Shah, S. R., Leckie, R. M., and Pearson, A., 2009, Global Cooling During the Eocene-Oligocene Climate Transition: Science, v. 323, no. 5918, p. 1187-1190.

Lough, A. C., Wiens, D. A., Grace Barcheck, C., Anandakrishnan, S., Aster, R. C., Blankenship, D. D., Huerta, A. D., Nyblade, A., Young, D. A., and Wilson, T. J., 2013, Seismic detection of an active subglacial magmatic complex in Marie Byrd Land, Antarctica: Nature Geoscience, v. 6, no. 12, p. 1031-1035.

Lucchi, R. G., Camerlenghi, A., Rebesco, M., Colmenero-Hidalgo, E., Sierro, F. J., Sagnotti, L., Urgeles, R., Melis, R., Morigi, C., Bárcena, M. A., Giorgetti, G., Villa, G., Persico, D., Flores, J. A., Rigual-Hernández, A. S., Pedrosa, M. T., Macri, P., and Caburlotto, A., 2013, Postglacial sedimentary processes on the Storfjorden and Kveithola trough mouth fans: Significance of extreme glacimarine sedimentation: Global and Planetary Change, v. 111, p. 309-326.

Luyendyk, B. P., 1995, Hypothesis for Cretaceous rifting of east Gondwana caused by subducted slab capture: Geology, v. 23, no. 4, p. 373-376.

Luyendyk, B. P., Sorlien, C. C., Wilson, D. S., Bartek, L. R., and Siddoway, C. S., 2001, Structural and tectonic evolution of the Ross Sea rift in the Cape Colbeck region, Eastern Ross Sea, Antarctica: Tectonics, v. 20, no. 6, p. 933-958.

Luyendyk, B. P., Wilson, D. S., and Siddoway, C. S., 2003, Eastern margin of the Ross Sea Rift in western Marie Byrd Land, Antarctica: Crustal structure and tectonic development: Geochemistry, Geophysics, Geosystems, v. 4, no. 10.

Lyle, M., Olivarez Lyle, A., Gorgas, T., Holbourn, A., Westerhold, T., Hathorne, E., Kimoto, K., and Yamamoto, S., 2012, Data report: Raw and normalized elemental data along the Site U1338 splice from X-ray fluorescence scanning, in Pälike, H., Lyle, M., Nishi, H., Raffi, I., Gamage, K., Klaus, A., and the Expedition 320/321 Scientists, eds., Proceedings of the Integrated Ocean Drilling Program, v. 320/321, Tokyo, Integrated Ocean Drilling Program Management International, Inc.

Mackiewicz, N. E., Powell, R. D., Carlson, P. R., and Molnia, B. F., 1984, Interlaminated ice-proximal glacimarine sediments in Muir Inlet, Alaska: Marine Geology, v. 57, no. 1, p. 113-147.

Mangini, A., Jung, M., and Laukenmann, S., 2001, What do we learn from peaks of uranium and of manganese in deep sea sediments?: Marine Geology, v. 177, no. 1, p. 63-78.

References

Mann, M. E., and Lees, J. M., 1996, Robust estimation of background noise and signal detection in climatic time series: Climatic change, v. 33, no. 3, p. 409-445.

Margolis, S. V., and Kennett, J. P., 1970, Antarctic Glaciation during the Tertiary Recorded in Sub-Antarctic Deep-Sea Cores: Science, v. 170, no. 3962, p. 1085-1087.

Marsh, R., Mills, R. A., Green, D. R., Salter, I., and Taylor, S., 2007, Controls on sediment geochemistry in the Crozet region: Deep Sea Research Part II: Topical Studies in Oceanography, v. 54, no. 18, p. 2260-2274.

Masson-Delmotte, V., M. Schulz, A. Abe-Ouchi, J. Beer, A. Ganopolski, J.F. González Rouco, E. Jansen, K. Lambeck, J. Luterbacher, T. Naish, T. Osborn, B. Otto-Bliesner, T. Quinn, R. Ramesh, M. Rojas, X. Shao and A. Timmermann, 2013, Information from Paleoclimate Archives, *in* Stocker, T.F., D. Qin, G.-K. Plattner, M. Tignor, S.K. Allen, J. Boschung, A. Nauels, Y. Xia, V. Bex and Midgley, P.M., eds., Climate Change 2013: The Physical Science Basis. Contribution of Working Group I to the Fifth Assessment Report of the Intergovernmental Panel on Climate Change. Cambridge University Press, Cambridge, United Kingdom and New York, NY, USA.

Mawbey, E. M., and Lear, C. H., 2013, Carbon cycle feedbacks during the Oligocene-Miocene transient glaciation: Geology, v. 41, no. 9, p. 963-966.

Mazzulo, J., and Graham, A., 1988, Handbook for shipboard sedimentologists: ODP Technical Note, v. 8, Ocean Drilling Program, Texas A&M University, College Station, TX, 67 pp.

McCollum, D., 1975, Diatom stratigraphy of the Southern Ocean: Initial Reports of the Deep Sea Drilling Project, v. 28, p. 515-571.

McKay, R., Browne, G., Carter, L., Cowan, E., Dunbar, G., Krissek, L., Naish, T., Powell, R., Reed, J., Talarico, F., and Wilch, T., 2009, The stratigraphic signature of the late Cenozoic Antarctic Ice Sheets in the Ross Embayment: GSA Bulletin, v. 121, no. 11-12, p. 1537-1561.

McKay, R., Dunbar, G., Naish, T., Barrett, P., Carter, L., and Harper, M., 2008, Retreat history of the Ross Ice Sheet (Shelf) since the Last Glacial Maximum from deep-basin sediment cores around Ross Island: Palaeogeography, Palaeoclimatology, Palaeoecology, v. 260, no. 1, p. 245-261.

McKay, R., Naish, T., Carter, L., Riesselman, C., Dunbar, R., Sjunneskog, C., Winter, D., Sangiorgi, F., Warren, C., Pagani, M., Schouten, S., Willmott, V., Levy, R., DeConto, R., and Powell, R. D., 2012a, Antarctic and Southern Ocean influences on Late Pliocene global cooling: Proceedings of the National Academy of Sciences, v. 109, no. 17, p. 6423-6428.

References

McKay, R., Naish, T., Powell, R., Barrett, P., Scherer, R., Talarico, F., Kyle, P., Monien, D., Kuhn, G., Jackolski, C., and Williams, T., 2012b, Pleistocene variability of Antarctic Ice Sheet extent in the Ross Embayment: Quaternary Science Reviews, v. 34, p. 93-112.

McKay, R. M., Barrett, P. J., Levy, R. S., Naish, T. R., Golledge, N. R., and Pyne, A., 2016, Antarctic Cenozoic climate history from sedimentary records: ANDRILL and beyond: Philosophical Transactions of the Royal Society of London A: Mathematical, Physical and Engineering Sciences, v. 374, no. 2059.

Mercer, J. H., 1983, Cenozoic glaciation in the Southern Hemisphere: Annual Review of Earth and Planetary Sciences, v. 11, p. 99-132.

Meyers, S., 2014, astrochron: An R Package for Astrochronology, http://cran.r-project.org/package=astrochron.

Meyers, S. R., and Sageman, B. B., 2007, Quantification of deep-time orbital forcing by average spectral misfit: American Journal of Science, v. 307, no. 5, p. 773-792.

Meyers, S. R., Sageman, B. B., and Arthur, M. A., 2012, Obliquity forcing of organic matter accumulation during Oceanic Anoxic Event 2: Paleoceanography, v. 27, no. 3.

Milankovitch, M., 1941, Kanon der Erdebestrahlung und seine Anwendung auf das Eiszeitenproblem, Special Publications 132, Section of Mathematics and Natural Sciences 33, Königlich Serbische Akademie, Belgrade, 633 pp.

Mildenhall, D., 1989, Terrestrial palynology, *in* Barrett, P., ed., Antarctic Cenozoic history from the CIROS-1 drillhole, McMurdo Sound: DSIR Bulletin, v. 245, Wellington, New Zealand, DSIR Publishing, p. 119-127.

Miller, K. G., Browning, J. V., Aubry, M.-P., Wade, B. S., Katz, M. E., Kulpecz, A. A., and Wright, J. D., 2008a, Eocene–Oligocene global climate and sea-level changes: St. Stephens Quarry, Alabama: Geological Society of America Bulletin, v. 120, no. 1-2, p. 34-53.

Miller, K. G., and Fairbanks, R. G., 1983, Evidence for Oligocene-Middle Miocene abyssal circulation changes in the western North Atlantic: Nature, v. 306, no. 5940, p. 250-253.

Miller, K. G., and Fairbanks, R. G., 1985, Oligocene to Miocene carbon isotope cycles and abyssal circulation changes, *in* Sundquist, E. T., and Broecker, W. S., eds., The Carbon Cycle and Atmospheric CO_2: Natural Variations Archean to Present, American Geophysical Union, Washington, D. C., p. 469-486.

References

Miller, K. G., Fairbanks, R. G., and Mountain, G. S., 1987, Tertiary oxygen isotope synthesis, sea level history, and continental margin erosion: Paleoceanography, no. 2, p. 1-19.

Miller, K. G., Kominz, M. A., Browning, J. V., Wright, J. D., Mountain, G. S., Katz, M. E., Sugarman, P. J., Cramer, B. S., Christie-Blick, N., and Pekar, S. F., 2005a, The Phanerozoic Record of Global Sea-Level Change: Science, v. 310, no. 5752, p. 1293-1298.

Miller, K. G., and Mountain, G. S., 1996, Drilling and Dating New Jersey Oligocene-Miocene Sequences: Ice Volume, Global Sea Level, and Exxon Records: Science, v. 271, no. 5252, p. 1092-1095.

Miller, K. G., Mountain, G. S., Wright, J. D., and Browning, J. V., 2011, A 180-million-year record of sea level and ice volume variations from continental margin and deep-sea isotopic records: Oceanography, v. 24, no. 2, p. 40-53.

Miller, K. G., Sugarman, P. J., Browning, J. V., Kominz, M. A., Hernández, J. C., Olsson, R. K., Wright, J. D., Feigenson, M. D., and Van Sickel, W., 2003, Late Cretaceous chronology of large, rapid sea-level changes: Glacioeustasy during the greenhouse world: Geology, v. 31, no. 7, p. 585-588.

Miller, K. G., Sugarman, P. J., Browning, J. V., Kominz, M. A., Olsson, R. K., Feigenson, M. D., and Hernández, J. C., 2004, Upper Cretaceous sequences and sea-level history, New Jersey Coastal Plain: Geological Society of America Bulletin, v. 116, no. 3-4, p. 368-393.

Miller, K. G., Wright, J., Katz, M., Browning, J., Cramer, B., Wade, B. S., and Mizintseva, S., A view of Antarctic ice-sheet evolution from sea-level and deep-sea isotope changes during the Late Cretaceous–Cenozoic, *in* Proceedings Antarctica: A Keystone in a Changing World. Proceedings of the 10th International Symposium on Antarctic Earth Sciences, Washington, DC, 2008b, The National Academies Press, p. 55-70.

Miller, K. G., Wright, J. D., and Browning, J. V., 2005b, Visions of ice sheets in a greenhouse world: Marine Geology, v. 217, no. 3–4, p. 215-231.

Miller, K. G., Wright, J. D., Browning, J. V., Kulpecz, A., Kominz, M., Naish, T. R., Cramer, B. S., Rosenthal, Y., Peltier, W. R., and Sosdian, S., 2012, High tide of the warm Pliocene: Implications of global sea level for Antarctic deglaciation: Geology, v. 40, no. 5, p. 407-410.

Miller, K. G., Wright, J. D., and Fairbanks, R. G., 1991, Unlocking the Ice House: Oligocene-Miocene oxygen isotopes, eustasy, and margin erosion: Journal of Geophysical Research: Solid Earth, v. 96, no. B4, p. 6829-6848.

References

Moncrieff, A. C. M., 1989, Classification of poorly-sorted sedimentary rocks: Sedimentary Geology, v. 65, no. 1, p. 191-194.

Moros, M., Endler, R., Lackschewitz, K. S., Wallrabe-Adams, H. J., Mienert, J., and Lemke, W., 1997, Physical properties of Reykjanes Ridge sediments and their linkage to high-resolution Greenland Ice Sheet Project 2 ice core data: Paleoceanography, v. 12, no. 5, p. 687-695.

Moucha, R., Forte, A. M., Mitrovica, J. X., Rowley, D. B., Quéré, S., Simmons, N. A., and Grand, S. P., 2008, Dynamic topography and long-term sea-level variations: There is no such thing as a stable continental platform: Earth and Planetary Science Letters, v. 271, no. 1–4, p. 101-108.

Mudelsee, M., Bickert, T., Lear, C. H., and Lohmann, G., 2014, Cenozoic climate changes: A review based on time series analysis of marine benthic δ18O records: Reviews of Geophysics, v. 52, no. 3, p. 333-374.

Mudelsee, M., and Raymo, M. E., 2005, Slow dynamics of the Northern Hemisphere glaciation: Paleoceanography, v. 20, no. 4.

Mukasa, S. B., and Dalziel, I. W. D., 2000, Marie Byrd Land, West Antarctica: Evolution of Gondwana's Pacific margin constrained by zircon U-Pb geochronology and feldspar common-Pb isotopic compositions: Geological Society of America Bulletin, v. 112, no. 4, p. 611-627.

Naish, T., Levy, R., Powell, R., and MIS Science and Operations Team Members, 2006, Scientific Logistics Implementation Plan for the ANDRILL McMurdo Ice Shelf Project, Lincoln-NE, University of Nebraska-Lincoln, ANDRILL Contribution, 117 p.:

Naish, T., Powell, R., Levy, R., Wilson, G., Scherer, R., Talarico, F., Krissek, L., Niessen, F., Pompilio, M., and Wilson, T., 2009, Obliquity-paced Pliocene West Antarctic ice sheet oscillations: Nature, v. 458, no. 7236, p. 322-328.

Naish, T., Wilson, G. S., Dunbar, G. B., and Barrett, P. J., 2008, Constraining the amplitude of Late Oligocene bathymetric changes in western Ross Sea during orbitally-induced oscillations in the East Antarctic Ice Sheet: (2) Implications for global sea-level changes: Palaeogeography, Palaeoclimatology, Palaeoecology, v. 260, no. 1–2, p. 66-76.

Naish, T., Woolfe, K. J., Barrett, P. J., Wilson, G. S., and et al., 2001, Orbitally induced oscillations in the East Antarctic ice sheet at the Oligocene/Miocene boundary: Nature, v. 413, no. 6857, p. 719-723.

References

Nam, S.-I., Stein, R., Grobe, H., and Hubberten, H., 1995, Late Quaternary glacial-interglacial changes in sediment composition at the East Greenland continental margin and their paleoceanographic implications: Marine Geology, v. 122, no. 3, p. 243-262.

Nowaczyk, N. R., 2001, Logging of magnetic susceptibility, Tracking environmental change using lake sediments, Springer, p. 155-170.

Ó Cofaigh, C., and Dowdeswell, J. A., 2001, Laminated sediments in glacimarine environments: diagnostic criteria for their interpretation: Quaternary Science Reviews, v. 20, no. 13, p. 1411-1436.

Ó Cofaigh, C., Dowdeswell, J. A., and Grobe, H., 2001, Holocene glacimarine sedimentation, inner Scoresby Sund, East Greenland: the influence of fast-flowing ice-sheet outlet glaciers: Marine Geology, v. 175, no. 1, p. 103-129.

Ogg, J. G., 2012, Geomagnetic Polarity Time Scale, *in* Gradstein, F. M., Ogg, J. G., Schmitz, M. D., and Ogg, G. M., eds., The Geologic Time Scale: Boston, Elsevier, p. 85-113.

Pagani, M., Huber, M., Liu, Z., Bohaty, S. M., Henderiks, J., Sijp, W., Krishnan, S., and DeConto, R. M., 2011, The Role of Carbon Dioxide During the Onset of Antarctic Glaciation: Science, v. 334, no. 6060, p. 1261-1264.

Pagani, M., Zachos, J. C., Freeman, K. H., Tipple, B., and Bohaty, S., 2005, Marked Decline in Atmospheric Carbon Dioxide Concentrations During the Paleogene: Science, v. 309, no. 5734, p. 600-603.

Paillard, D., 2010, Climate and the orbital parameters of the Earth: Comptes Rendus Geoscience, v. 342, no. 4–5, p. 273-285.

Pälike, H., Frazier, J., and Zachos, J. C., 2006a, Extended orbitally forced palaeoclimatic records from the equatorial Atlantic Ceara Rise: Quaternary Science Reviews, v. 25, no. 23–24, p. 3138-3149.

Pälike, H., Norris, R. D., Herrle, J. O., Wilson, P. A., Coxall, H. K., Lear, C. H., Shackleton, N. J., Tripati, A. K., and Wade, B. S., 2006b, The heartbeat of the Oligocene climate system: Science, v. 314, no. 5807, p. 1894-1898.

Paolo, F. S., Fricker, H. A., and Padman, L., 2015, Volume loss from Antarctic ice shelves is accelerating: Science, v. 348, no. 6232, p. 327-331.

Pascher, K., Hollis, C., Bohaty, S., Cortese, G., McKay, R., Seebeck, H., Suzuki, N., and Chiba, K., 2015, Expansion and diversification of high-latitude radiolarian assemblages in the late Eocene linked to a cooling event in the southwest Pacific: Climate of the Past, v. 11, no. 12, p. 1599-1620.

References

Passchier, S., 2011, Linkages between East Antarctic Ice Sheet extent and Southern Ocean temperatures based on a Pliocene high-resolution record of ice-rafted debris off Prydz Bay, East Antarctica: Paleoceanography, v. 26, no. 4, p. 1-13.

Passchier, S., Bohaty, S. M., Jiménez-Espejo, F., Pross, J., Röhl, U., van de Flierdt, T., Escutia, C., and Brinkhuis, H., 2013, Early Eocene to middle Miocene cooling and aridification of East Antarctica: Geochemistry, Geophysics, Geosystems, v. 14, no. 5, p. 1399-1410.

Passchier, S., Browne, G., Field, B., Fielding, C. R., Krissek, L. A., Panter, K., Pekar, S. F., and Team, a. A.-S. S., 2011, Early and middle Miocene Antarctic glacial history from the sedimentary facies distribution in the AND-2A drill hole, Ross Sea, Antarctica: Geological Society of America Bulletin, v. 123, no. 11-12, p. 2352-2365.

Passchier, S., and Krissek, L. A., 2008, Oligocene–Miocene Antarctic continental weathering record and paleoclimatic implications, Cape Roberts drilling Project, Ross Sea, Antarctica: Palaeogeography, Palaeoclimatology, Palaeoecology, v. 260, no. 1–2, p. 30-40.

Patterson, M., McKay, R., Naish, T., Escutia, C., Jimenez-Espejo, F., Raymo, M., Meyers, S., Tauxe, L., Brinkhuis, H., and Expedition, I., 2014, Orbital forcing of the East Antarctic ice sheet during the Pliocene and Early Pleistocene: Nature Geoscience, v. 7, no. 11, p. 841-847.

Paul, H. A., Zachos, J. C., Flower, B. P., and Tripati, A., 2000, Orbitally induced climate and geochemical variability across the Oligocene/Miocene boundary: Paleoceanography, v. 15, no. 5, p. 471-485.

Pearson, P. N., Foster, G. L., and Wade, B. S., 2009, Atmospheric carbon dioxide through the Eocene–Oligocene climate transition: Nature, v. 461, no. 7267, p. 1110-1113.

Pearson, P. N., and Palmer, M. R., 2000, Atmospheric carbon dioxide concentrations over the past 60 million years: Nature, v. 406, no. 6797, p. 695-699.

Pekar, S., and Miller, K. G., 1996, New Jersey Oligocene "Icehouse" sequences (ODP Leg 150X) correlated with global $\delta^{18}O$ and Exxon eustatic records: Geology, v. 24, no. 6, p. 567-570.

Pekar, S. F., Christie-Blick, N., Kominz, M. A., and Miller, K. G., 2002, Calibration between eustatic estimates from backstripping and oxygen isotopic records for the Oligocene: Geology, v. 30, no. 10, p. 903-906.

Pekar, S. F., and DeConto, R. M., 2006, High-resolution ice-volume estimates for the early Miocene: Evidence for a dynamic ice sheet in Antarctica: Palaeogeography, Palaeoclimatology, Palaeoecology, v. 231, no. 1–2, p. 101-109.

References

Pekar, S. F., DeConto, R. M., and Harwood, D. M., 2006, Resolving a late Oligocene conundrum: Deep-sea warming and Antarctic glaciation: Palaeogeography, Palaeoclimatology, Palaeoecology, v. 231, no. 1–2, p. 29-40.

Pinous, O. V., Akhmetiev, M. A., and Sahagian, D. L., 1999, Sequence stratigraphy and sea-level history of Oligocene strata of the northern Aral Sea region (Kazakhstan): Implications for glacioeustatic reconstructions: Geological Society of America Bulletin, v. 111, no. 1, p. 1-10.

Pole, M., Hill, B., and Harwood, D., 2000, Eocene Plant Macrofossils from Erratics, Mcmurdo Sound, Antarctica, *in* Stilwel, J. D., and Feldman, R. M., eds., Paleobiology and Paleoenvironments of Eocene Rocks: McMurdo Sound, East Antarctica, Volume 76: Washington, DC, American Geophysical Union, p. 243-251.

Pollard, D., and DeConto, R., 2007, A Coupled Ice-sheet/Ice-shelf/Sediment Model Applied to a Marine Margin Flowline: Forced and Unforced Variations, *in* Hambrey, M. J., Christoffersen, P., Glasser, N., and Hubbard, B., eds., Glacial Sedimentary Processes and Products, Wiley-Blackwell, p. 35-53.

Pollard, D., and DeConto, R. M., 2009, Modelling West Antarctic ice sheet growth and collapse through the past five million years: Nature, v. 458, no. 7236, p. 329.

Pollard, D., DeConto, R. M., and Alley, R. B., 2015, Potential Antarctic Ice Sheet retreat driven by hydrofracturing and ice cliff failure: Earth and Planetary Science Letters, v. 412, p. 112-121.

Poole, I., Cantrill, D., and Utescher, T., 2005, A multi-proxy approach to determine Antarctic terrestrial palaeoclimate during the Late Cretaceous and Early Tertiary: Palaeogeography, Palaeoclimatology, Palaeoecology, v. 222, no. 1–2, p. 95-121.

Powell, R., Krissek, L., and Van der Meer, J., 2000, Preliminary depositional environmental analysis of CRP-2/2A, Victoria Land Basin, Antarctica: palaeoglaciological and palaeoclimatic inferences: Terra Antartica, v. 7, no. 3, p. 313-322.

Powell, R., Laird, M., Naish, T., Fielding, C. R., Krissek, L., and van der Meer, J., 2001, Depositional environments for strata cored in CRP-3 (Cape Roberts Project), Victoria Land Basin, Antarctica: palaeoglaciological and palaeoclimatological inferences: Terra Antarctica, v. 8, p. 207-216.

Powell, R. D., 1984, Glacimarine processes and inductive lithofacies modelling of ice shelf and tidewater glacier sediments based on Quaternary examples: Marine Geology, v. 57, no. 1–4, p. 1-52.

References

Powell, R. D., and Cooper, J. M., 2002, A glacial sequence stratigraphic model for temperate, glaciated continental shelves: Geological Society, London, Special Publications, v. 203, no. 1, p. 215-244.

Powell, R. D., and Molnia, B. F., 1989, Glacimarine sedimentary processes, facies and morphology of the south-southeast Alaska shelf and fjords: Marine Geology, v. 85, no. 2–4, p. 359-390.

Prebble, J. G., Raine, J. I., Barrett, P. J., and Hannah, M. J., 2006, Vegetation and climate from two Oligocene glacioeustatic sedimentary cycles (31 and 24 Ma) cored by the Cape Roberts Project, Victoria Land Basin, Antarctica: Palaeogeography, Palaeoclimatology, Palaeoecology, v. 231, no. 1–2, p. 41-57.

Pritchard, H. D., Arthern, R. J., Vaughan, D. G., and Edwards, L. A., 2009, Extensive dynamic thinning on the margins of the Greenland and Antarctic ice sheets: Nature, v. 461, no. 7266, p. 971-975.

Pritchard, H. D., Ligtenberg, S. R. M., Fricker, H. A., Vaughan, D. G., van den Broeke, M. R., and Padman, L., 2012, Antarctic ice-sheet loss driven by basal melting of ice shelves: Nature, v. 484, no. 7395, p. 502-505.

Pross, J., Contreras, L., Bijl, P. K., Greenwood, D. R., Bohaty, S. M., Schouten, S., Bendle, J. A., Rohl, U., Tauxe, L., Raine, J. I., Huck, C. E., van de Flierdt, T., Jamieson, S. S. R., Stickley, C. E., van de Schootbrugge, B., Escutia, C., and Brinkhuis, H., 2012, Persistent near-tropical warmth on the Antarctic continent during the early Eocene epoch: Nature, v. 488, no. 7409, p. 73-77.

Pudsey, C., 2000, Sedimentation on the continental rise west of the Antarctic Peninsula over the last three glacial cycles: Marine Geology, v. 167, no. 3, p. 313-338.

Raine, J., and Askin, R., 2001, Terrestrial palynology of Cape Roberts Project Drillhole CRP-3, Victoria Land Basin, Antarctica: Terra Antartica, v. 8, no. 4, p. 389-400.

Richter, T. O., Van der Gaast, S., Koster, B., Vaars, A., Gieles, R., de Stigter, H. C., De Haas, H., and van Weering, T. C., 2006, The Avaatech XRF Core Scanner: technical description and applications to NE Atlantic sediments: Geological Society, London, Special Publications, v. 267, no. 1, p. 39-50.

Rignot, E., Bamber, J. L., van den Broeke, M. R., Davis, C., Li, Y., van de Berg, W. J., and van Meijgaard, E., 2008, Recent Antarctic ice mass loss from radar interferometry and regional climate modelling: Nature Geoscience, v. 1, no. 2, p. 106-110.

Rignot, E., Jacobs, S., Mouginot, J., and Scheuchl, B., 2013, Ice-Shelf Melting Around Antarctica: Science, v. 341, no. 6143, p. 266-270.

References

Rignot, E., Mouginot, J., and Scheuchl, B., 2011, Ice flow of the Antarctic ice sheet: Science, v. 333, no. 6048, p. 1427-1430.

Robert, C., and Kennett, J. P., 1997, Antarctic continental weathering changes during Eocene-Oligocene cryosphere expansion: Clay mineral and oxygen isotope evidence: Geology, v. 25, no. 7, p. 587-590.

Roberts, A. P., Wilson, G. S., Harwood, D. M., and Verosub, K. L., 2003, Glaciation across the Oligocene–Miocene boundary in southern McMurdo Sound, Antarctica: new chronology from the CIROS-1 drill hole: Palaeogeography, Palaeoclimatology, Palaeoecology, v. 198, no. 1–2, p. 113-130.

Robinson, S. G., 2001, Early diagenesis in an organic-rich turbidite and pelagic clay sequence from the Cape Verde Abyssal Plain, NE Atlantic: magnetic and geochemical signals: Sedimentary Geology, v. 143, no. 1–2, p. 91-123.

Rocchi, S., LeMasurier, W. E., and Di Vincenzo, G., 2006, Oligocene to Holocene erosion and glacial history in Marie Byrd Land, West Antarctica, inferred from exhumation of the Dorrel Rock intrusive complex and from volcano morphologies: Geological Society of America Bulletin, v. 118, no. 7-8, p. 991-1005.

Rollinson, H. R., 1993, Using geochemical data: evaluation, presentation, interpretation, Harlow, England, Pearson Prentice Hall, 352 p.:

Rose, K. C., Ferraccioli, F., Jamieson, S. S. R., Bell, R. E., Corr, H., Creyts, T. T., Braaten, D., Jordan, T. A., Fretwell, P. T., and Damaske, D., 2013, Early East Antarctic Ice Sheet growth recorded in the landscape of the Gamburtsev Subglacial Mountains: Earth and Planetary Science Letters, v. 375, p. 1-12.

Rosenthal, Y., Lam, P., Boyle, E. A., and Thomson, J., 1995, Authigenic cadmium enrichments in suboxic sediments: Precipitation and postdepositional mobility: Earth and Planetary Science Letters, v. 132, no. 1–4, p. 99-111.

Rothwell, R. G., and Croudace, I. W., 2015, Twenty Years of XRF Core Scanning Marine Sediments: What Do Geochemical Proxies Tell Us?, *in* Croudace, I. W., and Rothwell, R. G., eds., Micro-XRF Studies of Sediment Cores: Dordrecht, Springer, p. 25-102.

Rowley, D. B., Forte, A. M., Moucha, R., Mitrovica, J. X., Simmons, N. A., and Grand, S. P., 2013, Dynamic Topography Change of the Eastern United States Since 3 Million Years Ago: Science, v. 340, no. 6140, p. 1560-1563.

Ruddiman, W. F., 1997, Tectonic Uplift and Climate Change, New York, Plenum Press, 535 p.:

References

Ruddiman, W. F., 2014, Earth's climate - past and future, New York, W. H. Freeman and Company, 445 p.:

Ruffell, A., McKinley, J. M., and Worden, R. H., 2002, Comparison of clay mineral stratigraphy to other proxy palaeoclimate indicators in the Mesozoic of NW Europe: Philosophical Transactions of the Royal Society of London A: Mathematical, Physical and Engineering Sciences, v. 360, no. 1793, p. 675-693.

Salabarnada, A., Escutia, C., Nelson, H., Damuth, J. E., and Jimenez-Espejo, F., The Oligocene-Miocene transition at the East Antarctic Wilkes Land margin: IODP Site 1356, *in* Proceedings EGU General Assembly Conference Abstracts2015, Volume 17, p. 15698.

Scher, H. D., Whittaker, J. M., Williams, S. E., Latimer, J. C., Kordesch, W. E. C., and Delaney, M. L., 2015, Onset of Antarctic Circumpolar Current 30 million years ago as Tasmanian Gateway aligned with westerlies: Nature, v. 523, no. 7562, p. 580-583.

Scherer, R. P., Aldahan, A., Tulaczyk, S., Possnert, G., Engelhardt, H., and Kamb, B., 1998, Pleistocene collapse of the West Antarctic ice sheet: Science, v. 281, no. 5373, p. 82-85.

Schlich, R., Wise Jr, S., and Palmer Julson, A., The geologic and tectonic evolution of the Kerguelen Plateau: an introduction to the scientific results of Leg 120, *in* Proceedings Proceedings of the Ocean Drilling Program, Scientific Results1992, Volume 120, Texas A&M University College Station, TX, p. 5-30.

Schoof, C., 2007, Ice sheet grounding line dynamics: Steady states, stability, and hysteresis: Journal of Geophysical Research: Earth Surface, v. 112, no. F3.

Sexton, D. J., Dowdeswell, J. A., Solheim, A., and Elverhøi, A., 1992, Seismic architecture and sedimentation in northwest Spitsbergen fjords: Marine Geology, v. 103, no. 1, p. 53-68.

Shackleton, N., Imbrie, J., Pisias, N., and Rose, J., 1988, The evolution of oceanic oxygen-isotope variability in the North Atlantic over the past three million years [and discussion]: Philosophical Transactions of the Royal Society B: Biological Sciences, v. 318, no. 1191, p. 679-688.

Shackleton, N. J., Backman, J., Zimmerman, H., Kent, D. V., Hall, M., Roberts, D. G., Schnitker, D., Baldauf, J., Desprairies, A., and Homrighausen, R., 1984, Oxygen isotope calibration of the onset of ice-rafting and history of glaciation in the North Atlantic region: Nature, v. 307, no. 5952, p. 620-623.

Shackleton, N. J., Hall, M. A., Raffi, I., Tauxe, L., and Zachos, J., 2000, Astronomical calibration age for the Oligocene-Miocene boundary: Geology, v. 28, no. 5, p. 447-450.

References

Shackleton, N. J., and Kennett, J. P., 1975, Paleotemperature history of the Cenozoic and the initiation of Antarctic glaciation: oxygen and carbon isotope analyses in DSDP Sites 277, 279, and 281: Initial reports of the deep sea drilling project, v. 29, p. 743-755.

Shevenell, A. E., and Kennett, J. P., 2007, Cenozoic Antarctic cryosphere evolution: Tales from deep-sea sedimentary records: Deep Sea Research Part II: Topical Studies in Oceanography, v. 54, no. 21–22, p. 2308-2324.

Shevenell, A. E., Kennett, J. P., and Lea, D. W., 2004, Middle Miocene Southern Ocean Cooling and Antarctic Cryosphere Expansion: Science, v. 305, no. 5691, p. 1766-1770.

Shevenell, A. E., Kennett, J. P., and Lea, D. W., 2008, Middle Miocene ice sheet dynamics, deep-sea temperatures, and carbon cycling: A Southern Ocean perspective: Geochemistry, Geophysics, Geosystems, v. 9, no. 2.

Shigemitsu, M., Narita, H., Watanabe, Y. W., Harada, N., and Tsunogai, S., 2007, Ba, Si, U, Al, Sc, La, Th, C and 13C/12C in a sediment core in the western subarctic Pacific as proxies of past biological production: Marine Chemistry, v. 106, no. 3–4, p. 442-455.

Siddoway, C., 2008, Tectonics of the West Antarctic Rift System: new light on the history and dynamics of distributed intracontinental extension, *in* Cook, A. K., Barrett, P., Stagg, H., Storey, B., Stump, E., and Wise, W., eds., Antarctica: A Keystone in a Changing World: Washington, DC, The Naional Academic Press, p. 91-114.

Siddoway, C. S., Baldwin, S. L., Fitzgerald, P. G., Fanning, C. M., and Luyendyk, B. P., 2004, Ross Sea mylonites and the timing of intracontinental extension within the West Antarctic rift system: Geology, v. 32, no. 1, p. 57-60.

Siddoway, C. S., Sass, L. C., and Esser, R. P., 2005, Kinematic history of western Marie Byrd Land, West Antarctica: direct evidence from Cretaceous mafic dykes: Geological Society, London, Special Publications, v. 246, no. 1, p. 417-438.

Smellie, J., 2001, History of Oligocene erosion, uplift and unroofing of the Transantarctic Mountains deduced from sandstone detrital modes in CRP-3 drillcore, Victoria Land Basin, Antarctica: Terra Antartica, v. 8, no. 4, p. 481-490.

Sorlien, C. C., Luyendyk, B. P., Wilson, D. S., Decesari, R. C., Bartek, L. R., and Diebold, J. B., 2007, Oligocene development of the West Antarctic Ice Sheet recorded in eastern Ross Sea strata: Geology, v. 35, no. 5, p. 467-470.

Spofforth, D. J., Pälike, H., and Green, D., 2008, Paleogene record of elemental concentrations in sediments from the Arctic Ocean obtained by XRF analyses: Paleoceanography, v. 23, no. 1.

References

Stern, R., Ten Brink, U., and Bott, M., 1992, Numerical modelling of uplift and subsidence adjacent to the Transantarctic Mountains, *in* Yoshida, Y., Kaminuma, K., and Shiraishi, K., eds., Recent Progress in Antarctic Earth Science, Tokyo, Terra Scientific Publishing Company, p. 515-521.

Stern, T. A., Baxter, A. K., and Barrett, P. J., 2005, Isostatic rebound due to glacial erosion within the Transantarctic Mountains: Geology, v. 33, no. 3, p. 221-224.

Stocchi, P., Escutia, C., Houben, A. J. P., Vermeersen, B. L. A., Bijl, P. K., Brinkhuis, H., DeConto, R. M., Galeotti, S., Passchier, S., Pollard, D., Brinkhuis, H., Escutia, C., Klaus, A., Fehr, A., Williams, T., Bendle, J. A. P., Bijl, P. K., Bohaty, S. M., Carr, S. A., Dunbar, R. B., Flores, J. A., Gonzàlez, J. J., Hayden, T. G., Iwai, M., Jimenez-Espejo, F. J., Katsuki, K., Kong, G. S., McKay, R. M., Nakai, M., Olney, M. P., Passchier, S., Pekar, S. F., Pross, J., Riesselman, C., Röhl, U., Sakai, T., Shrivastava, P. K., Stickley, C. E., Sugisaki, S., Tauxe, L., Tuo, S., van de Flierdt, T., Welsh, K., and Yamane, M., 2013, Relative sea-level rise around East Antarctica during Oligocene glaciation: Nature Geoscience, v. 6, no. 5, p. 380-384.

Stoner, J. S., Channell, J. E. T., and Hillaire-Marcel, C., 1995, Magnetic properties of deep-sea sediments off southwest Greenland: Evidence for major differences between the last two deglaciations: Geology, v. 23, no. 3, p. 241-244.

Stow, D., and Piper, D., 1984, Deep-water fine-grained sediments: facies models: Geological Society, London, Special Publications, v. 15, no. 1, p. 611-646.

Stow, D. A., 1979, Distinguishing between fine-grained turbidites and contourites on the Nova Scotian deep water margin: Sedimentology, v. 26, no. 3, p. 371-387.

Stow, D. A., and Shanmugam, G., 1980, Sequence of structures in fine-grained turbidites: comparison of recent deep-sea and ancient flysch sediments: Sedimentary Geology, v. 25, no. 1-2, p. 23-42.

Strand, K., Passchier, S., and Näsi, J., 2003, Implications of quartz grain microtextures for onset Eocene/Oligocene glaciation in Prydz Bay, ODP Site 1166, Antarctica: Palaeogeography, Palaeoclimatology, Palaeoecology, v. 198, no. 1–2, p. 101-111.

Svendsen, J. I., Mangerud, J., Elverhøi, A., Solheim, A., and Schüttenhelm, R. T., 1992, The Late Weichselian glacial maximum on western Spitsbergen inferred from offshore sediment cores: Marine Geology, v. 104, no. 1-4, p. 1-17.

Taviani, M., and Beu, A. G., 2003, The palaeoclimatic significance of Cenozoic marine macrofossil assemblages from Cape Roberts Project drillholes, McMurdo Sound, Victoria Land Basin, East Antarctica: Palaeogeography, Palaeoclimatology, Palaeoecology, v. 198, no. 1–2, p. 131-143.

References

ten Brink, U., and Cooper, A., 1992, Modeling the bathymetry of Antarctic continental margins: Recent Progress in Antarctic Earth Science: Tokyo, Terra Scientific Publishing Co, p. 763-772.

ten Brink, U. S., Hackney, R. I., Bannister, S., Stern, T. A., and Makovsky, Y., 1997, Uplift of the Transantarctic Mountains and the bedrock beneath the East Antarctic ice sheet: Journal of Geophysical Research: Solid Earth v. 102, no. B12, p. 27603-27621.

The Shipboard Scientific Party, 1975a, Introduction: Initial Reports of the Deep Sea Drilling Project, v. 28, p. 5-18.

The Shipboard Scientific Party, 1975b, Shipboard site reports - sites 270, 271, 272: Initial Reports of the Deep Sea Drilling Project, v. 28, p. 211-234.

Thompson, G. R., and Hower, J., 1973, An explanation for low radiometric ages from glauconite: Geochimica et Cosmochimica Acta, v. 37, no. 6, p. 1473-1491.

Thomson, D. J., 1982, Spectrum estimation and harmonic analysis: Proceedings of the Institute of Electrical and Electronics Engineers, v. 70, no. 9, p. 1055-1096.

Thorn, V., 2001, Oligocene and early Miocene phytoliths from CRP-2/2A and CRP-3, Victoria Land Basin, Antarctica: Terra Antartica, v. 8, no. 4, p. 407-422.

Tripati, A., Backman, J., Elderfield, H., and Ferretti, P., 2005, Eocene bipolar glaciation associated with global carbon cycle changes: Nature, v. 436, no. 7049, p. 341-346.

Troedson, A. L., and Riding, J. B., 2002, Upper Oligocene to lowermost Miocene strata of King George Island, South Shetland Islands, Antarctica: stratigraphy, facies analysis, and implications for the glacial history of the Antarctic Peninsula: Journal of Sedimentary Research, v. 72, no. 4, p. 510-523.

Troedson, A. L., and Smellie, J. L., 2002, The Polonez Cove Formation of King George Island, Antarctica: stratigraphy, facies and implications for mid-Cenozoic cryosphere development: Sedimentology, v. 49, no. 2, p. 277-301.

Van Simaeys, S., Brinkhuis, H., Pross, J., Williams, G. L., and Zachos, J. C., 2005, Arctic dinoflagellate migrations mark the strongest Oligocene glaciations: Geology, v. 33, no. 9, p. 709-712.

Wade, B. S., and Pälike, H., 2004, Oligocene climate dynamics: Paleoceanography, v. 19, no. 4.

Walker, R. G., 1992, Turbidites and subamrine fans, *in* Walker, R. G., and James, N. P., eds., Facies models: response to sea level change, Geological Association of Canada, p. 239-263.

References

Warny, S., Askin, R. A., Hannah, M. J., Mohr, B. A. R., Raine, J. I., Harwood, D. M., Florindo, F., and Team, t. S. S., 2009, Palynomorphs from a sediment core reveal a sudden remarkably warm Antarctica during the middle Miocene: Geology, v. 37, no. 10, p. 955-958.

Weber, M., Clark, P., Kuhn, G., Timmermann, A., Sprenk, D., Gladstone, R., Zhang, X., Lohmann, G., Menviel, L., and Chikamoto, M., 2014, Millennial-scale variability in Antarctic ice-sheet discharge during the last deglaciation: Nature, v. 510, no. 7503, p. 134-138.

Weltje, G. J., Bloemsma, M. R., Tjallingii, R., Heslop, D., Röhl, U., and Croudace, I. W., 2015, Prediction of Geochemical Composition from XRF Core Scanner Data: A New Multivariate Approach Including Automatic Selection of Calibration Samples and Quantification of Uncertainties, *in* Croudace, I. W., and Rothwell, R. G., eds., Micro-XRF Studies of Sediment Cores, Volume 17, Springer Netherlands, p. 507-534.

Weltje, G. J., and Tjallingii, R., 2008, Calibration of XRF core scanners for quantitative geochemical logging of sediment cores: theory and application: Earth and Planetary Science Letters, v. 274, no. 3, p. 423-438.

Wilch, T. I., and McIntosh, W. C., 2000, Eocene and Oligocene volcanism at Mount Petras, Marie Byrd Land: implications for middle Cenozoic ice sheet reconstructions in West Antarctica: Antarctic Science, v. 12, no. 04, p. 477-491.

Williams, T., van de Flierdt, T., Hemming, S. R., Chung, E., Roy, M., and Goldstein, S. L., 2010, Evidence for iceberg armadas from East Antarctica in the Southern Ocean during the late Miocene and early Pliocene: Earth and Planetary Science Letters, v. 290, no. 3, p. 351-361.

Wilson, D. S., Jamieson, S. S., Barrett, P. J., Leitchenkov, G., Gohl, K., and Larter, R. D., 2012, Antarctic topography at the Eocene–Oligocene boundary: Palaeogeography, Palaeoclimatology, Palaeoecology, v. 335, p. 24-34.

Wilson, D. S., and Luyendyk, B. P., 2009, West Antarctic paleotopography estimated at the Eocene-Oligocene climate transition: Geophysical Research Letters, v. 36, no. 16.

Wilson, D. S., Pollard, D., DeConto, R. M., Jamieson, S. S. R., and Luyendyk, B. P., 2013, Initiation of the West Antarctic Ice Sheet and estimates of total Antarctic ice volume in the earliest Oligocene: Geophysical Research Letters, v. 40, no. 16, p. 4305-4309.

Wilson, G., Pekar, S. F., Naish, T., Passchier, S., and DeConto, R., 2009, The Oligocene-Miocene boundary - Antarctic climate response to orbital forcing, *in* Florindo, F., and Siegert, M., eds., Antarctic Climate Evolution, Amsterdam, Elsevier, p. 369-400.

References

Winberry, J. P., and Anandakrishnan, S., 2004, Crustal structure of the West Antarctic rift system and Marie Byrd Land hotspot: Geology, v. 32, no. 11, p. 977-980.

Wise, S. W. Jr., Breza, J. R., Harwood, D. M., and Wie, W., 1992, Paleogene glacial history of Antarctica, *in* McKenzie, J. A., Müller, D. W., and Weissert, H., eds., Controversies in Modern Geology, Cambridge, Cambridge University Press, p. 133-171.

Zachos, J. C., Breza, J. R., and Wise, S. W., 1992, Early Oligocene ice-sheet expansion on Antarctica: Stable isotope and sedimentological evidence from Kerguelen Plateau, southern Indian Ocean: Geology, v. 20, no. 6, p. 569-573.

Zachos, J. C., Dickens, G., and Zeebe, R., 2008, An early Cenozoic perspective on greenhouse warming and carbon-cycle dynamics: Nature, v. 451, no. 7176, p. 279-283.

Zachos, J. C., Flower, B. P., and Paul, H., 1997, Orbitally paced climate oscillations across the Oligocene/Miocene boundary: Nature, v. 388, no. 6642, p. 567-570.

Zachos, J. C., Pagani, M., Sloan, L., Thomas, E., and Billups, K., 2001a, Trends, Rhythms, and Aberrations in Global Climate 65 Ma to Present: Science, v. 292, no. 5517, p. 686-693.

Zachos, J. C., Quinn, T. M., and Salamy, K. A., 1996, High-resolution (104 years) deep-sea foraminiferal stable isotope records of the Eocene-Oligocene climate transition: Paleoceanography, v. 11, no. 3, p. 251-266.

Zachos, J. C., Shackleton, N. J., Revenaugh, J. S., Pälike, H., and Flower, B. P., 2001b, Climate Response to Orbital Forcing across the Oligocene-Miocene Boundary: Science, v. 292, no. 5515, p. 274-278.

Zhang, Y. G., Pagani, M., Liu, Z., Bohaty, S. M., and DeConto, R., 2013, A 40-million-year history of atmospheric CO_2: Philosophical Transactions of the Royal Society A: Mathematical, Physical and Engineering Sciences, v. 371, no. 2001, p. 20130096.

References

APPENDIX CD 1

Appendix

APPENDIX CD 2

Appendix